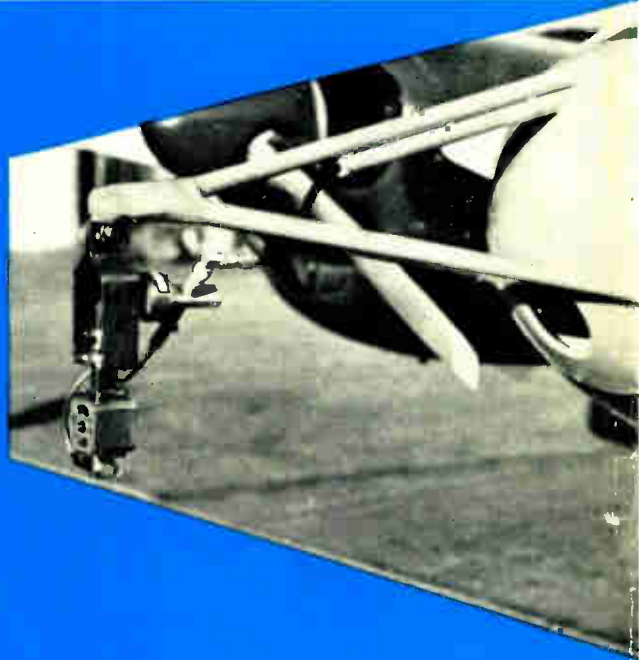


F81

Advances in RADIO RESEARCH

VOLUME 1

Edited by
J. A. SAXTON



ACADEMIC PRESS
LONDON AND NEW YORK

The lower atmosphere, or troposphere, has an all-important influence on the propagation of very short radio waves, the full understanding of which demands a knowledge in detail of the fine structure of the refractive index of the troposphere and its spatial and temporal variations. A description is given of the design and performance of microwave refractometers by means of which such knowledge may be obtained. There are also two chapters on the tropospheric refraction and attenuation of radio waves, leading to proposals for models of the atmosphere for application in radio communication problems.

A final chapter presents an up-to-date account of the theory of surface wave propagation, a topic for argument for many years since the early work of Zeu-neck and Sommerfeld until recently when the more important issues appear to have been resolved.

ELECTROMAGNETIC WAVE PROPAGATION

International Conference sponsored by the Postal and Telecommunications Group of the Brussels Universal Exhibition

Edited by M. DESIRANT, *Société Belge de Physique, Loverval, Belgium.*

and J. L. MICHIELS, *Laboratoire de Recherches Physiques, A.C.E.C., Charleroi, Belgium.*

1960, xiii + 730 pp., illus., 157s.

This volume presents a survey of research and progress in the field of electromagnetic wave propagation by scientists and engineers from eleven different countries and offers a fruitful comparison of work carried out in different parts of the world.

The importance of a wider and deeper knowledge of electromagnetic wave propagation for the continued progress of modern telecommunication needs no emphasis. Research on this subject has been particularly active in recent years and has led to advances of major interest. An outstanding illustration of this is the investigation of ionospheric and tropospheric scatter and its application to beyond-the-horizon communication.



ACADEMIC PRESS
LONDON AND NEW YORK

Berkeley Square House, Berkeley Square, London, W.1

111 Fifth Avenue, New York, New York 10003

ADVANCES IN RADIO RESEARCH

Edited by

Author:

J. A. SAXTON

*Scientific Attaché, British Embassy, Washington D.C.
formerly Deputy Director, Radio Research Station
Slough, England*

Volume 1



1964



ACADEMIC PRESS · LONDON · NEW YORK

ACADEMIC PRESS INC. (LONDON) LTD
BERKELEY SQUARE HOUSE
BERKELEY SQUARE
LONDON, W.1

U.S. Edition published by

ACADEMIC PRESS INC.
111 FIFTH AVENUE
NEW YORK 3, NEW YORK

Copyright © 1964 By Academic Press Inc. (London) Ltd

ALL RIGHTS RESERVED
NO PART OF THIS BOOK MAY BE REPRODUCED IN ANY FORM BY
PHOTOSTAT, MICROFILM, OR ANY OTHER MEANS, WITHOUT WRITTEN
PERMISSION FROM THE PUBLISHERS

1924
621.3841072 ✓

Library of Congress Catalog Card Number: 64-19688

Printed in Great Britain by The Whitefriars Press Ltd.
London and Tonbridge

**ADVANCES IN
RADIO
RESEARCH**

Volume 1

CONTRIBUTORS TO VOLUME I

B. R. BEAN, *Central Radio Propagation Laboratory, National Bureau of Standards, Boulder, Colorado, U.S.A.*

A. W. STRAITON, *The University of Texas, Austin, Texas, U.S.A.*

JAMES R. WAIT, *Central Radio Propagation Laboratory, National Bureau of Standards, Boulder, Colorado, U.S.A.*

PREFACE

This is the first volume of a new series, "Advances in Radio Research", in which up-to-date reviews will be made of research and developments in the techniques and practice of radiocommunications, and of research on aerials and on the propagation of radiowaves on which such communication depends. Attention will also be devoted to radio techniques developed primarily as a tool for other fields of research, but which may also have applications in the general field of radio communications. It is thus the aim of the series to present information of value to those engaged in research in radio physics and communications, and also to engineers wishing to obtain a background in the basic knowledge on which the practice of radio communication depends; and the editor hopes that readers will find that this dual aim has been achieved.

An understanding of the propagation of radio waves requires a knowledge of the refracting, scattering and absorbing properties of the medium through which the transmission occurs. In communication problems the earth's atmosphere is still the most important such medium, and it is intended to include in this series accounts of research on all the relevant characteristics of the atmosphere. Consideration will also be given to the propagation of waves over and through the earth (including the sea) and to propagation problems associated with space research and communications not dealt with in a companion series.

The troposphere, or lower atmosphere, is of predominant importance in the propagation of very short waves, at frequencies greater than about 30 Mc/s; whilst at longer wavelengths the upper atmosphere, in which the ionosphere occurs, exerts a controlling influence. The nature of the ground is also important in some propagation problems, but whereas at very short wavelengths it is the irregularity of the surface and the presence of diffracting or absorbing obstacles which matter most, at longer wavelengths the electrical properties of the ground—dielectric constant and conductivity—are of much greater significance than is topography, though the effects of mountainous terrain cannot always be ignored.

Volume 1 contains three chapters on the troposphere as a propagation medium. One of these chapters is concerned primarily with the techniques available for the measurement of the tropospheric refractive index; and particular attention is devoted to the powerful method developed during the past decade in which direct measurements of the index are made using microwave refractometers. It has been realized for some time that any major progress in the understanding of the detailed characteristics of radio propagation at very short wavelengths is most likely to come through a comprehensive knowledge of the fine structure of the refractive index of the

troposphere and its variations; and the microwave refractometer has much to offer in this field of study.

The second and third chapters deal with refraction in the troposphere and its general relation to meteorological conditions and climate, and with the attenuation arising from absorption and scattering by atmospheric gases—mainly oxygen and water vapour—and by clouds and various forms of precipitation. On the practical side these chapters have relevance, for example, to the planning of very short wave communication and broadcasting systems; to space communication, guidance and control problems; and also to the estimation and correction of errors which may occur in the determination of target ranges and elevations by means of radar.

The fourth and final chapter in Volume 1 presents a review of some aspects of surface wave propagation; that is, of the characteristics of electromagnetic waves which are propagated along the boundary surface separating two media of different electrical properties. This subject has excited much argument since the early work of Zenneck and Sommerfeld, and it is only in recent years that the more important issues have been resolved.

It is a pleasure for the editor to acknowledge the willing and helpful co-operation he has received from the contributors to this volume.

J. A. SAXTON

Washington
February, 1964

CONTENTS

CONTRIBUTORS TO VOLUME 1	v
PREFACE	vii

MEASUREMENT OF THE RADIO REFRACTIVE INDEX OF THE ATMOSPHERE

A. W. Straiton

I. INTRODUCTION	2
II. REFRACTIVE INDEX OF THE ATMOSPHERE	2
III. LABORATORY MEASUREMENTS PRIOR TO 1947	5
IV. HISTORY OF ATMOSPHERIC REFRACTOMETRY	6
V. THE CRAIN REFRACTOMETER	9
VI. THE BIRNBAUM REFRACTOMETER	14
VII. CHARACTERISTICS OF MICROWAVE CAVITIES	17
VIII. THE DEAM REFRACTOMETER	26
IX. CHARACTERISTICS OF COAXIAL CAVITIES	29
X. THE TOLBERT PHASE-SHIFT REFRACTOMETER	31
XI. THE HAY REFRACTOMETER	32
XII. RADIO REFRACTIVE INDEX MEASUREMENTS	34
ACKNOWLEDGMENT	50
REFERENCES	50

TROPOSPHERIC REFRACTION

B. R. Bean

I. RADIO RAY TRACING.	53
II. LIMITATIONS TO RADIO RAY TRACING	56
III. AN APPROXIMATION FOR HIGH INITIAL ELEVATION ANGLES	57
IV. THE STATISTICAL METHOD	57
V. SCHULKIN'S METHOD	58
VI. LINEAR OR EFFECTIVE EARTH'S RADIUS MODEL	59
VII. MODIFIED EFFECTIVE EARTH'S RADIUS MODEL	62
VIII. EXPONENTIAL MODEL	67
IX. THE INITIAL GRADIENT CORRECTION METHOD	77
X. THE BI-EXPONENTIAL MODEL	78

XI.	THE DEPARTURES-FROM-NORMAL METHOD	87
XII.	A GRAPHICAL METHOD	90
XIII.	EFFECT OF ATMOSPHERIC HORIZONTAL INHOMOGENEITY UPON RAY TRACING	91
XIV.	COMPARISON OF OBSERVED ATMOSPHERIC RADIO REFRACTION EFFECTS WITH VALUES PREDICTED THROUGH THE USE OF SURFACE WEATHER OBSERVATIONS	100
	REFERENCES	119

ATTENUATION OF RADIO WAVES IN THE TROPOSPHERE

B. R. Bean

I.	INTRODUCTION	121
II.	ATTENUATION BY ATMOSPHERIC GASES.	122
III.	ESTIMATES OF THE RANGE OF TOTAL GASEOUS ABSORPTION	132
IV.	TOTAL RADIO PATH ABSORPTION.	136
V.	DERIVATION OF ABSORPTION ESTIMATE FOR OTHER AREAS	137
VI.	ATTENUATION IN CLOUDS	141
VII.	ATTENUATION BY RAIN	142
VIII.	RAIN ATTENUATION EFFECTS ON RADIO SYSTEMS ENGINEERING.	147
IX.	ATTENUATION BY HAIL	151
X.	ATTENUATION BY FOG	152
XI.	THERMAL NOISE EMITTED BY THE ATMOSPHERE	153
	REFERENCES	155

ELECTROMAGNETIC SURFACE WAVES

James R. Wait

I.	INTRODUCTION	157
II.	DIPOLE OVER AN IMPEDANCE PLANE	159
III.	RELATED SURFACE WAVE PROBLEMS	166
IV.	AXIAL WAVES ON CYLINDRICAL RODS	171
V.	AZIMUTHAL WAVES ON CYLINDRICAL BOUNDARIES	172
VI.	PROPAGATION OVER A HOMOGENEOUS SPHERICAL EARTH	175
VII.	MIXED-PATH PROPAGATION	184
VIII.	WAVE PROPAGATION OVER AN INHOMOGENEOUS SPHERE	204
	REFERENCES	209
	ACKNOWLEDGMENT	212
	APPENDIX	212
	REFERENCES FOR APPENDIX.	217
	AUTHOR INDEX	219
	SUBJECT INDEX	223

MEASUREMENT OF THE RADIO REFRACTIVE INDEX OF THE ATMOSPHERE

A. W. STRAITON

*The University of Texas
Austin, Texas, U.S.A.*

I.	Introduction	2
II.	Refractive Index of the Atmosphere	2
	A. Definition and Basic Relationships	2
	B. Refractivity	3
	C. Frequency Dependence	4
III.	Laboratory Measurements Prior to 1947	5
IV.	History of Atmospheric Refractometry	6
V.	The Crain Refractometer	9
	A. General Principles	9
	B. Description of System	10
	C. Stabilized Oscillators	12
	D. Metering Amplifier and Discriminator	14
VI.	The Birnbaum Refractometer	14
	A. General Principles	14
	B. Method of Operation	15
	C. Time Delay Measurements	16
	D. Readout and Noise Evaluation	17
VII.	Characteristics of Microwave Cavities	17
	A. General Relationships	17
	B. Field Equations	18
	C. Frequency Variation with Index of Refraction	19
	D. Frequency Variation with Change in Dimensions	19
	E. Methods of Reducing Effects of Temperature Changes	20
	F. Pressure Effects	22
	G. Wall Condensation Effects	23
	H. Cavity Ventilation	24
VIII.	The Deam Refractometer	26
	A. General Principles	26
	B. Method of Operation	26
	C. Cavity Characteristics	28
IX.	Characteristics of Coaxial Cavities	29
	A. General Relationships	29
	B. Temperature Compensation	30
	C. Condensation Effects	30
	D. Refractive Index Variations Along the Cavity	30
X.	The Tolbert Phase-Shift Refractometer	31
XI.	The Hay Refractometer	32
	A. General Principles	32
	B. Description of System	33
	C. Sampling Capacitor	33
	D. Reference Capacitor	33
	E. Adaptations	34
	F. Condensation Effects	34

XII. Radio Refractive Index Measurements	34
A. Introduction	34
B. Refractive Index Calculated from Meteorological Parameters	35
C. Ground Based Refractometer Measurements	36
D. Airborne Refractometer Profile Measurements	38
E. Airborne Refractometer Fluctuation Measurements	41
F. Cloud Studies	46
G. Other Applications	49
Acknowledgment	50
References	50

I. INTRODUCTION

It is the purpose of this chapter to describe various new techniques which have been used in recent years for the direct measurement of the radio refractive index of the atmosphere. These measurements have caused major revisions in our concepts of the refractive index structure of the atmosphere.

The presentation will begin with a brief review of the factors determining refractive index, followed by a short account of how the investigation of these factors led to the development of atmospheric refractometers.

A description will then be given of the several types of refractometers now in use or which have been proposed for special applications. Particular attention will be given to the problems relating to the sampling element of these devices.

Illustrative examples of observations taken with refractometers for the purpose of obtaining detailed profile and fluctuation data will be shown and some of their more common features noted.

The presentation will be concluded by a brief account of other uses of refractometers involving measurement of the refractive properties of dust, smoke, and ionized gases, studies of molecular polarization and the measurement of the water vapor content of the atmosphere.

A less extensive survey of certain of the areas to be covered in this presentation has recently been made by McGavin (1962). His survey is primarily concerned with the accuracies of the various techniques employed in determining the radio refractive index both indirectly from meteorological data and directly through the use of refractometers with regard to the application of such data. As elaborated later in this presentation, the radiosonde evaluation technique is shown to be well suited to synoptic type analyses while the direct reading refractometer is essential to the higher accuracy required for radar and propagation studies.

II. REFRACTIVE INDEX OF THE ATMOSPHERE

A. DEFINITION AND BASIC RELATIONSHIPS

The refractive index of a dielectric, n , is the ratio of the velocity of a plane electromagnetic wave in a vacuum to its velocity in the dielectric. In a non-magnetic medium, the refractive index is equal to the square root of the

relative dielectric constant, K , i.e.

$$n^2 = K \tag{1}$$

Debye (1929) has shown that the dielectric constant and the refractive index may be related to the polarizability, α , by the relationship

$$\frac{K-1}{K+2} = \frac{n^2-1}{n^2+2} = \frac{4\pi}{3} \frac{m}{M} \rho \alpha \tag{2}$$

where ρ is the density, m is the number of molecules per unit volume and M is the molecular weight.

The polarizability may in turn be expressed in two terms as follows:

$$\alpha = \alpha_0 + \frac{\mu^2}{k3T} \tag{3}$$

where α_0 is the polarization effect due to distortion of charge distributions and $\mu^2/3kT$ is the effect associated with the orientation of polar molecules. In this expression, μ is the electric moment, k is Boltzmann's constant and T is the absolute temperature in degrees Kelvin.

B. REFRACTIVITY

The refractive index of the atmosphere differs from unity by a maximum of a few hundred parts per million. It is therefore convenient to introduce a term, N , called the refractivity, which is defined by

$$N = (n-1) \times 10^6 \tag{4}$$

Thus N represents the parts per million by which the refractive index differs from unity.

As a good approximation

$$n^2 - 1 = 2N \times 10^{-6} \tag{5}$$

Equation (2) may be written as

$$\frac{n^2-1}{n^2+2} = \frac{2N \times 10^{-6}}{3} = \frac{4\pi}{3} \frac{m}{M} \rho \alpha \tag{6}$$

or

$$N = 2\pi \times 10^6 \frac{m}{M} \rho \alpha \tag{7}$$

Substituting equation (3) into (7) gives

$$N = 2\pi \times 10^6 \frac{m}{M} \rho (\alpha_0 + \mu^2/3kT) \tag{8}$$

Since the density is proportional to the ratio of pressure to temperature and the constants for a particular gas may be combined, equation (8) may thus be written as

$$N = A' P/T + A'' P/T^2 \tag{9}$$

In the absence of precipitation or foreign particles, the atmosphere is essentially composed of nitrogen and oxygen in fixed amounts and water vapor in smaller but variable amounts. Nitrogen and oxygen have no permanent electric dipole moment, leaving water vapor as the only significant gas having a non-zero A'' term. Contributions due to traces of other gases in the atmosphere may be neglected.

Since the polarizability of a mixture of gases is additive, the refractivity for air may be written as

$$N = A'_{Ni} P_{Ni}/T + A'_O P_O/T + A'_{WV} P_{WV}/T + A''_{WV} P_{WV}/T^2 \quad (10)$$

$$\text{or} \quad N = A'_{DA} P_{DA}/T + A'_{WV} P_{WV}/T + A''_{WV} P_{WV}/T^2 \quad (11)$$

where Ni, O, WV and DA refer to nitrogen, oxygen, water vapor and dry air, respectively.

Equation (11) thus gives a means for obtaining the refractivity of the atmosphere if the constants are known. In order to establish these constants, it is necessary to have some direct means of measuring the dielectric constant or refractive index. The development of atmospheric refractometers was stimulated by laboratory experiments designed to measure these constants for air and for other gases.

Values of the constants in equation (11) have been given by a number of investigators starting with Jona (1919). Smith and Weintraub (1960) surveyed and evaluated the results of the various measurements and suggested the use of the following, where the pressure is expressed in mb:

$$A'_{DA} = 77.6, \text{ }^\circ\text{K}/\text{mb}$$

$$A'_{WV} = 72, \text{ }^\circ\text{K}/\text{mb}$$

$$A''_{WV} = 3.75 \times 10^5, \text{ } (^\circ\text{K})^2/\text{mb}$$

While there is some uncertainty in these values, variations in N resulting from the use of slightly different experimentally determined values of the constants are of no significance when compared, as Bean (1962) has shown, to the errors resulting from the inability to obtain accurate or representative values of pressure and temperature. The effect is further minimized, as will be discussed later in atmospheric applications, when consideration is given to the fact that a knowledge of relative changes in N is of much greater utility than are absolute values in studies of radio wave propagation.

Using the values suggested by Smith and Weintraub, equation (11) then becomes

$$N = \frac{77.6 P_{DA}}{T} + \frac{72 P_{WV}}{T} + \frac{3.75 \times 10^6 P_{WV}}{T^2} \quad (12)$$

C. FREQUENCY DEPENDENCE

Since there is no variation of the polarization effect due to distortion of charge distributions over the entire optical-radio electromagnetic frequency spectrum, the index of refraction of dry air is constant throughout this interval. On the other hand, a significant change occurs when water vapor

is considered between optical and radio refractive index because of the greatly enhanced field interaction at radio wavelengths with the water vapor polar molecule. This contribution is very small in the optical portion of the spectrum, increases sharply in the far infrared and submillimeter portion and then remains essentially constant throughout the entire radio spectrum. These characteristics of water vapor are well demonstrated by Essen and Froome (1951) and Froome (1955) who present data by various investigators whose techniques appear to provide a high degree of accuracy. These data, summarized by wavelengths, are shown in Table I and indicate that to the accuracy required in the refractivity equation, there is no variation in the atmospheric refractive index within the radio frequency spectrum. In addition to those shown in the table, other pertinent references are those of Birnbaum and Catterjee (1952) and Phillips (1950).

TABLE I. *Refractivity in N Units*

Frequency	Dry Air 0°C 760 mm Hg Pressure	Water Vapor 20°C 10 mm Hg Pressure	Source
0.5 Mc/s		61.3	Stranathan (1935)
0.5 Mc/s	288		Watson <i>et al.</i> (1934)
1 Mc/s		62.7	Sanger (1930)
1 Mc/s	288.5		Hector and Woernly (1946)
9 000 Mc/s	286	61.3	Crain (1948)
9 000 Mc/s	287.5		Birnbaum <i>et al.</i> (1951)
9 000 Mc/s	288.1	60.7	Essen (1953)
24 000 Mc/s	288	60.7	Essen and Froome (1951)
74 000 Mc/s	287.7	61.0	Froome (1955)
Optical (Long wavelength)		2.94	Barrell and Sears (1939)
Optical (Long wavelength)	287.8		Barrell (1951)

III. LABORATORY MEASUREMENTS PRIOR TO 1947

Direct measurements of refractive index or dielectric constant of the air and its constituent gases prior to 1947 were confined to the laboratory. These measurements, however, set the pattern for the techniques which were subsequently used in refractometers and also showed some of the difficulties which were later encountered in the field use of these instruments.

Jona (1919) reported measurements made on the refractive index of a number of gases including dry air and water vapor. His studies were made to confirm Debye's relationships for unpolarized and for polarized gases. He used a tuned circuit to control frequency with the sampling unit provided by a parallel plate condenser. Since this capacitance is directly proportional to the dielectric constant of the gas between the plates, a change in this dielectric of the gases will result in a change in the capacitance of the condenser. To examine the relationships given in equations (2) and (3), the value

of $K-1$ was plotted against the reciprocal of the absolute temperature. Jona noted a change in the slope of this curve near the liquification point for some of the gases studied.

Zahn (1926) reported similar measurements and also noted a break in the curve which he associated with a film of water on the condenser plates. This error introduced by the condensation of water is a problem which continues whenever the refractive index of water vapor or air containing water vapor is being measured.

Stranathan (1935) further examined the anomaly reported by Zahn and found that there are errors due not only to the film of water but also to the conductivity of the insulators used to separate the condenser plates. Stranathan's measurements and those reported by Sanger (1930) provided data in close agreement with the values chosen by Smith and Weintraub (1960) in the index of refraction equation for dry air and water vapor. The measurements prior to 1940 were all made at frequencies below 4 Mc/s. Tregidga (1940) reported dielectric constant values for water vapor at a frequency of 42 Mc/s. He also used a condenser for sampling the gases but with a standard capacitance in parallel with the measuring unit. When the capacitance of the sampling condenser changed due to a change in the index of refraction of the gas between its plates, compensation was made by changing the standard capacitance. From the amount of this change, he determined the change in capacitance of the sampling condenser. Kerr (1941) reported refractive index measurements at a radio frequency of 58 Mc/s in which he introduced a standing wave method using a coaxial tube as his sampling device. Saxton (1946) reported the first microwave measurements of the refractive index of water vapor and introduced the cavity technique for these measurements. Using reflex klystron tubes, his studies were made at frequencies of 3 300, 10 000 and 18 700 Mc/s. He matched the oscillator to the cavity by means of a telescopic coaxial line for the two lower frequencies and by the use of tuning stubs for the highest frequency. For the two lower frequencies a cavity oscillating in TM_{010} mode was used and plots were made of the resonance curve of the cavity as the frequency was varied over a wide enough range to determine the resonant frequency and the bandwidth of the cavity. From these data, he determined not only the dielectric constant but also the loss tangent of the gas. For the highest frequency, he used a cavity oscillating in the TE_{011} mode and, because of difficulty in tuning the klystron frequency, he adjusted the resonance cavity mechanically.

IV. HISTORY OF ATMOSPHERIC REFRACTOMETRY

The early laboratory measurements of the dielectric constant of various gases, including water vapor, were directed primarily toward obtaining the average dielectric constant of the individual gases, although as noted above, Saxton's 18 700 Mc/s studies also gave experimental evidence of loss in water vapor. The need for greater accuracy and the developments in refraction and scatter propagation, which involved requirements for direct refractive index probing of the atmosphere, led to the introduction of the

atmospheric refractometer starting in about 1947. Almost simultaneously, C. M. Crain of The University of Texas and George Birnbaum of the Bureau of Standards started work on devices which would measure directly the dielectric constant or refractive index of gases. These devices were very similar and each will be discussed in greater detail later. Each used 10 000 Mc/s resonant cavities to give the dielectric constant of the gas. In Crain's case the cavities were active; that is, they controlled the frequency of the generator and in Birnbaum's case, the cavities were passive with their impedance essentially measured by a sweep frequency technique. These instruments were originally developed in an effort to increase the accuracy with which dielectric constant measurements could be made of air, water vapor and other gases and each was later adapted to direct atmospheric sampling. The results of Crain's measurements and a description of his refractometer were given in his paper in the *Physical Review* (1948), while Birnbaum's instrument was described in his paper in the *Review of Scientific Instruments* (1950a).

Shortly after the development of their refractometers, both Crain and Birnbaum moved their instruments outdoors and noted for the first time the existence of rapid temporal variations of the index of refraction (Crain and Gerhardt, 1950; Birnbaum, 1951). These surface level fluctuations, which are discussed in more detail in Section XIIC, resulted from the combined effects of temperature and moisture variations created by atmospheric turbulence, both of the mechanical mixing and convective or thermal heating types. It might be well to point out at this time that the rapid response characteristics of these refractometers were ideally suited for the experimental verification of the theories of atmospheric turbulence which were just being developed at that time involving the existence of a continuous spectrum of frequencies, or eddy sizes. Previously, meteorologists had shown no great interest in, and had little knowledge of, the variations in atmospheric parameters on other than synoptic or weather-map distance and time scales.

The first airborne refractometer flight was made in April 1951 by A. P. Deam with a Crain refractometer in a blimp at Lakehurst, N.J. (Crain and Deam, 1952). A picture of the installation is shown in Fig. 1. The general type of atmospheric structure which has become so familiar through various types of profile measurements was noted with a rather strong inversion over the Atlantic Ocean at a height of about 5 000 ft and fluctuations generally decreasing with elevation save at levels where marked vertical stratification existed. In June 1951 the first aircraft sounding was made out of Wright Field by C. M. Crain with the refractometer inside the plane and the cavity extending outside the shell of the plane. These initial flights were subsequently followed by many other airborne-refractometer soundings throughout the world. Few of these measurement programs, however, have been on a continuous or systematic basis and the samples that are available, although numerous, are still somewhat intermittent in time and diverse in location.

Various changes have been made in the Birnbaum and Crain type refractometers and their construction has also been undertaken by a number of

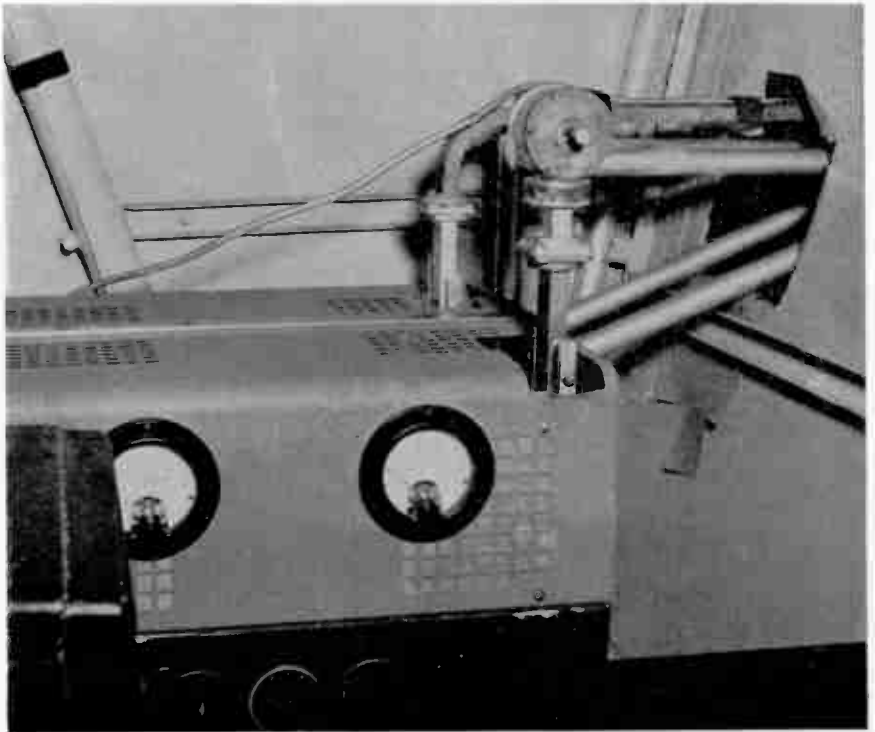
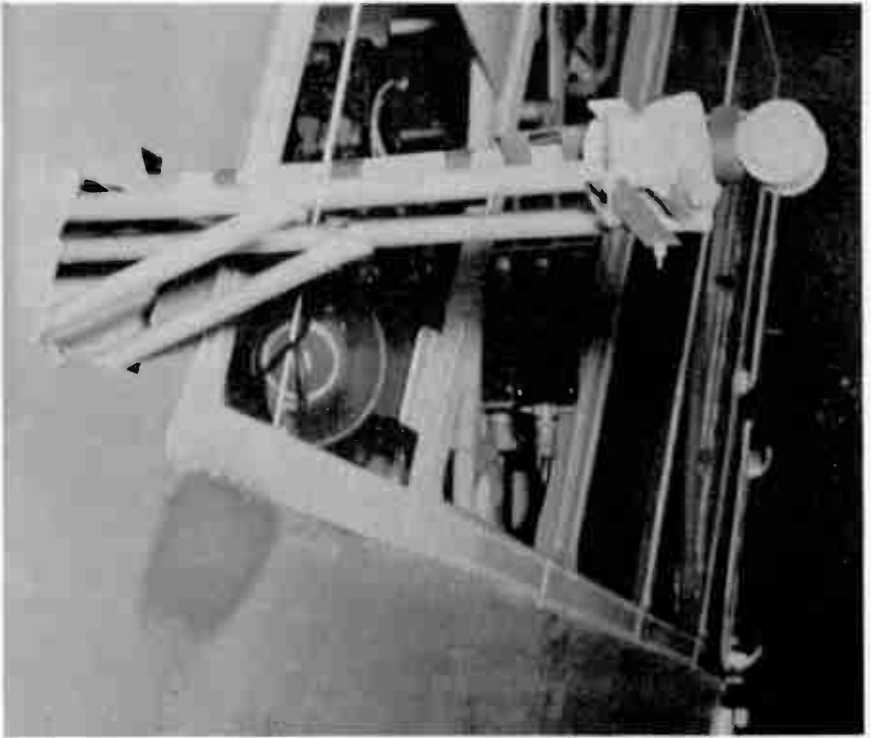


FIG. 1. Composite interior and exterior views of first airborne refractometer installation on a U.S. Navy blimp in 1951. The perforations in the Crain refractometer cavity are those which were used in all future flight programs for ventilation purposes.

different organizations. In 1959 A. P. Deam developed a lightweight refractometer operating at a frequency of about 400 Mc/s which could be dropped from an aircraft or flown by balloons with the data being recorded either in the aircraft or at a ground station. In 1960 Hay in Canada developed a variation of the refractometer which used a capacitor as the sensing element. This has been flown on a balloon and atmospheric refractive index data obtained with it. Several other varieties of capacity controlled refractometers have been developed and are being tried by a number of different groups.

The subsequent discussions of refractometer units will take up the Crain and Birnbaum types, the Deam type and the Hay type in that order. These may be classified in terms of the air sampling device and frequency of operation as follows:

1. Resonant cavities operating in the vicinity of 10 000 Mc/s.
2. Coaxial cavities operating in the vicinity of 400 Mc/s.
3. Condensers operating at frequencies below 10 Mc/s.

In general, the frequency change corresponding to a change of one N unit will be 10^{-6} times the nominal frequency of operation of the instrument. The exception occurs if the sampling device is in parallel with a similar device which does not change with the atmospheric index of refraction. For this condition, the sensitivity will be reduced.

There is some advantage in using a microwave system as opposed to one operating in the few megacycles per second range. For instance, one N unit change in a 10 000 Mc/s refractometer will produce a corresponding change in frequency of 10 000 cycles, whereas one N unit change in a 1 Mc/s device will produce a change of only 1 c/s. The refractive index-frequency relationship is given in more detail in Section VII.

Another important factor to be considered is the type of electric field used in the sensor. A field which does not terminate on the walls of the sensor will have a big advantage over one that does so terminate, since any slight deposit of moisture or dust on the walls will cause a far greater change when the electric field is terminated on the walls than when it is not. The problem of sensors is probably the most important and the most critical one in refractometry. For this reason, considerable detail will be given concerning the sampling elements in Section VII.

V. THE CRAIN REFRACTOMETER

A. GENERAL PRINCIPLES

The Crain atmospheric refractometer uses essentially the same principle as the laboratory instrument which he developed for the measurement of the constants in the equation for the index of refraction of water vapor (Crain, 1948). For atmospheric measurements, and particularly for the airborne ones, much greater stability and more rugged construction is necessary. An instrument to meet this requirement was reported by Crain (1950).

The Crain refractometer has the following identifying characteristics:

1. It uses two Pound stabilized oscillators (Pound, 1946), one controlled

by a reference cavity and one by a measuring cavity. The difference between the frequencies of these two stabilized oscillators is the measure of the index of refraction. The difference in resonance frequency between the two cavities is converted to a dc voltage and recorded on a meter.

2. A change in index of refraction is directly proportional to the change in the resonant frequency of the cavity. Crain's instrument has the advantage of being calibrated by a frequency meter and is independent of any stability problems in the klystron associated with it. It is, accordingly, much less subject to vibrations in the instrument than is a passive cavity device.

3. It has the disadvantage in that its circuitry is rather complex and that it requires the two oscillators. Furthermore, while any cavity system will suffer a degradation in Q with increasing loss tangent, as would be found, for example, in ionized gases, the Pound technique is under these conditions such as to make it more difficult to measure the real part of the dielectric constant than is the case with the passive, swept-frequency cavity of the Birnbaum type. The Crain unit is, however, ideally suited for atmospheric measurement and has been the one most extensively employed for airborne refractometer measurements since 1951.

There have been eight models of the Crain refractometer, several of them representing particular applications in the field, and others merely involving improvements in circuitry over the previous units. All operate on the same principle, however, and the description given in the following sections applies equally well to each model.

B. DESCRIPTION OF SYSTEM

The Crain microwave refractometers were designed for installation in aircraft to measure the changes in the index of refraction of the atmosphere as the airplane flew through it. The height interval over which a refractometer may be used will depend on the aircraft in which it is installed and the height of interest for the investigation concerned. The refractometers, in general, were designed to measure the index of refraction over a total range of variation of 400 N units on scales of 50 or 100 N units at a time. Smaller ranges with high pass filters can be used to measure rapid fluctuations of refractive index.

Typically, the Crain refractometer consists of three principal components as shown in Fig. 2. These are (1) the refractometer proper, (2) the power supply, and (3) the recording meter. The instrument makes use of two stabilized oscillators operating near 9 400 Mc/s arranged as shown in the system block diagram in Fig. 3. The frequency of each stabilized oscillator is determined by the resonant frequency of an associated cavity resonator. One oscillator, called the reference oscillator, is controlled by a sealed cavity resonator or reference cavity. The other oscillator, called the measuring oscillator, is controlled by an open cavity resonator or a measuring cavity. Changes of index of refraction of the atmosphere in the measuring cavity cause the resonant frequency to change and thus the difference frequency between the two stabilized oscillators. Since the change in resonant frequency

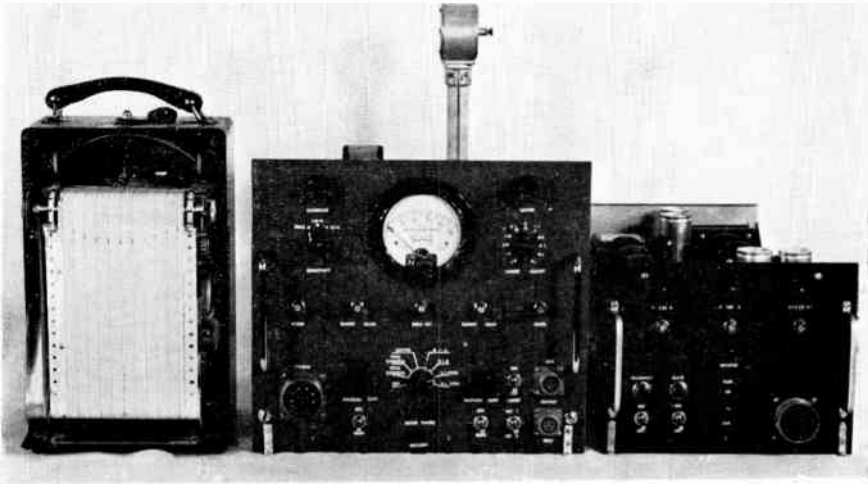


FIG. 2. A view of a typical model of the Crain 9 400 Mc/s refractometer showing from left to right the recorder, refractometer proper and power supply. The measuring cavity with its frequency perturbation screw is above the refractometer while the top part of the reference cavity can just be seen to the left of the measuring cavity. Later models made use of higher speed recorders to obtain fluctuation data.

of the measuring cavity is directly proportional to the change in index of refraction of the atmosphere it contains, the change in the difference frequency between the two oscillators is also directly proportional to the change in the index of refraction of the measuring cavity.

The outputs of the two stabilized oscillators are mixed in a hybrid junction and the difference frequency extracted. The signal at the difference frequency is amplified and limited by a conventional amplifier and applied to a discriminator having a linear slope characteristic over an approximate 4 Mc/s

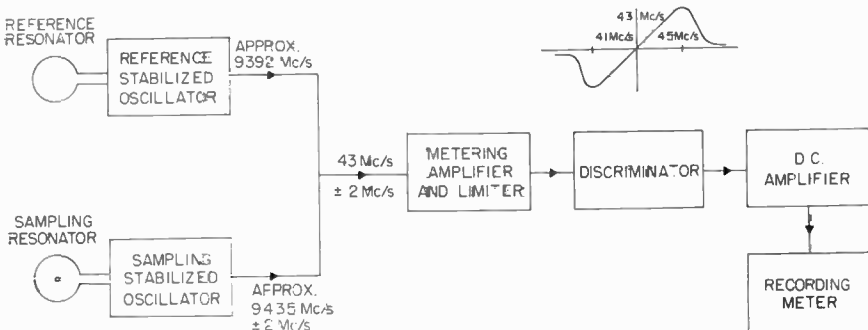


FIG. 3. Block diagram of the basic circuit for all models of the Crain refractometer.

range. The output of the discriminator is applied to a linear differential amplifier which in turn drives the pen of the recording meter. Thus, the change in the pen position of recording meter is in direct proportion to the change in index of refraction of the medium in the sampling resonator.

The resonant frequency of the cavity resonator is determined not only by the index of refraction of the gas it contains but also by the dimensions. For the change in pen position of the recording meter to be due entirely to a change in index of refraction of the gas in the measuring cavity, dimensions of both cavities must be independent of temperature and pressure. Discussions of the errors introduced by these factors will be contained in a later section since they are applicable to any type of refractometer using resonant cavities.

C. STABILIZED OSCILLATORS

Since the reference and sampling stabilized oscillators are identical electrically, the following description applies to either unit. The stabilized oscillators are, in fundamental principle, the same as described by Pound (1946), with the exception that the arms of the hybrid junction containing the receiver and modulator crystals have been interchanged as suggested by Tuller *et al.* (1948).

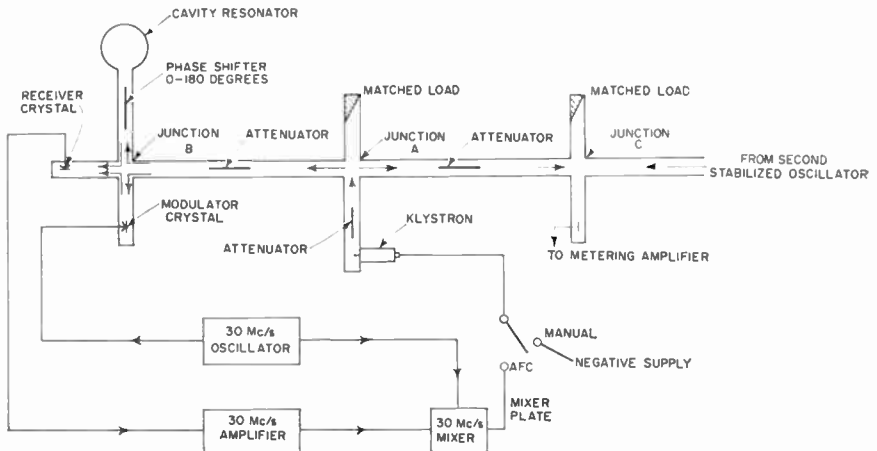


FIG. 4. Block diagram of the basic stabilized oscillator unit employed for all models of the Crain refractometer.

Figure 4 shows a block diagram of the stabilized oscillator unit. The output of the klystron oscillator divides at junction *A*, half going to junction *B* and half to junction *C* where it mixes with the output of the second stabilized oscillator to provide the difference frequency for the metering amplifier as indicated earlier. Power entering junction *B* divides approximately equally between the modulator crystal and the cavity resonator arms. The modulator crystal is matched when it has zero 30.4 Mc/s voltage across it. Hence,

when driven by the 30.4 Mc/s voltage from the i-f oscillator, it reflects sidebands of carrier (± 30.4 Mc/s) but no 9 400 Mc/s carrier. Ideally, it is nothing more than a suppressed carrier generator. The energy entering the cavity resonator arm is reflected from the cavity resonator according to the reflection coefficient of the cavity resonator and enters the receiver crystal arm and the arm containing the attenuator. The energy entering the attenuator arm is prevented from traveling to junction *B* by the hybrid junction *A*.

The signal from the modulating crystal may be expressed as

$$V_1 = D_1 \cos w_i t \sin w_c t \quad (13)$$

where w_i is 2π times the i-f frequency (30.4 Mc/s) and w_c is 2π times the carrier frequency (9 400 Mc/s).

The signal from the cavity is expressed as

$$V_2 = D_2 \sin (w_c t + \theta) \quad (14)$$

If square law detection for the receiver crystal is assumed, the i-f output of the crystal is given by

$$V_3 = D_3 \cos \theta \cos w_i t \quad (15)$$

The phase shifter is adjusted to make $\theta = 90^\circ$ for the condition at which the frequency of the oscillator is the same as the frequency of the cavity. Under these conditions, the resulting i-f output will be zero. The phase of the signal reflected from cavity shifts rapidly to minus 90° or plus 90° as the frequency of the klystron varies on one side of the cavity frequency or the other, and the sign of V_3 changes from plus to minus, providing an error signal output. The remaining terms in the square law detector are the dc component and the double carrier frequency component. These have no effect on the operation of the stabilizing system. A mismatch in the modulating crystal will cause a 30.4 Mc/s signal output of the receiver crystal. This should be minimized for proper operation of the unit.

As the oscillator frequency goes through the resonant frequency of the cavity resonator, the phase of the signal in the 30.4 Mc/s amplifier changes 180° corresponding to the change in the cavity resonator reactance from capacitive to inductive. The 30.4 Mc/s signal output from the receiver crystal is then transmitted through the amplifier and applied to the grid of the mixer tube. To the third grid of the same tube is applied the 30.4 Mc/s voltage directly from the oscillator as shown in Fig. 4. The output of the mixer tube will be a function of both of these signals and, in general, the plate current will be maximum when the two 30.4 Mc/s signals are in phase or 180° out of phase. The instrument has been built such that this optimum phase relationship exists. The output of the mixer tube is applied to the repeller voltage of the klystron closing the circuit on the stabilized oscillator. The attenuator between junctions *A* and *B* is set to give approximately 12 db attenuation and the one between junctions *A* and *C* is set to give about 3 db attenuation. Attenuation between arms *A* and *B* is maintained high to prevent the reflected signal from the cavity resonator from loading the oscillator.

D. METERING AMPLIFIER AND DISCRIMINATOR

The metering amplifier receives the difference frequency between the two stabilized oscillators at junction *C* as shown in Fig. 4. The amplifier has a center frequency near 43 Mc/s and a bandwidth of approximately 7.5 Mc/s. This bandwidth is necessary in order for the refractometer to have a linear range of approximately 400 *N* units and so that the voltage applied to the discriminator circuit will be practically constant over the 4 Mc/s range.

The recording meter amplifier is a differential amplifier with a recording meter connected between the plates. So that recording on a 50 or 100 *N* unit scale anywhere throughout the 400 *N* unit range of the refractometer may be possible, arrangements have been made to add a calibrated bucking voltage to the output of the discriminator; thus, if the index of refraction changes so as to cause the recording meter in the plate circuit of the dc amplifier to go off scale in either direction the operator may turn one switch position and move the pen 8/10 of the full scale in the desired direction. The range adjustment switch is provided with a zero position, five add and five subtract positions with the result that if one is recording on the 50 *N* unit scale, he may add or subtract as necessary up to 200 *N* units from the center position.

VI. THE BIRNBAUM REFRACTOMETER

A. GENERAL PRINCIPLES

Birnbaum developed the refractometer which bears his name for use at the National Bureau of Standards, U.S.A., for the measurement of the properties of polar molecules. In principle the instrument followed the general lines used by other investigators in the study of the index of refraction of solids and liquids. Such application has been described by Works *et al.* (1944) and presented by Montgomery (1947) as a microwave technique. Birnbaum and Franeau (1949) reported measurements on solids and liquids with instrumentation similar to that described by Works. The transition to measurements on gases required considerable refinement, and this established the pattern for the Birnbaum-type refractometer. He, himself, only made one airborne flight with his instrument (Bussey and Birnbaum, 1953), but made a number of measurements on buildings (Birnbaum, 1951) and on a 125-m tower (Birnbaum and Bussey, 1955).

Additional development of the Birnbaum type refractometer has been carried out by other investigators. A field model of the refractometer was made by A. P. Deam of The University of Texas under contract to the Bureau of Standards in 1950. Thompson and Vetter (1958) and others at the Bureau have reported further versions. A Birnbaum instrument was built by Lane *et al.* (1961) and another variation of it has been reported by Vetter (1962). Some of the features of these units will be discussed later. Vetter (1960) described an adaptation of the Birnbaum-type refractometer in which the resonant frequency of the sampling cavity was measured by maintaining coincidence of its frequency with that of the reference cavity by a servo-mechanism.

The significant features of the Birnbaum refractometer are as follows:

1. It uses transmission type microwave cavities as passive elements rather than as active elements as in the Crain refractometer.
2. The instrument uses only one klystron oscillator of which the frequency is swept by a saw-tooth wave, the output, in turn, being applied to a reference and to a measuring cavity. The time delay in the peak signals through the two cavities is measured to give the difference in the resonant frequency of the two cavities.
3. It has a relatively simple microwave system.
4. It is subject to stability and vibration problems in the oscillator since its frequency response is a characteristic of the klystron as well as that of the cavity resonators.
5. It has the advantage that it is readily tunable over a wide range of sensitivities and can be used to measure large changes in index with high loss tangents.

B. METHOD OF OPERATION

The block diagram for the Birnbaum refractometer is shown in Fig. 5. The output of a saw-tooth generator is applied to the repeller of the klystron

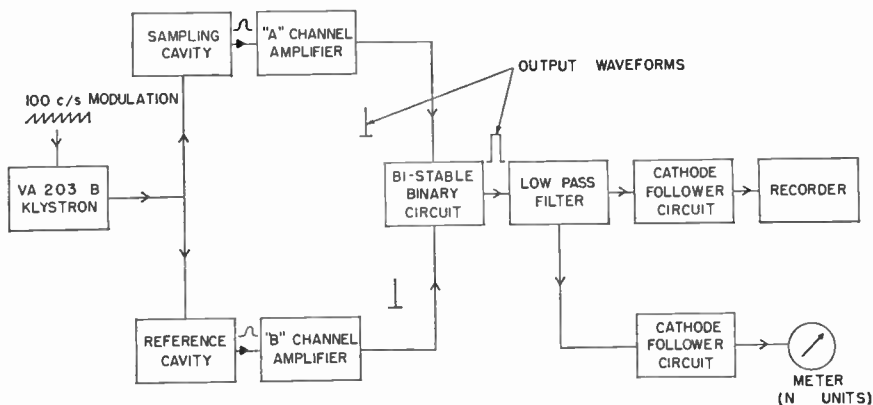


FIG. 5. Block diagram of the basic circuit for the various models of the Birnbaum refractometer.

and sweeps the frequency over a range of approximately 4 Mc/s corresponding to a change in refractivity of 400 N units. The output of the klystron is then applied through a waveguide to a magic tee in which the signal is divided approximately equally, half going to a sampling cavity and half to a reference cavity. Attenuators in the waveguide in front of the cavities prevent feedback to the klystron. Ferrite isolators were used in the Thompson models of the Birnbaum refractometer in order to prevent feedback of the reflected signal from affecting the klystron operation.

The sweep generator is a blocking oscillator and is operated at a repetition

rate of 120 c/s in the original Birnbaum unit, at 100 c/s in the Lane device and at 10 kc/s in the Thompson version. The saw-tooth sweep voltage applied to the klystron repeller is of the order of 20 V. A modification of this instrument which has shown excellent electrical stability has been developed by Schunemann and Steffan (1958).

C. TIME DELAY MEASUREMENTS

The output of the klystrons is applied at a port of each of the cavities and the output signal from the cavity is taken from another port. The time delay between the maximum response of the reference and measuring cavities is determined by techniques which are somewhat different in the various modifications of the unit.

1. A null difference technique, previously reported by Works *et al.* (1944), and others, was used by Birnbaum for measuring relatively large and slow changes in refractive index. This consisted of manually adjusting a calibrated tuning screw on the reference cavity to bring its frequency to that of the reference cavity. The lack of sensitivity and the time required for this method made it undesirable for atmospheric measurements.

2. In the Birnbaum atmospheric measurement unit, the outputs of the two cavities are applied to crystal detectors. After amplification and sharpening, one of the pulses starts a modified Eccles-Jordan trigger circuit and the other pulse stops it. The output is a rectangular wave form of constant amplitude with a width proportional to the difference in frequency between the two cavity resonators. Hence, the average value of output is proportional to the difference in refractivity.

3. In the Thompson versions of the refractometer, the difference in resonant frequency is determined by the use of a phase measuring circuit. This circuit consists of two amplitude selector circuits, a bistable multi-vibrator and a two-channel recording circuit. Each of the amplitude selector circuits is designed to produce a timing pulse which tends to maintain a fixed relationship to the peak of the respective voltage even with varying signal amplitudes. In each channel, automatic volume control is provided to insure freedom from amplitude changes resulting from vibrations of the coaxial cables or waveguides.

The width of the plate voltage pulse of the multivibrator is a nearly linear function of the phase difference between the two timing pulses. Variations in the width are converted into variations in the average voltage from a low pass filter circuit.

4. Vetter (1960, 1962) uses the technique of comparing the resonant frequency of the two cavities with the klystron frequency by obtaining an output from the klystron modulated by a small sine-wave voltage on its repeller. The wave shape of the 12 kc/s voltage from a detector operating on the cavity output is determined by the relative values of the cavity's center frequency and the center frequency of the klystron. If the two frequencies coincide the cavity provides an even transmission function and the output only has even harmonics of the original modulation signal. If the cavity's center frequency is lower or higher than that of the klystron, the output

contains a fundamental frequency but the phase is sifted by 180 degrees for the two cases. By comparing the phase of any fundamental component of the modulating frequency found in the output of the original modulating frequency, it is possible to develop an error signal which, when applied to the klystron repeller, will tend to lock the latter's center frequency to that of the cavity. By reversing this process, it is possible to servo the cavity tuning to follow the klystron frequency. This process is accomplished by taking the sum and difference information from the two cavities. The sum is used to keep the klystron within the cavity operating range and the difference to tune the reference cavity to the measuring cavity. By calibration of the screw setting and its servodrive, the refractivity may be read off directly. The response of the system is about 1 c/s.

D. READOUT AND NOISE EVALUATION

In the Thompson model two outputs are provided, one through a band-pass filter to cover the range from 1/2 to 40 c/s to drive a recorder with a maximum full-scale sensitivity of 0.03 *N* unit and the other output through a low-pass filter to drive a recorder with a full-scale sensitivity of 200 *N* units and to cover the frequency range from 0 to 1 c/s. The overall equipment noise may be evaluated in two ways. The first consists of closing the sampling cavity to the free passage of air by means of two caps. This does not provide a hermetic seal but does permit evaluation of the high frequency noise component which must be taken into consideration in order to obtain unbiased, high frequency, free atmosphere turbulence measurements. The second method consists of assuming that the quietest open-cavity record obtained in actual use is the effective noise of the system. In practice, on occasions it has been found that the open cavity measurements at about 12 000 ft elevation were only a few times larger than the closed cavity records. The system noise appears to be the order of 0.1 of a *N* unit.

VII. CHARACTERISTICS OF MICROWAVE CAVITIES

A. GENERAL RELATIONSHIPS

This section is concerned with a study of the properties of cavities used as sensors and references. Separate consideration is given to these elements because of the fact that they are the most critical part of the refractometer and in many cases the largest source of errors in the measurements. In addition, the problems relating to cavities are common to all types of refractometers. Although there is no theoretical or practical reason why a wide variety of frequencies and configurations could not be used, the sampling devices, as discussed earlier, which have been applied to refractometers, fall into three groups as follows:

1. Resonant cavities operating in the region of 10 000 Mc/s.
2. Coaxial cavities operating around 400 Mc/s.
3. Condensers operating at or below 10 Mc/s.

Each of these types of elements will be considered separately in connection with the refractometer types with which they are used.

The resonant cavities operating in the vicinity of 10 000 Mc/s have been circular cylindrical ones using the TE_{011} mode for the following reasons:

1. This waveguide mode has no electric flux lines terminating on the walls and therefore has a small value of electric field in the vicinity of the walls. This greatly reduces the effect of moisture or dust particles depositing on the walls.

2. The TE_{011} mode has no current flowing between the side wall and the end plates. This simplifies construction in that no electrical connection is necessary at the end plates and the loss of Q from the lack of good electrical contact is avoided. Finally, since the dimensions of the cavity, and hence its resonant frequency, change with temperature, these effects can be minimized in a relatively simple manner by constructing end plates and walls of materials of different thermal expansion so that expansion relative to each other can lead to the preservation of an essentially constant resonant frequency over a wide temperature range. The temperature compensation concept is discussed more fully later in this section.

B. FIELD EQUATIONS

For the TE_{011} mode, the field equations in the cavity are given by

$$\left. \begin{aligned} E_{\phi} &= AJ_1\left(\frac{3.83}{a}r\right)\sin\pi z/l \\ H_r &= -j\frac{A}{2l\mu f}J_1\left(\frac{3.83}{a}r\right)\sin\pi z/l \\ H_z &= j\frac{0.610A}{a\mu f}J_0\left(\frac{3.83}{a}r\right)\sin\pi z/l \end{aligned} \right\} \quad (16)$$

$$\text{and} \quad f = \frac{c}{2n} \sqrt{\frac{1}{l^2} + \frac{1.59}{a^2}} \quad (17)$$

where

r, ϕ, z are the components of the cylindrical coordinate system

l and a are the cavity length and radius, respectively

f is the resonant frequency

c is the velocity of a plane wave in a vacuum

n is the index of refraction

μ = permeability ($4\pi \times 10^{-7}$ henries/meter for air)

$J_1\left(\frac{3.83}{a}r\right)$ and $J_0\left(\frac{3.83}{a}r\right)$ are the first and zero order Bessel functions of argument $\left(\frac{3.83}{a}r\right)$.

These equations make the usual assumption that each equation varies according to $e^{j2\pi ft}$ and that the conductivity of the walls is very high.

C. FREQUENCY VARIATION WITH INDEX OF REFRACTION

The resonant frequency, f , of a cavity filled with air of index, n , is given in terms of the frequency, f_0 , when the cavity is evacuated, as follows:

$$f = f_0/n \tag{18}$$

When the refractivity, N , is introduced,

$$f = \frac{f_0}{1 + N \times 10^{-6}} \tag{19}$$

and

$$N = \frac{(f_0 - f)}{f} 10^6 \tag{20}$$

Correspondingly,

$$\Delta N = N_2 - N_1 = 10^6 \left(\frac{f_0 - f_2}{f_2} - \frac{f_0 - f_1}{f_1} \right) \tag{21}$$

$$\cong - \frac{\Delta f}{f} 10^6 \tag{22}$$

where

$$f = f_2, f_1, \text{ or } f_0.$$

D. FREQUENCY VARIATION WITH CHANGE IN DIMENSIONS

The resonant frequency of the cavity may be written as

$$f = \frac{c}{2nl} \sqrt{1 + 1.59 \left(\frac{l}{a} \right)^2} \tag{23}$$

For cavities so made that the temperature coefficient of expansion, δ , is the same for the radius and length of the cavity, the resonant frequency will be inversely proportional to the length. Replacing l by $l_1(1 + \delta\Delta T)$, where ΔT is the anticipated temperature change, we have

$$f - \Delta f = \frac{c}{2nl_1(1 + \delta\Delta T)} \sqrt{1 + 1.59 \left(\frac{l}{a} \right)^2} \tag{24}$$

$$\cong \frac{c}{2nl_1} \sqrt{1 + 1.59 \left(\frac{l}{a} \right)^2} [1 - \delta\Delta T] \tag{25}$$

$$\cong f_1(1 - \delta\Delta T) \tag{26}$$

or

$$\frac{\Delta f}{f_1} \cong -\delta\Delta T \tag{27}$$

If this change in frequency is interpreted as a change in refractivity, the apparent index change would be

$$\Delta N = \delta\Delta T 10^6 \tag{28}$$

Thus, if the temperature coefficient is 10^{-6} per degree centigrade, there will be a change in indication of 1 *N* unit for each degree centigrade change in the temperature of the cavity material.

Since airborne refractometers may be subject to changes in temperature of the order of 50°C, the temperature error may be quite large. There are a number of methods of coping with this problem, some of which are described below.

E. METHODS OF REDUCING EFFECTS OF TEMPERATURE CHANGES

1. *Use of Low Temperature Expansion Materials*

The use of a cavity material with a low temperature coefficient of expansion will obviously reduce the errors due to changes in dimensions caused by changes in temperature. The most common material used for refractometer cavities has been invar. For a good grade of invar, temperature coefficients are given as 0.5 to 0.8 parts per million per degree centigrade. Care should be taken, however, in indiscriminately using a quoted coefficient in evaluating cavity performance. The temperature coefficient tends to vary with temperature and is a function of the machining and silvering processes used in the cavity construction.

Ceramic materials may have much lower temperature coefficients and such cavities have been developed for laboratory use at the National Bureau of Standards by Thompson *et al.* (1958). Structural problems have, however, delayed their application to airborne units. As in the case of invar cavities, the temperature coefficient of the cavity may be a function of the temperature range involved, the baking and silvering techniques employed as well as the nominal value of expansion coefficient of the material.

2. *Use of Common Block*

When a comparison is made between a sampling and a reference cavity, the error indication may be avoided if the sampling and the reference cavities are maintained at the same temperature. One scheme to accomplish this temperature balance is to machine both cavities out of the same block. This method is quite satisfactory for laboratory measurements when there is adequate time to obtain a temperature balance throughout the block. Difficulty is experienced, however, in atmospheric refractometers due to the cumbersome structure which would need to be exposed to the air stream and to the fact that gradients in temperature exist within the block. The perforated end plates used in the sampling cavity to permit free access of air will be subject to variable temperature air flow and will change temperature at a different rate from that of the body. In addition, since tuning screws are frequently employed for adjustment of the frequency of either cavity, such adjustment with equipment external to the aircraft presents obvious difficulties.

3. *Temperature Compensation of Cavities*

Crain and Williams (1957) have described a method for the temperature compensation of a cavity which has subsequently been commonly used on

refractometers. This is based on the principle that an increase in the radius of the cavity may be compensated by a decrease in length. In the equation

$$f = \frac{c}{2n} \sqrt{\frac{1}{l^2} + \frac{1.59}{a^2}} \tag{29}$$

frequency and index will remain constant if

$$\frac{\Delta l}{\Delta a} = -1.59 l^3/a^3 \tag{30}$$

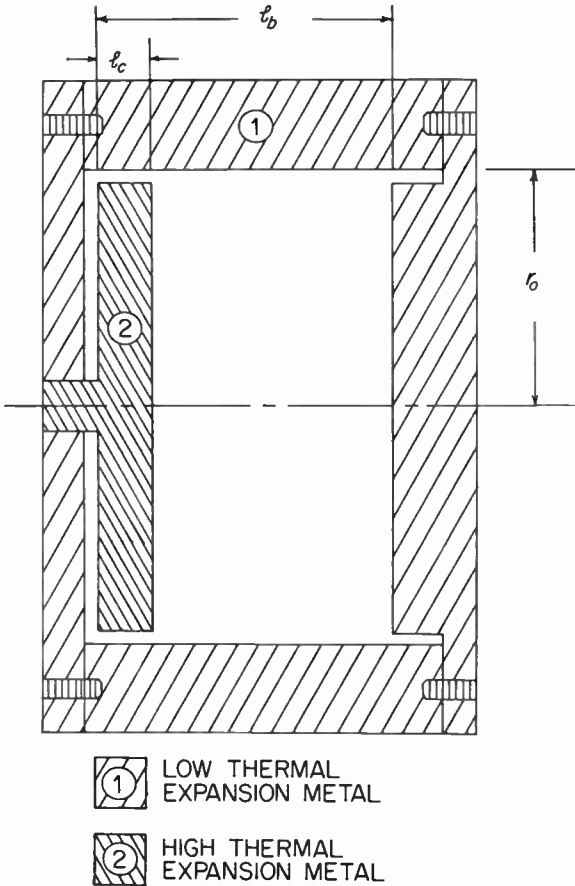


FIG. 6. Parts and assembly sketch of temperature compensation technique employed in the microwave cavities of the Crain refractometer.

This relationship may be approached by a cavity design as shown in Fig. 6. A steel insert mounted on a post on the end of the cavity has a much higher temperature coefficient of expansion than has the invar cavity body. As the invar body expands due to a change in temperature, the steel insert will

expand at a faster rate and reduce the effective length of the cavity. By the proper choice of the materials used and the length of the steel insert, the condition of equation (30) may be approached. In practice, the insert is made slightly longer than predicted and ground down step by step on the basis of measured temperature-index curves plotted over the range of temperatures for which the cavity is to be used. Changes in the properties of the metal with time, however, may cause a deterioration of the compensation over a long time interval. It is possible to obtain overall effective temperature coefficients for the cavity with this technique as low as 10^{-7} per degree centigrade over a temperature range from about -20°C to 40°C , although great pains and care must be taken. This type of compensation results in consistent temperature-frequency characteristics free of hysteresis type effects which is not the case when compensation involves the use of solid end plates of a different temperature coefficient from that of the body.

4. *Measurement of Cavity Temperature*

A correction may be applied for a change in cavity temperature if a measurement of its temperature is possible. The technique of imbedding a thermocouple in the cavity walls has been tried with some success but the resulting measurement complications and the necessity of correcting the measured data have precluded its general use.

5. *Periodic Calibration*

In the laboratory, the standard of comparison is the evacuated cavity. It has been suggested that in the aircraft installation of refractometers it might be possible to evacuate the measuring cavity or fill it with a gas of known index of refraction at regular intervals. If this could be done without change in the dimension of the cavities due to temperature or pressure effects, it would be possible to provide a calibration which would permit correction for temperature.

Periodic calibrations may also be accomplished by measuring the temperature, pressure and humidity with meteorological instruments. Ground checks before flight and in-flight measurements also provide reference for gross corrections. Sometimes it is possible to fly at elevations where the air is relatively calm and the index fairly constant. Measurements made simultaneously at these heights provide a reasonably good absolute calibration. As an expedient, it is sometimes possible to compare high altitude, nearby, radiosonde data with refractometer soundings to get an absolute index reference point.

F. PRESSURE EFFECTS

Changes in air pressure do not normally affect the dimensions of the sampling cavity, but may cause change in the sealed reference cavity. Crain has found that for a typical reference cavity of this design, a change in pressure of one millibar will cause the resonator frequency to change by an amount corresponding to 0.015 N unit. For a height equivalent to 10 000 ft, the pressure may be reduced by as much as 300 mb and the associated change

in reference index of refraction would be 4.5 *N* units. By use of the pressure calibration curve supplied with the refractometers, a correction can be made as a function of pressure on the reference cavity. Crain found that it was easier to prevent leaks in or out of the reference cavity if it were filled with air at a pressure somewhat below one atmosphere rather than if it were completely evacuated. Crain and Williams (1957) used a glass cup over the tuning screw to insure sealing of the reference cavity. Pressure compensation of the reference cavity may be effected by the use of small sealed empty spaces behind the inner end plates so that these plates experience no difference in pressure due to changes in outside pressure. Pressure coefficients as low as 0.003 *N* unit/mb have been obtained.

G. WALL CONDENSATION EFFECTS

An approximate estimate of the change in frequency due to the addition of a small amount of lossless dielectric may be obtained by perturbation techniques. The extra energy stored in the electric field of the dielectric must be balanced by an increase in the energy stored in the magnetic field. Since the magnetic field in equation (16) is inversely proportional to frequency, the energy stored will be inversely proportional to the square of frequency. Equating the energy change, we have

$$\frac{1}{2}\Delta K E_{\max}^2 \tau = -2 \frac{\Delta f}{f} U_{H_{\max}} \tag{31}$$

where

- ΔK is the change in dielectric constant for the foreign material
- E_{\max} is the maximum electric field averaged over the volume of the foreign material
- τ is the volume of the foreign material
- $U_{H_{\max}}$ is the maximum energy stored in the cavity field.

Thus,

$$\frac{\Delta f}{f} = - \frac{\Delta K E_{\max}^2 \tau}{4 U_{H_{\max}}} \tag{32}$$

For cylindrical cavities operating in the TE_{011} mode, the electric field will approach zero near the walls. A dielectric deposited on the walls will therefore be in a region of small field and the resulting perturbation in frequency will be minimized. Birnbaum and Bussey (1955) concluded that the error due to the deposit varied as the cube of the thickness of the film formed on the walls, a change of 1 *N* unit being associated with a uniform film of 0.03 mm thickness. Although water at 10 000 Mc/s is not a lossless material, and calculations have not been made taking this effect into account, it is nevertheless obvious from the approximate perturbation analysis described above that even thin films of condensed water can result in extensive cavity frequency changes. This problem is normally encountered only in measurement programs where large temperature changes are encountered, as in rapid altitude descents, for example, into highly saturated layers below a temperature inversion or through precipitation. The problem is minimized with the

high ventilation speeds and relatively slow altitude changes employed in aircraft sounding procedures and, in theory, could be eliminated by artificial, constant, temperature heating of the cavity walls above ambient conditions.

H. CAVITY VENTILATION

It is necessary to ensure that the air to be examined gets into the measuring cavity. In a moving air stream this is not very difficult and natural ventilation is normally sufficient even with relatively small end plate openings, although ground based installations may require the use of suction fans. Nevertheless, a significant amount of research has been carried out on techniques to

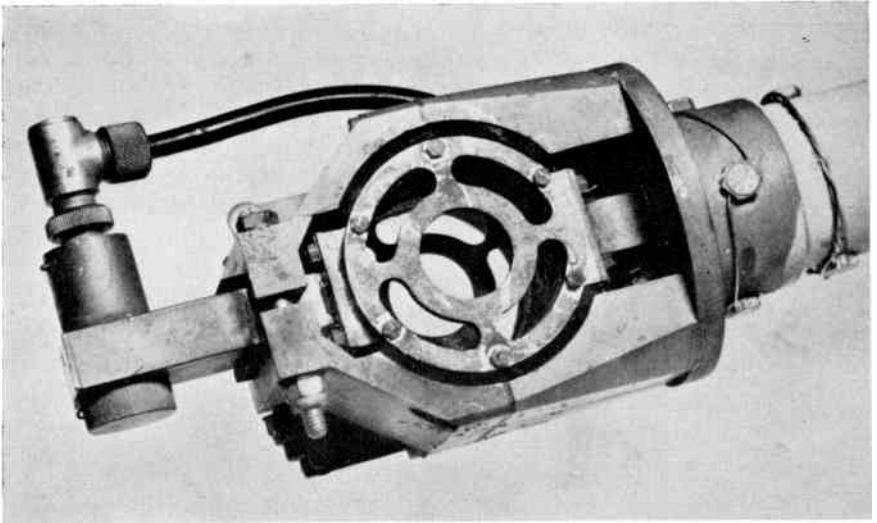


FIG. 7. A view of the ventilation employed with a measuring cavity in a microwave refractometer developed by Lane *et al.* (1961) following the Birnbaum principle. Somewhere around 75 per cent of the end plate material is removed to permit free access of air.

permit unimpeded flow through the cavity. Thompson *et al.* (1959) developed a cavity following the procedure suggested by Adey (1957) where a ring with supporting crossbars in the end plate provided a termination for the cavity sufficient for the latter not to suffer from too great a loss in Q . The ring is located at the distance from the axis at which the current would be a maximum in a solid end plate. This prevented, however, the temperature compensation procedure which is used with the normal end plate. A picture of such a cavity as used by Lane *et al.* (1961) where some 75 per cent of the end plate material has been removed is shown in Fig. 7. Thorn and Straiton (1959) proposed a rectangular waveguide type of cavity which was completely open except for a narrow dividing strip through the waveguide which served as the terminations for the cavity. The Q of this cavity was relatively low but it was found capable of operating the Crain refractometer.

The problem of whether a varying air flow through an airborne cavity

causes appreciable error in the recordings has been given some attention. Crain has tried experiments in which the speed of an aircraft was varied from approximately 110 to 220 m.p.h. and the resulting change in the index of refraction was only about 1 N unit. Normally in practice, therefore, any error should be small since aircraft in ordinary sampling procedures fly at reasonably constant speeds. Crain also tried putting various types of housings around the cavity in the general form of a teardrop to control the velocity of

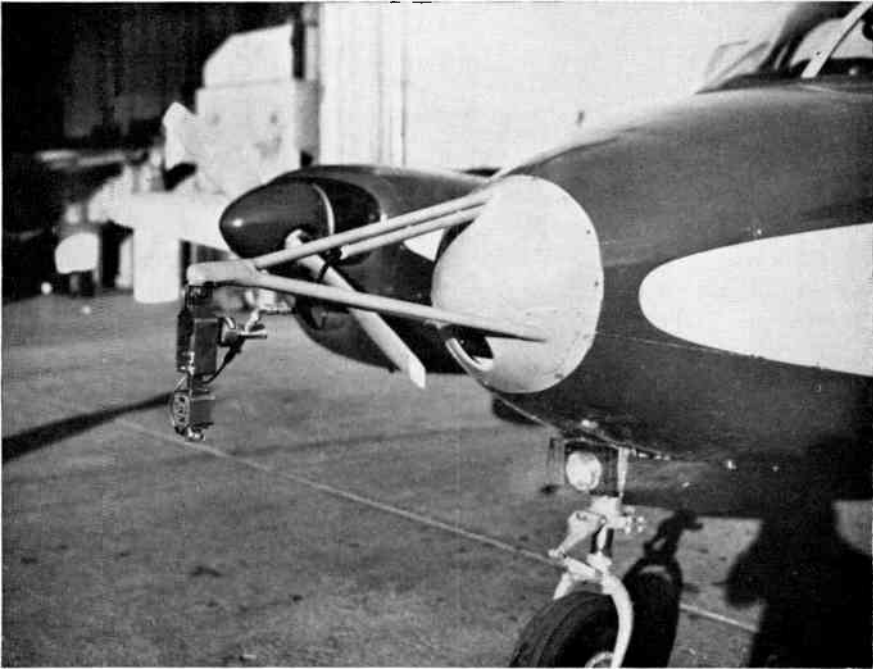


FIG. 8. A view of a refractometer installation designed to minimize aircraft interference with the free airstream. This nose cone adaptation on a light-weight plane was made by the National Bureau of Standards for use with the Birnbaum refractometer.

air through the cavity but found that it did not make any major difference whether or not the air was slowed down as it flowed through the cavity.

Another problem which has been investigated is the effect of having the cavity near the skin of the aircraft and, by wind tunnel studies, this was found to be insignificant if the cavity was 6 in or more away from the surface. Care should be taken in propeller driven aircraft, however, to see that the cavity is not located in such a position that it samples the wind passing through the propeller blades, as this may cause a modulation at the propeller speed, or that it is located near any sources of engine heat. An example of one of the many types of aircraft installations designed to optimize free air sampling is shown in Fig. 8, where a nose cone adaptation

on a light-weight aircraft is employed with a Birnbaum type refractometer to place the sampling cavity in advance of the air stream.

Finally, it has been found possible to eliminate certain of the ventilation problems involved with higher speed aircraft and to minimize cavity wall wetting due to condensation, precipitation or clouds, by mounting the cavity in an air duct system whose outlet and inlet are flush with the aircraft surface; an example has been reported by Sherr (1961). Care, however, must be taken to ensure a true ambient air temperature environment within the cavity.

VIII. THE DEAM REFRACTOMETER

A. GENERAL PRINCIPLES

Deam (1962) has described a balloon-borne, light-weight refractometer based on the Pound stabilized oscillator principle but with a number of unique features. The principal features of the Deam refractometer are as follows:

1. The oscillator associated with the sampling cavity is packaged separately from the reference oscillator. This separate package weighs about 6 lb and may be sent aloft on a balloon or dropped by parachute from an aircraft.
2. The operating frequency is reduced to 400 Mc/s to permit the use of an inexpensive triode as the oscillator.
3. The sampling cavity is a half-wave coaxial cavity made of silver coated glass rod and glass tubing for inexpensive construction.
4. The receiver may be carried in an aircraft or used at a ground station with a magnetic tape recorder or a pen recorder free of vibration.

B. METHOD OF OPERATION

The Deam refractometer is essentially one-half of the Crain refractometer operating at 400 Mc/s instead of 10 000 Mc/s. The unit weighs approximately 6 lb and has been elevated by balloons and dropped from aircraft with the signal generated transmitted either to a phase lock receiver in the airplane or on the ground. This receiver compares the frequency of the sampling resonant cavity to the frequency generated within the receiver by crystal control and frequency multiplier techniques. The sampling unit is battery-operated and its output signal of 0.1 W is capable of being received at distances of approximately 20 miles in the line of sight. A picture of the Deam unit is shown in Fig. 9 and the block diagram is shown in Fig. 10. The unit is built around three aluminum bulkheads which are spaced with aluminum tubing. The coaxial cavity, along with the ring circuit, runs the length of the two compartments formed by the bulkhead. The cavity is open at both ends and loop excited at the center. Electronic components are located in the compartment near the parachute container. The stabilizing amplifier and stabilizer oscillator are separate modular units such that either or both units may be removed for service or replacement. Although the stabilized oscillator chassis is not visible, it is just to the rear of the amplifier.

Batteries are assembled in the right-hand compartment and may assume

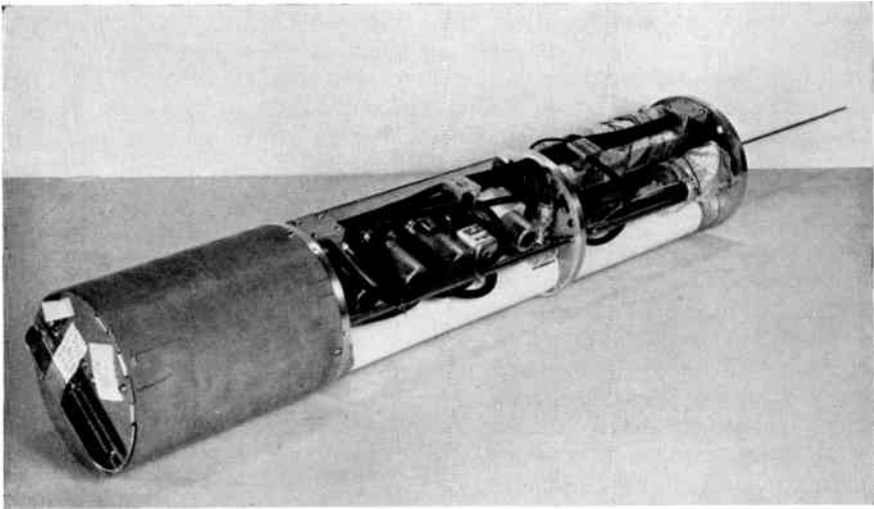


FIG. 9. A view of the 400 Mc/s light-weight refractometer as developed by Deam, complete with the exception of the removal of the aluminum cylindrical covers.

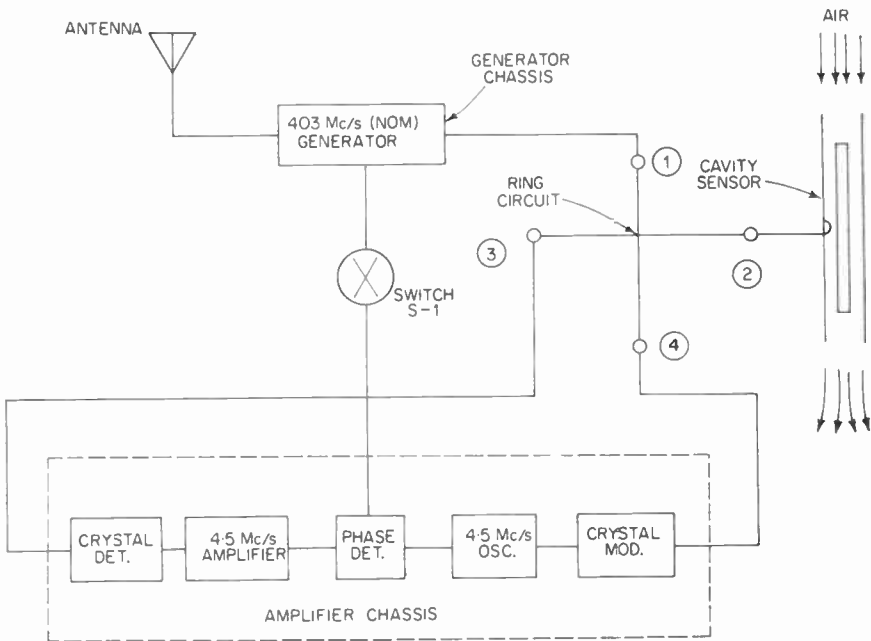


FIG. 10. Block diagram of the basic circuit of the 400 Mc/s Deam refractometer.

various configurations. Radiation from the instrument is through a quarter-wavelength antenna at the right end. Although the thin-rolled aluminum cover has been removed for the photograph, it is easily seen that this cover serves as a ground plane for the antenna. The ring circuit is visible in the photograph and is constructed of coaxial cable cut to provide the proper phase shift at 403 Mc/s. Interconnections between amplifier, ring circuit and oscillator are made with standard fittings and coaxial cable. Exception to this is made in connecting the modulator crystal to the ring circuit where a selected length of coaxial cable is used to provide the proper reflection coefficient at the ring circuit connection. The only other critical length is that connecting the cavity to the ring circuit and it must be adjusted for proper phasing of the feed-back from the cavity and the stabilized loop.

No particular elaboration is necessary as regards the stabilizing amplifier other than to say it is a tuned amplifier operating at 4.5 Mc/s with its output fed into a synchronous detector whose reference is obtained from a 4.5 Mc/s crystal controlled oscillator. Output from the synchronous detector is compensated and used to control the frequency of the stabilized oscillator with the aid of a solid state variable capacitor. Degenerative frequency shift is minimized at the input of this amplifier by the damping of the crystal detector. Damping is necessary since amplitude variation of the output of the stabilized oscillator causes changes in crystal impedance which in turn can cause undesired shifts in frequency of the stabilized oscillator.

The UHF generator or stabilized oscillator employs a triode whose tank circuit is in a parallel wire system. Mechanical tuning is provided at the end of the line together with the electrical tuning by the solid state capacitors. A small loop pick-up is used to excite the stabilizing circuit and a larger loop for the antenna excitation. A resistor is inserted in the antenna pick-up loop to minimize pulling of the oscillator's frequency by the antenna, while the resistor in the small pick-up loop provides damping for wave return from the ring circuit. The oscillator is stabilized against frequency changes due to temperature variation by proper choice of capacitors connecting the solid state capacitor of the tank circuit.

C. CAVITY CHARACTERISTICS

Stability of the Pound oscillator is principally controlled by the stability of the cavity, and this item is the main obstacle to producing a sonde insensitive to errors. The half-wavelength cavity used is shown in Fig. 11, although prototype quarter-wavelength models have also been developed. The cavity is constructed using a special, low expansion ceramic tubing for the outer conductor and a fused quartz rod for the inner conductor, each rendered conductive by the usual silver-plating techniques. This process was used in order to produce an inexpensive cavity that required no machining. The parts for the cavity are assembled using an epoxy resin which is baked at recommended temperatures. Although the length of the center rod is the primary control of frequency and can be cut with high accuracy, second order effects produced by eccentricity in the outer conductor have caused some variation in the resonant frequency of a group of twenty-five cavities

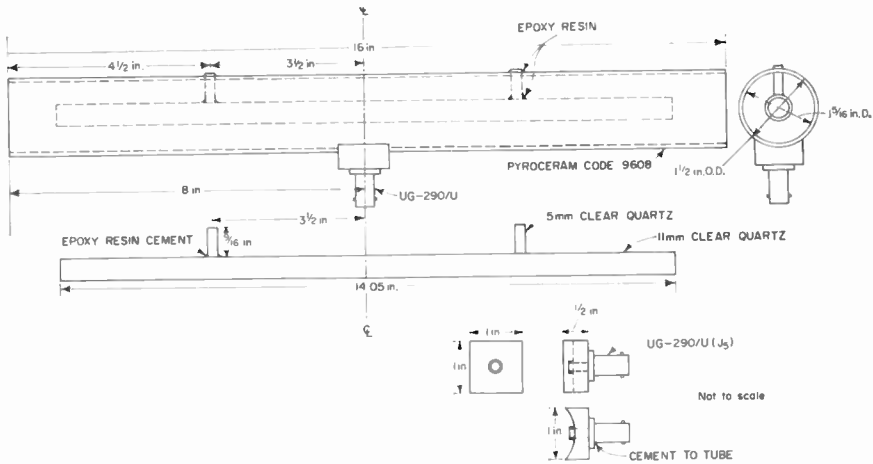


FIG. 11. Schematic view of the ceramic, open-end half-wavelength coaxial cavity employed with the 400 Mc/s Deam refractometer.

which were so made. The frequencies were randomly scattered between 404 and 402 Mc/s. The unloaded Q of this cavity as constructed and measured is approximately 2 000. Results obtained by dropping this unit and sending it up in a balloon are described later.

IX. CHARACTERISTICS OF COAXIAL CAVITIES

A. GENERAL RELATIONSHIPS

In the construction of the Deam refractometer, the objective was primarily that of building a low cost, expendable unit which would be light enough in weight to be sent up on a balloon or dropped on a small parachute. No attempt was made in constructing the half-wavelength cavity to provide temperature compensation, since the objective was primarily that of obtaining an accurate measure of relative changes in index of refraction over short time or distance intervals. Such an instrument can accurately detect and record variations resulting from atmospheric layers or stratifications but it is not designed to obtain an accurate profile over large altitude ranges where long term, large temperature variations are encountered.

With the half-wavelength cavity, both ends could be completely opened. In practice, fine screens were provided for a certain amount of filtering of foreign particles and to prevent electrical feedback from the antenna into the coaxial cavity. With the coaxial cavity, it is possible to get nearer the theoretical Q than it is with almost any other cavity. The reason for this seems to be that in the coaxial cavity there are no bends or sharp points which need to be silver plated, and thus the difficulty of getting a smooth connection between such elements is eliminated.

B. TEMPERATURE COMPENSATION

Cogdell *et al.* (1960) have described a method for the temperature compensation of coaxial cavities. Their work was concerned with quarter-wavelength cavities as used by Deam in his prototype model. The technique was that of adding a plate across the end of the cavities at an appropriate distance from the end of the center post. The capacitance introduced by this end plate provides a loading of the equivalent transmission line. If all of the dimensions increase in the same proportion, the frequency will be decreased due to the increased length of the center post. An increase in the distance between the center rod and the end plate will cause a decrease in the capacitance and an increase in frequency. Proper location of the end plate will thus tend to make the cavity insensitive to temperature changes.

An alternative method suggested by Cogdell is that of using a bimetallic arrangement. The center post may be made of a low expansion coefficient material recessed in the end plate of the shorted end of the quarter-wavelength cavity. The material in which it is recessed may have a high temperature coefficient and be of such a length that the exposed part of the center rod is temperature insensitive.

C. CONDENSATION EFFECTS

The electric field of the coaxial cavity is given approximately by

$$E = A \frac{1}{r} \sin \frac{\pi}{2l} z \quad (33)$$

where r and z are cylindrical coordinates with z measured from the center of the half-wavelength cavity. The electric flux lines are disposed radially from the center conductor to the outer conductor except near the end. If a thin coating of dielectric is formed on one of the plates, equation (32) may again be applied to give the perturbation in frequency. As a rough approximation, the coaxial cavity may be considered as a parallel plate condenser with uniform field between the plates. The perturbation in frequency is then given by

$$\frac{\Delta f}{f} = - \frac{\Delta K}{2} \frac{\text{volume of foreign matter}}{\text{volume of cavity}} \quad (34)$$

For water, with a dielectric constant of 80, there will be the equivalent of a 40 N unit change in frequency due to the foreign matter if it has a volume of one-millionth of that of the cavity. This again emphasizes the difficulty caused by a high electric field at the cavity walls. Again it is recognized that water is not a lossless material, but the approximation is much better at this lower frequency.

D. REFRACTIVE INDEX VARIATIONS ALONG THE CAVITY

Perturbation theory may also be used to give a measure of the sensitivity

of a cavity to a change in atmospheric index of refraction. Since

$$\frac{\Delta f}{f} \cong - \frac{\Delta K E_{\max}^2 \tau}{4 U_{H_{\max}}} \quad (35)$$

it is seen that the sensitivity to a change in index of refraction will be different for different parts of the cavity, depending on the value of the electric field intensity. For half-wave coaxial cavities, where the field varies from a maximum near the ends to a minimum near the center, the most sensitive part will be near the ends while the center section will be a relatively insensitive region. A step function change in refractive index will need to travel the full length of the cavity for full response. For quarter-wavelength coaxial cavities the maximum response will be near the open circuit end and a step function of refractive index change will produce nearly full response in less than the entire cavity length since the field is large only near the open end.

X. THE TOLBERT PHASE-SHIFT REFRACTOMETER

Tolbert and Straiton (1951) have described a prototype refractometer based on a different principle from those previously described. This refractometer uses a short transmission path either in a waveguide or through the atmosphere. The phase change over this path, which is proportional to the refractive index of the air along the path, is compared with the phase shift along a reference path. A waveguide or open path length of approximately one meter is normally used, but this distance could be increased to any distance for which extraneous reflections can be eliminated. This refractometer is an integrating rather than a point-measurement device and its applications may be in somewhat different fields from those of the Crain or Birnbaum type refractometers. It involves the transmission of microwave energy over two paths, one a measuring path and the other a reference path. The transmission along the reference path is modulated by a rotary phase shifter at 133 c/s. The relative phase of the microwave signals at the ends of the two paths is maintained in the 133 c/s frequency that is obtained by beating the waves transmitted on the two paths. Using the phase multiplier system, the relative phase is multiplied by 1 875, raising the frequency to 250 kc/s. The phase change of the 250 kc/s signal measures a change in the phase over the transmission path. A frequency stabilized klystron supplies energy at a frequency of 9 375 Mc/s to a magic tee where one-half of the energy goes over the reference path and one-half over the transmission path. Fixed attenuator pads are located in each of these paths to reduce the effect of cross-feed. With this arrangement, a change of 1° in the relative phase of the 133 c/s signal at the input of the phase multiplier will produce a change of $1\ 875^\circ$ in the relative phase of the 250 kc/s signal at the output of the phase multiplier.

For the waveguide used as a sampling device, the air, whose changes in index of refraction are to be measured, is drawn into the waveguide through an opening in one end and exhausted at the other. The section which constitutes the measuring path is sealed off from the rest of the system with mica

windows. Extremely high sensitivity may be obtained with this system by extending the length of the path or by increasing the phase multiplication. There are, however, a number of inherent disadvantages which limit its use to fairly special applications. These disadvantages are changes in dimensions caused by thermal expansion or by external forces on the system, particularly when free-space transmission is used, by changes in temperature of the air in the reference path, by reflection of the signals from nearby objects, and by drifts in the amplifier. A block diagram is shown in Fig. 12.

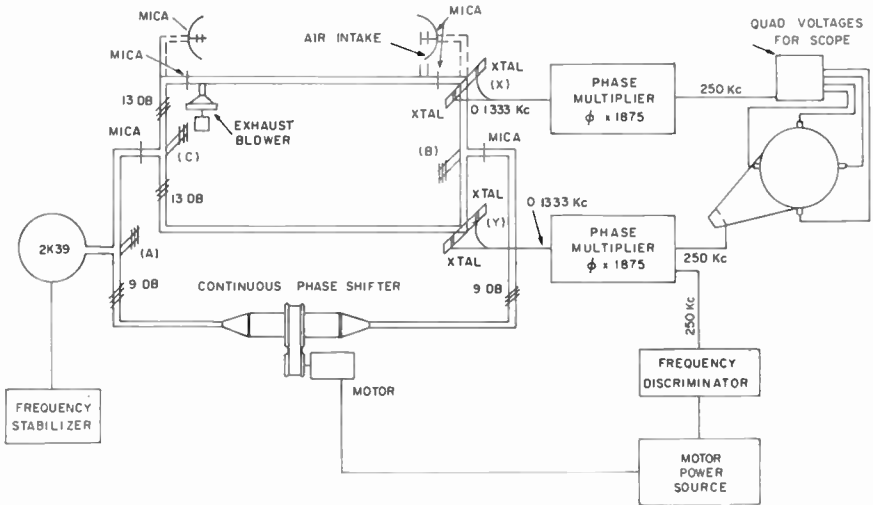


FIG. 12. Block diagram of the Tolbert phase shift refractometer.

XI. THE HAY REFRACTOMETER

A. GENERAL PRINCIPLES

Since the work of Jona (1919), the condenser has been used as a sampling device for measuring refractive index changes in gases, liquids, and solids. The condenser is included in a resonant circuit the frequency of which varies when the dielectric constant of the material between the condenser plates is changed.

The principal features of this system are as follows:

1. The frequency generated in a separately packaged sampling system is transmitted to a receiver at a distant point where the resonant frequency is compared with that of a reference frequency.
2. A rather simple resonant circuit can be used with ordinary radio frequency components for the sampling oscillator. Compact and light-weight construction permits the unit to be sent aloft on a radiosonde type balloon.
3. It may be subject to difficulties in calibration if capacitances other than that of the sampling condenser are present in the circuit.

4. The use of the lower frequency necessary with a capacity-controlled oscillator means that there is less change in frequency for a 1 N unit change in refractive index than there is for microwave systems.

5. Errors which may be introduced due to changes in the temperature, to the conductivity of the condenser spacer and to other losses affect the applicability of the unit.

B. DESCRIPTION OF SYSTEM

One of the more promising recent developments in the capacity controlled refractometer was introduced by Hay *et al.* (1961) for balloon-borne use in the lower atmosphere. Since the capacitance of a condenser is proportional to the dielectric constant of the material between the plates, it is possible to let the atmosphere flow between condenser plates and control the resonant frequency of the circuit. In the Hay refractometer a frequency of 10 Mc/s is chosen as being a compromise between the lower frequencies for which the radio circuitry would be relatively simple and the higher frequencies for which multipath propagation is easier to avoid and for which larger changes in frequency occur for a given change in index of refraction. In order to isolate his oscillator from the antenna, Hay introduces a frequency doubling circuit which converts the 10 Mc/s signal to 20 Mc/s before it is sent to the antenna. This 20 Mc/s signal is transmitted to a receiver on the ground which, through a reference oscillator, measures the change in frequency resulting from changes in the capacitance of the condenser. The 10 Mc/s signal is obtained from a Clapp (1948) oscillator. The frequency of the oscillator is determined essentially by a 6.1 μ H inductor in series with a 50 μ F sensing capacitor. Good frequency stability is obtained by making the Q of this inductor high and by appropriate circuitry to prevent interaction between the output and oscillator circuits.

C. SAMPLING CAPACITOR

A flat plate configuration in the air-sensing capacitor is chosen for simplicity in construction. The spacing between the capacitor plates required for free air flow to obtain may be estimated from the thickness of the boundary layer at these plates. From the theory of fluid dynamics, the thickness of the boundary layer is related to the kinematic viscosity of the air, the length of the condenser plates and the velocity of the air. Hay found that plates spaced 0.25 in apart would provide for free flow through the condenser, and used a set of six plates on each side of the refractometer, each of dimensions 6 in \times 0.63 in.

D. REFERENCE CAPACITOR

In order to provide a standard signal, a sealed reference capacitor is incorporated in the balloon-borne refractometer and arrangements are made to switch between the sampling and the reference capacitor at intervals of approximately 15 sec. The Clapp oscillator frequency remains essentially constant during this interval for the rates of temperature change encountered in normal ascents. The reference capacitor is constructed of quartz and

invar to make its temperature coefficient comparable to that of the air-sensing capacitor.

E. ADAPTATIONS

An earlier laboratory model of a 13 Mc/s capacitance controlled oscillator which was used as the sensor in an atmospheric refractometer was developed by Severin and Crain (1957) although appreciable steady state and transient temperature induced errors were encountered. A modification of the capacitance principle has been reported by Berry *et al.* (1962) in which a cylindrical capacitor is employed as the sensor in a model designed for drop-sonde applications. The instrument to date, however, is in the laboratory development phase.

F. CONDENSATION EFFECTS

In equation (34) the frequency perturbation was approximated for the coaxial cavity. A similar approximation holds for the condenser and, as before for $\Delta K = 80$ and for a volume of foreign matter equal to one-millionth of the volume of the condenser, an error of 40 *N* units will be introduced. It has been pointed out by Stranathan (1935) that water vapor may be absorbed upon the spacers of the condenser plates: Hay has reduced effects due to this by putting the supports in the region of weak electric fields outside of the capacitor. He also recommends depositing thin water-repellent films on the spacers and on the capacitor plates to discourage the accumulation of absorbed water.

XII. RADIO REFRACTIVE INDEX MEASUREMENTS

A. INTRODUCTION

This section gives a description of various measurements which have been made of the radio refractive index of the atmosphere and some of the equipment arrangements used in these measurements. There are six broad classes of refractive index measurements which will be described as follows:

1. Refractive index calculated from meteorological instruments such as thermometers, hygrometers and pressure measuring devices.
2. Refractive index measurements with fixed refractometers on the ground or on towers.
3. Refractive index measurements as a function of height with refractometers carried in aircraft or by balloons, or dropped from aircraft or balloons and designed primarily to obtain representative average vertical profiles for use in evaluating refraction effects.
4. Measurements, usually taken by refractometers in aircraft, to provide information on the rapid variations of the refractive index due to turbulence and the spectrum of these variations, a knowledge of which is essential to the evaluation of scatter propagation effects.
5. Refractive index studies of clouds.

6. Special applications of refractometers as in the measurement of the moisture content of the atmosphere, the dielectric constants of smokes or aerosols and the ionizing effects of radiation.

B. REFRACTIVE INDEX CALCULATED FROM METEOROLOGICAL PARAMETERS

The index of refraction of the atmosphere may be calculated through the use of equation (12) if the temperature, pressure and partial water vapor pressure are known. By far the greatest amount of information available on the radio refractive index structure of the atmosphere has been obtained in this manner. This information is in two general categories:

1. Variations at the earth's surface as a function of time and geographical location.
2. Variations with elevation, as observed using radiosondes.

Bean and Meaney (1955) have presented data, in terms of monthly medians, on the refractivity at the earth's surface and on the difference in refractivity between the ground and an elevation of 1 km above ground, and they give maps showing contours of this refractive index difference for the United States. Bean (1962), in a summary paper, describes a survey of refractive index for the United States at ground level as determined from the temperature and humidity, and deduces contours of mean values of the index. Radiosonde soundings are taken at regular intervals at many weather stations and compilations of data of this type are available at the National Weather Records Center in Asheville, North Carolina, and these data are valuable for the determination of refractive index profiles. Such profiles, evaluated from standard meteorological derivations, are primarily useful for the examination of climatological effects, and are less applicable to the study of day-to-day changes in characteristics or of the variations which may affect radiowave propagation conditions for specific paths and times. The sensors used for radiosonde measurements, particularly for water vapor, are relatively slow in response. There is a further disadvantage in that the refractive index must be calculated from the meteorological observations, a process which, on a large scale, can be very time consuming. In radiosonde observations temperature and humidity are alternately sampled at finite pressure intervals and the data telemetered to a receiving station on the ground. This alternate sampling means that instantaneous data for all three of the parameters is not available. In addition, some difficulty is experienced with the humidity measuring strips in the radiosondes, due to their large response time, in going from moist to dry air, and due to the fact that measurements below a relative humidity of about 25 per cent are not possible with the strips now in use.

The problem of converting from the meteorological data to radio refractive index can, however, be simplified by the use of nomograms or computers. A number of these have been devised, one example of the nomogram technique being that given by Burgoyne (1945). Two proposals have been made for computing the radio refractive index directly from meteorological sensors without having to record the meteorological data. One of these is

described by Hirao and Akita (1957), who thus measured the refractive index by the use of kytoons up to heights of 500 m. Clinger and Straiton (1960) have examined the possibility of converting a standard radiosonde for the direct output of refractive index information, and have found that by a certain rearrangement of components such a conversion could be made to give an approximation of the refractive index directly in the output of the unit.

A survey of the status and developments in the field of synoptic radio meteorology has recently been presented by Bean *et al.* (1962) involving representative profiles for various air masses, various parametric forms of refractive index data applicable to radio meteorologists, and illustrations of the resulting three dimensional refractive index structure of a storm system traveling across the North American continent. Similar studies have also been reported by Jehn (1960a, 1960b, 1961).

C. GROUND BASED REFRACTOMETER MEASUREMENTS

A full appreciation of the high frequency and magnitude of the refractive index variations, particularly near the earth's surface, was not obtained until refractometers were developed with their essentially instantaneous response to changes in refractive index. The primary limitation of this technique is that of getting the air into and out of the sampling cavities. In ground based studies where the wind speed is not adequate to achieve this it may be accomplished by drawing the air through the cavities with a suction fan.

Several uses of refractometers as ground based instruments will be described in this section. These are only examples and are not intended to be a detailed account of each use of the refractometer. The reports mentioned have a certain historical significance and also are illustrative of the type of applications that can be made with ground based refractometers. Crain and Gerhardt (1952) have described studies of refractive index made from 10 in to 50 ft above ground. They also measured simultaneously the temperatures and the index of refraction and examined the cross-correlation between the two. From these and other studies, it was ascertained that the general pattern was normally a high degree of correlation with large magnitude and high frequency fluctuations near the ground and a reduced correlation, magnitude and frequency with elevation. The high observed ground level cross-correlations of 0.6 to 0.8 resulted from the ground acting as a common moisture and heat source, with turbulent transport affecting both parameters in a nearly identical fashion. The sign of the correlation, however, was variable and depended on the relative intensities of the source parameters. Thus, with a moist ground and little heat transport, humidity fluctuations were found to predominate over temperature fluctuations, giving a direct association between increases and decreases in temperature and refractive index. A hot desert surface, however, gave rise to large temperature variations with little, if any, humidity effects and, from equation (12), the inverse temperature association would result in opposite sign index and temperature variations. It should be noted that the water vapor contribution to refrac-

tivity is approximately three times as high per unit millibar change as it is per unit temperature change ($^{\circ}\text{C}$) at standard pressures and temperatures.

Birnbaum and Bussey (1955) have reported a series of measurements on a 125 meter tower at Brookhaven National Laboratory, Long Island, N.Y. By using a number of cavities separated in space, they were able to obtain cross-correlation functions from which scales of turbulence were computed based on the time required for the cross-correlation function to drop to $1/e$ of its maximum value. By multiplying this time by the average wind speed, this time correlation was converted to a distance scale. They found these scales to be of the order of 180 m and were able to find a relation between these scales and the amplitude of the fluctuations involving a 1.6 power of the scale size. These and other determinations of scale sizes, r.m.s. values of fluctuations, and cross-correlation functions should be examined very carefully in terms of the length of the data sample taken. As pointed out by Birnbaum and Bussey (1955), one of the most striking features of the data taken was the variability in the characteristics of the fluctuations, indicating the non-uniform, non-stationary nature of the atmospheric turbulence encountered. This is a property which may be observed in all such data and indicates very strongly that the atmospheric variation of index of refraction cannot be described as a statistically stationary process.

Although it is not possible nor desirable to make any extensive association here with the comprehensive work that has been carried out in turbulence theory, it should be re-emphasized that the frequency variation of the fluctuations encountered is continuous from global through viscosity-heat dissipation distances; that there is a more or less universally recognized functional form due to Kolmogoroff (1941) relating the intensity of the variations encountered in the inertial subrange of sizes (frequencies from approximately 10^{-3} to 10^3 c/s where energy is constantly being transferred downward in size) to the $-5/3$ power of the wave number; and that, as a result, there is no such thing as the scale of turbulence. It is a mathematical concept only and, depending on the model employed, represents at best merely some effective average. A thorough review of this problem has been made by Hinze (1959).

Straiton *et al.* (1962) have described spectra of refractive index fluctuations observed at ground level and on a small tower, and have shown that the amplitudes of the fluctuations, the cross- and auto-correlation functions, and scales deduced from them are also a function of the length of the sample used. This is because the spectral range of the refractive index variations continually increased with increasing time for both the ground and tower based data, even over the longest intervals in which the data were taken. As a consequence the very slow speed changes swamp out the effect of the higher frequency changes of the amplitude, scale, and correlation functions. Thus, inevitably in practice, any evaluation of scales or intensities of turbulence due to such variations is carried out within a limited portion of the spectrum. The selection of the spectrum interval considered is sometimes made consciously, or sometimes unconsciously by the use of the filtering devices or recording techniques which emphasize the effects of certain fre-

quencies and minimize others. Crain and Gerhardt (1951) had previously reported similar investigations using temperature sensors alone. By plotting the r.m.s. of the temperature difference between sensors for various spacings, a measure of the cross-correlation was sought. It was found that the fluctuations of the temperature difference versus separation tended to level off for large separations, but a constant value was never actually reached.

D. AIRBORNE REFRACTOMETER PROFILE MEASUREMENTS

Although ground based refractometers have provided very interesting data from the meteorological standpoint, observations with airborne refractometers are much more pertinent to radio propagation studies. In many studies of radiowave propagation, the atmosphere is assumed to be horizontally stratified. For this reason, much of the early interest in airborne refractometry was centered in obtaining vertical profiles of the refractive index of the atmosphere in order to predict the effects of atmospheric refraction on radio propagation.

With the availability of the airborne refractometer in 1951, it became possible to carry out a number of combined radio propagation and refractive index measurement experiments. One of the more interesting of these involved a series of flights by the Wright Air Development Center where microwave signals were transmitted between aircraft flying away from each other at various levels in the troposphere. It was at this time that the phenomenon known as the "radio hole" was observed, an effect occurring at certain separations near to the altitude of a marked index stratification where the refraction was such as to cause significant radio energy divergence and resulting loss of signal. Wong (1958) was able to show the existence of a high correlation between refractive index profiles and radio holes as predicted by ray tracing techniques, and many profiles of refractive index in the vicinity of Dayton, Ohio, were studied. In conjunction with radio propagation studies for these purposes, it was common practice to fly an aircraft in either a spiral or slant ascent or descent and reduce the data to obtain index of refraction values at each 100-ft elevation interval. This produced a great deal of smoothing but still provided data which was in much finer detail than that obtainable by radiosondes. A later improvement in this technique has involved the use of $x-y$ plotters to obtain a direct index of refraction-altitude profile. A further refinement has been reported by Shaw and Cunningham (1962) involving a digital output of refractive index data.

By 1957 3 000 such profiles had been obtained by several different groups in the United States. The characteristics of these and their applications have been described by Crain *et al.* (1954), and Crain (1955, 1956, 1957). Figure 13 presents a set of profiles taken with the Crain refractometer over the eastern Caribbean (Ament, 1959) which illustrates the great uniformity that can exist in the structure of the moist tradewind layer. Figure 14 shows a set of profiles taken over the Pacific Ocean off the California coast which is also characterized by a semi-permanent, but colder, marine layer inversion. These layers may be observed in essentially the same form for great distances over the sea, but are significantly modified over land areas. The soundings

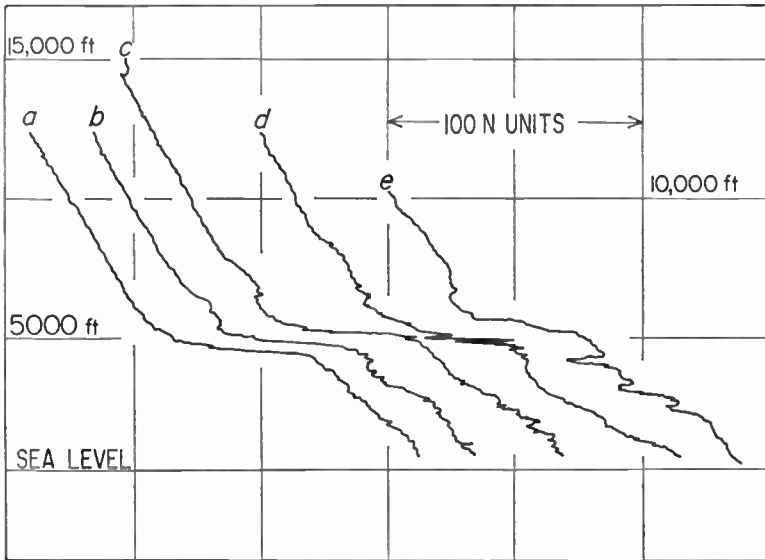


FIG. 13. Refractive index profiles obtained with the Crain refractometer in a Naval Research Laboratory aircraft over the period 0128-0423 E.S.T., 7 December 1956. The soundings were made during ascents at various locations between Patrick Air Force Base, Florida and Nassau. The marked irregularities at about 5 000 ft are due to mixing of wet and dry air at the top interface of the moist tradewind layer.

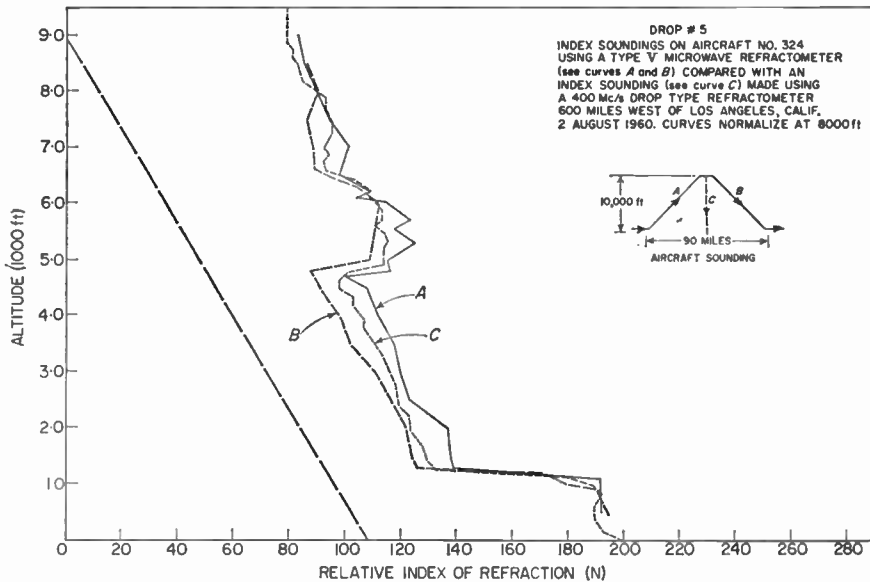


FIG. 14. A comparison of the two profiles obtained over the Pacific Ocean with a Naval Research Laboratory aircraft incorporating both the fixed installation Crain refractometer and the free falling Deam refractometer.

taken in Fig. 14 involved the use of different types of instruments at different frequencies. An airborne Crain refractometer operating at 10 000 Mc/s was flown in an aircraft by the Naval Research Laboratory while at the same time, free fall releases were made using the Deam refractometer, operating at 400 Mc/s. A sounding using the 10 000 Mc/s refractometer was made as the airplane climbed to elevation for dropping the Deam unit and another was taken as the airplane returned to a lower elevation. These profiles show a very remarkable similarity considering that the start and finish of the aircraft soundings were at considerable distances from the point at which the 400 Mc/s instrument fell into the ocean. Both of the above sets of data were

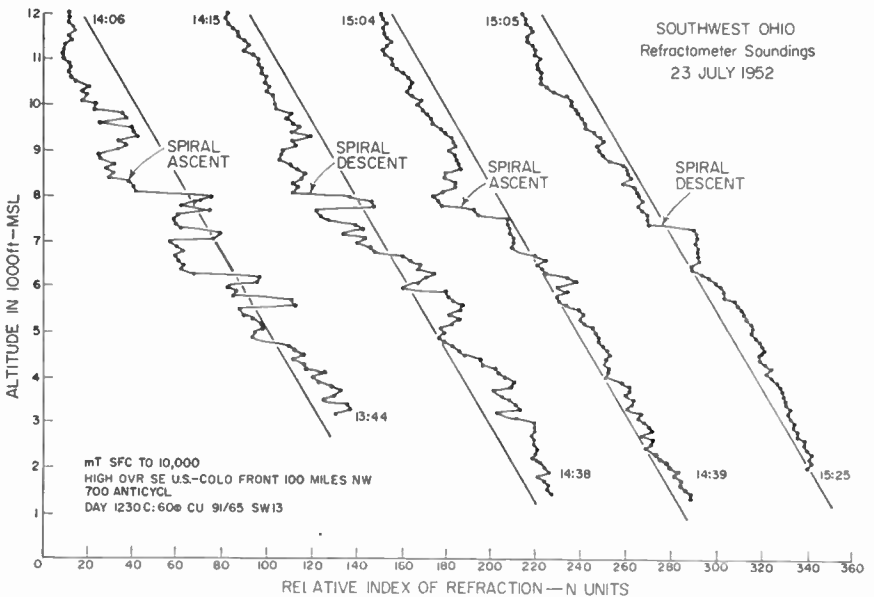


FIG. 15. A series of aircraft soundings made with the Crain refractometer in an area over central Ohio over a period of one hour illustrating the rapidity with which the shape of the profiles may vary due to topographic and convective effects.

taken in a U.S. Naval Research Laboratory program designed to determine the feasibility of using marine-layer refractive index ducts to facilitate over-water radio communication. The studies have included the Caribbean area (Ament, 1959), the Pacific Ocean from California to Hawaii and the Atlantic from Brazil to Ascension Island (Ringwalt and MacDonald, 1961).

An illustration of the lack of correlation of soundings taken in one area is shown in Fig. 15. These measurements were made over central Ohio and illustrate the inconsistency which may occur at times in such profiles, particularly in overland tests, due to topographic and non-uniform convection effects. While these profiles may show some major features which are similar, there are a great many details which are not duplicated from one sounding to the next.

E. AIRBORNE REFRACTOMETER FLUCTUATION MEASUREMENTS

Superimposed on the more regular changes which take place with height are rapid fluctuations of the refractive index of the atmosphere both in horizontal and vertical directions which are always present to a greater or smaller extent. These variations are of great significance in connection with the scatter propagation theories of radio transmission which were developed at about the same time that refractometer measurements became available. In the first flight of the refractometer in the blimp (Crain *et al.*, 1953) such rapid fluctuations were noted in passing over the shoreline of New Jersey where alternate patches of marshy land and dry land caused very rapid fluctuations in the moisture content of the atmosphere. Bussey and Birnbaum (1953), in their initial aircraft flight, also noted rapid fluctuations in the index of refraction and from these obtained a measure of a scale of turbulence. Crain *et al.* (1954b) examined considerable amounts of radio refractive index data, taking individual fluctuations in refractive index and evaluating their amplitudes and scales, but, since particular short samples of data were chosen for examination, a filtering process was introduced and the scales reported are now known to have no general significance. The 1 200 samples examined, however, do give illustrations of the types of jumps in refractive index which may occur in a short interval of time.

Edmonds (1960) has described a study of a set of measurements made in Colorado in which an aircraft flew horizontally at a number of different elevations. He determined fluctuation spectra from the various samples of data and examined the variation of these spectra with height. Comparisons were made with the radio signal amplitudes calculated from measured transmission losses of various National Bureau of Standards transmission paths having scatter common volumes generally within the refractometer sampling area. For one particular sample there was a predominant region of fluctuations in the vicinity of 17 000 ft elevation which was associated with strong turbulence and marked index stratification at that height. Other soundings have shown such enhanced fluctuations existing at heights from a few thousand to 10 000 ft with no particular preference for any given elevation. A typical spectrum of the fluctuations encountered at an altitude of 12 000 ft is shown in Fig. 16. Sherr (1961) has presented fluctuation data obtained at altitudes of about 40 000 ft using a Crain Type VIII refractometer with the cavity mounted in an air duct inside a standard commercial jet type aircraft. By transcribing from the original recordings, variations ranging up to 1.5 N units were obtained with periodicities from about 10 sec to 2 min. However, he erroneously interpreted the quoted $\pm 1 N$ unit accuracy of the refractometer and questioned the reality of the observed variations: in fact relative changes can be observed with these instruments to well within 0.1 N unit.

An examination has been made by Straiton *et al.* (1962) of a set of airborne data taken near Austin, Texas, in which an airplane flew horizontally for a distance of about one mile at each 500-ft interval of height up to about 5 000 ft. Two Deam refractometers were mounted on the wings of the light aircraft

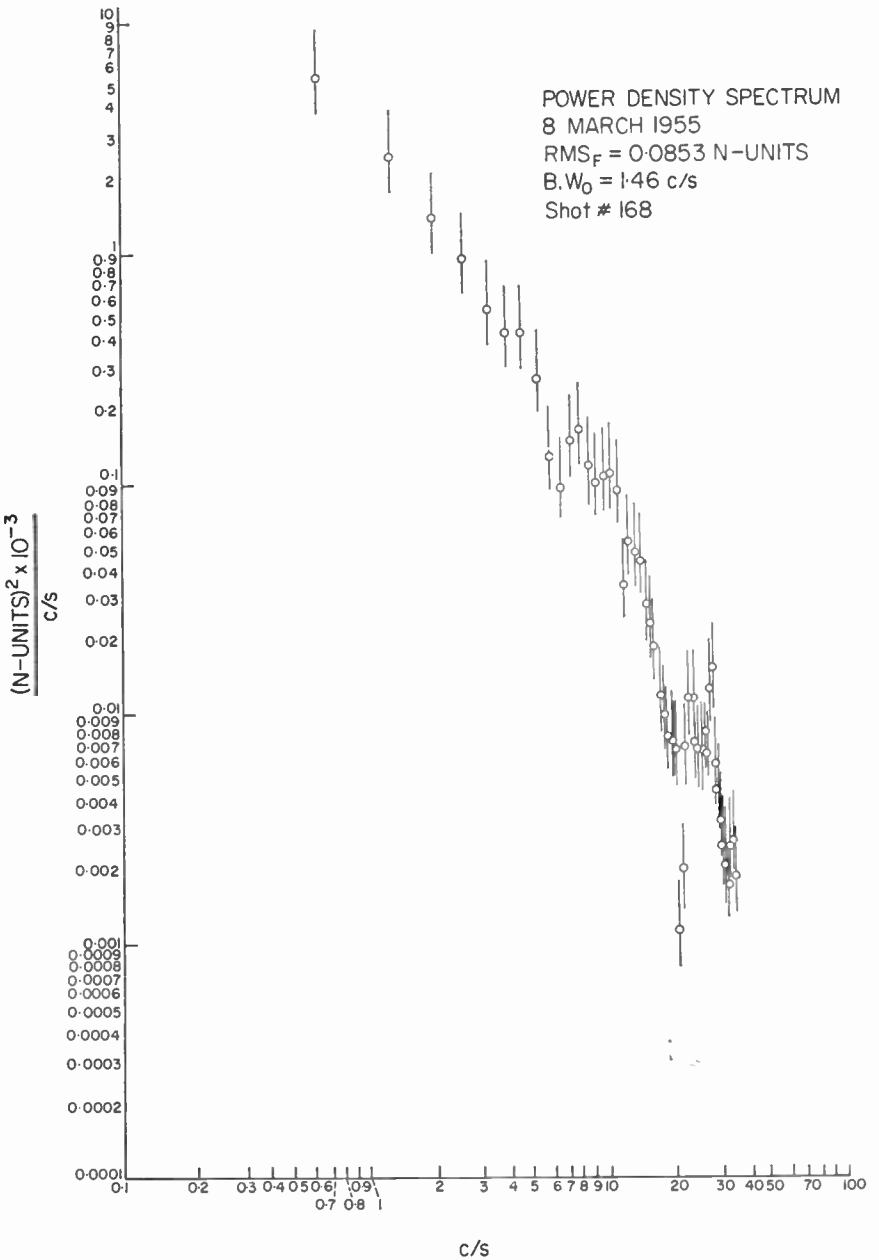


FIG. 16. A typical power spectrum obtained from the fluctuations observed at 12 000 ft with an airborne installation of the Crain refractometer in the central Colorado area. The 90 per cent confidence limits are indicated by the vertical line passing through each point.

and the separate refractometer signals were transmitted to ground based receivers. The output of one receiver gave the individual response of one of the two refractometers while the output of the other receiver measured the difference signal. Each was recorded directly on magnetic tape. Fluctuation spectra obtained from these refractive index soundings showed the

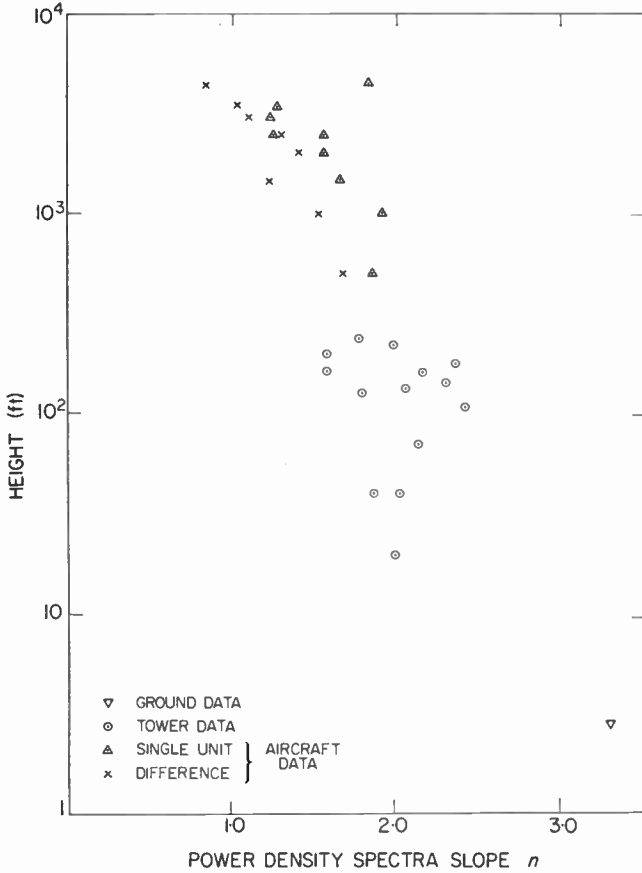


FIG. 17. Slopes of the power spectra of refractive index fluctuations as a function of height obtained over a limited time interval for ground, tower and airborne measurements with the Deam refractometer.

general trend of consistently increasing in amplitude with increasing scale. The index fluctuations (actually in terms of N^2) were plotted as a function of the wave number, which is 2π times the fluctuation frequency divided by the velocity of the air relative to the refractometer. For the airborne data, this velocity is the speed of the aircraft and for ground based data, also reported in this paper, the velocity is the mean wind speed; and thus a comparison of the airborne and ground based fluctuation spectra was possible. The

slopes of the spectra (which were approximated by straight lines on a log-log plot), from the ground based and airborne refractometer data are shown in Fig. 17. An r.m.s. of the fluctuations may be used if this is restricted to a particular part of the spectrum. An example of this is shown in Fig. 18, where only scales under 15 ft are considered. The variability of these results again emphasizes the fact that the atmospheric index of refraction cannot be classified as a statistically stationary process. Still greater variability is

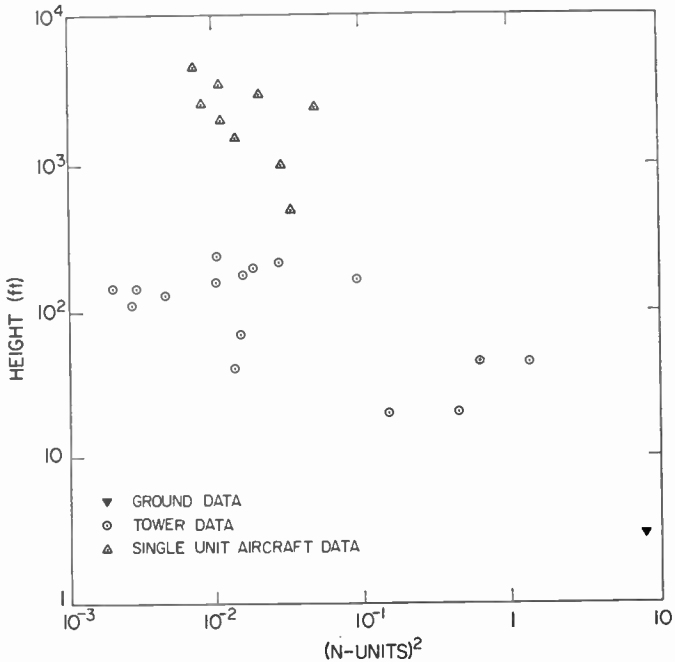
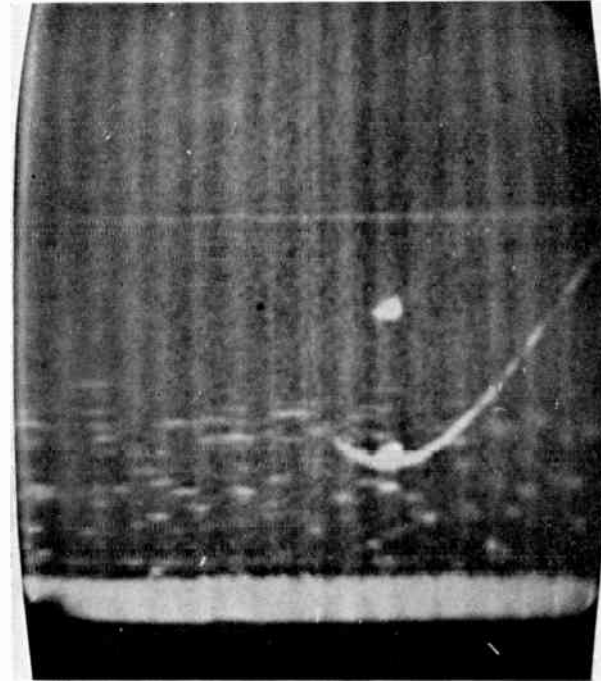
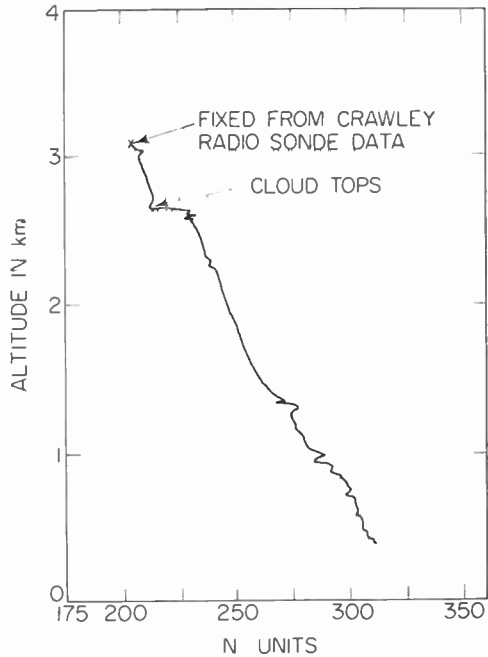


FIG. 18. Mean square values of refractive index fluctuations versus height obtained over a limited time interval for ground, tower and aircraft installations of the Deam refractometers. The values as discussed in the text have been restricted to a particular portion of the spectrum, i.e. for scales less than 15 ft and illustrate the extreme variability associated with a non-stationary process.

experienced for different locations or seasons of the year. It would appear that scatter propagation models based on any simple homogeneous and isotropic field of turbulence can at best provide only a first approximation to the true state of affairs.

Measurements of variations in index of refraction on a much wider scale also contribute to our knowledge of meteorology from a climatological standpoint. As an example of this, Wagner (1957) has described a study of refractive index data taken across the northeastern U.S. An aircraft flying at 4 000 ft elevation recorded only very minor index fluctuations, less than 0.1 *N* unit r.m.s., until a region of relatively unstable, converging air was encountered where the fluctuations increased by a factor of approximately 10.



18 JULY 1961:1400 GMT. HIGH PRESSURE TO WEST; LOW PRESSURE OVER S.W. ENGLAND. CLOUD: $\frac{4}{8}$ AT 10,000 ft, $\frac{3}{8}$ AT 2500 ft.

FIG. 19. An example of the combined vertical radar reflection and refractive index data obtained by Saxton. The solid curved trace is that of the aircraft carrying the refractometer.

This could not be attributed to rain, frontal systems or clouds. The nearly constant index area was identified as one where the wind field was divergent as a result of subsidence from higher elevations, resulting in uniformly stable, dry air. The convection and vertical motion present in the convergent area gave rise to significant moisture variability and resulting index fluctuations at the 4 000 ft level.

Gerhardt *et al.* (1956) have given illustrations of the type of refractive index fluctuations which may be encountered in a number of different geographical locations. They show that detailed observations with refractometers provide a means of studying atmospheric moisture distributions and variations at and below the synoptic scale, and thus make possible the analysis of those atmospheric processes which contribute to or produce tropospheric mixing, i.e. convection, mechanical lifting due to frontal squall lines, topography, frictional turbulence and wind shear. They further discuss the effects of thermal, convective cloud systems, and comment on the fact that small cumulus clouds in Colorado have shown sharp index changes of over 30 *N* units, equivalent to 6–7 mb of vapor pressure, in less than 10 ft of flying into the cloud with generally less than 2°C change in temperature. The same effect has been observed in flying through the invisible thermals associated with such clouds and prior to actual cloud formation.

Saxton (1964) has shown a close interrelationship between turbulence and tropospheric echoes observed with a vertical sounding radar. Simultaneous measurements of refractive index profiles and radar returns have shown that in many cases the echoes originate in regions of sharp changes in refractive index. He concludes, however, that an echo is generally not so much due to reflection caused by the refractive index discontinuity, but rather is due to incoherent scattering arising from turbulent refractive index fluctuations within the associated layer. In each case, when significant radar returns were observed, it was possible to measure an index of refraction change at the same height as the echo, but not all index discontinuities gave echoes. Rapid fluctuations in the vicinity of a discontinuity were usually associated with cases where radar returns were noted. An illustration of simultaneous radar and refractive index observations is shown in Fig. 19.

F. CLOUD STUDIES

Two airborne meteorological laboratories have made simultaneous soundings of a number of meteorological parameters and the refractive index of the atmosphere. These are the Naval Research Laboratory (Ament, 1959), and the Geophysics Research Directorate, AFCRL (Shaw and Cunningham, 1962). Cunningham *et al.* (1956) have described measurements made when flying an airplane through clouds at various levels. An example of the simultaneous recordings made with refractive index, temperature, vapor pressure and liquid water content sensors is shown in Fig. 20 for a constant level flight through a cumulus cloud. Horizontal refractometer recordings made at various elevations within such a cloud are shown in Fig. 21. The sharp changes in index of refraction in the cloud represent the difference in median index of refraction at the elevation of the sample and that

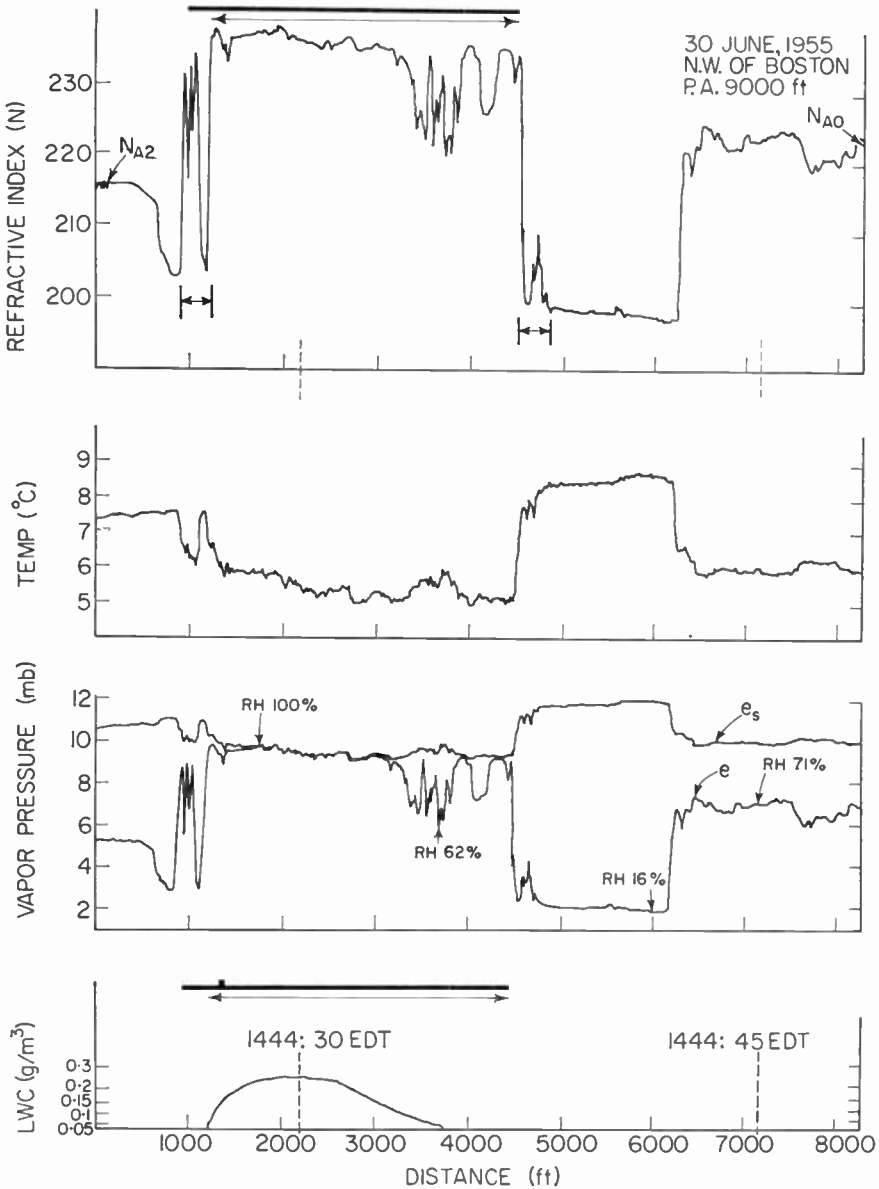


FIG. 20. Selected simultaneous recordings of refractive index, temperature, vapor pressure, and liquid water content made by Cunningham at a constant level through a cumulus cloud represented in extent by the thick bar. The index changes occur in the order of a few feet, the minimum resolvable distance in the type of recording employed.

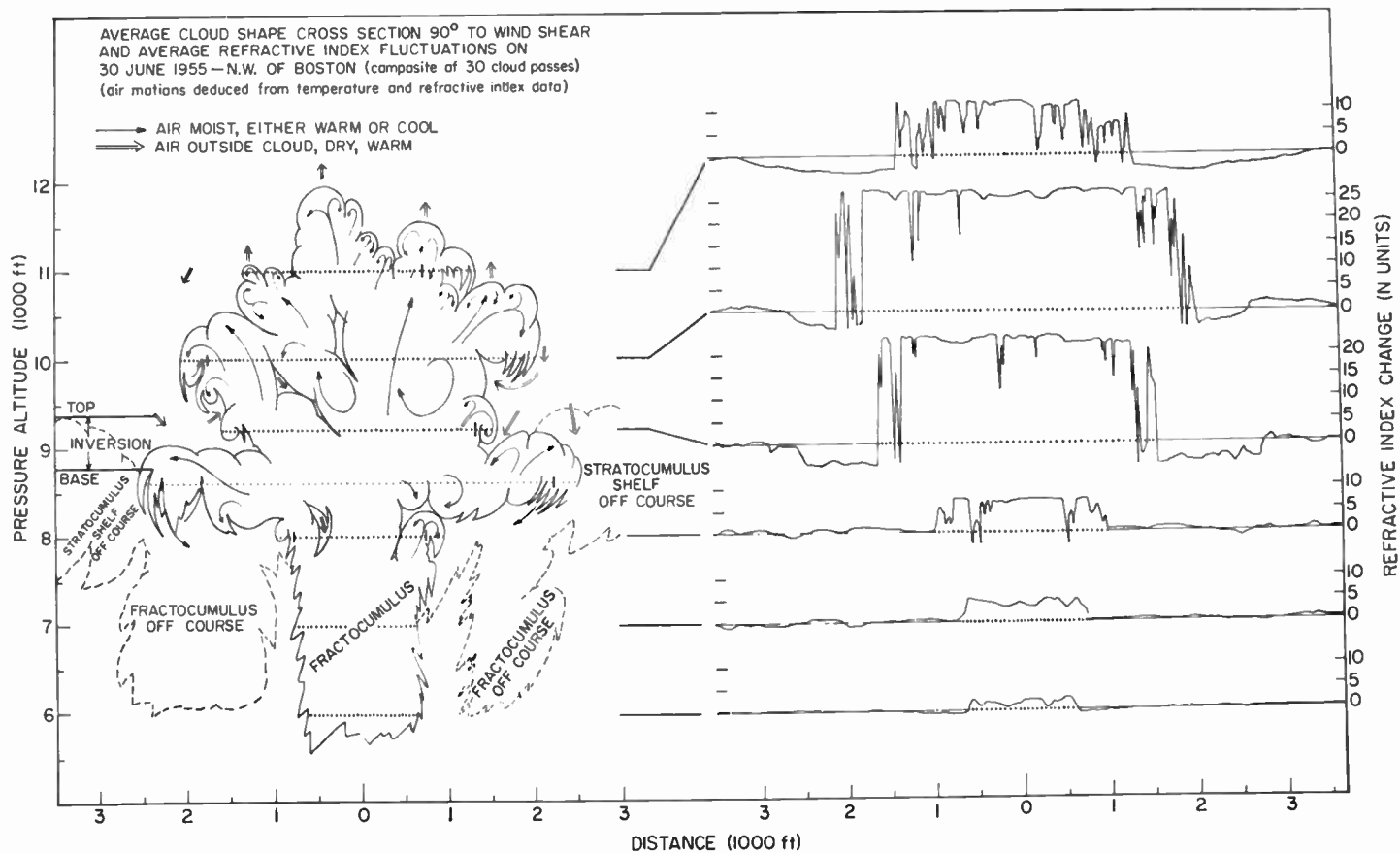


FIG. 21. Horizontal refractive index recordings made at various elevations within a cumulus cloud showing the variation of the intensity of the cloud-free air refractive index difference as a function of elevation.

at a considerably lower elevation from which the moisture was pushed upward by the thermal action in the cloud. Some of the most abrupt changes observed represent index variations of 20 N units or more over distances of no more than a few feet. Cunningham (1962) subsequently analyzed these data in terms of cloud climatology and models of cloud structure.

G. OTHER APPLICATIONS

As previously discussed, the index of refraction of air may be calculated if the pressure, temperature and water vapor content are known. This suggests that if the index of refraction, temperature and pressure are known, the water vapor content may be deduced. High speed temperature sensors may be used with the fast response of the refractometer to measure rapid changes in water vapor. Several hygrometers based on this principle have been devised in which the general technique is to maintain the air input to the refractometer at a fixed temperature above ambient so that the refractometer responds only to moisture variations. Provisions must also be made for periodic dry air sampling for calibration purposes by using some kind of hygroscopic material or cold trap auxiliary input. Magee and Crain (1958) have described one version of this device and Sargent (1959) another.

The above discussions concerning refractive index have all tacitly implied that the atmosphere is made up of oxygen, nitrogen and uncondensed water vapor only. This assumption is very well justified in most cases since the amounts of the rarer gases or foreign particles in the atmosphere are usually quite small, and of course, it is not easy to determine these amounts in a particular region of the atmosphere. The dielectric constant, dipole moments and polarizability of such other gases which may occur in the atmosphere have been examined in the laboratory by the same techniques as those used to determine the constants in the gaseous refractive index equations; and the atmospheric refractometer has proved to be an excellent tool in such studies. Temperature effects may be eliminated by immersing the cavities in oil baths. Illustrations of these uses for several types of refractometer have been given by Birnbaum (1950b), Boggs *et al.* (1957) and by Boggs and Deam (1960).

As in the case of the rarer atmospheric gases, the effect of dust, smoke and other solid particles in the atmosphere is in most cases negligible. There are instances, however, when their concentration is large enough to make a significant contribution to the refractive index. Crain *et al.* (1957a, 1957b) have examined the effects of smokes and aerosols with the refractometer technique and found that finely divided solid particles contributed in proportion to their volume and index of refraction. Much of the index of refraction changes associated with smokes other than the contribution from the solid particles may be attributed to the entrapped water vapor or to changes in temperature.

The effect of an ionized gas on the resonant frequency of a refractometer cavity has been used to study the properties of such gases. One method is to run a glass tube along the axis through the cavity and measure the perturbation of the resonance characteristics caused by ionization of the gas

within the tube, as described by Deakins and Crain (1956). Another method is that of exposing the cavity to radiation either through an opening in the cavity or by penetration through the cavity (Crain, 1958). The interpretation of these experiments is not a simple one since the primary source of electrons will probably be the cavity walls and the secondary source will be the collisions of the electrons ejected from the walls with the gas molecules. The Pound stabilized oscillator as used by Crain is sensitive to small amounts of ionization, but high conductivity in the gas causes a deterioration in the Q of the cavity with a corresponding loss in sensitivity. Relatively large changes in index of refraction and the loss tangent may be measured with sufficient accuracy by using a transmission type cavity and observing the resonance curve of the cavity as the frequency is varied.

ACKNOWLEDGMENT

The assistance of Mr. John R. Gerhardt in providing many helpful suggestions in the preparation of this material, and of various workers in the field of refractometry in supplying reprints and photographs is gratefully acknowledged.

REFERENCES

- Adey, A. W. (1957). *Canad. J. Tech.* **34**, 519-521.
- Ament, W. S. (1959). *Proc. Inst. Radio Engrs, N. Y.* **47**, 756-761.
- Barrell, H. (1951). *J. opt. Soc. Amer.* **41**, 295-299.
- Barrell, H., and Sears, J. E. (1939). *Phil. Trans.* **238A**, 1-64.
- Bean, B. R. (1962). *Proc. Inst. Radio Engrs, N. Y.* **50**, 260-273.
- Bean, B. R., and Meaney, F. M. (1955). *Proc. Inst. Radio Engrs, N. Y.* **43**, 1419-1431.
- Bean, B. R., Horn, J. D., and Riggs, L. P. (1962). *Tech. Note nat. Bur. Stand.* no. 98, 87 pp.
- Berry, R. L., Mohan, T. J., and Stout, C. D. (1962). *Rep. Res. Lab. Division Bendix Corp.* no. 2057, 39 pp.
- Birnbaum, G. (1950a). *Rev. sci. Instrum.* **21**, 169-171.
- Birnbaum, G. (1950b). *Phys. Rev.* **77**, 144-145.
- Birnbaum, G. (1951). *Phys. Rev.* **82**, 110-111.
- Birnbaum, G., and Bussey, H. E. (1955). *Proc. Inst. Radio Engrs, N. Y.* **43**, 1412-1418.
- Birnbaum, G., and Catterjee, S. K. (1952). *J. appl. Phys.* **23**, 220-223.
- Birnbaum, G., and Franeau, J. (1949). *J. appl. Phys.* **20**, 110-111.
- Birnbaum, G., Kryden, S. J., and Lyons, H. (1951). *J. appl. Phys.* **22**, 95-102.
- Boggs, J. E., and Deam, A. P. (1960). *J. chem. Phys.* **32**, 315-316.
- Boggs, J. E., Thompson, C. M., and Crain, C. M. (1957). *J. phys. Chem.* **61**, 1625-1627.
- Burgoyne, R. H. (1945). "Nomograms for Computation of Modified Index of Refraction," *Radiation Lab. Rep.* no. 55, Massachusetts Institute of Technology.
- Bussey, H. E., and Birnbaum, G. (1953). *J. Res. nat. Bur. Stand.* **51**, 171-178.
- Clapp, J. K. (1948). *Proc. Inst. Radio Engrs, N. Y.* **36**, 356-358.
- Clinger, A. H., and Straiton, A. W. (1960). *Bull. Amer. met. Soc.* **41**, 250-252.
- Cogdell, J. R., Deam, A. P., and Straiton, A. W. (1960). *Trans. Inst. Radio Engrs, N. Y. MTT8*, 151-155.

- Crain, C. M. (1948). *Phys. Rev.* **74**, 691–693.
- Crain, C. M. (1950). *Rev. sci. Instrum.* **21**, 456–457.
- Crain, C. M. (1955). *Proc. Inst. Radio Engrs, N. Y.* **43**, 1405–1411.
- Crain, C. M. (1956). *Electronics* **29**, 150–154.
- Crain, C. M. (1957). *Onde élect.* **37**, 442–444.
- Crain, C. M. (1958). *J. appl. Phys.* **29**, 1605–1606.
- Crain, C. M., and Deam, A. P. (1952). *Rev. sci. Instrum.* **23**, 149–151.
- Crain, C. M., and Gerhardt, J. R. (1950). *Bull. Amer. met. Soc.* **31**, 330–335.
- Crain, C. M., and Gerhardt, J. R. (1951). *J. Met.* **8**, 363–365.
- Crain, C. M., and Gerhardt, J. R. (1952). *Proc. Inst. Radio Engrs, N. Y.* **40**, 50–54.
- Crain, C. M., and Williams, C. E. (1957). *Rev. sci. Instrum.* **28**, 620–623.
- Crain, C. M., Deam, A. P., and Gerhardt, J. R. (1953). *Proc. Inst. Radio Engrs, N. Y.* **41**, 284–290.
- Crain, C. M., Gerhardt, J. R., and Williams, C. E. (1954a). *Trans. Inst. Radio Engrs, N. Y. PGAP-2*, 15–22.
- Crain, C. M., Straiton, A. W., and Von Rosenberg, C. E. (1954b). *Trans. Inst. Radio Engrs, N. Y. PGAP-1*, 43–46.
- Crain, C. M., Boggs, J. E., and Thorn, D. C. (1957a). *Trans. Inst. Radio Engrs, N. Y.* **16**, 246–251.
- Crain, C. M., Thorn, D. C., and Boggs, J. E. (1957b). *J. phys. Chem.* **61**, 806–808.
- Cunningham, R. M. (1962). *Geophys. Res. Papers* no. 51, Air Force Cambridge Research Laboratories, AFCRL-62-252.
- Cunningham, R. M., Plank, V. G., and Campen, C. M. (1956). *Geophys. Res. Papers* no. 51, Air Force Cambridge Research Center, AFCRC-56-210.
- Deakins, G. E., and Crain, C. M. (1956). *Rev. sci. Instrum.* **27**, 606–608.
- Deam, A. P. (1962). *Rev. sci. Instrum.* **33**, 438–441.
- Debye, P. (1929). “Polar Molecules,” 172 pp. Dover Publications, New York.
- Edmonds, F. N. (1960). In “Statistical Methods of Radio Wave Propagation,” pp. 197–211. Pergamon Press, London.
- Essen, L. (1953). *Proc. phys. Soc. Lond.* **66B**, 189–193.
- Essen, L., and Froome, K. D. (1951). *Proc. phys. Soc. Lond.* **64B**, 862–875.
- Froome, K. D. (1955). *Proc. phys. Soc. Lond.* **68B**, 833–835.
- Gerhardt, J. R., Crain, C. M., and Chapman, H. (1956). *Bull. Amer. Meteor. Soc.* **37**, 251–261.
- Hay, D. R., Martin, H. C., and Turner, H. E. (1961). *Rev. sci. Instrum.* **32**, 693–697.
- Hector, L. G., and Woernly, D. L. (1946). *Phys. Rev.* **69**, 101–105.
- Hinze, J. O. (1959). “Turbulence,” 586 pp. McGraw-Hill, New York.
- Hirao, K., and Akita, K. T. (1957). *J. Radio Res. Lab.* **4**, 423–437.
- Jehn, K. H. (1960a). *Bull. Amer. met. Soc.* **41**, 304–312.
- Jehn, K. H. (1960b). *J. Meteor.* **17**, 264–269.
- Jehn, K. H. (1961). *Bull. Amer. met. Soc.* **42**, 71–76.
- Jona, M. J. (1919). *Phys. Z.* **20**, 14–21.
- Kerr, F. J. (1941). *Nature, Lond.* **148**, 751–752.
- Kolmogoroff, A. N. (1941). *C. R. Acad. Sci. U.R.S.S.* **30**, 301–305.
- Lane, J. A., Froome, D. S., and McConnell, G. J. (1961). *Proc. Instn elect. Engrs* **108**, 398–402.
- Magee, J. B., and Crain, C. M. (1958). *Rev. sci. Instrum.* **29**, 51–54.
- McGavin, R. E. (1962). *Tech. Note nat. Bur. Stand.* no. 99, 37 pp.
- Montgomery, C. G. (1947). In “Techniques of Microwave Measurements,” Radiation Laboratory Series Vol. 11, pp. 403–407. McGraw-Hill, New York.
- Phillips, W. E. (1950). *Proc. Inst. Radio Engrs, N. Y.* **38**, 786–790.

- Pound, R. V. (1946). *Rev. sci. Instrum.* **17**, 490–505.
- Ringwalt, D. L., and MacDonald, F. C. (1961). *Trans. Inst. Radio Engrs, N.Y. AP-9*, 377–383.
- Sanger, R. (1930). *Phys. Z.* **31**, 306–315.
- Sargent, J. A. (1959). *Rev. sci. Instrum.* **30**, 348.
- Saxton, J. A. (1946). In “Meteorological Factors in Radio-Wave Propagation,” Report of a Conference held on 8 April 1946 by The Physical Society and The Royal Meteorological Society, pp. 215–238, Physical Society, London.
- Saxton, J. A., Lane, J. A., Meadows, R. W., and Matthews, P. A. (1964). *Proc. Instn elect. Engrs* **111**, 275–283.
- Schunemann, R., and Steffan, W. (1958). *Trans. 6027 nat. Bur. Stand.*
- Severin, J. A., and Crain, C. M. (1957). *Rep. elect. Eng. Res. Lab. Univ. Tex.* no. 5-29, 25 pp.
- Shaw, R. H., and Cunningham, R. W. (1962). *Air Force Cambridge Res. Lab. Rep.* no. 20 (AFCRL-62-298).
- Sherr, P. E. (1961). *J. Meteor.* **18**, 494–500.
- Smith, E. K., and Weintraub, S. (1960). *Proc. Inst. Radio Engrs, N.Y.* **41**, 1035–1037.
- Straiton, A. W., Deam, A. P., and Walker, G. B. (1962). *Trans. Inst. Radio Engrs, N.Y. AP-10*, 732–736.
- Stranathan, J. D. (1935). *Phys. Rev.* **48**, 538–544.
- Thompson, M. C., Jr., and Vetter, M. J. (1958). *Rev. sci. Instrum.* **29**, 1093–1096.
- Thompson, M. C., Jr., Freethey, F. E., and Waters, D. M. (1958). *Rev. sci. Instrum.* **29**, 865–868.
- Thompson, M. C., Jr., Freethey, F. E., and Waters, D. M. (1959). *Trans. Inst. Radio Engrs, N.Y. MTT7*, 388.
- Thorn, D. C., and Straiton, A. W. (1959). *Trans. Inst. Radio Engrs, N.Y. MTT7*, 389.
- Tolbert, C. W., and Straiton, A. W. (1951). *Rev. sci. Instrum.* **22**, 162–165.
- Tregidga, A. C. (1940). *Phys. Rev.* **57**, 294–297.
- Tuller, W. G., Galloway, W. C., and Zaffarano, F. P. (1948). *Proc. Inst. Radio Engrs, N.Y.* **36**, 794–800.
- Vetter, M. J. (1960). *Rep. nat. Bur. Stand.* no. 6700.
- Vetter, M. J. (1962). To be published.
- Wagner, N. K. (1957). *Bull. Amer. met. Soc.* **38**, 494–496.
- Watson, H. E., Rao, G. O., and Ramaswany, K. L. (1934). *Proc. roy. Soc.* **143A**, 558–588.
- Wong, M. S. (1958). *Proc. Inst. Radio Engrs, N.Y.* **46**, 1628–1638.
- Works, C. N., Dakin, T. W., and Boggs, F. W. (1944). *Trans. Amer. Inst. elect. Engrs* **63**, 1092–1098.
- Zahn, C. T. (1926). *Phys. Rev.* **27**, 329–340.

TROPOSPHERIC REFRACTION

B. R. BEAN

*Central Radio Propagation Laboratory,
National Bureau of Standards, Boulder, Colorado, U.S.A.*

I. Radio Ray Tracing	53
II. Limitations to Radio Ray Tracing	56
III. An Approximation for High Initial Elevation Angles	57
IV. The Statistical Method	57
V. Schulkin's Method	58
VI. Linear or Effective Earth's Radius Model	59
VII. Modified Effective Earth's Radius Model	62
VIII. Exponential Model	67
IX. The Initial Gradient Correction Method	77
X. The Bi-Exponential Model	78
XI. The Departures-from-Normal Method	87
XII. A Graphical Method	90
XIII. Effect of Atmospheric Horizontal Inhomogeneity upon Ray Tracing	91
XIV. Comparison of Observed Atmospheric Radio Refraction Effects with Values Predicted through the Use of Surface Weather Observations	100
References	119

I. RADIO RAY TRACING

If a radio wave is propagated in free space, where there is no atmosphere, the path followed by a ray is a straight line. However, a ray that is propagated through the earth's atmosphere encounters variations in atmospheric refractive index along its trajectory that cause the ray path to become curved. The geometry of radio ray refraction is shown in Fig. 1. The total angular refraction of the ray path between two points, commonly called the "bending" of the ray, is designated by τ , and is the central refraction parameter used throughout this chapter. The atmospheric radio refractive index, n , always has values slightly greater than unity near the earth's surface (e.g. 1.0003), and approaches unity with increasing height.

If it is assumed that the refractive index is a function only of height above the surface of a smooth, spherical earth (which means that the refractive index structure is taken to be horizontally homogeneous), then the path of a radio ray will obey Snell's law for polar co-ordinates:

$$nr \cos \theta = n_0 r_0 \cos \theta_0 = \text{constant} \quad (1)$$

or, setting $N = (n-1)10^6$

$$(1 + N \times 10^{-6})(a+h) \cos \theta = (1 + N_s \times 10^{-6})(a+h_s) \cos \theta_0 \quad (2)$$

where the radial distance from the center of the earth, r , equals $a+h$. The zero or s subscripts in (2) refer to the initial values at the earth's surface.

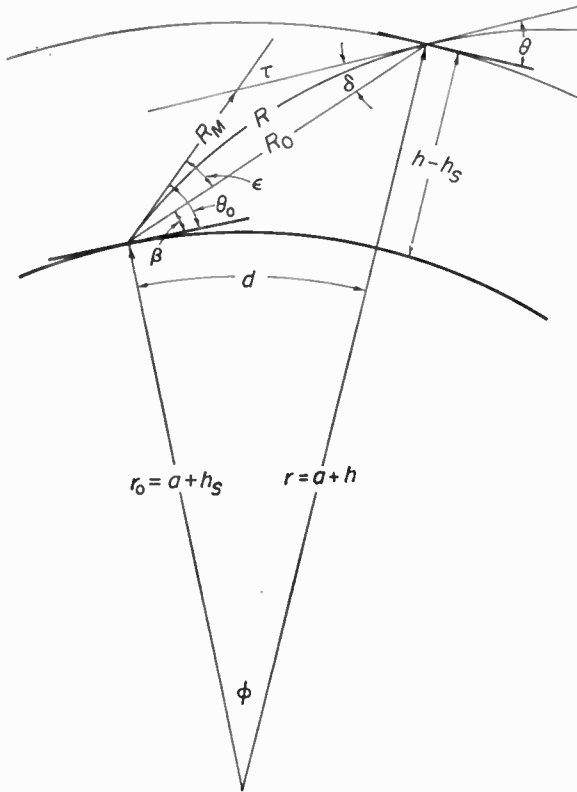


FIG. 1. Geometry of the refraction of radio waves.

Equation (2) may be used to calculate the local elevation angle, θ , at any point along the ray and thus affords a complete description of the ray path. If

$$n_2 r_2 \cos \theta_2 = n_1 r_1 \cos \theta_1$$

and

$$n_2 = n_1 + \Delta n$$

$$r_2 = r_1 + \Delta r$$

and

$$\theta_2 = \theta_1 + \Delta \theta$$

where Δn , Δr , and $\Delta \theta$ are infinitesimals, then

$$n_1 r_1 \cos \theta_1 = (n_1 + \Delta n)(r_1 + \Delta r) \cos (\theta_1 + \Delta \theta) \tag{3}$$

and in the limit, as Δr approaches zero, this becomes

$$n_1 r_1 \cos \theta_1 = (n_1 + dn)(r_1 + dr)(\cos \theta_1 - d\theta \sin \theta_1) \tag{4}$$

If (4) is expanded and products of differentials are omitted, then one obtains

the differential equation

$$\tan \theta d\theta = \frac{dn}{n} + \frac{dr}{r} \tag{5}$$

or
$$d\theta = \frac{dn}{n} \cot \theta + \frac{dr}{r} \cot \theta \tag{6}$$

Noting that $dr \cot \theta / r = rd\phi / r = d\phi$ and, from geometry, $d\theta = d\phi - d\tau$, one obtains the expression for the bending of a radio ray

$$d\tau = -\frac{dn}{n} \cot \theta$$

or
$$\tau_{1,2} = -\int_{n_1}^{n_2} \frac{dn}{n} \cot \theta \tag{7}$$

Note that (7) defines downward bending as a positive quantity.

Equation (7) is the basic measure of the effects of atmospheric refraction used throughout this chapter. Although these effects may be expressed in many ways, the bending offers a convenient method of calculation often used in classical astronomy. Once values of θ and τ have been obtained, they may be used to derive all other refraction variables. The elevation angle error, ε , may be obtained from

$$\varepsilon = \tau - \text{Arc tan} \left[\frac{\frac{n_s}{n} - \cos \tau - \sin \tau \tan \theta_0}{\sin \tau - \cos \tau \tan \theta_0 + \frac{n_s}{n} \tan \theta} \right] \tag{8}$$

The true elevation angle, β , is then:

$$\beta = \theta_0 - \varepsilon \tag{9}$$

Further, the angular distance, ϕ , and the distance along the earth's surface, d , are obtained from

$$\phi = \frac{d}{a + h_s} = \tau + \theta - \theta_0 \tag{10}$$

while the true range, R_0 , is obtained from the law of sines as:

$$R_0 = \frac{(a + h) \sin \phi}{\cos \beta} \tag{11}$$

The geometric path length, R , is obtained by summation of the chord lengths from point to point along the ray path:

$$\Delta(R) = \sqrt{r_2^2 + r_1^2 - 2r_1 r_2 \cos(\phi_2 - \phi_1)} \tag{12}$$

where $r \equiv a + h$.

The "optical" or effective radio path length is obtained by means of

$$R_e = \int_0^R n dR \quad (13)$$

Finally, the radio-range error, ΔR_e , and the geometric path length difference, ΔR , are evaluated as:

$$\Delta R_e = R_e - R_0 \quad (14)$$

and

$$\Delta R = R - R_0 \quad (15)$$

It must be remembered that all of the above refraction results are obtained under the assumption that the refractive index is horizontally homogeneous.

The integral for τ , (7), cannot be evaluated directly without a knowledge of the behavior of n as a function of height. Consequently, the approach of the many workers in this field has been along two distinct lines: the use of numerical integration techniques and approximation methods to evaluate τ without full knowledge of n as a function of height, and the construction of model n -atmospheres in order to evaluate average atmospheric refraction. The following sections are devoted to a discussion of these methods.

II. LIMITATIONS TO RADIO RAY TRACING

It should be kept in mind that the equations given in the preceding section are subject to the following restrictions of ray tracing:

- (1) The refractive index should not change appreciably in a wavelength.
- (2) The fractional change in the spacing between neighboring rays (initially parallel) must be small in a wavelength.

Condition (1) will be violated if there is a discontinuity in the refractive index (which will not occur in nature), or if the gradient of refractive index, dn/dr , is very large, in which case condition (2) will also be violated. Condition (1) should be satisfied if

$$\frac{(dn/dh) \text{ per km}}{N} < 0.002 f_{kc/s}$$

where refractivity, N , is defined as $N = (n-1) \times 10^6$ and $f_{kc/s}$ is the carrier frequency (Bean and Thayer, 1959). Condition (2) is a basic requirement resulting from Fermat's principle for geometrical optics. An atmospheric condition for which both conditions (1) and (2) are violated is known as "trapping" of a ray, and it can occur whenever a layer of refractive index exists with a vertical decrease of N greater than 157 N -units per kilometer. A layer of this type is called a "duct", and the mode of propagation through such a layer is similar to that occurring in a waveguide (Booker and Walkinshaw, 1947). Taking into account refractive index gradients, a cut-off frequency may be derived for waveguide-like propagation through a ducting layer (Kerr, 1951).

In addition to the above limitations, it should be remembered that the postulate of horizontal homogeneity, made in order to use equation (1), is not realized under actual atmospheric conditions; some degree of horizontal inhomogeneity is always present.

III. AN APPROXIMATION FOR HIGH INITIAL ELEVATION ANGLES

A method may be derived for determining ray-bending from a knowledge only of n at the end points of the ray path, if the initial elevation angle is large. Equation (7) in terms of refractivity, N , is equal to

$$\tau_{1,2}(\theta_0) = - \int_{N_1}^{N_2} \cot \theta dN \cdot 10^{-6} \quad (16)$$

assuming $n \cong 1$ in the denominator.

Integration by parts yields:

$$\begin{aligned} \tau_{1,2}(\theta_0) &= - \int_{N_1}^{N_2} \cot \theta dN \cdot 10^{-6} \\ &= - [N \cot \theta \cdot 10^{-6}]_{N_1}^{N_2} - \int_{\theta_1}^{\theta_2} \frac{N}{\sin^2 \theta} d\theta \cdot 10^{-6} \end{aligned} \quad (17)$$

Note that the ratio, $N/\sin^2 \theta$, becomes smaller with increasing θ . If point 1 is taken at the surface, then $\theta_1 = \theta_0$ and $N_1 = N_s$. Then for $\theta_0 = 10^\circ$, $N_2 = 0$ and $\theta_2 = \pi/2$, the last term of (17) amounts to only 3.5 per cent of the entire equation, and for the same values of N_2 and θ_2 but with $\theta_0 = 87$ mrad ($\sim 5^\circ$) the second term of (6) is still relatively small (~ 10 per cent). Thus it would seem reasonable to assume that for

$$\theta_0 \geq 87 \text{ mrad } (\sim 5^\circ)$$

the bending, $\tau_{1,2}$, between the surface and any point, r , is given sufficiently well by

$$\tau_{1,2}(\theta_0) = - [N \cot \theta \times 10^{-6}]_{N_s}^{N_r}$$

$$\text{or} \quad \tau_{1,2}(\theta_0) = N_s \cot \theta_0 \times 10^{-6} - N_r \cot \theta_r \times 10^{-6} \quad (18)$$

The term $-N_r \cot \theta_r \times 10^{-6}$ is practically constant and small with respect to the first term, for a given value of θ_0 and r , in the range $\theta_0 \geq 87$ mrad and $\tau_{1,2}(\theta_0)$ is essentially a linear function of N_s . For bending through the entire atmosphere (to a point where $N_r = 0$), and for $\theta_0 > 87$ mrad, (18) reduces to

$$\tau(\theta_0) = N_s \cot \theta_0 \times 10^{-6} \quad (19)$$

IV. THE STATISTICAL METHOD

Another method for determining high-angle bending is the statistical linear regression technique developed by Bean and Cahoon (1957). It has been

found that for normal conditions and all heights the right-hand integral of (17) is approximately a linear function of $N_s(\theta_0, r \text{ constant})$ for $\theta_0 > 17 \text{ mrad}$ ($\sim 1^\circ$) and that the second term of (18) tends to be constant. Thus (17) reduces to a linear equation,

$$\tau_{1,2} = bN_s + a \quad (20)$$

where b and a are constants and N_s is the surface refractivity.

The form of (20) is very attractive, since it implies two things:

- (1) $\tau_{1,2}$ may be predicted with some accuracy as a function only of N_s (surface height and θ_0 constant), a parameter which may be observed from simple surface measurements of the common meteorological elements of temperature, pressure, and humidity.
- (2) The simple linear form of the equation indicates that, given a large number of calculated, or observed, $\tau_{1,2}$ versus N_s values for many values of h and θ_0 , the expected (or best estimate) values of b and a can be obtained by the standard method of statistical linear regression. This is what was done to obtain the tables given by Bean *et al.* (1960a), where a large number of refractive index profiles were so chosen as to represent the range of profile conditions likely to be encountered in nature. The applicability of this sample to represent both calculated and observed climatic and synoptic variations of τ is discussed in Section XIV.

These tables also show the values of the standard error of estimate, SE , to be expected in predicting the bending, and the correlation coefficients, r , for the data used in predicting the lines. Linear interpolation or graphical methods can be used between the heights given to obtain a particular height that is not listed in the tables.

V. SCHULKIN'S METHOD

Schulkin (1952) has presented a relatively simple, numerical integration method of calculating bending for N -profiles obtained from ordinary significant-level radiosonde (or "RAOB") data. The N -profile obtained from the RAOB data consists of a series of values of N for different heights; one then assigns to $N(h)$ a linear variation with height between the tabulated profile points, so that the resulting N versus height profile is that of a series of interconnected linear segments. Under this assumption, (7) is integrable over each separate linear N -segment of the profile (after dropping the n term in the denominator, which can result in an error of no more than 0.04 per cent in the result), yielding the following result:

$$\Delta\tau_{1,2} \cong - \int_{n_1}^{n_2} \cot \theta \, dn \cong \frac{2(n_1 - n_2)}{\tan \theta_1 + \tan \theta_2}$$

$$\text{or} \quad \Delta\tau_{1,2}(\text{mrad}) \cong \frac{2(N_1 - N_2) \times 10^{-3}}{\tan \theta_1 + \tan \theta_2} \quad (21)$$

The bending for the whole profile is obtained by summing up the $\Delta\tau_{1, 2}$ for each pair of profile levels:

$$\tau_n \approx \sum_{k=0}^n \frac{2(N_k - N_{k+1})}{\theta_k + \theta_{k+1}} \tag{22}$$

This is Schulkin's result. The degree of approximation of (22) is quite high, and most recent "improved" methods of calculating τ will reduce to Schulkin's result for the accuracy obtainable from RAOB or other similar data. Thus, provided that the N -profile is known, (22) is a most useful form for computing bending for communications or radar-engineering applications.

VI. LINEAR OR EFFECTIVE EARTH'S RADIUS MODEL

The classical method of accounting for the effects of atmospheric refraction of radio waves is to assume an effective earth's radius, $a_e (= ka)$ where a is the true radius of the earth and k is the effective earth's radius factor. This method, advanced by Schelling *et al.* (1933), assumes an earth appropriately larger than the actual earth so that the curvature of the radio ray may be absorbed in the curvature of the effective earth, thus leaving the relative curvature of the two the same and allowing radio rays to be drawn as straight lines over this effective earth rather than as curved lines over the

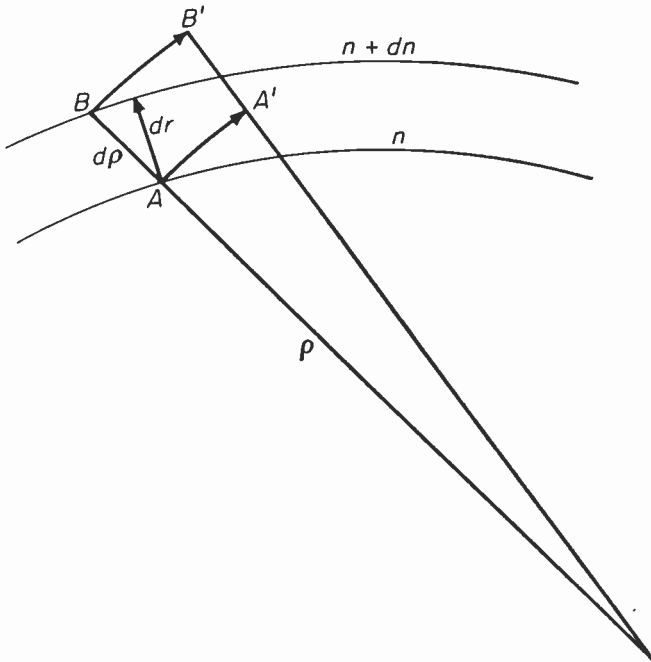


FIG. 2. Differential geometry used in the derivation of the effective-earth's-radius-model atmosphere.

true earth. This method of accounting for atmospheric refraction permits a tremendous simplification in the many practical problems of radio propagation engineering, although the height distribution of refractive index implied is not a very realistic representation of the atmosphere. Consideration will now be given to the refractive index structure assumed by the effective earth's radius model and to how this differs from the observed refractive index structure of the atmosphere. Further, the limits of applicability of the effective earth's radius approach will be explored and a physically more realistic model, the exponential, will be described for those conditions where the effective earth's radius model is most in error.

It is instructive to give a derivation of the expression relating the curvature of radio rays to the gradient of refractive index. In Fig. 2 a wave front moves from AB to A'B' along the ray path. If the phase velocity along AA' is v and $v + dv$ along BB', then, from considering the angular velocity,

$$\frac{v}{\rho} = \frac{v + dv}{\rho + d\rho} \quad (23)$$

and

$$\frac{dv}{v} = \frac{d\rho}{\rho} \quad (24)$$

where ρ is the radius of curvature of the arc AA'. Now, since the phase velocity, v , is

$$v = \frac{c}{n} \quad (25)$$

where c is the velocity of light *in vacuo*, one obtains

$$\frac{dv}{v} = - \frac{dn}{n} \quad (26)$$

combining (24) and (25), the familiar equation for ray curvature, $1/\rho$,

$$\frac{1}{\rho} = - \frac{1}{n} \frac{dn}{d\rho} \quad (27)$$

is obtained. If the ray path makes an angle θ with the surface of constant refractive index

$$dr = d\rho \cos \theta \quad (28)$$

and

$$\frac{1}{\rho} = - \frac{1}{n} \frac{dn}{dr} \cos \theta \quad (29)$$

If the curvature of the effective earth is defined as

$$\frac{1}{a_e} = \frac{1}{a} - \frac{1}{\rho} \quad (30)$$

then

$$a_e = ka = \frac{1}{1/a - 1/\rho} \quad (31)$$

and
$$k = \frac{1}{1 + \frac{a}{n} \frac{dn}{dh} \cos \theta} \tag{32}$$

For the small values of θ normally used in tropospheric propagation, $\cos \theta$ may be set equal to unity. Further, by setting the n gradient constant,

$$\frac{dn}{dh} \equiv -\frac{1}{4a} \tag{33}$$

one obtains the familiar value of $k = 4/3$ for the effective earth's radius factor. By assuming that the gradient of n is constant, a linear model of N versus height has been adopted that has the advantage of replacing a curved ray in the atmosphere by a straight ray over an imaginary earth larger in radius, by the factor k , than the real earth, thus maintaining the relative curvature between the earth and the radio ray.

For this model the bending

$$\tau_{1,2} = - \int_{n_1}^{n_2} \cot \theta \, dn \tag{34}$$

is written
$$\tau_{1,2} = \int_{h_1}^{h_2} \frac{\cot \theta}{4a} \, dh \tag{35}$$

since
$$N = N_0 - \frac{h}{4a} 10^6 \tag{36}$$

and
$$dn = dN \times 10^{-6} = -\frac{dh}{4a} \tag{37}$$

Further, for the case $h_1 = 0$, and $0 \leq \theta_0 \leq 10^\circ$, where θ_0 is the initial elevation angle of a ray, (35) may be approximated by

$$\tau_{0,h} = - \int_0^h \frac{dh}{4a\theta} \tag{38}$$

The angle θ may be determined from

$$\theta_h = \left(\theta_0^2 + 2(N - N_0) + \frac{2}{a}(h - h_0) \cdot 10^6 \right)^{\frac{1}{2}} \tag{39}$$

or
$$\theta_h = \left(\theta_0^2 + \frac{3}{2} \frac{h}{a} 10^6 \right)^{\frac{1}{2}} \text{ in milliradians} \tag{40}$$

For the case when $\theta_0 = 0$ (38) becomes

$$\tau_{0,h} = \frac{1}{2\sqrt{6a}} \int_0^h \frac{dh}{\sqrt{h}} = \frac{1}{\sqrt{6}} \left[\sqrt{h/a} \right]_0^h \tag{41}$$

i.e.
$$\tau_{0,h} = \frac{1}{\sqrt{6}} \sqrt{h/a} \quad (42)$$

Now, from the geometrical relationship,

$$\tau = \frac{d_{0,h}}{a} + (\theta_0 - \theta_h) \quad (43)$$

one finds, for $\theta_0 = 0$

$$d_{0,h} = a(\tau_{0,h} + \theta_h) \quad (44)$$

which upon substitution from (42) and (40) gives

$$d_{0,h} = \sqrt{2h(4/3)a} \quad (45)$$

or, more familiarly,

$$d_{0,h} = \sqrt{2kah} \quad (46)$$

A very convenient working formula is derived from (46) by setting $k = 4/3$, $a = 3960$ miles and using units of miles for the ground distance to the radio horizon, $d_{0,h}$, and feet for the antenna height, h :

$$d_{0,h} = \sqrt{2h} \text{ miles} \quad (47)$$

This is the familiar expression often used in radio propagation engineering for the distance to the radio horizon.

VII. MODIFIED EFFECTIVE EARTH'S RADIUS MODEL

The effective earth's radius model, although very useful for engineering practice, is not a very good representation of actual atmospheric N structure. For example, the data on Fig. 3 represent the average of individual radio-sonde observations over a five-year period at several locations chosen to represent the extremes of refractive index profile conditions within the United States. The Miami, Florida, profile is typical of warm, humid sea-level stations that tend to have maximum refraction effects, while the Portland, Maine, profile is associated with nearly minimum sea-level refraction conditions. Although Ely, Nevada, has much smaller surface N values than either Miami or Portland, it is significant that when its N profile is plotted in terms of altitude above sea level, it falls within the limits of the maximum and minimum sea level profiles. It is to take advantage of this simplification that altitude above sea level rather than height above ground is frequently used throughout this chapter. The N distribution for the 4/3 earth atmosphere is also shown on Fig. 3. It is quite evident that the 4/3 earth distribution has about the correct slope in the first kilometer above the earth's surface but decreases much too rapidly above that height. It is also seen from Fig. 3 (the N -scale is logarithmic) that the observed refractivity distribution is more nearly an exponential function of height than a linear one as assumed with the 4/3 earth atmosphere.

One might wonder, in the light of the data of Fig. 3, why the effective earth's radius approach has served so well for so many years. It appears

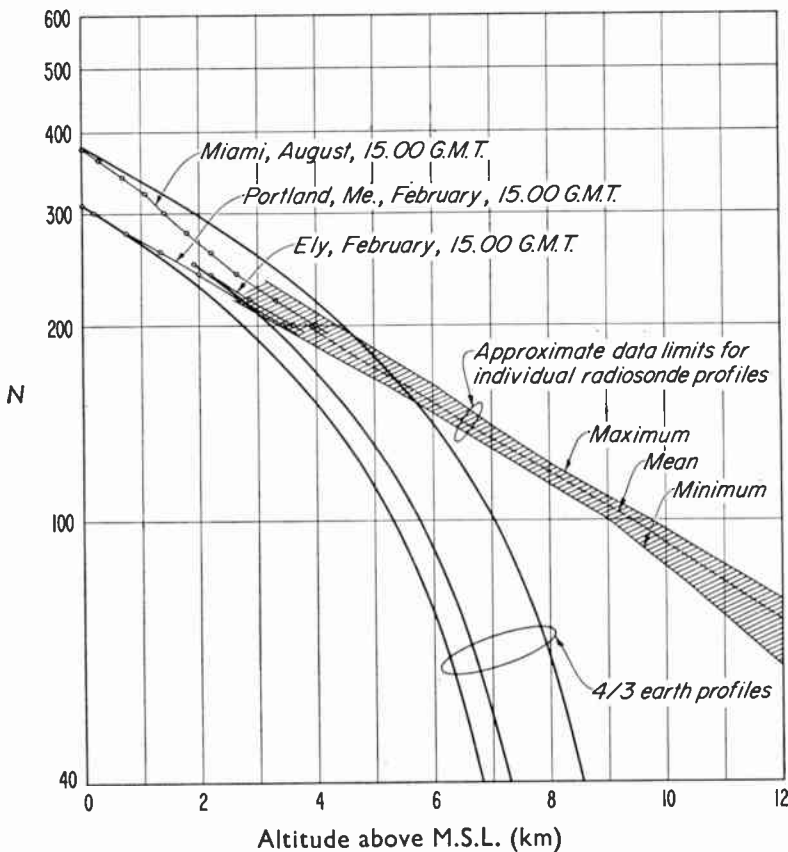


FIG. 3. Typical N -versus-height distributions.

that this success is due to the fact that the model assumed is in essential agreement with the average N structure near the earth's surface, and it is this N structure which largely controls the refraction of radio rays at the small values of θ_0 common in tropospheric communications systems.

It would seem that the deficiency of the effective earth's radius approach could be lessened by modifying that theory in the light of the average N structure of the atmosphere. An indication of the average N structure has been obtained by examining a number of N profiles carefully selected from a variety of individual radiosonde observations to represent the range of N profile conditions during summer and winter at thirteen climatically diverse locations. The results of this examination are given in Table I.

It is interesting to note that the range of N values has a minimum at 8 to 9 km above sea level, but is systematically greater above and below that altitude. The average value of 104.8 at 9 km corresponds to a similar value reported by Stickland (1946) as typical of the United Kingdom. Further,

TABLE I. *Refractivity Statistics as a Function of Altitude Above Sea Level as Derived from Individual Radiosonde Observations*

Altitude in Kilometers	\bar{N}	Maximum N	Minimum N	Range†
4	197.1	209.5	186.5	23.0
5	172.3	184.0	165.0	19.0
6	151.4	161.0	146.0	15.0
7	134.0	139.5	129.5	10.0
8	118.4	121.5	113.3	8.2
9	104.8	108.0	100.0	8.0
10	92.4	97.0	86.0	11.0
11	81.2	86.0	70.0	16.0
12	70.7	76.0	60.5	15.5
14	53.2	60.0	44.5	15.5

† Range = Maximum N - Minimum N .

the altitude of 8 km corresponds to that reported by Humphreys (1940), where the atmospheric density is nearly constant regardless of season or geographical location. It seems quite reasonable, then, to adopt a constant value of $N = 105$ for 9 km, thus further facilitating the specification of model atmospheres. Further, when the values of Table I are plotted, as on Fig. 3, it is seen that the data strongly suggest that N may be represented by an exponential function of height of the form:

$$N(h) = N_0 \exp \{-bh\}$$

in the altitude range of 1 to 9 km above sea level.

When the effective earth's radius assumption is used, height is calculated as a function of distance, for a ray with $\theta_0 = 0$, with the equation $h = d^2/2ka$, where d is the distance, k is the effective earth's radius factor, and a is the true radius of the earth (~ 6373 km). The errors likely to be incurred when using this equation, assuming as a true atmosphere an exponential $N(h)$ profile as given in the following section, will not exceed 5 per cent for heights of 1 km or less.

The preceding background discussion has presented the material necessary for the consideration of the suitability of various models of refractivity to describe atmospheric refraction of radio waves. As a guide to what follows, let us ask what a logical sequence of models (or assumptions) would be to describe the effects of atmospheric refraction. One such sequence might be:

(1) Assume an invariant model that is near to the actual average conditions and facilitates the calculation of radio field strengths. This has been done by the 4/3 earth model.

(2) Assume a variable effective earth's radius factor for the calculation of radio field strengths in various climatic regions. This approach has been

followed by Norton *et al.* (1955). When it becomes apparent that the effective earth's radius approach is inadequate, one might proceed by:

(3) Correcting the effective earth's radius model by assuming a more realistic N structure in the region where that model is most in error. This "modified effective earth's radius" model would then maintain, for some applications, the advantages of the original model.

(4) Assume an entirely new model of N structure guided by the observed average N structure of the atmosphere.

It is assumed that models (3) and (4) would allow for seasonal and climatic changes of the average refractive index structure of the atmosphere. In the following sections these models will be described and tested for their relative agreement with the ray bendings obtained from actual long-term average N profiles.

Consider first the model of atmospheric refractivity based upon the effective earth's radius concept in the first kilometer. In this atmosphere N is assumed to decay linearly with height from the surface h_s to 1 km above the surface $h_s + 1$. This linear decay is given by

$$N(h) = N_s + (h - h_s)\Delta N, \quad h_s \leq h \leq h_s + 1 \quad (48)$$

$$\text{where} \quad -\Delta N = 7.32 \exp(0.005577 N_s) \quad (49)$$

for the U.S.

and $-\Delta N = 9.30 \exp(0.004565 N_s)$ for Western Europe (Bean *et al.*, 1962).

These last two relationships come from the observed relationship between 6- to 8-year averages of daily observations of N_s and ΔN , the difference between N_s and the value of N at 1 km above the earth's surface:

$$-\Delta N = N_s - N(1 \text{ km})$$

It is evident from Fig. 4 that for average conditions a relationship exists between ΔN and N_s . The least squares determination given by (49) was based upon 888 sets of monthly mean values of $\overline{\Delta N}$ and \overline{N}_s from forty-five United States weather stations representing many diverse climates. This relationship between $\overline{\Delta N}$ and \overline{N}_s is expected to represent the best estimate of a majority of individual profiles and certainly will closely agree with average conditions for the United States with one notable exception, southern California in the summer. The ray bendings based upon the ΔN obtained from (49) are in rather good agreement with the values calculated from actual N profiles, even those observed in southern California.

Equation (49) offers a convenient method of specifying various models of the refractivity structure of the atmosphere, since it allows an estimation of the value at N at 1 km in addition to the two values already known; i.e. N_s and $N = 0$ at $h = \infty$.

It may be further assumed that N decreases exponentially from $h_s + 1$ to a constant value of 105 at 9 km above sea level. In this altitude range N is

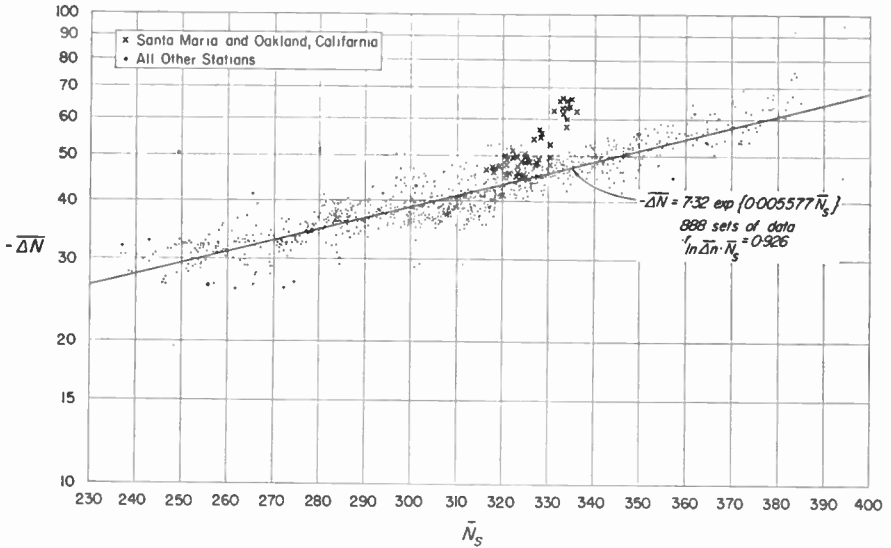


FIG. 4. Eight-year average N_s versus 6-yr average ΔN at 0300 and 1500 GMT.

defined by:

$$N = N_1 \exp \{-c(h - h_s - 1)\}, \quad h_s + 1 \leq h \leq 9 \text{ km} \quad (50)$$

where

$$c = \frac{1}{8 - h_s} \ln \frac{N_1}{105}$$

and N_1 is the value of N at 1 km above the surface.

Above the altitude of 9 km, where less than 10 per cent of the total bending occurs, a single exponential decrease of N may be assumed. The coefficients in the exponential expression:

$$N = 105 \exp \{-0.1424(h - 9)\}, \quad h \geq 9 \text{ km} \quad (51)$$

were determined by a least squares analysis of the Rocket Panel data (1952). This expression is also in agreement with the ARDC Model Atmosphere—1956 and Dubin's (1954) conclusion that a standard density-distribution may be used to determine the refractivity distribution at altitudes in excess of 20 000 ft.

The three-part model of the atmosphere expressed by (49)–(51), called the CRPL Reference Atmosphere—1958, has the advantage of the effective earth's radius approach, particularly for such applications as point-to-point radio relaying over distances up to, say, 150 km, where the radio energy is generally confined to the first kilometer of height, and in addition is in reasonably good agreement with the average N structure of the atmosphere. The specific combinations of N_s , h_s , and ΔN , that define the CRPL Reference Atmosphere—1958 are given in Table II.

TABLE II. Constants for the CRPL Reference Atmosphere—1958

N_s	h_s feet	a' miles	$-\Delta N$	k	a_e miles	c per km
0	0	3 960·0000	0	1·00000	3 960·00	0
200	10 000	3 961·8939	22·3318	1·16599	4 619·53	0·106211
250	5 000	3 960·9470	29·5124	1·23165	4 878·50	0·114559
301	1 000	3 960·1894	39·2320	1·33327	5 280·00	0·118710
313	700	3 960·1324	41·9388	1·36479	5 403·88	0·121796
350	0	3 960·0000	51·5530	1·48905	5 896·66	0·130579
400	0	3 960·0000	68·1295	1·76684	6 996·67	0·143848
450	0	3 960·0000	90·0406	2·34506	9 286·44	0·154004

Note: a_e is the effective earth's radius and is equal to $a'k$, $a' = a + h_s$, where a is the altitude of the earth's surface above sea level.

$$a = 3\,960 \text{ miles}, c = \frac{1}{8-h_s} \ln \frac{N_1}{105}$$

The station elevations corresponding to given combinations of N_s and ΔN were chosen to correspond with an average decay of N with station elevation. Although the error in neglecting this height dependence has been estimated to be no more than a few per cent, it could be important in such high precision applications as radar tracking of earth satellites. It should be remembered in subsequent applications that a unique feature of these reference atmospheres is the dependence of N_s on the altitude of surface above sea level. This feature was built in so that the reference atmospheres would be completely specified by the single parameter N_s .

VIII. EXPONENTIAL MODEL

The next model of the atmosphere to be considered may be specified by assuming a single exponential distribution of N :

$$N = N_s \exp \{-c_e(h-h_s)\} \quad (52)$$

where

$$c_e = \ln \frac{N_s}{N(1 \text{ km})} = \ln \frac{N_s}{N_s + \Delta N} \quad (53)$$

and these equations are used to determine N at all heights. This model of atmospheric refractivity is a close representation of the average refractivity structure within the first 3 km; and it has been adopted for use within the National Bureau of Standards with specific values of the constants in (52) and (53) which are given in Table III, so defining the CRPL Exponential Reference Atmosphere—1958.

Figure 5 compares the N structure of the above two models together with that of the simple 4/3 earth model. It can be seen that the latter model agrees with the reference atmosphere in the first kilometer, which is to be expected since $N_s = 301$ is the value required to yield 4/3 gradient from (49). Figure 5

TABLE III. *Table of the Constant c_e for the CRPL Exponential Radio Refractivity Atmosphere*

$$N = N_s \exp \{-c_e(h-h_s)\}$$

ΔN	N_s	c_e per km
0	0	0
22·3318	200·0	0·118400
29·5124	250·0	0·125625
30·0000	252·9	0·126255
39·2320	301·0	0·139632
41·9388	313·0	0·143859
50·0000	344·5	0·156805
51·5530	350·0	0·159336
60·0000	377·2	0·173233
68·1295	400·0	0·186720
70·0000	404·9	0·189829
90·0406	450·0	0·223256

illustrates the essential agreement of the reference atmosphere with the Rocket Panel and ARDC data. The exponential reference atmosphere is also shown on Fig. 5 for $N_s = 313$, the average value for the United States. The exponential reference atmosphere appears to be a reasonable single line representation of N throughout the height interval shown.

The differences between the various models become more apparent by examining their agreement with observed N profiles over the first 10 km as in Fig. 6. The reference and exponential reference atmospheres are given for the N profiles corresponding to near-maximum N_s (Lake Charles, La.) and near minimum-at-sea-level N_s conditions (Caribou, Me.). The two reference atmospheres were determined solely from the N_s values of each profile. Several observations can be made on these data. First, the 4/3 earth model closely represents the slope of the minimal N_s profile over the first kilometer, but then decreases too rapidly with height. Note, however, that the 4/3 earth model with its constant decay of 39·2 N units per kilometer would be a very poor representation of the maximum profile which decreases over 66 N units in the first kilometer. The exponential reference atmosphere is in good agreement with the initial N distribution, but tends to give values systematically low above approximately 3 km. At first glance, the exponential reference atmosphere does not appear to be as good a representation of the two observed profiles as the reference atmosphere, particularly above approximately 5 km. A later analysis of the refraction obtained from these two model atmospheres will show that this systematic disagreement of the exponential reference atmosphere in the 5- to 20-km interval is a minor defect of the model compared to its closer agreement with observed N

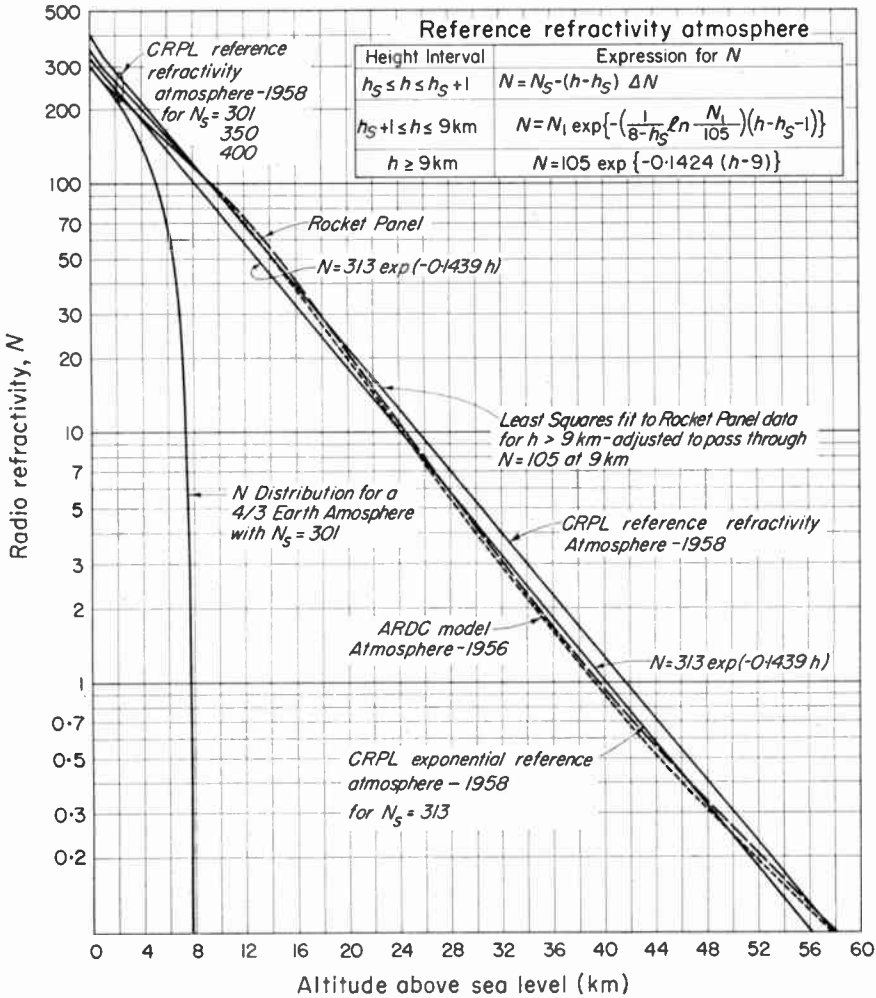


FIG. 5. CRPL reference refractivity atmospheres—1958.

distributions over the first 1 to 3 km. This is particularly true for the higher values of N_s such as that for Lake Charles. Both of the latter models are more in agreement with long-term mean N profiles than is the 4/3 earth model, and the application in mind must aid in deciding which of the reference atmospheres would be the more useful. To aid in distinguishing between the various models, some consideration will now be given to a comparison of the ray bending to be expected in the different atmospheres, where systematic differences in behavior will be seen to appear.

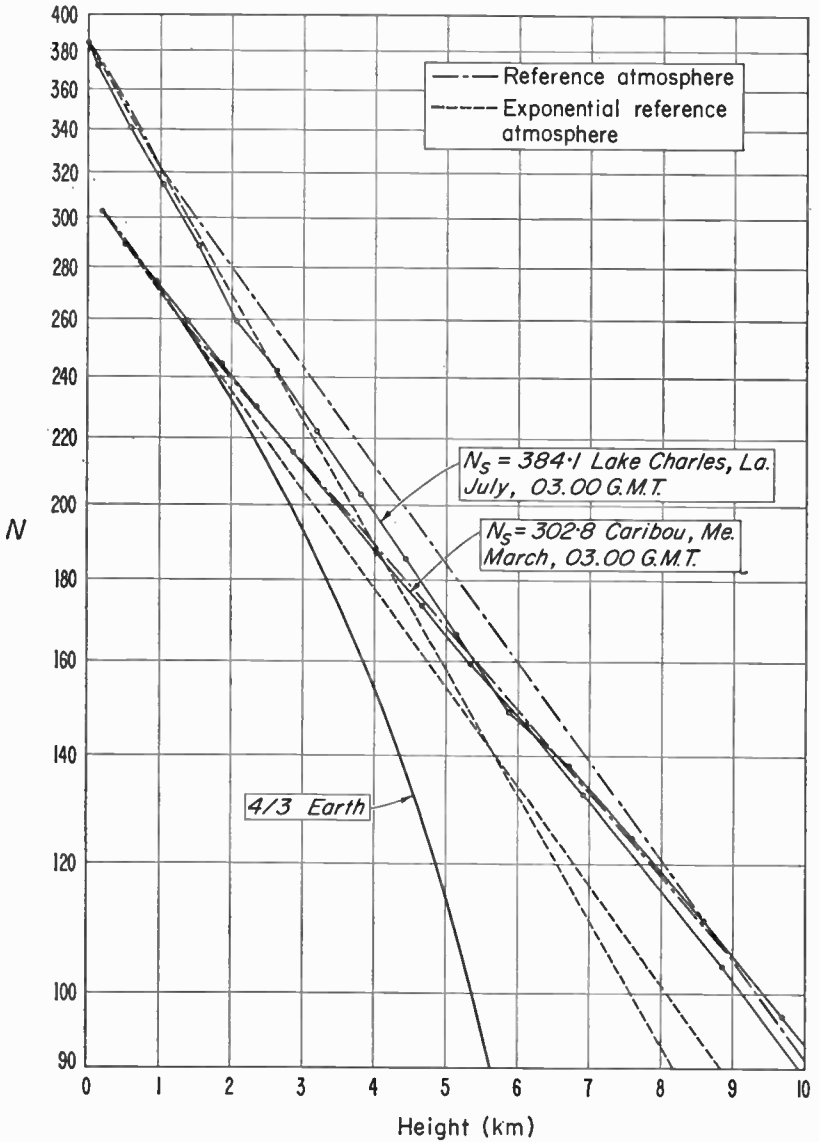


FIG. 6. Comparison of reference atmospheres with observed N profiles.

Such a comparison is given in Fig. 7 for a distance of 200 miles and a height of 14 000 ft and in Fig. 8 for a distance of 800 miles and a height of

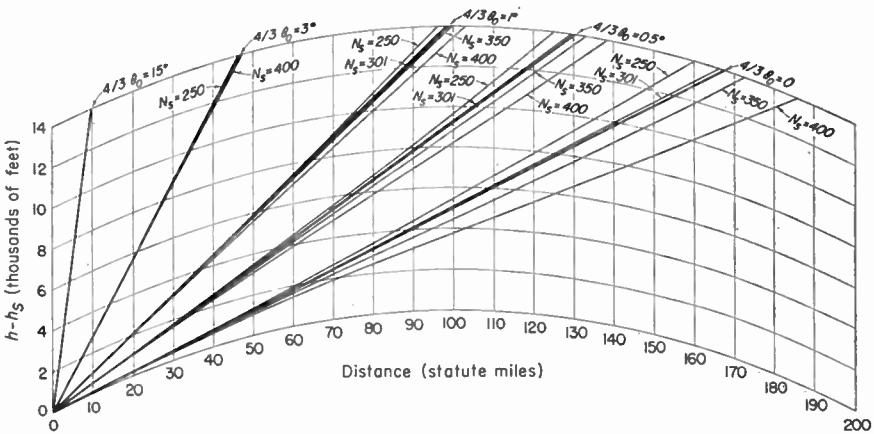


FIG. 7. Comparison of rays in the CRPL reference refractivity atmospheres—1958 and the 4/3 earth atmosphere.

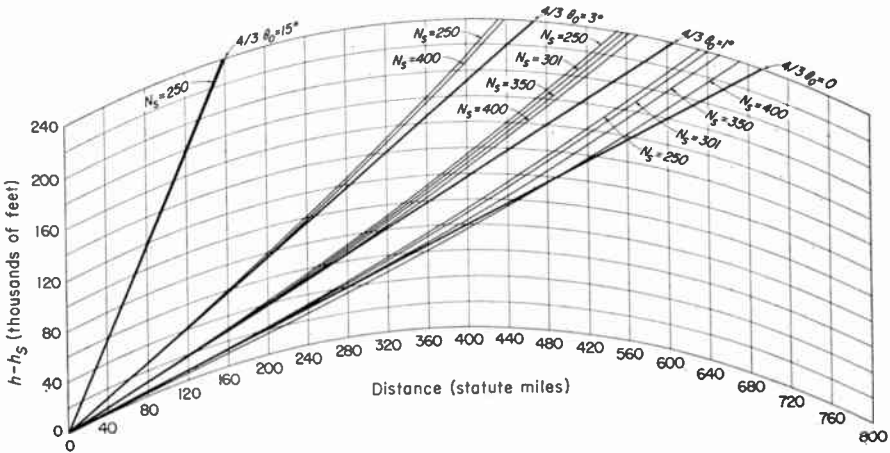


FIG. 8. Comparison of rays in the CRPL reference refractivity atmospheres—1958 and the 4/3 earth atmosphere.

240 000 ft. The particular graphical presentation used in Figs. 7 and 8 shows the 4/3 earth rays as straight lines. It is noted that the 4/3 earth ray at $\theta_0 = 0$ is in relatively good agreement with that in the reference atmosphere for distances out to 200 miles and heights up to 14 000 ft, but systematically departs from it for greater distances and heights. For a range of 600 miles, where the ray reaches heights of about 200 000 ft, the 4/3 earth ray is some 9 000 ft lower than that in the $N_s = 400$ reference atmosphere and 36 000 ft

lower than in the $N_s = 250$ reference atmosphere. This height discrepancy is due to the 4/3 earth model's unrealistically large N gradient at great heights with resultant increased bending.

The bending in the 4/3 earth atmosphere is compared with that in the exponential reference atmosphere in Fig. 9. The bending in an average atmosphere is also given. The important point made by Fig. 9 is that the 4/3

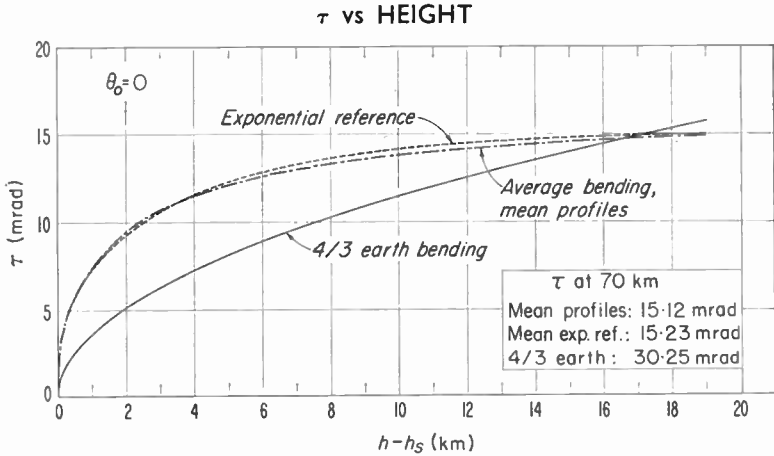


FIG. 9. Comparison of total bending in the exponential reference atmosphere, the 4/3 earth atmosphere, and as calculated from mean N profiles.

earth model is systematically in disagreement with average bending; at low heights it gives too little bending, while at high altitudes it gives too much bending. The exponential reference atmosphere does not appear to be systematically biased, and deviates less than 5 per cent from the average atmosphere. It is significant that the exponential reference and the average atmosphere are in essential agreement as to the shape of the τ -height curve.

It is now instructive to compare the bendings obtained from the various theoretical models with values derived from each of the 5-year mean N profiles which have been obtained for both summer and winter for a variety of climates as represented by the states of Florida, Texas, Maine, Illinois, Nevada, California, North Dakota, Washington, Nebraska, Wyoming, and by the District of Columbia. The results of such a comparison are given in Figs. 10 and 11, which have been selected to illustrate the range of agreement between the models and the expected long-term average bendings. Figure 10 gives a comparison for a small initial elevation angle, $\theta_0 = 0$, and a small height increment, $h-h_s = 3$ km, and shows that both reference atmospheres tend to set a lower limit to the bendings. In this case, the exponential reference atmosphere appears to be in better agreement with the expected long-term mean bendings than does the reference atmosphere. The numbered data points for Washington, D.C., Omaha, Nebraska, and Santa Maria, California, are of special interest. Washington and Omaha have the only long-

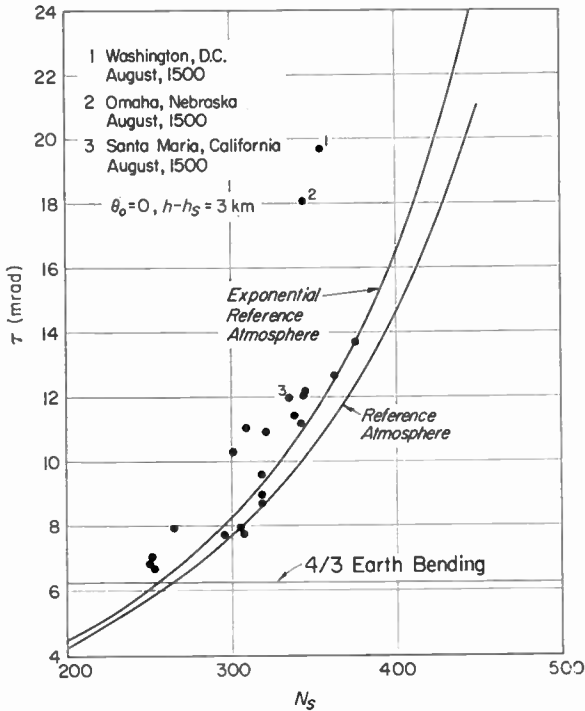


FIG. 10. Comparison of τ vs N_s as obtained from CRPL reference atmospheres—1958 and 5-yr mean radiosonde data.

term mean N profiles with initial N gradients (i.e. $-112/\text{km}$ and $-106/\text{km}$, respectively) that are significantly greater than would be expected from the ΔN vs N_s relationship. Both of these stations have an unusually large humidity decrease near the ground. The third point, Santa Maria, California, is of interest since it is in relatively good agreement with the reference atmospheres, even though it represents the southern California summer climate which was excluded from the original ΔN vs N_s relationship. This agreement is attributed to the fact that the reference atmosphere is a good representation of the N distribution below the California elevated inversion and to the fact that the majority of the bending is accomplished below the elevated inversion height of about 500 m. Further, it can be easily shown that the bending integral is increasingly insensitive to strong N discontinuities as the height increases. Figure 11 shows a similar comparison for a high initial elevation angle, $\theta_0 = 15^\circ$ and a large height increment, $h - h_s = 70 \text{ km}$. This comparison shows that both of the reference atmospheres are in closer agreement with the long-term mean bendings than are the 4/3 earth bendings. Note that, whether τ is predicted from N_s or ΔN , the 4/3 earth model gives but a single value of bending that is outside the limits of the values of τ obtained from the long-term profiles.

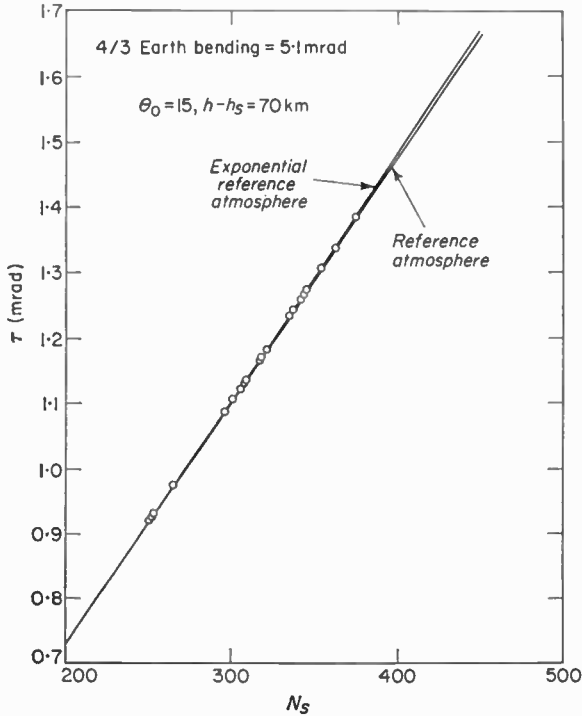


FIG. 11. Comparison of τ vs N_s as obtained from CRPL reference atmospheres—1958 and 5-yr mean radiosonde data.

In considering the comparisons of Figs. 10 and 11, one might ask if they reflect the form of the basic equation for bending; namely, at low angles is τ determined by the N gradient throughout the N profile, and at high angles is τ essentially a function of the value of N at both ends of the N profile (i.e. the limits of integration)? Thus one might expect the deviations to be smaller if the comparisons were made on the basis of a function of the N gradient such as ΔN , particularly for small values of θ_0 . Such a comparison is given by Figs. 12 and 13 for the same initial elevation angles and height increment as before. It is seen that the ΔN -specified reference atmospheres improve the agreement for the low-angle case, but decidedly decrease the agreement for the high-angle case.

A numerical evaluation of the root mean square (r.m.s.) deviation of the long-term mean bendings from both the reference atmospheres determined as a function of both ΔN and N_s has been made for a variety of initial elevation angles for the height increments 3 and 70 km. (Root mean square deviations were not calculated for the 4/3 earth model since this model is obviously in marked disagreement with the long-term mean bendings under these conditions.) Figure 14 summarizes the r.m.s. deviations for the height

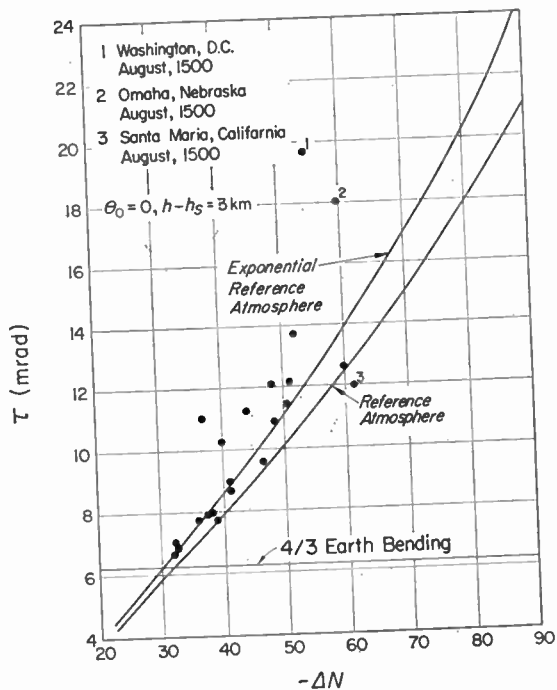


FIG. 12. Comparison of τ vs ΔN as obtained from CRPL reference atmospheres—1958 and 5-yr mean radiosonde data.

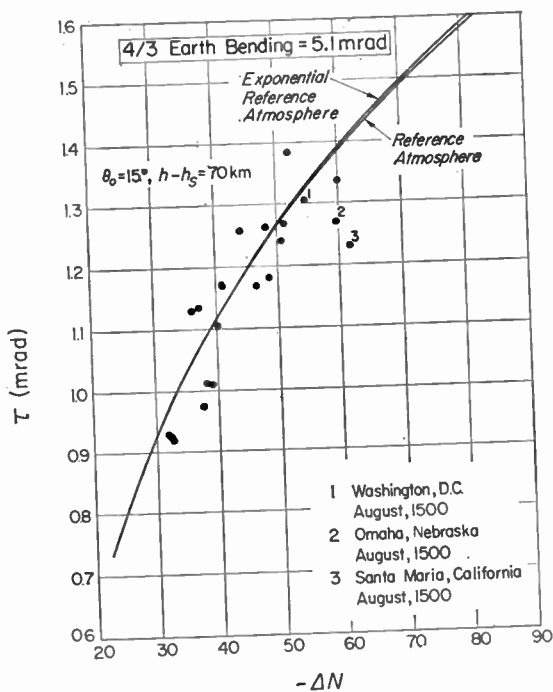


FIG. 13. Comparison of τ vs ΔN as obtained from CRPL reference atmospheres—1958 and 5-yr mean radiosonde data.

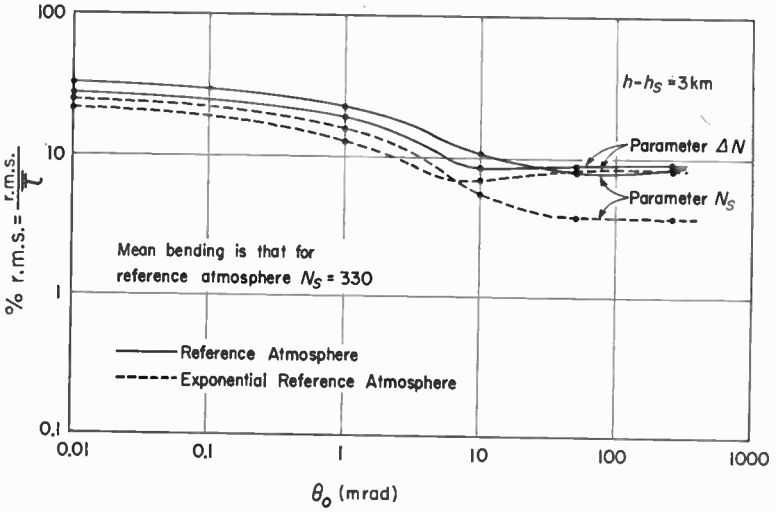


FIG. 14. Comparison of per cent r.m.s. deviations of 5-yr mean profile bendings about CRPL reference atmospheres using two parameters, N_s and ΔN .

interval ($h-h_s$) of 3 km. It is seen that for $\theta_0 < 10$ mrad (about 0.5°), the ΔN -specified reference atmospheres have the smaller r.m.s. deviations. Also, the exponential reference atmospheres, whether specified by ΔN or N_s , have smaller r.m.s. deviations than the reference atmospheres. For the height interval of 70-km case (Fig. 15) the N_s -specified reference atmospheres have a significantly smaller r.m.s. deviation than the ΔN -specified atmospheres

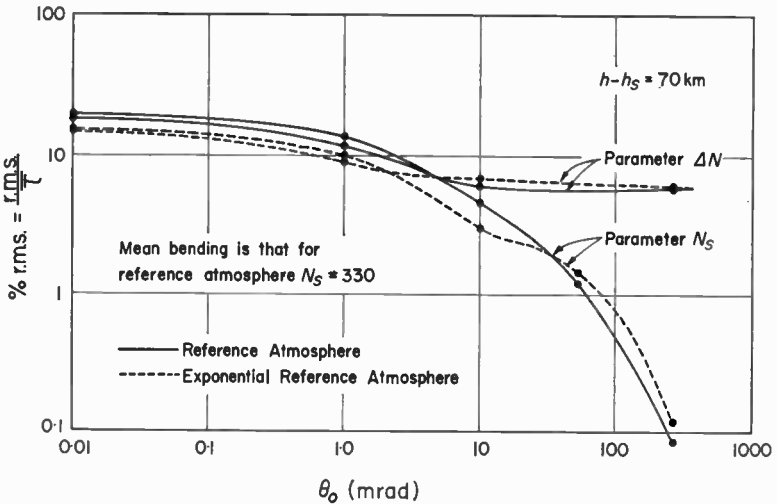


FIG. 15. Comparison of per cent r.m.s. deviations of 5-yr mean profile bendings about CRPL reference atmospheres using two parameters, N_s and ΔN .

for $\theta_0 > 5$ mrad. Again it may be noted that the exponential reference atmosphere generally has the smaller r.m.s. deviation for values of θ_0 less than 10 mrad. However, the slightly smaller r.m.s. deviations associated with the reference atmosphere for $\theta_0 > 10$ mrad reflects that model's closer agreement with the actual N structure of the atmosphere at high altitudes.

IX. THE INITIAL GRADIENT CORRECTION METHOD

The importance of the initial gradient in radio propagation, where the initial elevation angle of a ray path is near zero, has long been recognized. The effect of anomalous initial N -gradients on ray propagation at elevation angles near zero, and for gradients less than ducting

$$(dN/dh > -157 N \text{ units/km})$$

may be quite large. A method has been developed for correcting the predicted refraction (from the exponential reference atmosphere) to account for such anomalies, assuming that the actual value of the initial gradient is known (Bean and Thayer, 1959a). The result is

$$\tau_h = \tau_h(N_s, \theta_0) + [\tau_{100}(N_s^*, \theta_0) - \tau_{100}(N_s, \theta_0)] \tag{54}$$

where $\tau_h(N_s) = \tau$ at height h , for the exponential reference atmosphere corresponding to N_s , and N_s^* is the N_s for the exponential reference atmosphere that has the same initial gradient as the observed initial gradient; τ_{100} is τ at a height of 100 m. This procedure has the effect of correcting the predicted bending by assuming that the observed initial gradient exists

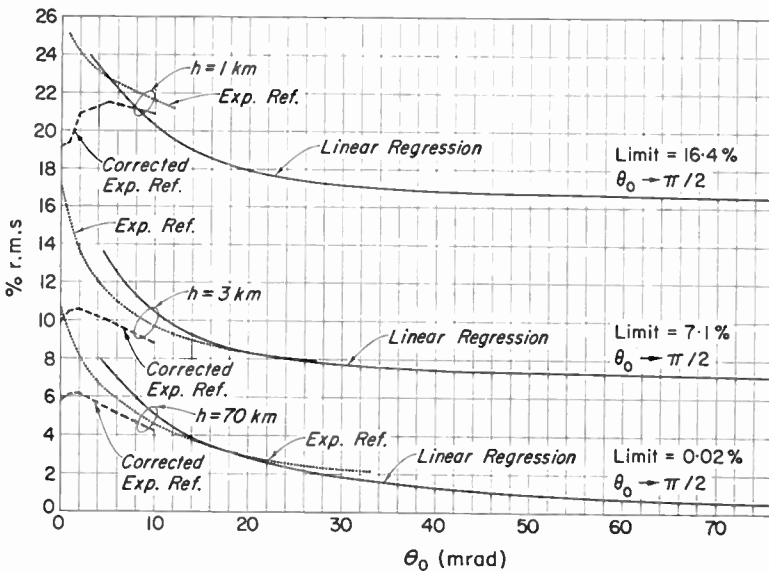


FIG. 16. R.M.S. error of predicting τ at various heights as a percentage of mean τ excluding super-refraction.

throughout a surface layer 100 m thick, calculating the bending at the top of the 100-m thick layer, then assuming that the atmosphere behaves according to the exponential reference profile corresponding to the observed value of N_s for all heights above 100 m. This approach has proved quite successful in predicting τ for initial elevation angles under 10 mrad, and will, of course, predict trapping when it occurs.

A comparison of the residual errors of predicting τ by the use of the Exponential Reference Atmosphere, the corrected exponential reference and the statistical regression method is given on Fig. 16. It is seen, for all combinations of target height and elevation angle greater than 10 mrad, that the statistical method yields sufficiently small residual errors as to justify its use in practical applications, especially considering the complexity of the other methods.

X. THE BI-EXPONENTIAL MODEL

The simple exponential model has been found to represent, to a first approximation, the average refractive index structure within a few kilometers above the ground for the United States (Bean and Thayer, 1959a), France (Misme, 1958), and Japan (Tao and Hirao, 1960). All of these investigations have reported varying degrees of departure of the actual atmosphere from this model, and Misme *et al.* (1960) have endeavored to delineate the regions of the world where the exponential model is most applicable. Subsequent analysis of several types of data, however, has shown this model to be more generally applicable than at first seemed likely and not unreasonable for use even in arctic and tropic locations (Bean and Thayer, 1960).

Suppose that $N = D + W$ where

$$D = \frac{77.6P}{T}$$

and

$$W = \frac{3.73 \times 10^5 e'}{T^2}$$

where P and e' are respectively the total pressure and partial pressure of water vapor in mb, then one may consider the height variation of each term separately. A model of the form

$$N(z) = D_0 \exp \left\{ -\frac{z}{H_d} \right\} + W_0 \exp \left\{ -\frac{z}{H_w} \right\}$$

may be used to describe the average decrease of N with height. D_0 and W_0 are the values of the D and W components at the earth's surface. This particular form has been found useful by Katz (1951), in his derivation of the potential refractive modulus and by Zhevankin and Troitskii (1959) in their treatment of atmospheric absorption. H_d and H_w are the scale heights of D and W respectively. It would be well in what follows to note that scale height, as used in this study, is merely the height at which the value of the atmospheric property has decreased to $1/e$ of its surface value. Typical values of D_0 , W_0 , and N_0 are listed for arctic, temperate and tropical locations

in Table IV. It is seen that the contribution of W to the total value of N is nearly negligible in the arctic but becomes greater as one passes from temperate to tropical climates. There is, of course, generally an inverse correlation between the magnitude of D and W since, at sea-level, where $P \sim 1000$ mb, the low arctic temperature increases the D term and, combined

TABLE IV. *Typical Average Values of D and W*

Station and Climate	D_0	W_0	N_0
Isachsen (78° 50'N) arctic	332.0	0.8	332.8
Washington, D.C. (38° 50'N) Temperate	266.1	58.5	324.6
Canton Island (2° 46'S) tropic	259.4	111.9	371.3

with low atmospheric water vapor capacity, decreases the wet term. Conversely, the higher temperatures of the temperate and tropical climates depress the D term and provide a greater water vapor capacity with the result that W may have a sizeable contribution to the total N .

One may examine N structure in a standard atmosphere as a guide to its general characteristics in the free atmosphere. As an example, the I.C.A.O. standard atmosphere (Minzner *et al.*, 1958), given in Fig. 17, may be con-

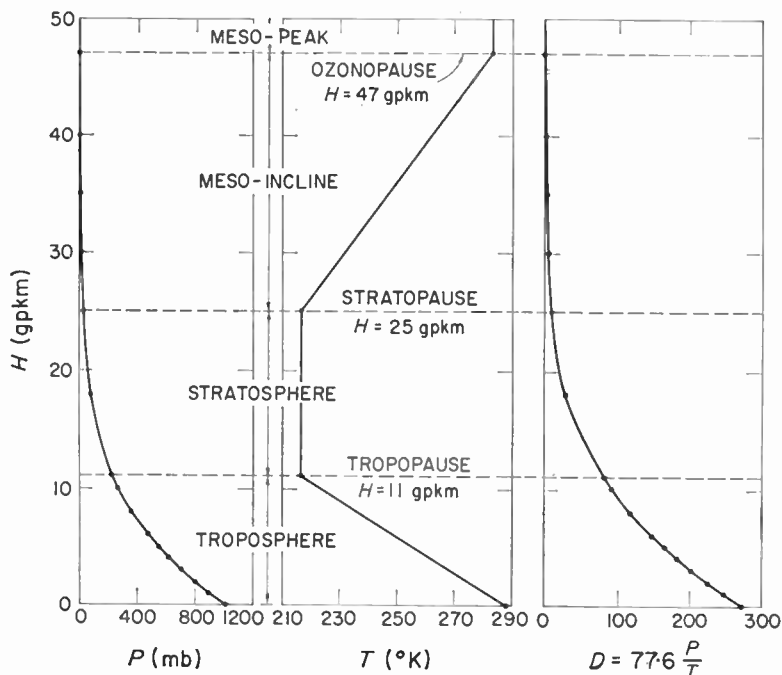


FIG. 17. The I.C.A.O. standard atmosphere (with an extension proposed in the U.S.).

sidered. The conditions specified for this atmosphere are an approximately exponential decrease of pressure (and therefore also of D) with respect to height and a linear temperature decrease from ground level to the tropopause. Figure 18 shows what these conditions mean in terms of the radio

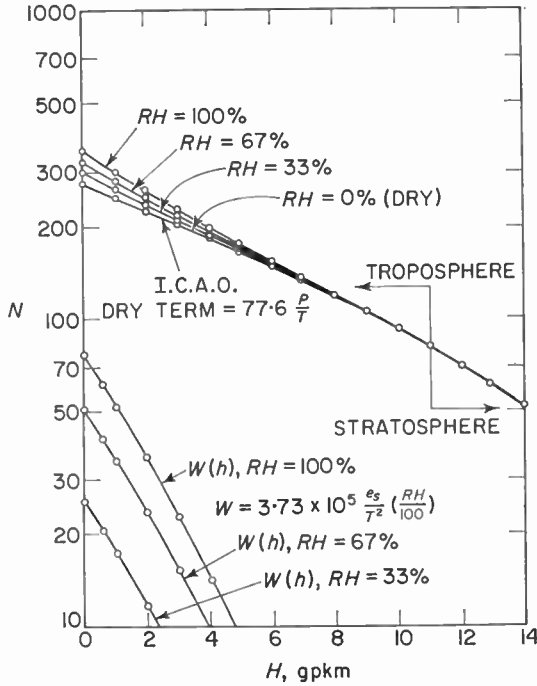


FIG. 18. N distribution for the I.C.A.O. standard atmosphere.

refractive index, and both D and W are seen to display an approximately exponential distribution from the surface to the tropopause. This conclusion is based upon the observation that the distribution is nearly linear, as one would expect if one wrote the function

$$y = A \exp(-h/c)$$

as

$$\ln y = -h/c + \ln A$$

which is the equation of a straight line on semi-logarithmic paper. The exponential distribution of W with height in this atmosphere follows naturally from the definition of constant relative humidity since the saturation vapor pressure, e_s , is itself, to a first approximation, an exponential function of temperature. It is evident that the value of W can significantly affect the surface values of N but has no appreciable effect upon the value of N at the tropopause.

An examination of long-term means from observations in the actual atmosphere shows that this same general bi-exponential trend is observed in practice, for temperate climates at least. Examples are given on Figs. 19 and 20 for Bismarck (North Dakota) and Brownsville (Texas). Bismarck is

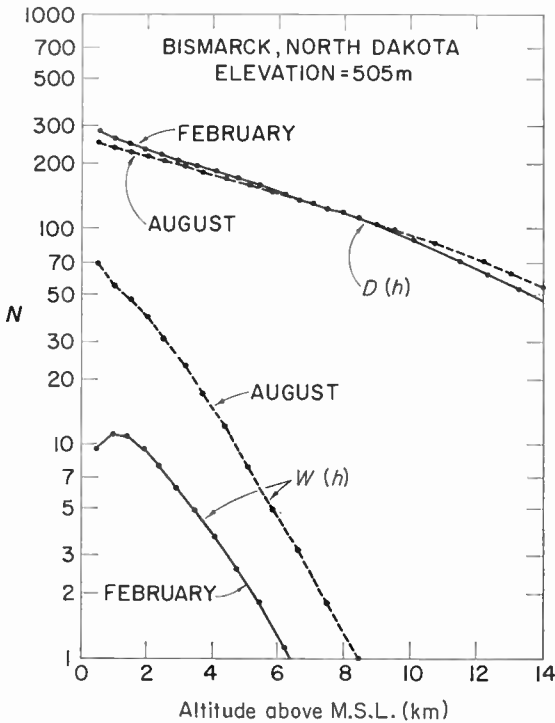


FIG. 19. N distribution for Bismarck, N. Dakota. (Note that altitude rather than geopotential height is used here to facilitate the eventual calculation of radio ray bending through actual atmospheric layers.)

typical of the high, dry, great plains region of North America which are frequently subjected to strong intrusions of arctic air; while Brownsville represents the humid periphery of the Gulf of Mexico. Even in these very dissimilar climates one finds a strong tendency towards a bi-exponential distribution of N , particularly when W is large.

Average values of D and W versus height have been determined for twenty-two U.S. radiosonde stations distributed at random about the country from published values of mean pressures, temperatures, and humidities for the United States (Ratner, 1945) which may then be converted into mean values of the refractive index with negligible error (Bean and Horn, 1959). The method of least squares has been used to determine the scale heights of the wet term, H_w , and of the dry term, H_d . Examination of

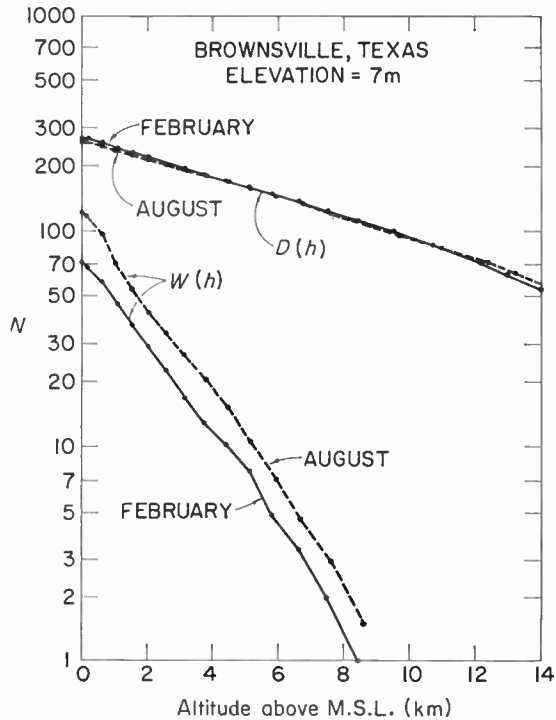


FIG. 20. N distribution for Brownsville, Texas.

these scale heights does not reveal any simple method of predicting their geographic and seasonal behavior, other than simply to map them. Such maps have been prepared for the United States for both winter (February) and summer (August); and the immediate conclusion that one reaches from these maps, Figs. 21 to 24, is that H_w has a year-round, country-wide average value of perhaps 2.5 km while H_d has an average value of about 9 km.

Since the scale height is the height at which the value of an atmospheric property has decreased to $1/e$ of its surface value it reflects the degree of stratification of the property. For example, cold arctic air is very stratified and has very little vertical motion with the result that its density scale height would be expected to be low. By contrast, tropical maritime air that has moved over land is characteristically unstable with convective activity thoroughly mixing the original moist surface air throughout the entire troposphere, and here the density scale height is relatively larger than in the case of arctic air. The dry term scale height on Figs. 21 and 23 shows a distinct tendency to be larger during the warm summer months when the atmosphere is well mixed to great heights with a consequent slower decrease of D with height. A slight geographical pattern is observed in the H_d maps: the coastal regions display somewhat higher values than the inland regions.

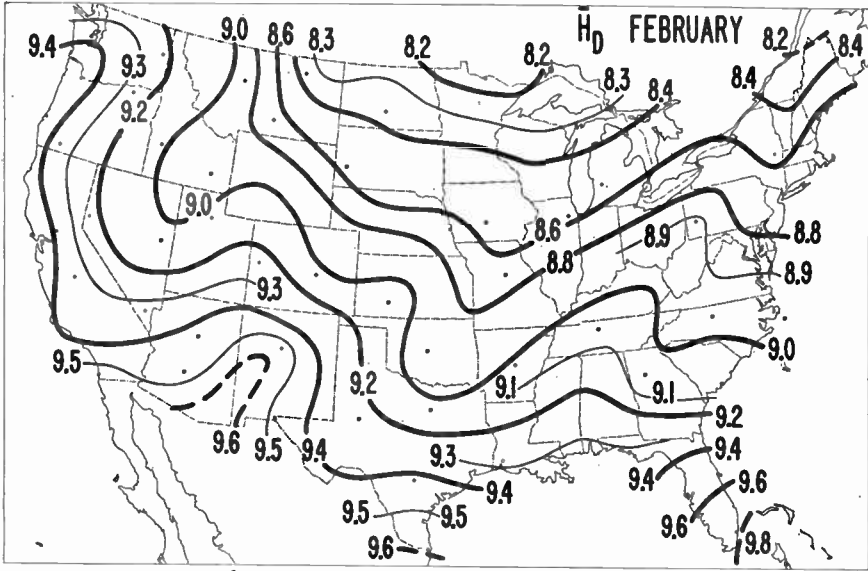


FIG. 21. Dry term scale height, \bar{H}_d , in kilometers, for February.

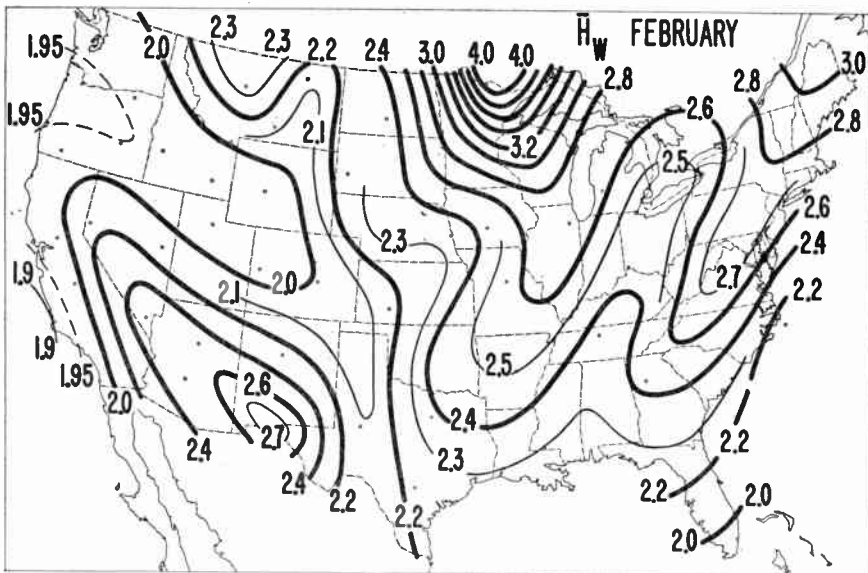


FIG. 22. Wet term scale height \bar{H}_w , in kilometers, for February.

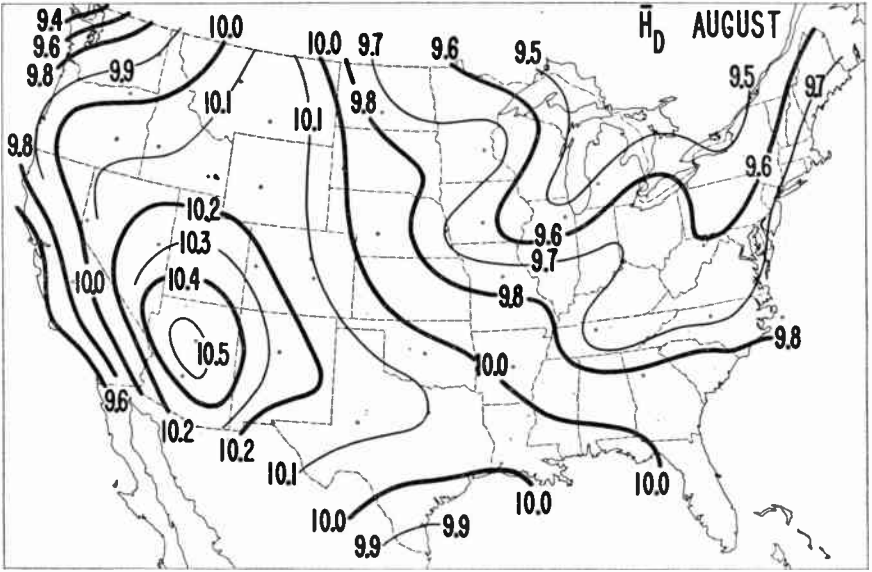


FIG. 23. Dry term scale height, \bar{H}_D , in kilometers, for August.

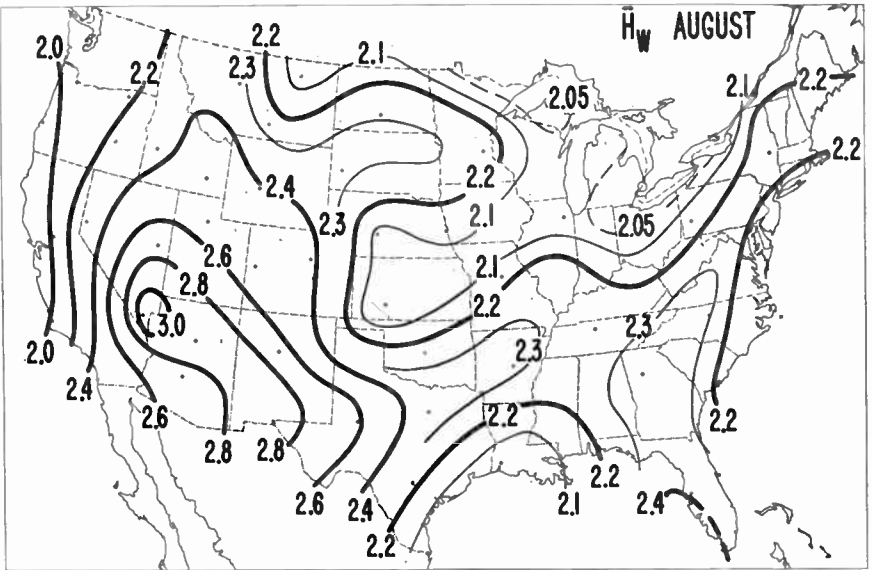


FIG. 24. Wet term scale height, \bar{H}_W , in kilometers, for August.

The north-south direction of the isopleths along the west coast on the February H_d map definitely reflects the uniform onshore advection of low-density maritime air. By contrast the east coast shows an east-west isopleth pattern, the high values in Florida reflecting the well-mixed nature of sub-tropical air, and the lower values in New England indicating the presence of the more dense and stratified continental air that customarily flows off-shore during the winter months. The same pattern is repeated on the summer-time map along the west coast, but is less pronounced on the east coast due to the combination of more uniform heating and also onshore advection of maritime air produced by the circulation pattern of the Bermuda high pressure area. The high value of $H_d = 10.5$ km observed in the southwest during the summer appears to be due to the intense heating with resultant convective mixing to great heights so common in that desert area. A somewhat opposite pattern is evidenced by the H_w maps. For example, the coastal areas generally have the lowest values and thus reflect the characteristic strong humidity stratification of maritime air. The smaller humidity gradients of the inland regions produce somewhat larger scale heights for that area. The summer H_w map is quite surprising in that very little variation is shown, perhaps indicating uniform vertical convection of the available moisture at all locations throughout the country. The strong convection indicated in the southwest on the summer H_d map is again reflected by the high value of $H_w = 3.0$ km for that same area.

The test of a model of atmospheric refractive index is the degree to which it represents the average N structure of the atmosphere. A further critical test is the degree to which the refraction, or bending, of a radio ray is represented by this atmosphere. The bending is given as the angular change of a radio ray as it passes from n_1 to n_2 in a spherically stratified atmosphere as represented by equation (7), and it has been obtained by numerical methods for the mean N profiles for one-half of the twenty-two United States weather stations mentioned earlier. The values of τ predicted by the bi-exponential model for these same stations has also been obtained by preparing U.S. maps of H_d and H_w from the other half of the data, selecting values of H_d and H_w for the test stations, calculating the bending and obtaining r.m.s. differences between these values and those obtained from the mean N profiles. These r.m.s. differences are shown on Fig. 25. Also, for comparison, the r.m.s. errors obtained from the C.R.P.L. exponential atmosphere are shown. This atmosphere, based upon a single exponential curve passing from the surface value, N_s , to the value at 1 km, N_1 , is founded upon equation (49).

It is quite evident from Fig. 25 that within the troposphere, $h \leq 10$ km, the bi-exponential model has a lower r.m.s. error for the common, near-zero angles of departure used in tropospheric propagation of radio waves. Both models yield about a 12 per cent error in determining τ for $\theta_0 = 0$ and $h = 11$ km. At $\theta_0 = 100$ mrad, however, the percentage error decreases to 4 per cent for the bi-exponential model and 7 per cent for the exponential reference atmosphere. The rather marked errors of the single exponential model at 10 km simply reflect the fact that that model is deliberately fitted to the average N structure over the first few kilometers with the result that this

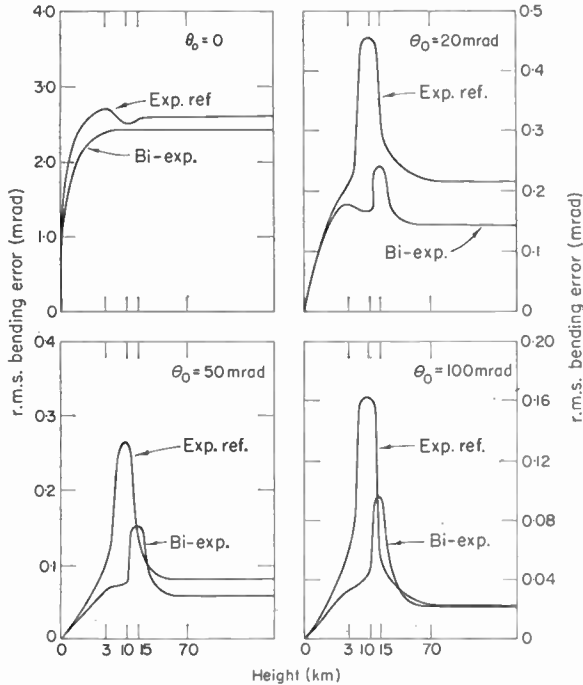


FIG. 25. R.M.S. errors of predicting bending for both the bi-exponential refractive index model and the CRPL (single) exponential atmosphere. Height is used here to indicate the actual thickness of atmosphere traversed by the radio ray.

model systematically departs from the average atmospheres in the vicinity of the tropopause. This is particularly apparent at the higher values of θ_0 where the integral tends to become proportional to the difference of the limits of integration. That is, using the theorem of the mean for integrals,

$$\tau = - \int_{n_s}^n \cot \theta \, dn \sim - \cot \theta_0 \int_{n_s}^n dn = [N_s - N] 10^{-6} \cot \theta_0$$

under the assumption that $\cot \theta$ may be replaced by $\cot \theta_0$ over the interval of integration. For $\theta_0 \leq 20$ mrad this assumption introduces less than a 10 per cent error for the interval $0 \leq h \leq 10$ km. It is apparent that the error in predicting τ for large θ_0 is then simply a matter of how closely the model approaches the true value of n in the atmosphere. At θ_0 near zero, however, the integral for τ is very heavily weighted towards the effect of n gradients near the earth's surface. Since the values of θ_0 normally involved in radio communication paths through the troposphere are near to zero, and both models show comparable r.m.s. errors for $\theta_0 = 0$, one concludes that there is no clear advantage to the bi-exponential model for this application. Furthermore, charts of H_d , H_w , D_0 , and W_0 are not available, and to

use the single exponential model one need only to refer to existing regional or world-wide maps (Bean and Horn, 1959; Bean *et al.*, 1960b). An obvious advantage of the bi-exponential model is that the scale heights do reflect the physical properties of the atmosphere in a much clearer way than does the single exponential model.

The data discussed above relate to the continental United States and one wonders if the same approach might be of utility in other regions. As a brief check the D and W term scale heights have been determined for conditions typical of the long arctic night (Isachsen, N.W.T., for February) and for humid tropical areas (Canton Island, South Pacific, February) from 5-year means of N versus height; and they are listed in Table V.

TABLE V. H_d and H_w for Arctic and Tropical Locations

Station	H_d km	H_w km
Canton Island	9.4	2.0
Isachsen	6.3	6.5

The extreme meteorological differences of these two locations are quite evident. The $H_d = 9.4$ km and $H_w = 2.0$ km at Canton Island indicate a warm atmosphere with a strong humidity gradient, while the value of $H_d = 6.3$ km at Isachsen indicates very stratified air with high surface density and a strong density decrease with height. The value of $H_w = 6.5$ km at Isachsen is due to a very low humidity gradient; in fact, at no point in the troposphere does W exceed 3 N units for this location and season. The value of $H_w = 2.6$ km reported for the characteristic altitude of water vapor for the middle belt of the U.S.S.R. (Zhevankin and Troitskii, 1959) also appears to be in agreement with the values given above for the U.S.

XI. THE DEPARTURES-FROM-NORMAL METHOD

A method of calculating bending by the use of the exponential model of $N(h)$ together with an observed $N(h)$ profile has been given by Bean and Dutton (1960). This method is primarily intended to point out the difference between actual ray-bending and the average bending that is predicted by the exponential $N(h)$ profile and is a powerful method of identifying air mass refraction effects. The exponential model described in Section VIII can be expected to represent average refractivity profile characteristics at any given location, but it cannot be expected to depict accurately any single refractivity profile selected at random, even though it may occasionally do so. In order to study the differences between individual observed $N(h)$ profiles and the mean profiles predicted by the exponential model, a variable called the A -unit has been developed; it is defined simply as the sum of the observed N at any height, h , and the refractivity decrease from the surface to the height, h , which is predicted by the exponential profile for a given value of N_s .

That is:

$$A(N_s, h) = N(h) + N_s(1 - \exp\{-c_e h\}) \tag{55}$$

Thus (55) adds to $N(h)$ the average decrease of N with height, so that if a particular profile should happen, by coincidence, to be the same as the corresponding exponential profile, the value of $A(N_s, h)$ for this profile would be equal to N_s for all heights. The above analysis shows that the difference between $A(N_s, h)$ and N_s , $\delta A(N_s, h)$, is a measure of the departure of $N(h)$ from the normal, exponential profile:

$$\delta A(N_s, h) = A(N_s, h) - N_s = N(h) - N_s \exp\{-c_e h\} \tag{56}$$

It seems logical to expect that the application of the A -unit to bending would indicate the departures of bending from normal, in some way, just as it indicates departures of refractivity, N , from normal. This is indeed the case, as can be seen in Fig. 26, where, for an $N_s = 313.0$ exponential atmosphere,

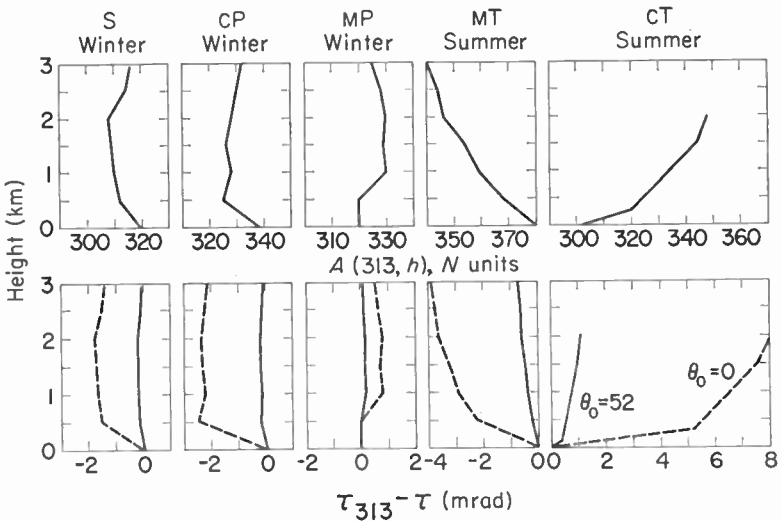


FIG. 26. Departure of N structure and bending from that expected in the $N_s = 313$ exponential reference atmosphere. Air mass classification: S, Superior; cP, Polar Continental; MP, Polar Maritime; MT, Tropical Maritime; cT, Tropical Continental.

$A(313.0, h)$ is plotted on one set of graphs for various typical air masses, and the corresponding bending departures from normal are shown in the second set of graphs corresponding to the same air masses. Obviously, the bending departures between layers are highly analogous to the A -unit variation. It can be seen from Fig. 26 that the similarity exists, although it is less, for higher initial elevation angles. The similarity also decreases with increasing height, owing to the fact that the bending departures from normal are an integrated effect, and at low initial elevation angles are more sensitive to N -variations at the lower heights. This causes an apparent damping of

the bending departures from normal at greater heights. However, the A -unit variation is not similarly influenced; hence, a loss of similarity arises at large heights above the earth's surface.

If (55) is differentiated and substituted into (7) the following equation results:

$$\tau_{0,h} \underset{\text{(rad)}}{\cong} \tau_{N_s}(h) + \sum_{k=0}^{k_h} - \frac{2}{\theta_k + \theta_{k+1}} \left[\frac{\Delta A(N_s)}{N_k} \right]^{N_{k+1}} \times 10^{-6} \quad (57)$$

where

$$\Delta A(N_s) = \Delta N(h) + \Delta [N_s \{1 - \exp(-c_e h)\}] = \Delta N(h) + N_s c_e \exp(-c_e h) \Delta h$$

$\tau_{N_s}(h)$ is the value of τ tabulated for various exponential atmospheres (Bean and Thayer, 1959b), θ_k and θ_{k+1} arc in milliradians and must be from the N_s exponential atmosphere used. $\Delta A(N_s)$ is obtained from subtraction of the A value at layer level, k , from the value of A at layer, $k+1$. The A value may be obtained by adding any given $N(h)$ value, obtained from radiosonde or other similar data, to a value of $N_s [1 - \exp\{-ch\}]$ for the same height, which may be obtained from Fig. 27. Since $\tau_{N_s}(h)$ has been calculated only

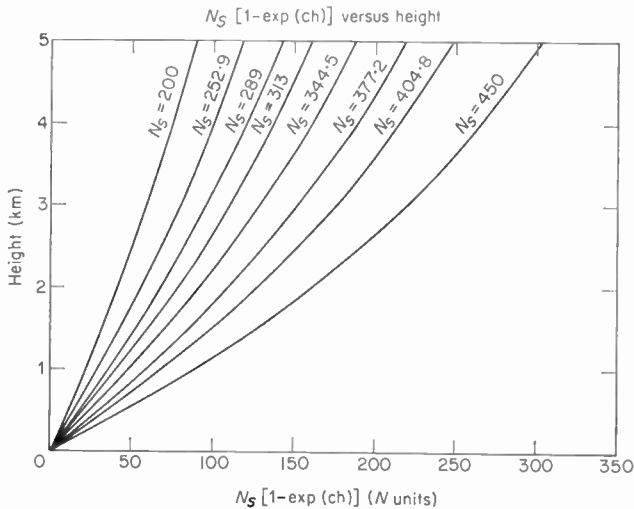


FIG. 27. $N_s [1 - \exp(ch)]$ versus height.

for a few of the exponential atmospheres, these being the $N_s = 200.0, 252.9, 289.0, 313.0, 344.5, 377.2, 404.8,$ and 450.0 atmospheres, one of these atmospheres must be used in the calculation of bending by the departures method. The selection of the particular atmosphere to be used is based on the value of the gradient of $N, dN/dh$, between the surface of the earth and the first layer considered. The ranges of the gradient for the choice of a particular exponential atmosphere are shown in Table II.

XII. A GRAPHICAL METHOD

Weisbrod and Anderson (1959) have presented a convenient graphical method for computing refraction in the troposphere. Rewriting and enlarging (21), one obtains

$$\tau(\text{mrad}) = \sum_{k=0}^n \frac{N_{k+1} - N_k}{500(\tan \theta_k + \tan \theta_{k+1})} \tag{58}$$

where τ will be the total bending through n layers. Terms for the denomi-

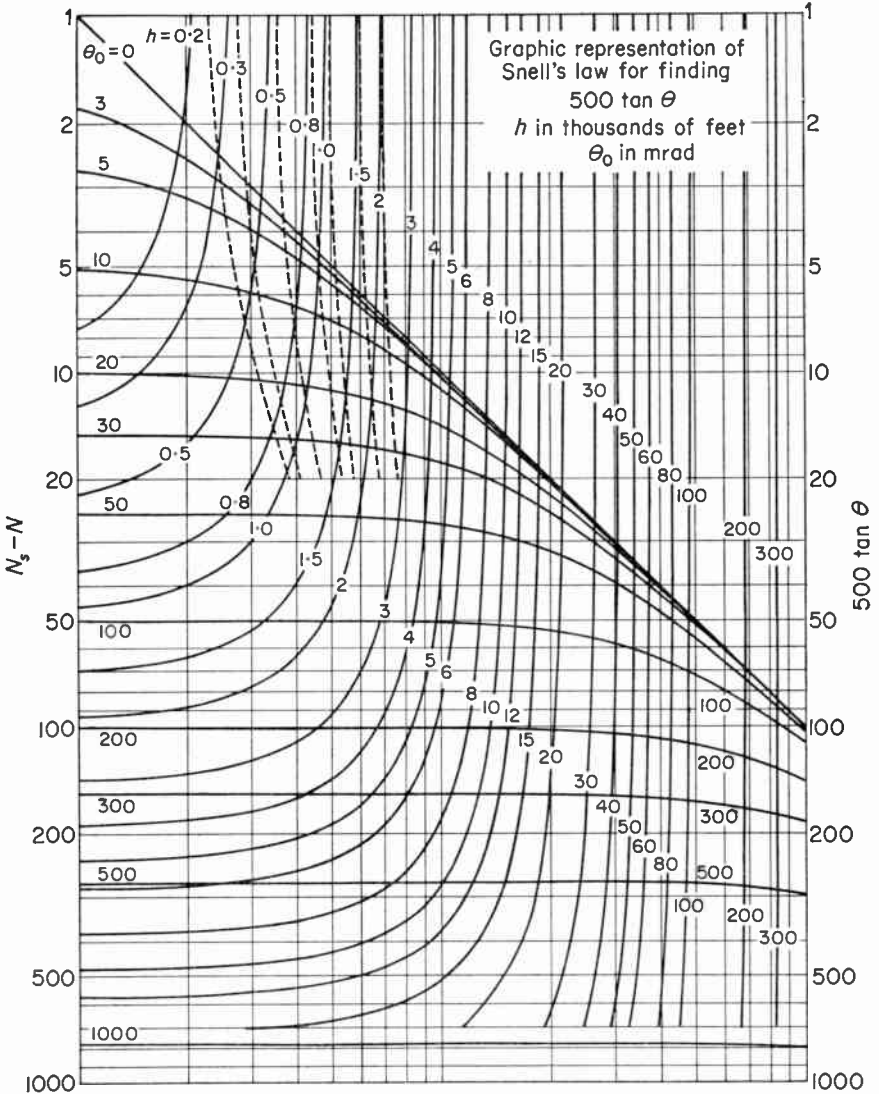


FIG. 28. Graphic representation of Snell's Law for finding $500 \tan \theta$.

ator can be determined from Fig. 28. Equation (58) is essentially Schulkin's result with only the approximation, $\tan \theta_k \cong \theta_k$, for small angles omitted. The procedure for using Fig. 28 follows. Enter on the left margin at the appropriate $N_s - N(h)$. Proceed horizontally to the proper height, h , interpolating between curves if necessary. Use the solid height curves when $N_s - N(h)$ is positive and the dashed curves when $N_s - N(h)$ is negative. Then proceed vertically to the assumed θ_0 and read $500 \tan \theta$ along the right margin.

XIII. EFFECT OF ATMOSPHERIC HORIZONTAL INHOMOGENEITY UPON RAY TRACING

It is common in ray tracing studies to assume that the refractive index of the atmosphere is spherically stratified with respect to the surface of the earth. Thus, the effect of refractive index changes in the horizontal direction is normally not considered, although Wong (1958) has considered the effect of mathematically smooth horizontal changes in airborne propagation problems.

Neglecting the effect of horizontal gradients seems quite reasonable in the troposphere because of the relatively slow horizontal change of refractive index in contrast to the rapid decrease with height. In fact, examination of climatic data indicates that one must compare sea level stations located 100 km from each other on the earth's surface in order to observe a difference in refractive index values which would be comparable to that obtained by making any one of these locations and comparing its surface value with the refractive index 1 km above the location. Although the assumption of small horizontal changes of the refractive index appears to be true in the average or climatic sense, there are many special cases such as variations occurring in frontal zones and land-sea breeze effects where one would expect the refractive index to change abruptly within the horizontal distance (80 km or so) traversed by a tangential ray passing through the first kilometer in height.

Two cases of such marked horizontal change of refractive index conditions have been studied: one which occurred over the Canterbury Plain in New Zealand and the other at Cape Canaveral,† Florida. Although these particular sites were chosen for several reasons such as land-to-sea paths and a sub-tropical location (where marked changes in refraction conditions are common) the major consideration was that detailed aircraft and ground meteorological observations were available for prolonged periods. These detailed measurements allow a quantitative evaluation to be made of the error which may be incurred by assuming that the refractive index is horizontally stratified. First one determines the refractive index structure vertically over the transmitter and assumes that this same structure describes the atmosphere vertically everywhere. Rays are then traced through this horizontally laminated atmosphere. These ray paths may then be compared with those obtained by the step-by-step ray tracing through the detailed convolutions of refractive index structure in the two cases under study to

† Now Cape Kennedy.

evaluate the degree of confidence to which standard prediction methods may be used under conditions of horizontal inhomogeneity.

The Canterbury data were compiled by a radio meteorological team working from September 1946, through November 1947, on the South Island of New Zealand under the leadership of R. S. Unwin (Report of Canterbury Project, 1951). The report was very carefully prepared, giving minute details of the experiment on a day-to-day basis. Anson aircraft and a trawler were used for meteorological measurements over the sea, and three mobile sounding trucks for observations on land. The trucks and the trawler carried wiresonde equipment, whereby elements for measuring temperature and humidity up to a height of 150 m to 600 m (depending on wind conditions) were raised by means of balloons or kites. Standard meteorological instruments provided a continuous record of wind, surface pressure, temperature, and humidity at stations at the coast and 14 km and 38 km inland. The headquarters of the project were at Ashburton Aerodrome, and the observations extended out to sea on a line perpendicular to the coastline of Canterbury Plain. Aircraft were equipped with a wet-bulb and dry-bulb psychrometer, mounted on the portside above the wing. Readings were taken three or four times on each horizontal flight leg of 2 or 3 min duration. Special lag and airspeed corrections were applied, resulting in accuracy of $\pm 0.1^\circ\text{C}$. It was found that, under the variety of conditions in which observations were made, the aircraft flights were more or less parallel to the surface isobars; hence, the sea-level pressure as recorded at the beach site was considered to hold over the whole track covered by the aircraft. The relationship used for calculating the pressure, P , in millibars at a height h in feet was:

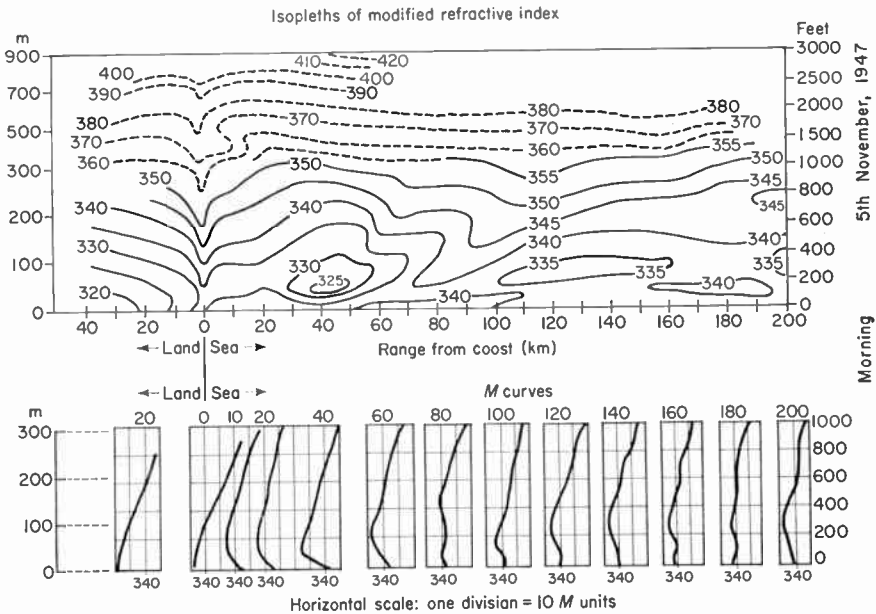
$$P(h) = P_0 - h/30$$

where P_0 is the surface pressure. This approximation (determined by averaging the effect of the temperature and humidity distributions on pressure in a column of air) resulted in a maximum error in the refractivity of 0.5 per cent at 900 m. Radiosonde ascents at Hokitika on the west coast of South Island and Paraparaumu and Auckland on North Island were used to supplement the aircraft measurements, particularly in the altitude levels above 1 km.

The synoptic situation for the morning of 5 November 1947, has been selected as an example of unusually heterogeneous conditions since it revealed a surface-ducting gradient near the coast with an elevated layer about 100 km offshore. A cross-section of the area from Ashburton to a point 200 km offshore has been plotted with all available data, and isopleths of modified refractive index, M , drawn to intervals of 2.5 units.

$$M = (n - 1 + K_e h)10^6$$

where $K_e = (15.70) (10^{-8})/\text{m}$. A simplified version of the lower portion of this cross-section with the corresponding M curves is accompanied by a sketch of the general location of the experiment in Fig. 29. Some smoothing has proved necessary, particularly near the sea surface and in those areas



Note: vertical scale change above 300m

(Adapted from Canterbury project)

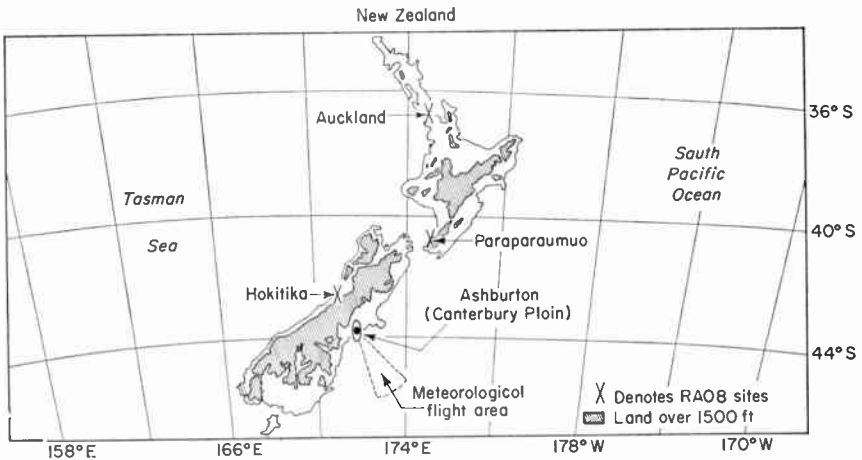


FIG. 29. Isopleths and curves of refractive index for 5 November 1947, at Canterbury, with a map locating sources of meteorological data. (Reproduced by courtesy of the Canterbury project.)

where aircraft slant ascents and descents caused lag errors in altimeter readings and in temperature and humidity elements. Isopleths over land have been plotted above surface rather than above sea level with an additional adjustment in the scale ratios of height and distance in an attempt to simplify the reading of values from the diagram.

The second data source is the Cape Canaveral to Nassau path for the period of 24 April to 8 May 1957. This material was supplied by the Wave Propagation Branch of Naval Research Laboratories and the University of Florida. The particular case chosen for study is the meteorological profile of 7 May 1957 (2 000 e.s.t.), due to its heterogeneous nature, which shows a well-defined elevated layer at about 1 500 m. Fourteen refractometer soundings from aircraft measurements taken at various locations along the 487-km path (Fig. 30) and six refractive index profiles (deduced from radiosonde ascents from Cape Canaveral, Grand Bahama Island, and Eleuthera Island) have been read in order to plot a cross-section of the atmosphere representing as closely as possible the actual refractive conditions at that time. Unfortunately the data near the surface (up to 300 m) were quite sparse compared to those recorded in the Canterbury Project, and calibration and lag errors had not been noted as carefully in the report which was available; some interpolation and considerable smoothing of refractive index values have therefore been necessary when drawing isopleths.

One may evaluate the bending of a radio ray by successive application of the formulas of Section I. Normally the use of these equations is quite straightforward. When considering horizontal changes in n , however, one must satisfy these equations by iterative methods. In the present application, since n has to be determined by graphical methods, it is considered to be sufficient to assume a constant distance increment of 250 to 500 m, solve for appropriate height increment from

$$\Delta h = \Delta d \tan \theta_1 \left[1 + \frac{h}{a} \right]$$

graphically determine N for the point $d_1 + \Delta d$, $h_1 + \Delta h$ and then determine θ_2 and $\tau_{1,2}$. This type of ray tracing has been done for various rays of initial elevation angles between 261.8 mrad (15°) and 10 mrad ($\sim 0.5^\circ$). The calculations were not carried to smaller elevation angles since the method is not valid within surface ducts for initial elevation angles below the angle of penetration (Kerr, 1951; Bean, 1959).

Although both of the calculated ray paths correspond to oversea propagation with coastal transmission sites, they are quite different in other aspects. Canterbury Plain is located southeast of the 10 000-ft chain of the Southern New Zealand Alps at a latitude of 44°S (the equatorward edge of the westerly belt of winds in November). Cape Canaveral is located on a sea level peninsula at 28°N (the poleward edge of the northeast trade circulation in May). While the Canterbury profile shows superrefractive tendencies, the Canaveral profile illustrates subrefraction at the surface counterbalanced by an elevated trade wind inversion layer, indicating that the total bending values of Canterbury should be higher than normal, while the Canaveral

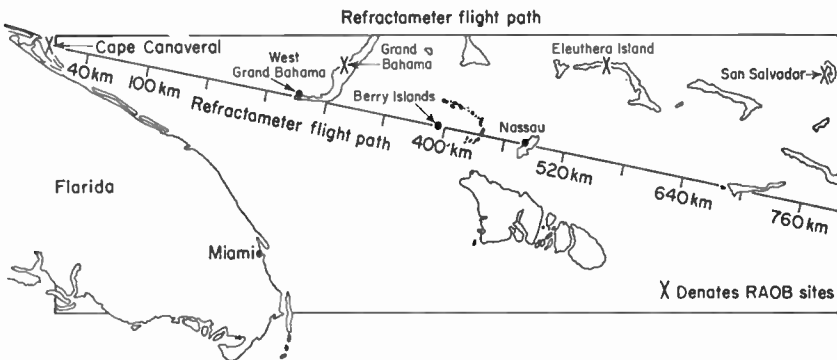
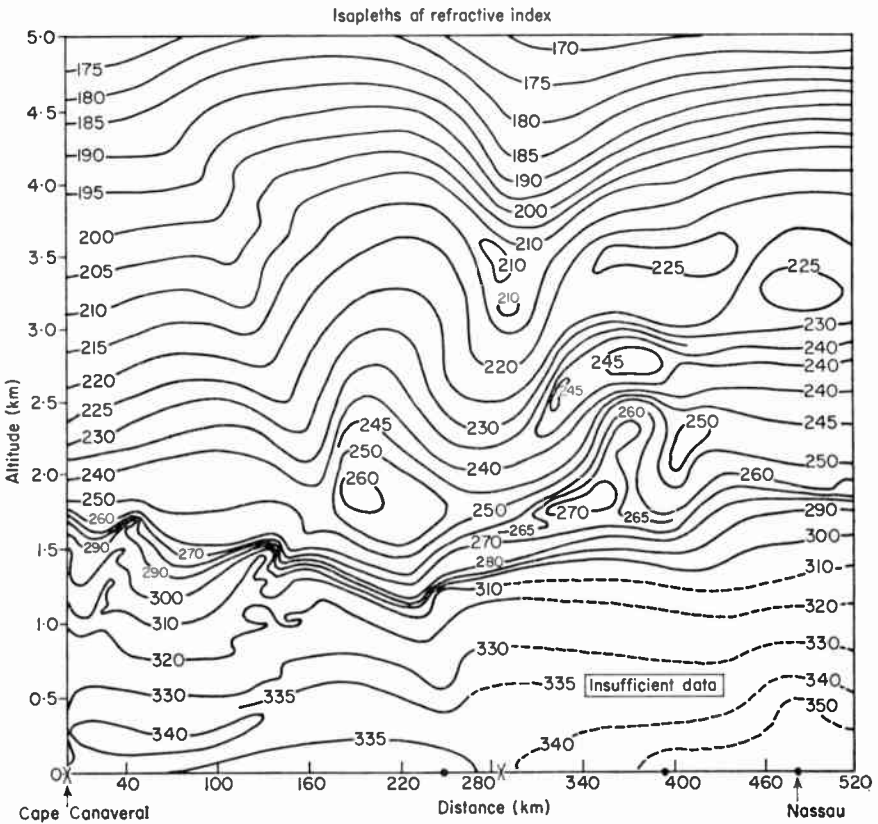


FIG. 30. Isopleths of refractive index and map of refractometer flight for 7 May 1957, Cape Canaveral to Nassau.

example should have values near or lower than normal. These differences are illustrated by Figs. 31 and 32 where the bending, τ , in milliradians is plotted versus altitude in kilometers. The effect of horizontal changes is most pronounced for rays with initial elevation angles of 10 mrad. On these figures the term "vertical" ray is used to designate the ray path through the horizontally homogeneous n structure determined from the refractive index vertically over the station. The term "horizontal" ray designates the ray path through the complex actual n structure. It is quite evident that a consistent difference in bending of about 1 mrad exists between the "vertical"

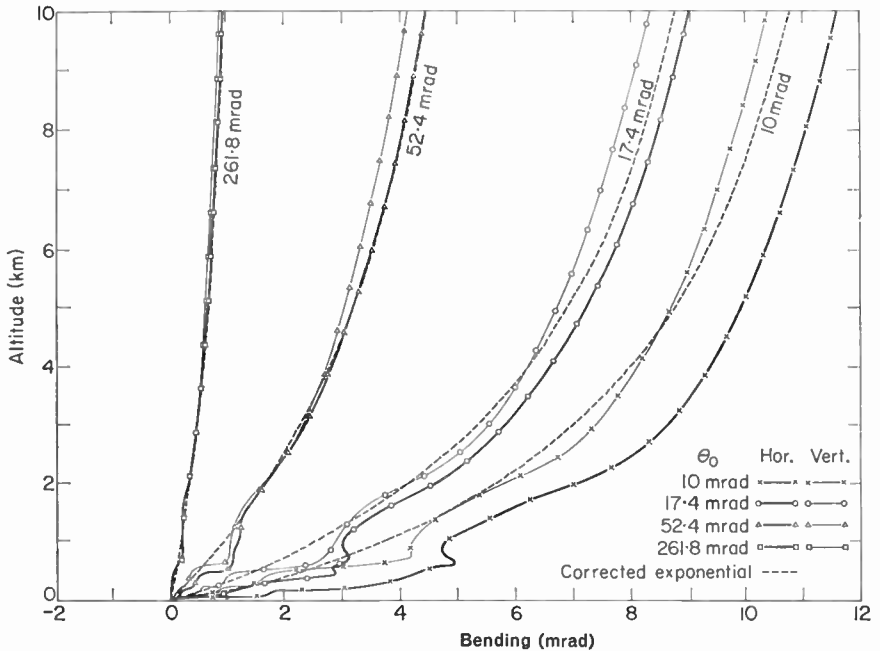


FIG. 31. Canterbury, 0 to 10 km, altitude versus ray bending.

and "horizontal" rays at Canterbury above 1 km for $\theta_0 = 10$ mrad. This would be expected since the vertical M profile at the beach (our hypothetical transmitter site) is nearly normal in gradient while as little as 10 km out to sea a duct exists, thus indicating a near maximum difference between the "horizontal" and the "vertical" rays at any initial elevation angle small enough to be affected by the duct. This is in contrast, however, with the case of Cape Canaveral where, except for the region of the elevated duct centered at about 1 500 m, the "vertical" and "horizontal" rays are in quite close agreement. These two examples illustrate that horizontal variations near to the surface produce the greatest effects. The importance of the altitude of the variation is due to the fact that refraction effects are very heavily weighted toward the initial layers (Bean, 1959).

Also shown on Figs. 31 and 32 are the values of the bending which would be predicted from the Central Radio Propagation Laboratory corrected exponential reference atmosphere (Bean and Thayer, 1959). These values have been derived from the value of N at the transmitter site as corrected by the vertical gradient over the first 100 m. It is noted that, for $\theta_0 = 10$ mrad at Canterbury, the value of bending predicted by the model is in essential agreement with the "vertical ray" bending but underestimates the "horizontal ray" (which has the largest variation of n with horizontal distance) by about 1.25 mrad. For Cape Canaveral at $\theta_0 = 10$ mrad, the model

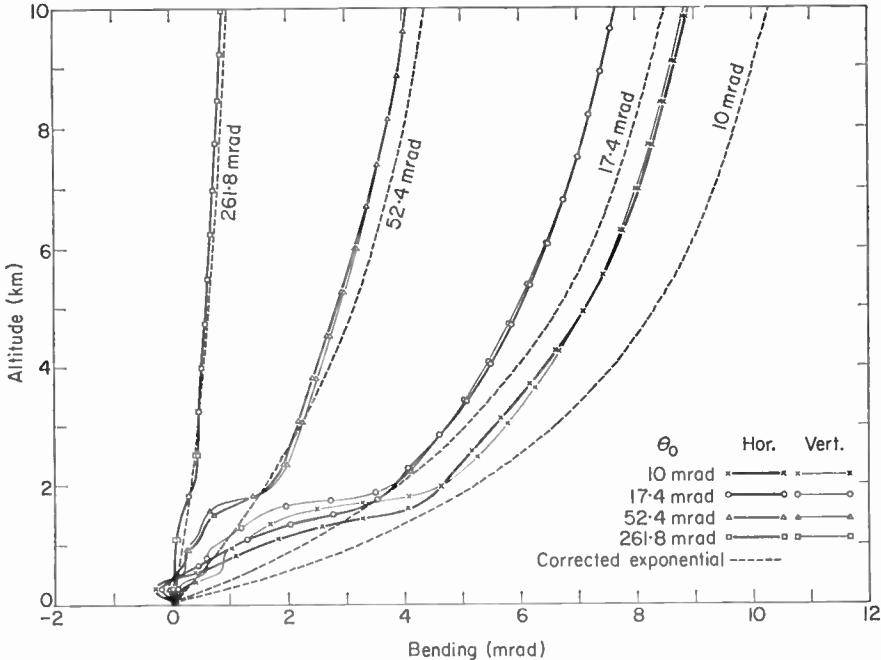


FIG. 32. Cape Canaveral, 0 to 10 km, altitude versus ray bending.

atmosphere overestimates the bending by about 1.25 mrad for altitudes in excess of 2 km. It should be emphasized that, although the model exponential atmosphere appears to represent the average of the two specific cases studied, the departure from this average arises from quite different causes in each case. The differences in the Canterbury case arise from the marked effect of horizontal variation of n , as is indicated by the agreement of the vertical ray bending with the model atmosphere. The disagreement in the Canaveral case is due to the presence of a very shallow surface layer of nearly normal gradient topped by a strong subrefractive layer; it therefore represents a shortcoming of the model rather than an effect of horizontal changes of n .

The preceding analysis of bending throws the refractive differences in

each case into sharp relief. The effect of refraction, of course, is to vary the ray path. Figures 33 and 34 show the ray paths corresponding to the bendings of Figs. 31 and 32. Note that for Canterbury at $\theta_0 = 10$ mrad the effect of

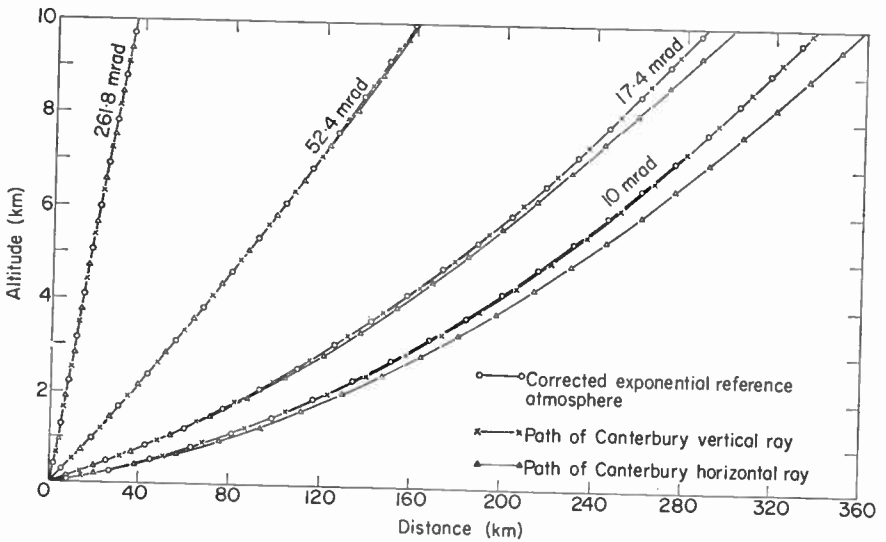


FIG. 33. Canterbury, 0 to 10 km, altitude of ray versus distance.

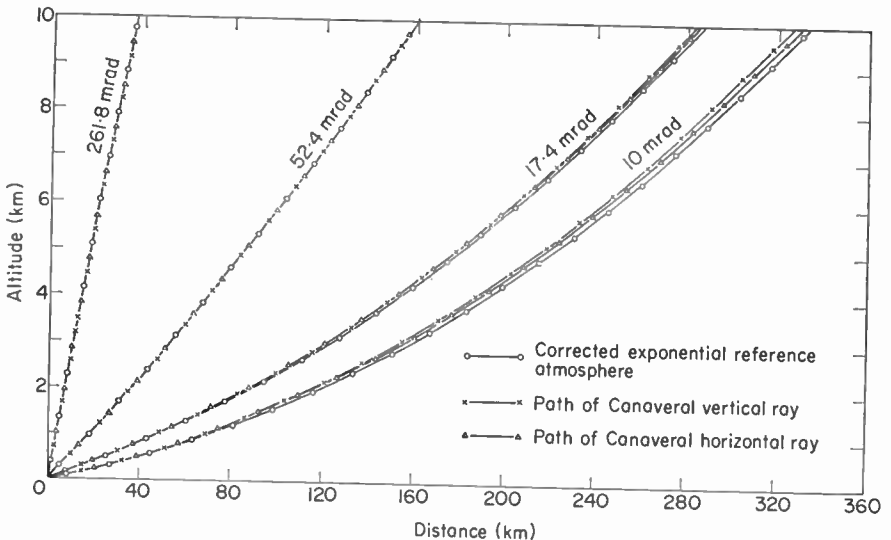


FIG. 34. Cape Canaveral, 0 to 10 km, altitude of ray versus distance.

the horizontal variation of n is to produce a difference in estimation of about 1 km in height or 20 km in ground distance at 300 km from what would be obtained from considering the vertical n profile as a representation of the

entire path. The effect of the subrefractive layer at Cape Canaveral is not so large, but it does cause an overestimation of the ground distance by about 5 km and an underestimation of the height by less than one-quarter of a kilometer at a ground distance of 300 km by assuming that the vertical profile may be used throughout the entire ray path.

It should be pointed out that the ducting case at Canterbury represents an extreme refraction condition and is not necessarily typical of conditions observed in other regions or, indeed, at Canterbury. The Canterbury project was purposely restricted to a study of ducting conditions with the result that less than 20 per cent of the total observations for the 15 months are reported. Therefore, because one of the more extreme cases is represented by the 5 November example, one might conclude that much less than 20 per cent of the observations would show the same degree of horizontal n change as the profile studied.

If one further hypothesizes that the greatest horizontal n change would be associated with ducting conditions, then the percentage incidence of ducts as evaluated from radiosonde observations, listed for various stations in Table VI, would indicate that the effects of horizontal changes of n sufficient to cause variations in the ray path as large as those of the present study would be observed less than 15 per cent of the time, regardless of geographic

TABLE VI. *Percentage Occurrence of Surface Ducts During the Years 1952 to 1956*

Station	% Incidence			
	February	May	August	November
Fairbanks, Alaska	9.4	0.4	0.4	6.2
Columbia, Mo.	0.7	2.5	8.4	1.3
Washington, D.C.	0.7	4.8	4.3	1.4
Canton Island	10.0	9.2	12.4	11.5
Miami, Fla.	0.7	3.5	8.5	2.7

TABLE VII. *Percentage Occurrence of Surface Subrefractive Layers During the Years 1952 to 1956*

Station	% Incidence			
	February	May	August	November
Fairbanks, Alaska	0.0	0.0	1.2	0.4
Columbia, Mo.	0.0	1.6	0.6	4.0
Washington, D.C.	0.9	2.2	5.8	2.7
Canton Island	0.0	0.0	0.0	0.3
Miami, Fla.	0.7	0.3	0.9	0.7

locations. The probable importance of subrefractive layers upon the prediction of refraction effects has emerged as a secondary result of the present study. Although subrefraction is normally neglected, it is potentially a very important refractive factor for distances of, say, less than 40 km. Even though the percentage occurrence of subrefractive layers can be as large as 6 per cent (see Table VII), this effect is frequently offset by the concurrent occurrence of an adjacent superrefractive layer, as is illustrated by the Cape Canaveral example.

XIV. COMPARISON OF OBSERVED ATMOSPHERIC RADIO REFRACTION EFFECTS WITH VALUES PREDICTED THROUGH THE USE OF SURFACE WEATHER OBSERVATIONS

The atmospheric radio refraction effects considered here are of two general types: errors in measuring distance by means of timing the transit of radio signals between two points, known as radio range errors, and errors in estimating the elevation angle of a target by means of measuring the angle of arrival of radio signals from the target, known as elevation angle errors. The systematic bias due to these refraction effects may be removed by use of the surface value of the radio refractivity, N_s , a quantity which can be measured directly with a microwave refractometer, or calculated from the ordinary meteorological variables of temperature, pressure, and humidity, to predict values of either range error or elevation angle error as discussed previously.

The elevation angle error, ϵ , is the difference between the apparent direction to a target, as indicated by the angle of arrival of a normal to the radio wavefront, and the true direction. This error is primarily a function of the refraction, or bending, of the radio ray. For targets beyond the atmosphere the two quantities are asymptotically equal (with increasing range). The values of ϵ and τ at any point on the ray path obey the following inequality:

$$\tau/2 \leq \epsilon \leq \tau$$

Recalling that the bending of a radio ray may be expressed by an equation of the form

$$\tau = a + bN_s$$

where a and b are functions of the initial elevation angle of the ray, θ_0 , and the height (or range) along the ray path at which the bending is to be calculated. This assumption can be checked by examining the behavior of values of τ , ray-traced for a number of observed height-profiles of radio refractive index, plotted against the corresponding values of N_s . Such a plot is shown in Fig. 35, for a small initial elevation angle, 50 mrad (about 3°), and a "target" height beyond the atmosphere, 70 km. The family of N -profiles used in ray-tracing this sample of bending values is referred to as the CRPL Standard Sample. It can be seen from inspection of Fig. 35 that the assumption of linearity expressed in (1) is justified for this case. A similar conclusion can be reached from examination of data for other cases, including low target heights and elevation angles down to zero degrees, although for these

extremes the degree of correlation between ε and N_s is not as marked as that shown in Fig. 35.

The other refraction variable, the radio range error, ΔR_e , is here defined as being that error incurred in measuring the distance between two points by means of timing the transit of radio signals between the points assuming

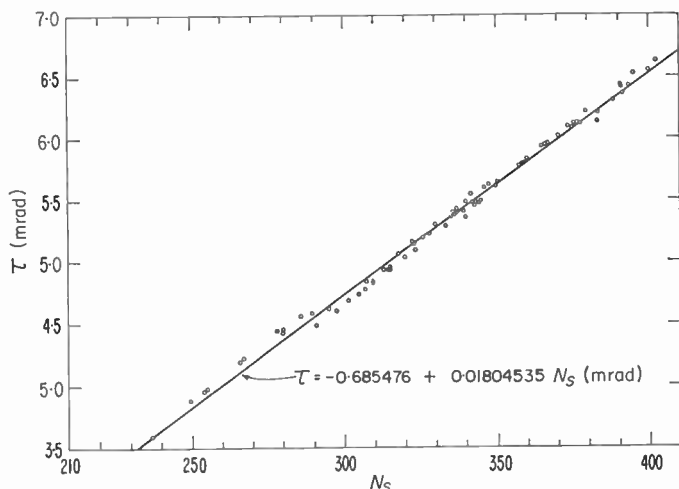


FIG. 35. Total refraction at $\theta_0 = 50$ mrad, $h = 70$ km, for the CRPL standard sample.

that the velocity of propagation is equal to that of free space. For the case of a radio ray, this error is composed of two parts: the difference between the curved length of the ray path, the geometric range, R_g , and the true slant range, R_0 ; and the discrepancy caused by the lowered velocity of propagation in a refractive medium. The geometric range is given by

$$R_g = \int_0^{h_t} \operatorname{cosec} \theta \, dh$$

and the apparent, or radio, range by

$$R_e = \int_0^{h_t} n \operatorname{cosec} \theta \, dh$$

Thus the total radio range error, $\Delta R_e = R_e - R_0$, is given by

$$\Delta R_e = \int_0^{h_t} n \operatorname{cosec} \theta \, dh - R_0$$

$$\text{or} \quad \Delta R_e = 10^{-6} \int_0^{h_t} N \operatorname{cosec} \theta \, dh + \int_0^{h_t} \operatorname{cosec} \theta \, dh - R_0 \quad (59)$$

The first term on the right-hand side of (59) is the “ velocity ” or “ refractivity ” error, ΔR_N ; the last two terms represent the geometric range error, ΔR_g , which is the difference in length between the straight path, R_0 , and the curved ray path, R_g . Table VIII gives some typical and extreme values of range errors ray-traced for observed N -profiles.

TABLE VIII. *Typical and Extreme Values of Range Errors for Targets Beyond the Atmosphere*

	Typical $N_s \cong 320$			Extreme $N_s \cong 400$			Maximum %
θ_0	ΔR_g Meters	ΔR_N	ΔR_e	ΔR_g	ΔR_N	ΔR_e	$\Delta R_g/\Delta R_e$
0	10	100	110	60	165	225	~ 27
20 mrad	2.5	62.5	65	4.5	73	77.5	6
50 mrad	0.7	38.1	38.8	1.0	43	44	2.3
100 mrad	0.14	22.26	22.4	0.2	24.8	25	0.8
200 mrad	0.02	11.9	11.9	0.03	13.0	13.0	0.23
500 mrad	0.001	5.01	5.01	0.002	5.50	5.50	0.04

From Table VIII it can be seen that the geometric range error, ΔR_g , does not represent a significant portion of the total range error except at very small initial elevation angles, between zero and about 3° . This being so, the behavior of the total range error will be primarily a function of the first integral in (59) for elevation angles greater than about 3° . The integral expression

$$\Delta R_e \cong 10^{-6} \int_0^{h_z} N \operatorname{cosec} \theta \, dh$$

may be rewritten as

$$\Delta R_e \cong \operatorname{cosec} \theta_0 \times 10^{-6} \int_0^{h_z} \frac{N \, dh}{1 - 2 \sin^2 \left(\frac{\theta - \theta_0}{2} \right) + \cot \theta_0 \sin(\theta - \theta_0)}$$

or

$$\Delta R_e \cong \operatorname{cosec} \theta_0 10^{-6} \int_0^{h_z} N \, dh + \sum_{i=1}^{\infty} (-1)^{i+1} 10^{-6} \times \int_0^{h_z} N \left[\cot \theta_0 \sin(\theta - \theta_0) - 2 \sin^2 \left(\frac{\theta - \theta_0}{2} \right) \right]^i \quad (60)$$

for $\sin \theta < 2 \sin \theta_0$, $\theta_0 > 0$.

This expression is analogous to that derived for the case of ray-bending, and similarly the integral series on the right-hand side of (60) contributes only

3 per cent or less to the value of ΔR_e for θ_0 larger than about 10° . From (3) one would thus suspect that the radio range error might be well estimated as a linear function of the integral of N with respect to height. In treating this integral, it is informative to note that any given $N(h)$ profile may be represented by three primary components:

$$N(h) = N'(N_s, h) + N''(h + h_s) + \delta N(h)$$

where N' is that part of the profile which can best be expressed as a function of N_s and height, N'' is a standard distribution of refractivity with respect to altitude above mean sea level ($h + h_s$) which is independent of N_s , especially above the tropopause, and δN represents a random component of the profile which cannot in general be accounted for *a priori*.

The N' component is generally effective over the first few kilometers, while above 6 or 7 km altitude the N'' component forms the bulk of the profile (Bean and Thayer, 1959). Thus the integral of the N profile with respect to height may be written as:

$$\int_0^{h_t} N dh = \int_0^{h_t} N'(N_s, h) dh + \int_{h_s}^{h_t+h_s} N''(h+h_s) dh + \int_0^{h_t} \delta N(h) dh$$

or
$$\int_0^{h_t} N dh = F_1(N_s, h_t) + F_2(h_s, h_t) + \delta F(h_t)$$

where δF is the random contribution to the integral. For any particular h_t then

$$\int_0^{h_t} N dh = F_1(N_s) + F_2(h_s) + \delta F$$

or
$$\int_0^{h_t} N dh = F_2(h_s = 0) + F_1(N_s) - F_3(h_s) + \delta F \tag{61}$$

where
$$F_3 = \int_0^{h_s} N''(h+h_s) dh, \text{ and } F_2(h_s = 0) \text{ is a constant.}$$

It has been found empirically, from integrated $N(h)$ profiles, that

$$\int_0^{h_t} N dh \cong a + b_1 N_s - b_2 h_s \pm S.E. \tag{62}$$

and the correspondence between (61) and (62) is plain, where the standard error of estimate of (62), "S.E.", represents the standard deviation of δF of (61). The results of such an empirical study are shown in Fig. 36, for the CRPL Standard N -profile Sample†, for h_t beyond the atmosphere. For any particular application of (62) at a single location the term $b_2 h_s$ will be absorbed into the constant a , since h_s does not vary. However, the introduction of this term is necessary to explain the station elevation dependence of integrated $N(h)$ profiles when taken from a sample containing stations at widely differing elevations, such as the Standard Sample.

† See page 105.

It is thus apparent that radio range errors, at least at the higher elevation angles, are primarily a linear function of N_s . That this is also true at comparatively low angles is shown in Fig. 37, for $\theta_0 = 50$ mrad (about 3°) for the same profile sample. It is particularly important to note the similarity of the distributions of the points about the regression lines between Figs. 36 and 37, showing that the range errors at about 3° are still primarily a function

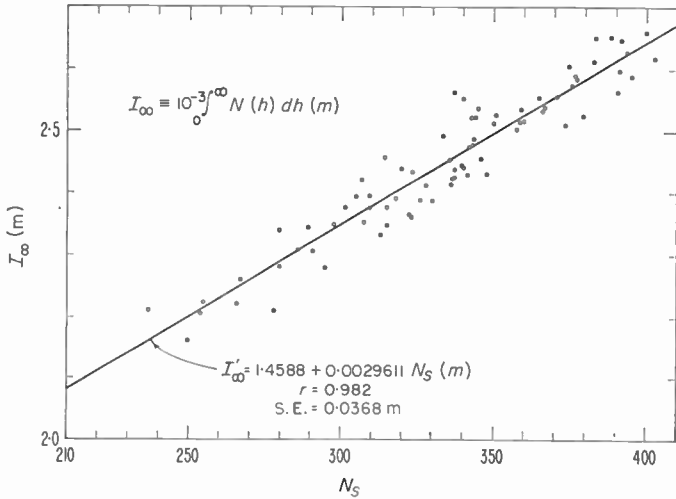


FIG. 36. Integrated refractive index profiles for the CRPL Standard Sample.

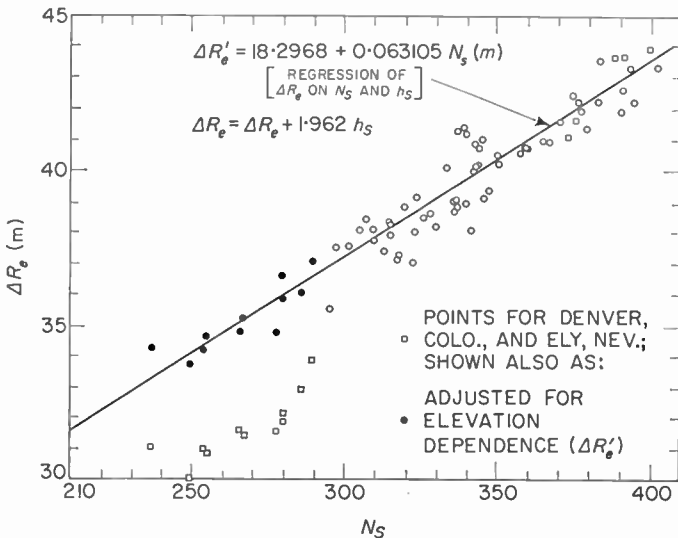


FIG. 37. Total range error at $\theta_0 = 50$ mrad, $h = 70$ km, for the CRPL Standard Sample.

of the integral of N with respect to height, or the range error at 90° . It has been demonstrated therefore that, theoretically, it should be possible to estimate both the angle of refraction of radio rays and errors in radio range measurements from measurement of the refractive index at the surface of the earth. This should be true for targets in or beyond the atmosphere, at elevation angles down to, and possibly lower than, 3° . In addition, if the behavior of refractive index profiles is similar in different parts of the world, it should be possible to specify "universal" values of the coefficients in these equations and to predict these values in advance by analysis of a large heterogeneous sample of refractive index profiles. Further it appears that, theoretically, it should be possible to estimate either radar elevation angle errors or radio range errors at any particular location by means of a system of linear equations in N_s , where the coefficients are functions of the target position. The target position can be specified by either the apparent elevation angle and target height, or the apparent range and target height (or as a third possibility, the apparent range and elevation angle), each having advantages in different situations. The equations recommended are:

$$\varepsilon = a_1(\theta_0, h_t) + b_1(\theta_0, h_t)N_s \pm S.E._1(\theta_0, h_t) \quad (63)$$

$$\Delta R_e = a_2(R_e, h_t) + b_2(R_e, h_t)N_s \pm S.E._2(R_e, h_t) \quad (64)$$

Values of the coefficients may be obtained by performing linear regressions of ε or ΔR_e , as ray-traced for an appropriate sample of radio refractive index profiles, upon N_s for a large number of target positions. As a by-product of these calculations one also obtains, for each target position, a value of the residual error (the standard error of estimate) to be expected for the particular type of profile sample used.

In order to obtain a general set of equations to be useful under arbitrary conditions of location, climate, and weather, a large sample of N -profiles has been assembled at the Central Radio Propagation Laboratory of the National Bureau of Standards, which is believed to be representative of both mean climatic and geographic trends and the larger synoptic variations which may be encountered. Thirteen radiosonde stations have been chosen to be representative of the major geographic and climatic types of the world, and a selection made from each station of six N -profiles of particular types, two of which are typical of the extremes of monthly mean conditions for that location, and the other four of which are typical of some of the variations which are found at that location (Bean and Cahoon, 1957). The result is a sample of seventy-seven† N -profiles which has been found over a period of years to be a sound cross-section of general refractive conditions and has thus been named the CRPL Standard Atmospheric Radio Refractive Index Profile Sample, hereafter referred to as the CRPL Standard Sample. Although the locations chosen for this sample are heavily weighted towards the U.S., it has been found that the general behavior of the refractive index structure as inferred from the standard sample is typical of conditions experienced in most parts of the world (Misme *et al.*, 1960).

† One of the types could not be found for one of the stations used.

Since the refraction measurements described here consist of samples taken at particular locations over comparatively short periods of time, they should provide a test for the general set of coefficients derived from the Standard Sample; not only is the general theoretical approach tested against measured values, but, the measurements coming from places of more or less homogeneous nature, they provide a check as to whether or not coefficients derived for a large heterogeneous sample of data are applicable also to individual places and times; i.e. they should reveal how much of the observed correlation of the heterogeneous sample is derived from correlation between "classes" of data (in the statistical sense). For a more thorough treatment of the CRPL Standard Sample and the associated regression coefficients for range error and elevation angle error the reader is referred to Bean and Thayer (1963). For the Standard Sample the standard error of estimate is equal to the standard prediction error within ± 1 per cent over the range of N_s from 200 to 470, and will be used interchangeably with the latter.

Before turning to an examination of the experimental refraction data and the degree of success realized in applying the theoretical prediction model to these data, it seems appropriate to examine the accuracy of the prediction model when applied to some independent theoretical (i.e. ray-traced) data. For this purpose four check stations have been selected which are not only independent in the sense of not having been included in the original thirteen station Standard Sample, but are from locations widely differing from the region of selection of the original sample. One station is representative of an arctic type climate, one temperate, one tropical, and one is from a "problem" climate area.

Amundsen-Scott station at the South Pole (lat. 90°S) is the arctic type; this station might be expected to present the most rigorous test of the prediction model (as based on the Standard Sample) that can be obtained anywhere in the world. In the first place the extreme arctic-continental climate, with almost no water-vapor contribution to the refractive index and the nearly incessant temperature inversion, is more alien to the Standard Sample than any other type; in the second place, the station elevation is 9 200 ft, which is 2 950 ft in excess of the highest station (Ely, Nevada, 6 250 ft) included in the Standard Sample. These two effects should augment each other as regards refraction. Dakar, Senegal, on the western coast of Africa, represents a "problem" climate station; an inverse relationship exists there between N_s and ΔN (the N -gradient over the first kilometer above the surface). A Congo basin station, Bangui, represents the tropical location, and Moscow, U.S.S.R., the temperate location.

In order to combine brevity with comprehensiveness, ray tracings have been carried out to determine the total refraction (bending at 70 km target height) at two elevation angles, 20 mrad and 100 mrad, for six profiles from each location. The six profiles were selected as representing roughly the range of N_s in winter (February), summer (August), and spring-fall (May and November), two profiles being selected from February, two from August, and one from each of May and November. The 20 mrad elevation angle was selected as representing roughly the lower limit of elevation angles for

which the bending is expected to be strongly correlated with N_s (say $r > 0.9$), while at 100 mrad (about 6°) the correlation is expected to be extremely high (say $r > 0.99$) and the refraction should be reasonably free of random profile effects. The results of the ray-tracings and the comparison with predicted values are shown in Fig. 38. As expected, the results from the South Pole seem to depart significantly from the predicted values at least for the 20 mrad elevation angle. At the 100 mrad elevation angle some of the calculated points lie more than one standard deviation from the predicted line (the theoretical prediction error is too small to show clearly on the graph); however, in all four cases the differences are less than $50 \mu\text{rad}$, a figure which, as will be seen later, may represent the limit of accuracy obtainable from the atmosphere in actual practice. At angles over 100 mrad the errors would be smaller, in fact they should tend to decrease in inverse proportion to the square of the initial elevation angle, as indeed they do between 20 and 100 mrad.

A conclusion which may be drawn from these results is that any regions where the prediction model based on the Standard Sample would not be expected to provide the theoretical accuracy are probably regions of climatic extremes, and at least for the case of angular errors the effects will be negligible for elevation angles of a few degrees or more. As an interesting aside it may be noted that apparently the Antarctic may be a desirable area for tracking systems location, at least from the point of view of consideration of atmospheric refraction effects, since (most likely because of the lack of substantial water vapor and the relatively homogeneous conditions) the prediction error for $\theta_0 = 20$ mrad is only about one-fifth as large as for temperate climates, indicating a possibly more stable atmosphere (even 90 per cent confidence limits for the Antarctic S.E. yield a value less than half of the theoretical temperate value of ± 0.286 mrad).

Before comparing the theoretical and experimental results it is appropriate to examine what one would expect to observe on the basis of propagation theory. In the case of angular errors it is expected that propagation through the real, turbulent atmosphere will produce random variations in the shape of the incoming wavefront, so that measurements made with systems in which the receiving antenna is aligned with the incoming signal will have random variations introduced in addition to the ordinary refraction effects; implying that the residual variance in predicting the elevation angle errors will probably always be greater than predicted from theoretical (static) considerations, and that there will probably be some minimum value of this variance for very large elevation angles. Thus in some cases the residual errors will probably not decrease steadily with increasing elevation angle, but will tend to assume a more or less constant value above some certain angle. These effects will be complicated, in comparing one set of data with another by such things as differences in the location and of time of day or season in which data are taken, and instrumental effects such as aperture averaging. The case of range errors is more straightforward. The effects of turbulent atmospheric inhomogeneities are expected to average out over regions of abnormally high or low density, or water vapor concentration,

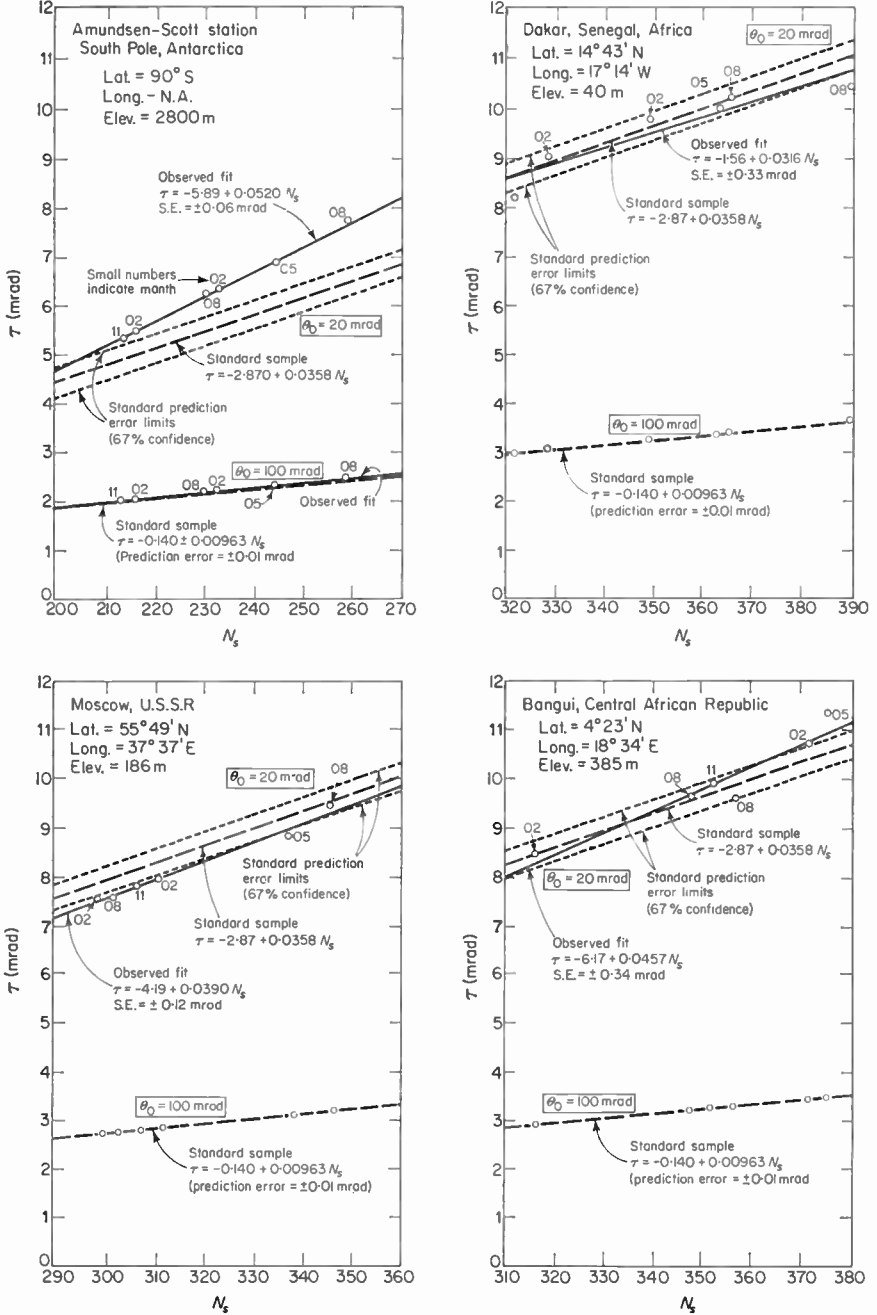


FIG. 38. Comparison of predicted refraction at $h = 70$ km for $\theta_0 = 20$ mrad and 100 mrad from regressions of the CRPL Standard Sample and ray-traced values from four independent locations.

when considering the transit-time of particular points on the wave front. Hence the effect on the residual range errors is expected to be small, and the observed values are expected to compare rather well with the predicted (theoretical) values.

Turning first to the comparison of observed and predicted elevation angle errors, Fig. 39 shows some data on the mean refraction of 1.85 cm radio waves received from the sun, a target at essentially infinite range, so that the elevation angle error is identical with the total angular bending of the

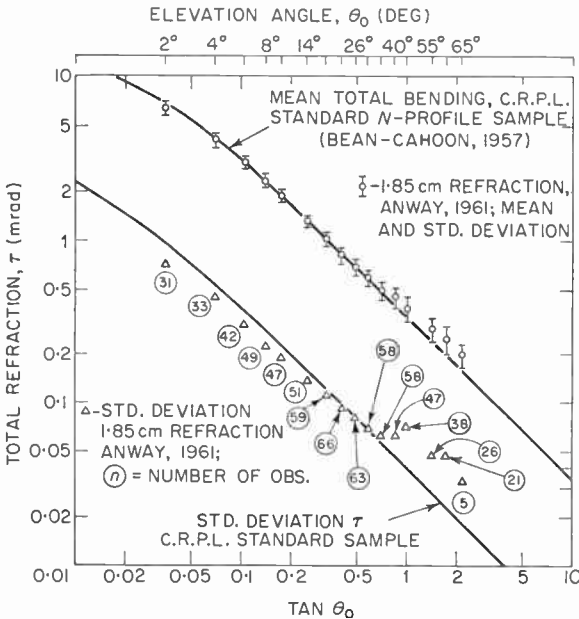


Fig. 39. Comparison of measured total atmospheric refraction of 1.85 cm radio waves at Cedar Rapids, Iowa, with values predicted from N_s .

radio ray, τ . The data shown in Fig. 39 were obtained by tracking the sun with a precise radio sextant developed by the Collins Radio Company, and were collected in August through December of 1959 at Cedar Rapids, Iowa (Anway, 1961). These data represent essentially instantaneous measurements. The mean of all observations at each elevation angle is plotted for elevation angles ranging from 2° to 65°, and the mean value of N_s associated with each point is about 332; the curve for the mean bending of the CRPL Standard Sample corresponds to the mean value of N_s of 334.6 for that sample and hence the data should be comparable. The standard deviation "wings" refer to the standard deviation of the individual "instantaneous" data, not to the standard error of estimate of the mean value. The close agreement observed for elevation angles between 2° and 35° constitutes not only a confirmation of the usefulness of the Standard Sample, but also a verification of the accuracy of ray-tracing theory in estimating radio wave

refraction in the actual, and thus heterogeneous, atmosphere. The standard deviation of the Collins data (shown on the lower part of Fig. 39 is generally lower than for the Standard Sample, but this is to be expected in view of the larger range of climatic variation contained in the CRPL Standard Profile Sample. The apparent discrepancies in the measurements made at elevation angles over 40° are apparently due to some slight inaccuracies in the calibration procedure used on the radio sextant during the period of data acquisition.† In fact, the data shown in Fig. 39 are almost precisely what one would expect to observe if all of the measured values of refraction were increased by a systematic calibration error of about $50 \mu\text{rad}$ over their correct values. The standard deviations in Fig. 39 tend to become constant at high elevation angles. The largest difference between the observed data and the predicted curve in Fig. 39 at elevation angles over 30° , is only about $50 \mu\text{rad}$ or 10 seconds of arc (the angular diameter of the planet Mars at its average distance from the earth is $10''$, an angle not discernible to the naked eye). Although this discrepancy might be significant in some applications, it is only about $\frac{1}{2}$ per cent of the diameter of the target sun and is probably near the limit of accuracy of the equipment used.

Figure 40 shows the results of the specific measurements reported by Anway for the radio sextant for all cases at an elevation angle of $8^\circ \pm 0.09^\circ$; each point represents an "instantaneous" reading. The solid line represents the linear regression of the measured refraction data on the values of N_s ; the dashed line shows the predicted linear relationship derived from least squares fits to the CRPL Standard Sample ray-traced refraction data. The mean bias between the two lines is about $40 \mu\text{rad}$, interestingly close to, and in the same direction as the apparent calibration error noted in the mean refraction data at high elevation angles. The standard error of estimate is considerably higher than predicted; however, the r.m.s. uncertainty of $\pm 0.052^\circ$, or $\pm 0.91 \text{ mrad}$, in the apparent elevation angle would be sufficient by itself to increase the standard error of estimate to about $\pm 0.017 \text{ mrad}$, which is four times larger than the predicted value. It is not known how much of the total standard error of $\pm 0.12 \text{ mrad}$ is due to measurement errors as opposed to unforeseen fluctuations in actual atmospheric refraction.

Figure 41 shows some results of measurements taken at Cape Canaveral, Florida, on 1-3 November 1959, at a very low elevation angle, about 0.7 mrad or 0.04° . These are "instantaneous" measurements, taken at half-hourly intervals, of the phase difference fluctuations between the signals from a beacon as they arrived at the upper and lower terminals of a vertical 24-ft baseline, thus being very closely equivalent to a measurement of the fluctuations in the angle of arrival of the wave front at the centerpoint of the baseline (the altitude difference between this point and the target beacon is referred to as the "mean" target height). Since only the fluctuations and not the

† The data for the highest elevation angles in Fig. 39 were necessarily collected during the early part of the period when the sun was higher in the sky. In a private communication, Anway states that the mean N_s applicable to the data at 60° - 65° was 358 rather than 332; this difference would account for about one-third of the discrepancies noted, reducing the residual bias to a maximum of about $40 \mu\text{rad}$.

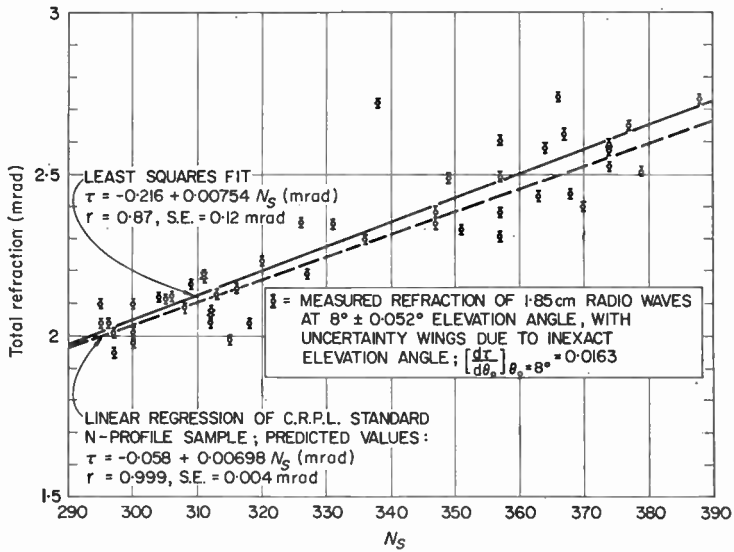


FIG. 40. 1.85 cm radio refraction at an elevation angle of 8° , at Cedar Rapids, Iowa. (After Anway, 1961.)

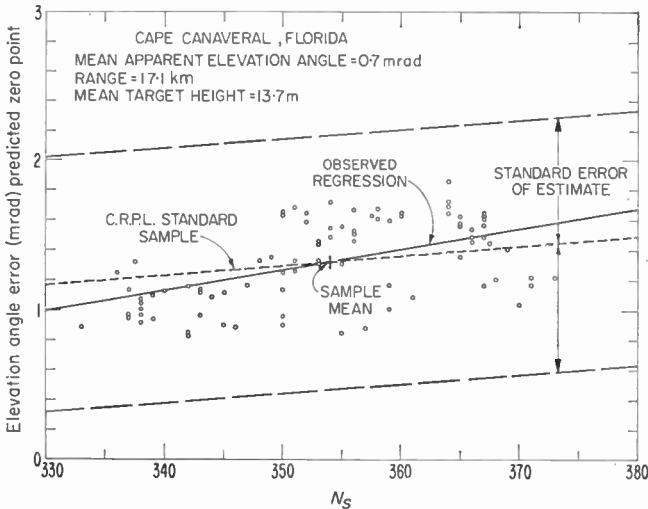


FIG. 41. Elevation angle fluctuations from phase differences taken across a 24-ft vertical baseline, at Cape Canaveral, Florida.

total phase differences were measured, only the slope and scatter of the elevation angle errors as a function of the observed N_s data can be compared with the predicted values from the CRPL Standard Sample. The zero point on the graph is set by the predicted mean value for the sample. The correlation coefficient is, as predicted from the Standard Sample, about 0.55. In this case the scatter of the observed data is well inside the limits of the standard error of estimate of the regression for the Standard Sample, even at this very small elevation angle where horizontal changes in the N profile can exert a large effect on elevation angle errors.

Figure 42 shows the results of a comparison between predictions of elevation errors estimated from the CRPL Standard Sample and some measurements made with a 6-cm radar at Tularosa Basin, New Mexico

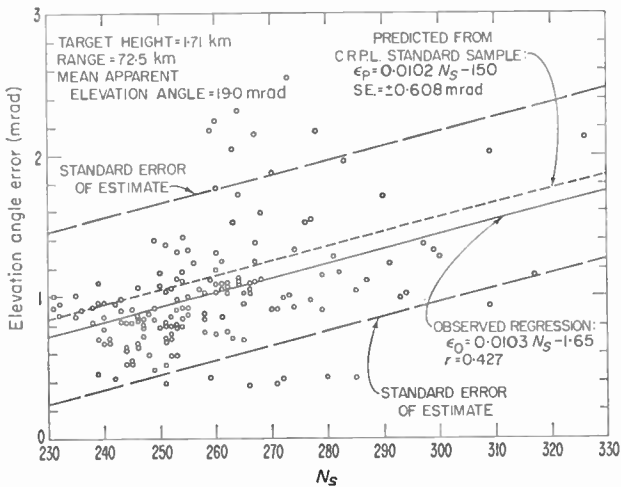


FIG. 42. Measured refraction of C-band radar at Tularosa Basin, N. Mexico.

(Anderson *et al.*, 1960). Each point represents the mean of five “instantaneous” readings made at 1-min intervals over a period of 4 min. The standard deviation of each five-reading group averaged 0.16 mrad, and the maximum deviation in any one group was 0.58 mrad. The radio energy was propagated over a 45-mile path at a mean apparent elevation angle of 18 mrad; the target was a beacon located on a mountain peak 5610 ft higher than the desert surface where the radar was located. The data in Fig. 42 show that even for this rather extreme case, where the degree of correlation between N_s and ϵ is 0.4, agreement is obtained between:

- (1) the predicted and observed mean refraction,
- (2) the observed and predicted slopes of the ϵ versus N_s relation,
- (3) the observed and predicted residual errors of predicting ϵ from N_s alone.

The small discrepancy between the intercepts (i.e. between the mean

refraction) of the observed and predicted ϵ versus N_s lines may be perhaps attributed to, for example, antenna lobe pattern distortion caused by differential refraction, or defocusing (Wilkerson, 1962). The remaining data examined were of necessity taken in such a manner as to have a rather high degree of autocorrelation (trends). Such data are not as suitable for confirming the accuracy of a regression prediction process as are independent data.

Turning to examination of radio range errors, Fig. 43 shows the results of some measurements of apparent radio range fluctuations over a 25-km path on the island of Maui, Hawaii, on 9–11 November 1956 (Norton *et al.*,

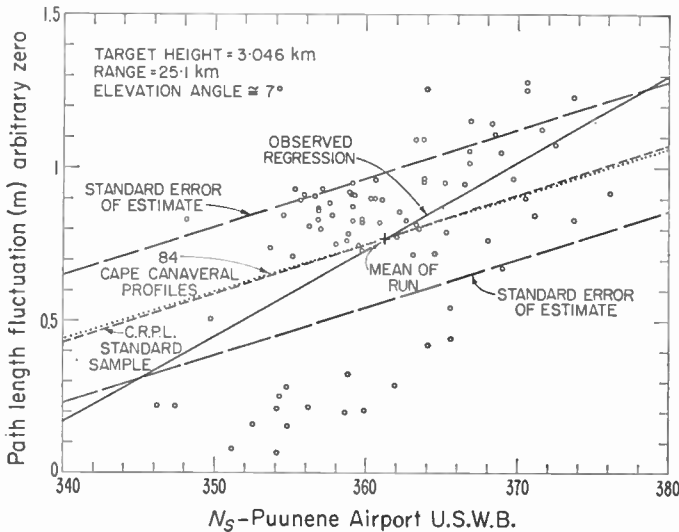


FIG. 43. Range error fluctuations observed on Maui Path.

1961). These measurements were made at 1-hr intervals, and are essentially "instantaneous" values. The target beacon was situated on the summit of Mount Haleakala at an elevation of 10 025 ft, while the "ground" station was near Puunene Airport at an elevation of 104 ft, thus yielding a target height of 3.046 km, in a region of critical target heights for prediction of radio range errors. The measured range fluctuations (absolute errors not measured) are plotted against values of N_s taken at about the same time (mostly 15 to 20 min later) by U.S. Weather Bureau personnel at the Puunene Airport weather station. The agreement between observation and prediction is fair considering that only thirty-two of the eighty-six points lie outside of the predicted standard error of estimate limits, while chance would indicate that twenty-nine points would exceed these limits. Also it should be kept in mind that in this case, as for all except the Collins data, the target beacon is located on the surface of the earth, whereas the predictions from the CRPL Standard Profile Sample are derived for targets in the free atmosphere; there is undoubtedly some bias introduced in this way.

As a part of a continuing investigation into the atmospheric limitations imposed on electronic distance measuring equipment, some measurements have been made recently by the Lower Atmosphere Physics Section, NBS, of both range errors and range difference errors (across a phase-differencing baseline) over a propagation path near Boulder, Colorado. Figures 44 and 45 are based on some of the preliminary results of these measurements (Thompson, 1962). Figure 44 shows the results of measurements of the fluctuations

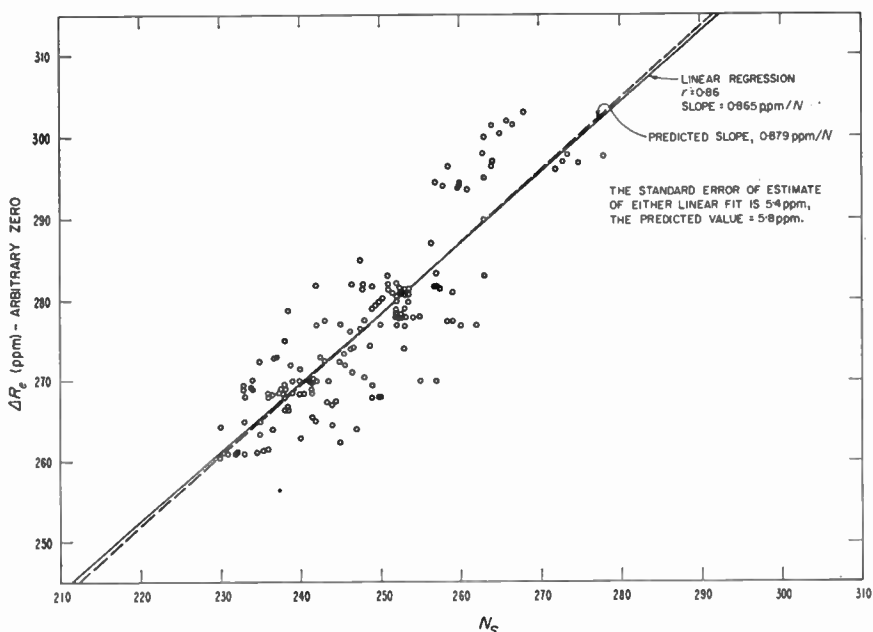


FIG. 44. Range error fluctuations observed over the Boulder Creek-Green Mountain Path, Colorado.

in apparent range, made at half-hour intervals on 9–11 May 1961, over a 15.5-km path between a transmitting beacon on Green Mountain at an elevation of 7 380 ft and a receiving antenna located near Boulder Creek at an elevation of 5 100 ft, the true target height thus being 2 280 ft. The apparent range fluctuations, expressed in parts-per-million of the 15.5-km path length (with an arbitrary zero since the total range was not measured), are plotted as a function of the surface value of the refractive index taken at a point quite close to the lower terminal. Quite good agreement is seen between the simple linear regression of the observed ΔR_e values on N_s and the predicted linear relationship obtained from the CRPL Standard Sample. Note that both lines have statistically equal standard errors of estimate with respect to the observed data.

Figure 45 shows the results of the range difference measurements made over a 460-m baseline essentially in line with the transmission path, where

the second antenna was farther from the target beacon than the primary antenna. Here the range difference fluctuations (again with an arbitrary zero) have been plotted as a function of the mean value of N_s , measured at each end of the baseline. The zero point on the graph is set by the predicted mean of the sample. In this case there seems to be some discrepancy between

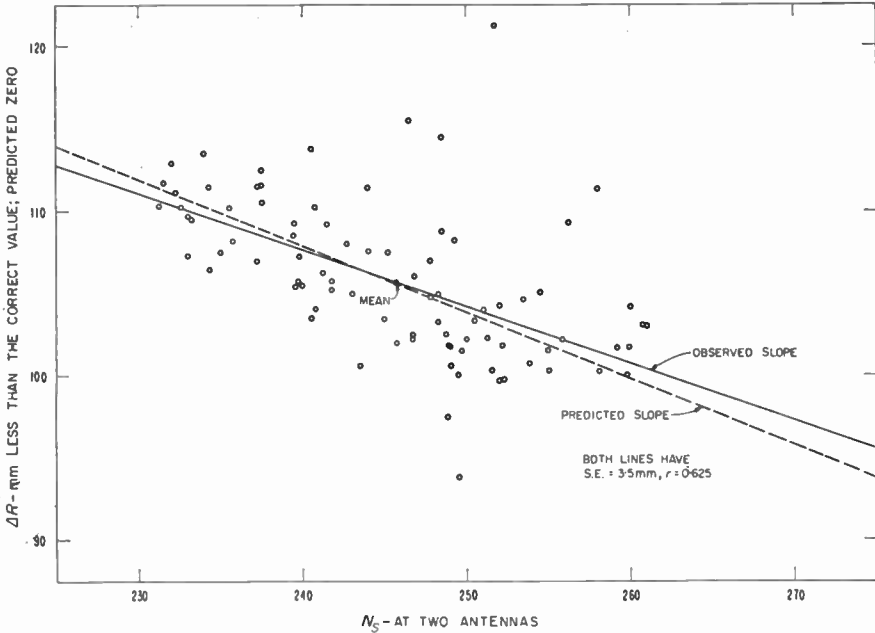


FIG. 45. Range difference fluctuations - observed over a 460-m in-line baseline, Boulder Creek-Green Mountain Path, Colorado.

the regression of the data and the predicted slope; however, it may be noted that the standard errors of estimate for the two lines are, to two significant figures, equal, indicating that the difference in the slopes is probably statistically insignificant.

There are some data points in Fig. 45 having a rather large deviation from the regression lines. Statistical theory (using the "Student" t -distribution for 84° of freedom) shows that, if the data points are drawn from a normally distributed population, there should be only one point having a deviation of more than ± 9 mm from the observed regression line. There are in fact five such points in Fig. 45, four above and one below the line. If these five points are rejected on the grounds that they weight too heavily the extremes of the distribution of data points (this is especially true when using least squares regression), and the regression is then redone using the remaining eighty-one data points, the resulting value of the slope is -0.385 mm/ N unit, with $r = 0.77$ compared to the predicted slope of -0.381 mm/ N unit, a rather close agreement.

As a summary of the results of the experimental versus theoretical comparisons given in the preceding section, a statistical analysis has been made of the significance of the differences between the slopes of the observed and predicted regression lines. In order to make the tests more stringent, it was assumed that the slopes derived from the Standard Sample should be taken to be the slopes of the population regression lines (β), thus yielding an estimate of the significance of the departure of the observed slope from the assumed population value.

A value of t was first calculated for each case using the relation (Bennett and Franklin, 1954).

$$t_{j-2} = \frac{|b - \beta_0| \sqrt{\sum(x_i - \bar{x})^2}}{S.E.}$$

where b is the observed slope, β_0 the assumed population, or theoretical, slope, x refers to the independent variable in each regression, N_s , $S.E.$ is the standard error of estimate, and t_{j-2} is the value of t for $j-2$ degrees of freedom. From t_{j-2} , confidence limits for β at the $100(1-\alpha)$ per cent level can be calculated from (*ibid.*)

$$b - \frac{t_{j-2, \alpha} S.E.}{\sqrt{\sum(x_i - \bar{x})^2}} < \beta < b + \frac{t_{j-2, \alpha} S.E.}{\sqrt{\sum(x_i - \bar{x})^2}}$$

The probability that the observed value b would have fallen outside of these limits by chance is α . Many statisticians consider a value of t_{j-2} falling below the $100\alpha = 5$ per cent level not to be significant, between the 5 per cent and 1 per cent levels to be of questionable significance, and over the 1 per cent level to be significant (*ibid.*). An observed slope b falling

$$|b - \beta_0| > \frac{t_{j-2, 0.01} S.E.}{\sqrt{\sum(x_i - \bar{x})^2}}$$

would thus be taken to represent a significant departure from the value β_0 , and would thus imply the possibilities

- (a) β_0 does not represent β , or
- (b) b represents the regression of data from a population different from that used in determining β_0 , or
- (c) both.

Before making the significance tests, however, the value of j , the number of independent observations going into the determination of b , must be known. In general, data of the type presented here are more or less highly autocorrelated, and hence not all independent. These data, with the possible exception of the Collins data and the Tularosa Basin data for which the calculations could not be performed, have autocorrelation coefficients r_k , for lag k ($k = 1, 2, 3$, units of time between successive measurements) that can be approximately described by

$$r_k \cong (r')^k$$

and for this type of data the effective number of pieces of independent data, j , is given by (Brooks and Carruthers, 1953).

$$j = n \left[\frac{1 - r'}{1 + r'} \right]$$

For the data treated here weighted mean values of r' were calculated from

$$r' \cong \frac{r_1 + 4r_2^{1/2} + 9r_3^{1/3} + \dots + k^2 r_k^{1/k}}{1 + 4 + 9 + \dots + k^2} \quad (65)$$

where k was the largest lag for which the autocorrelation coefficient was calculated, usually 4 or 5. No special justification is offered for the use of equation (65), other than the obvious fact that r_k is to be approximated by the k th power of r' , and hence a function of k would seem to be the most logical weighting function to use; the use of k^2 as a weighting function seemed to give the best overall fit to the series of r_k encountered with these data.

Table IX shows the results of the significance tests on the slopes of the various experimental and theoretical (predicted) regression lines. The number of pieces of data is shown in the first column, the observed slope b and theoretical slope β in the second and third columns, the autocorrelation coefficient for lag of one time unit in the fourth column, and the weighted mean r' as defined in (65) in the fifth column. In column 6 the effective number of independent pieces of data, j , is shown, while in column 7 the value of t_{j-2} is shown for the difference between b and β . The next column shows the value of $t_{j-2, 0.5}$, the value for the 50 per cent significance level for $j-2$ degrees of freedom. Only one of the t values turns out to be significant at the 50 per cent level, which means that there is a better-than-even chance that such differences would have occurred by chance in the other cases. In the case of the Collins data at $\theta_0 \cong 8^\circ$, the value of $t = 1.01$ would not be significant at the 25 per cent level; the value $t_{46} = 1.01$ corresponds to $\alpha = 0.34$, or a 34 per cent chance that the observed deviation $|b - \beta|$ is of a random nature, and thus not significant. The results of these tests are such that no significance can be attached to any of the apparent discrepancies between theory and observation, and given reason to believe that the values of β are theoretically sound, it may be said that the results are significantly positive in nature.

From the experimental data which are available at the present time it may be concluded that:

(1) Radio range and elevation angle errors can be predicted from the surface value of the radio refractive index, and the accuracy obtained will be generally commensurate with the estimates of residual errors made from theoretical ray-tracing considerations.

(2) The functional dependence of either angular refraction or range errors on the surface value of the refractive index as derived from the CRPL Standard N -profile Sample may be applied to arbitrary locations or climates

TABLE IX. *Experimental versus Theoretical Slope*

ε vs N_s	n	β	r_1	r'	j	t_{j-2}	$t(0.50, j-2)$	Is $ b-\beta $ significant at $\alpha = 50\%$ level?	
Collins Data 8°	48	0.00754	0.00698	—	—	(48)	1.01	0.68	Yes
Tularosa Basin	161	0.0103	0.0102	—	—	(161)	0.031	0.676	No
Cape Canaveral	86	0.01356	0.00648	.870	.860	6.5	0.708	0.73	No
ΔR_s vs N_s									
Maui Data	86	0.02833	0.01610	.974	.950	2.2	3.56	7.6	No
Boulder Creek-Green Mt.	155	0.865	0.879	.944	.950	4.0	0.32	0.82	No
$\Delta(\Delta R)$ vs N_s									
Boulder Creek-Green Mt.	86	-0.344	-0.381	.957	.946	2.4	0.60	2.0	No

TABLE X. *Comparison of Slopes for Independent Check*Predicted Slope at $\theta_0 = 20$ mrad: 0.358 mrad/ N_s

Station	Observed Slope	Difference $b-\beta_0$	$\sqrt{\Sigma(N_s-\bar{N}_s)^2}$	t	100 σ %	Significance
Amundsen-Scott	0.0520	+0.0162	37.9	10.2	<0.1%	Very high
Dakar	0.0316	-0.0042	56.5	0.72	52%	None
Bangui	0.0457	+0.0099	47.2	1.37	25%	Very low
Moscow	0.0390	+0.0032	44.3	1.18	31%	Very low

without noticeable decrease in accuracy over that obtained with a sample from the location under consideration.

(3) The effects of horizontal inhomogeneities of the refractive index, which certainly must have been prevalent over the transmission paths for which experimental data have been presented, do not appear to introduce any bias or additional residual variance into the values of observed refraction variables over those predicted from surface observations.

REFERENCES

- Anderson, L. J. (1958). *Trans. Amer. geophys. Un.* **39**, 208–212.
- Anderson, W. L., Beyers, N. J., and Rainey, R. J. (1960). *Trans. Inst. Radio Engrs, N. Y. on Antennas and Propagation AP-8*, 456.
- Anway, A. C. (1961). *Collins Res. Rep.* No. CRR-242S, Collins Radio Company, Cedar Rapids, Iowa.
- Bean, B. R. (1959). *J. Res. nat. Bur. Stand.* **63D**, 29.
- Bean, B. R., and Cahoon, B. A. (1957). *Proc. Inst. Radio Engrs, N. Y.* **45**, 1545–1546.
- Bean, B. R., and Dutton, E. J. (1960). *J. Res. nat. Bur. Stand.* **64D(3)**, 259–263.
- Bean, B. R., and Horn, J. D. (1959). *J. Res. nat. Bur. Stand.* **63D**, No. 3, 259–273.
- Bean, B. R., and Thayer, G. D. (1959a). *Proc. Inst. Radio Engrs, N. Y.* **47**, 740–755.
- Bean, B. R., and Thayer, G. D. (1959b). *Nat. Bur. Stand. Monograph* No. 4.
- Bean, B. R., and Thayer, G. D. (1960). *Proc. Inst. Radio Engrs, N. Y.* **48**, 1499–1501.
- Bean, B. R., and Thayer, G. D. (1963). *J. Res. nat. Bur. Stand.* **67D**, No. 3, 273–285.
- Bean, B. R., Cahoon, B. A., and Thayer, G. D. (1960a). *Tech. Note nat. Bur. Stand.* No. 44.
- Bean, B. R., Horn, J. D., and Ozanich, A. M., Jr. (1960b). *Nat. Bur. Stand. Monograph* No. 22.
- Bean, B. R., Thayer, G. D., and Cahoon, B. A. (1960c). *J. Res. nat. Bur. Stand.* **64D**, 487–492.
- Bean, B. R., Fehlhaber, L., and Grosskopf, J. (1962). *J. Res. nat. Bur. Stand.* **66D**, 5, 593–599.
- Bennett, C. A., and Franklin, N. L. (1954). “Statistical Analysis in Chemistry and the Chemical Industry,” John Wiley and Sons, New York.
- Booker, H. G., and Walkinshaw, W. (1947). *Phys. Soc. and Roy. Met. Soc. Conference*, London, England, 1946, pp. 80–127.
- Brooks, C. E. P., and Carruthers, N. (1953). “Handbook of Statistical Methods in Meteorology,” Her Majesty’s Stationery Office, London.
- Dubin, M. (1954). *J. geophys. Res.* **59**, 339–344.
- “Handbook of Geophysics for Air Force Designers” (1957). *Geophys. Res. Directorate, AFRC, ARDC, USAF*, pp. 1–2 to 1–37.
- Humphreys, W. J. (1940). “Physics of the Air,” p. 82. McGraw-Hill Book Co., New York.
- Katz, I. (1951). “Propagation of Short Radio Waves,” by D. E. Kerr, McGraw-Hill Book Co., New York.
- Kerr, D. E. (1951). “Propagation of Short Radio Waves,” pp. 9–22, McGraw-Hill Book Co., New York.
- Minzner, R. A., Ripley, W. S., and Condron, T. P. (1958). U.S. Extension to the ICAO Standard Atmosphere, Tables and Data to 300 Standard Geopotential Kilometers, G.P.O., Washington 25, D.C.
- Misme, P. (1958). *Ann. Télécomm.* **13**, 303–310.

- Misme, P., Bean, B. R., and Thayer, G. D. (1960). *Proc. Inst. Radio Engrs, N.Y.* 48, 1498–1501.
- Norton, K. A., Rice, P. L., and Vogler, L. E. (1955). *Proc. Inst. Radio Engrs, N.Y.* 43, 1488–1526.
- Norton, K. A., Herbstreit, J. W., Janes, H. B., Hornberg, K. O., Peterson, C. F., Barghausen, A. F., Johnson, W. E., Wells, P. I., Thompson, M. C. Jr., Vetter, M. J., and Kirkpatrick, A. W. (1961). *Nat. Bur. Stand. Monograph* No. 33.
- Ratner, B. (1945). *Rep. Weather Bur., Wash.* Upper air average values of temperature, pressure and relative humidity over the United States and Alaska. Report of Factual Data from the Canterbury Project, Dep. Sci. Indus. Res., Wellington, New Zealand (1951).
- Schelling, J. C., Burrows, C. R., and Ferrell, E. B. (1933). *Proc. Inst. Radio Engrs, N.Y.* 21, 427–463.
- Schulkin, M. (1952). *Proc. Inst. Radio Engrs, N.Y.* 40, 554–561.
- Smart, W. M. (1931). “Spherical Astronomy,” Ch. 3, Cambridge University Press, London.
- Stickland, A. C. (1946). Conference on Meteorological Factors in Radio-Wave Propagation, The Royal Institute, London, 253–267.
- Tao, Kazuhiko, and Hirao, Kunio (1960). *J. Radio Res. Labs., Japan* 7, 85–93.
- The Rocket Panel (1952). *Phys. Rev.* 88, 1027–1032.
- Thompson, M. C., Jr. (1962). Private Communication.
- Weisbrod, S., and Anderson, L. J. (1959). *Proc. Inst. Radio Engrs, N.Y.* 47, 1770–1777.
- Wilkerson, R. E. (1962). *J. Res. nat. Bur. Stand.* 66D, 479.
- Wong, Ming S. (1958). *Proc. Inst. Radio Engrs, N.Y.* 46, 1628–1639.
- Zhevankin, S. A., and Troitskii, V. S. (1959). *Radioteknika i Elektronika* 4, 21–27.

ATTENUATION OF RADIO WAVES IN THE TROPOSPHERE

B. R. BEAN

*Central Radio Propagation Laboratory,
National Bureau of Standards, Boulder, Colorado, U.S.A.*

I. Introduction	121
II. Attenuation by Atmospheric Gases	122
III. Estimates of the Range of Total Gaseous Absorption	132
IV. Total Radio Path Absorption	136
V. Derivation of Absorption Estimate for Other Areas	137
VI. Attenuation in Clouds	141
VII. Attenuation by Rain	142
VIII. Rain Attenuation Effects on Radio Systems Engineering	147
IX. Attenuation by Hail	151
X. Attenuation by Fog	152
XI. Thermal Noise Emitted by the Atmosphere	153
References	155

I. INTRODUCTION

The advent of tropospheric forward scatter techniques has made possible communications over longer distances with higher frequencies than has been heretofore thought practicable. The limitations imposed by gaseous absorption, and by scattering by raindrops, upon the power requirements of a communications system for this application become more important with increasing distance and frequency. It has been common in the past to evaluate propagation path attenuation due to absorption by multiplying the ground separation of the terminals by the value of the absorption calculated for surface meteorological conditions (Bussey, 1950) or to avoid the problem by restricting the communications system to frequencies that are essentially free of absorption (Davidson and Pote, 1955). In contrast Bean and Abbott (1957) evaluated the absorption along the actual ray path.

The following sections of this chapter will be devoted to a descriptive treatment of absorption of radio waves by raindrops and gaseous oxygen and water vapor in the atmosphere. Unless otherwise specified the following conditions obtain: (1) All attenuations are expressed in terms of decibel loss per unit length of the propagation path (db/km). The attenuations due to different causes are simply added to give the total attenuation in decibels. (2) Average values of temperature, droplet size, and droplet distribution are used for the estimation of attenuation over a given radio path; this being sufficiently accurate for most practical purposes.

The attenuation experienced by radio waves is the result of two effects: (1) absorption and (2) scattering. At wavelengths greater than a few centimeters, absorption by atmospheric gases may be regarded as negligibly small except where very long distances are concerned. However, attenuation

due to cloud and rain has to be considered at wavelengths less than 10 cm, and is particularly pronounced in the vicinity of 1 and 3 cm.

It is well known that, when an incident electromagnetic wave passes over an object whose dielectric properties differ from those of the surrounding medium, (a) some of the energy from the wave is absorbed by the object and heats the absorbing material (this is called true absorption) and (b) some energy is scattered, the scattering being generally smaller and more isotropic in direction the smaller the scatterer is with respect to the wavelength of the incident energy. In the case of point-to-point radio communications we are interested in the total attenuation of the transmitted energy caused by losses resulting from both the true absorption and the scattering.

II. ATTENUATION BY ATMOSPHERIC GASES

The major atmospheric gases that need to be considered as absorbers in the frequency range of 100 Mc/s to 50 Gc/s are water vapor and oxygen. For these frequencies the gaseous absorption arises principally in the 1.35 cm line (22.235 Gc/s) of water vapor and the series of lines centered around 0.5 cm (60 Gc/s) of oxygen (Van Vleck, 1947a). The variations of these

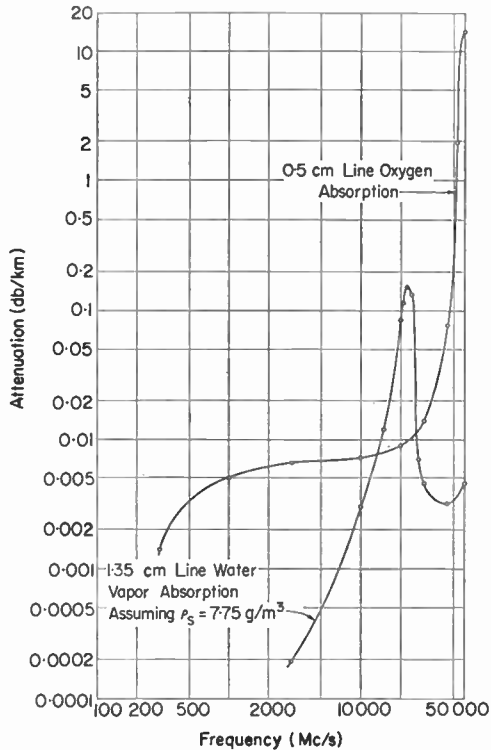


FIG. 1. Atmospheric absorption by the 1.35 cm line of water vapor and the 0.5 cm line of oxygen.

absorptions with pressure, frequency, temperature, and humidity have been described by Van Vleck (1947a, b). The frequency dependence of these absorptions is shown in Fig. 1 (Van Vleck, 1947a).

In Fig. 1, the water vapor absorption values have been adjusted to correspond to the mean absolute humidity, ρ (grams of water vapor per cubic meter), for Washington, D.C., 7.75 g/m^3 . The reason for this adjustment is that water vapor absorption is directly proportional to the absolute humidity (Van Vleck, 1951), and thus for normal concentrations of water vapor observed in the troposphere variations in signal intensity due to water vapor absorption may be specified directly in terms of the variations in the absolute humidity of the atmosphere. It can be seen from Fig. 1 that the water vapor absorption exceeds the oxygen absorption in the frequency range 13 Gc/s to 32 Gc/s, indicating that in this frequency range the total absorption will be sensitive to changes in the water vapor content of the air, while outside this frequency range the absorption will be more sensitive to changes in oxygen density. Only around the resonant frequency corresponding to $\lambda = 1.35 \text{ cm}$ is the water vapor absorption greater than the oxygen absorption. The absorption equations and the conditions under which they are applicable have been discussed by Van Vleck (1947a).

The Van Vleck theory describes these absorptions in the following manner: the oxygen absorption at $T = 293^\circ\text{K}$ and standard atmospheric pressure in decibels per kilometer, γ_1 , is given by the expression:

$$\gamma_1 = \frac{0.34}{\lambda^2} \left[\frac{\Delta v_1}{\frac{1}{\lambda^2} + \Delta v_1^2} + \frac{\Delta v_2}{\left(2 + \frac{1}{\lambda}\right)^2 + \Delta v_2^2} + \frac{\Delta v_2}{\left(2 - \frac{1}{\lambda}\right)^2 + \Delta v_2^2} \right] \quad (1)$$

where λ is the wavelength for which the absorption is to be determined and where Δv_1 and Δv_2 are line width factors with dimensions of cm^{-1} . This formula is based on the approximations of collision broadening theory, which postulates that, although the electromagnetic energy is freely exchanged between the incident field and the molecules, some of the electromagnetic energy is converted into thermal energy during molecular collisions and thus a part of the incident electromagnetic energy is absorbed. The term in equation (1) involving Δv_1 gives the non-resonant absorption arising from the zero frequency line of oxygen molecules, while the terms involving Δv_2 describe the effects of the several natural resonant absorptions of the oxygen molecule which are in the vicinity of 0.5 cm wavelength. The $(2 \pm 1/\lambda)$ (cm^{-1}) terms are the portion of the shape factors that describe the decay of the absorption at frequencies away from the resonant frequency (the number 2 is the reciprocal of the centroid resonant wavelength 0.5 cm).

The water vapor absorption at 293°K arising from the 1.35 cm line, γ_2 , is given by:

$$\frac{\gamma_2}{\rho} = \frac{3.5 \times 10^{-3}}{\lambda^2} \left[\frac{\Delta v_3}{\left(\frac{1}{\lambda} - \frac{1}{1.35}\right)^2 + \Delta v_3^2} + \frac{\Delta v_3}{\left(\frac{1}{\lambda} + \frac{1}{1.35}\right)^2 + \Delta v_3^2} \right] \quad (2)$$

where ρ is the absolute humidity and $\Delta\nu_3$ is the line width factor of the 1.35 cm water vapor absorption line. The additional absorption arising from absorption bands at $\lambda < 1.35$ cm, γ_3 , is described by:

$$\frac{\gamma_3}{\rho} = \frac{0.05\Delta\nu_4}{\lambda^2} \quad (3)$$

where $\Delta\nu_4$ is the effective line width of these absorption bands. The non-resonant term has been increased by a factor of 4 over the original Van Vleck formula in order better to satisfy experimental results (Becker and Autler, 1946).

Although Van Vleck gives estimates of the various line widths, more recent experimental determinations have been used here whenever possible. The line width values used in this chapter are summarized in Table I.

TABLE I. *Line Width Factors Used to Determine Atmospheric Absorption*

Line Width	Temperature	Value	Sources
$\Delta\nu_1$	293°K	0.018 cm ⁻¹ atm. ⁻¹	Birnbaum and Maryott (1955)
$\Delta\nu_2$	300°K	0.049 cm ⁻¹ atm. ⁻¹	Artman and Gordon (1954)
$\Delta\nu_3$	318°K	0.087 cm ⁻¹ atm. ⁻¹	Becker and Autler (1946)
$\Delta\nu_4$	318°K	0.087 cm ⁻¹ atm. ⁻¹	Becker and Autler (1946)

The preceding expressions for gaseous absorption are given as they appear in the literature and do not reflect the pressure and temperature sensitivity of either the numerical intensity factor or the line width. This sensitivity must be considered for the present application since it is necessary to determine the manner in which the absorption varies with temperature and pressure variations throughout the atmosphere. The dependence of intensity factors upon atmospheric pressure and temperature variations may be taken to be that given by the Van Vleck theory. The magnitude and temperature dependence of line widths is a question not completely resolved. Both theory and experiment indicate the line width to vary as $1/T^x$, $x > 0$. Different measurements on the same line of oxygen have given values of x ranging from 0.71 to 0.90, with differences in the magnitude of $\Delta\nu$ of about 20 per cent (Tinkham and Strandberg, 1955; Hill and Gordy, 1954). For example, two curves of oxygen absorption around 60 Gc/s are given in Fig. 2, one at one atmosphere and the other at one quarter of an atmosphere pressure. It is seen that with decreasing pressure the multitude of individual absorption lines begins to appear, the delineation becoming more pronounced the lower the pressure. Experiments have also clearly indicated that the line width changes from line to line, with maximum fluctuations of about 15 per

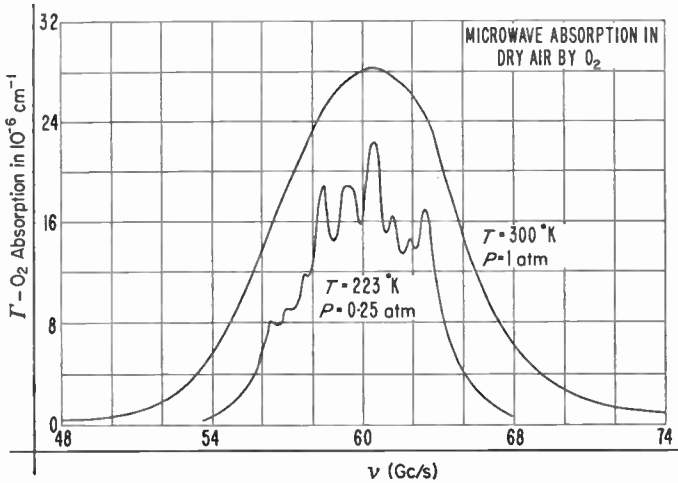


FIG. 2. Pressure variation of O₂ absorption near 60 Gc/s.

cent. In the frequency region considered in this chapter (10–45 Gc/s) the centroid frequency approximation for oxygen is valid and a mean line width can be used with good accuracy, but in the region of the resonant frequencies of oxygen, the line-to-line width variations must be taken into account. The expressions used here to calculate the absorptions are given in Table II.

TABLE II. Values Used in the Calculation of Atmospheric Absorption

Absorption (db/km)	Intensity Factor	Line Width
γ_1	$\frac{0.34}{\lambda^2} \left(\frac{P}{1013.25} \right) \left(\frac{293}{T} \right)^2$	$\Delta\nu_1 \left(\frac{P}{1013.25} \right) \left(\frac{293}{T} \right)^{\frac{1}{2}}$ and $\Delta\nu_2 \left(\frac{P}{1013.25} \right) \left(\frac{300}{T} \right)^{\frac{1}{2}}$
$\frac{\gamma_2 \dagger}{\rho}$	$\frac{0.0318}{\lambda^2} \left(\frac{293}{T} \right)^{\frac{1}{2}} \exp \left(-\frac{644}{T} \right)$	$\Delta\nu_3 \left(\frac{P}{1013.25} \right) \left(\frac{318}{T} \right)^{\frac{1}{2}} (1 + 0.0046\rho)$
$\frac{\gamma_3 \dagger}{\rho}$	$\frac{0.05}{\lambda^2} \left(\frac{293}{T} \right)$	$\Delta\nu_4 \left(\frac{P}{1013.25} \right) \left(\frac{318}{T} \right)^{\frac{1}{2}} (1 + 0.0046\rho)$

† ρ is water vapor density in g/m³.

The reference temperatures given are those at which the appropriate experimental determinations were made, and the pressures are to be expressed in millibars. A detailed discussion of the theoretical aspects of the pressure and temperature dependence is given by Artman (1953).

Experimental measurements on the absorption of microwaves by the atmosphere show different values of the loss from those obtained by existing theoretical prediction methods. There is reasonably good agreement between the predicted and measured loss for oxygen, but the measured loss of water vapor is considerably greater than that of the predicted amount, particularly above 50 Gc/s (Straiton and Tolbert, 1960). These observed discrepancies have little effect upon the present study, which is confined to frequencies less than 50 Gc/s. A major disagreement exists concerning the resonant line width factor for oxygen, $\Delta\nu_2$. The laboratory determinations of Birnbaum and Maryott (1955), and Artman and Gordon (1954), give impressive agreement with a centroid value of $\Delta\nu_2 = 0.05 \text{ cm}^{-1}$, whereas outdoor measurements by Straiton and Tolbert (1960) and Bell Telephone Laboratories (1955) give strong support to a value of $\Delta\nu = 0.02 \text{ cm}^{-1}$. The physical reason for the differences between laboratory and outdoor measurements has not been clarified in the literature. The line widths used for the calculation of the illustrative examples of this chapter are those given in Table I, obtained from laboratory measurements. Part of the reason for the choice of the laboratory values is that a clear delineation of the contributions of both resonant absorption and the effect of the wings of other absorption lines at higher frequencies is made; a factor not treated by Straiton and Tolbert. The results of the present study, for the frequency range 100 Mc/s–50 Gc/s, do however agree with those obtained by Tolbert and Straiton (1957) in their field experiments at Cheyenne Mountain and Pikes Peak, Colorado, at altitudes of 14 000 ft.

By taking into account the temperature and pressure dependence of the line widths it is seen that, for a given quantity of water vapor, the attenuation is proportional to

$$P^{-1} \text{ and } T^{-2} \exp\left(-\frac{644}{T}\right)$$

at the resonance line, to

$$P \text{ and } T^{-3} \exp\left(-\frac{644}{T}\right)$$

at the sides of the curve, and to

$$P \text{ and } T^{-3/2}$$

well away from resonance. In applying the above considerations to absorption approximations, it also must be remembered that for a given relative humidity, the density will vary considerably with temperature. Table III shows attenuation caused by water vapor at various temperatures and wavelengths.

TABLE III. *Water Vapor Attenuation (One way) in db/km. After Gunn-East*
P, pressure in atmospheres; W, water vapor content in g/m⁻³

<i>T</i> (°C)	$\lambda = 10$ cm	$\lambda = 5.7$ cm	$\lambda = 3.2$ cm	$\lambda = 1.8$ cm	$\lambda = 1.24$ cm	$\lambda = 0.9$ cm
20	$0.07 \times 10^{-3} PW$	$0.24 \times 10^{-3} PW$	$0.7 \times 10^{-3} PW$	$4.3 \times 10^{-3} PW \dagger$	$22.0 \times 10^{-3} p^{-1} PW \dagger$	$9.5 \times 10^{-3} PW$
0	$0.08 \times 10^{-3} PW$	$0.27 \times 10^{-3} PW$	$0.8 \times 10^{-3} PW$	$4.8 \times 10^{-3} PW \dagger$	$23.3 \times 10^{-3} p^{-1} PW \dagger$	$10.4 \times 10^{-3} PW$
-20	$0.09 \times 10^{-3} PW$	$0.30 \times 10^{-3} PW$	$0.9 \times 10^{-3} PW$	$5.0 \times 10^{-3} PW \dagger$	$24.6 \times 10^{-3} p^{-1} PW \dagger$	$11.4 \times 10^{-3} PW$
-40	$0.10 \times 10^{-3} PW$	$0.34 \times 10^{-3} PW$	$1.0 \times 10^{-3} PW$	$5.4 \times 10^{-3} PW \dagger$	$26.1 \times 10^{-3} p^{-1} PW \dagger$	$12.6 \times 10^{-3} PW$

† The pressure dependencies shown are only approximate. Near the 1.35 cm wavelength water vapor absorption line (between 1.0 cm and 2.0 cm) no simple power is accurate.

TABLE IV. *Pressure and Temperature Correction for Oxygen Attenuation for Wavelengths between 0.7 and 10 cm. After Gunn-East*

<i>T</i> (°C)	Factor
	(<i>P</i> is pressure in atmospheres)
20	$1.00 P^2$
0	$1.19 P^2$
-20	$1.45 P^2$
-40	$1.78 P^2$

The behavior of water vapor attenuation near the resonant line is very remarkable, as can be seen by inspecting equation (2). Since Δv_3 is small compared to $\frac{1}{\lambda}$, it may be neglected in the denominator of equation (2) for non-resonant wavelengths. The attenuation per unit density of water vapor is thus directly proportional to Δv_3 and hence to the total pressure for these frequencies. But at the resonant frequency, the dominant term in the expression is proportional to $\frac{1}{\Delta v_3}$, and thus inversely proportional to the pressure. In the atmosphere, the water vapor density is proportional to vapor pressure, and thus the attenuation at the resonant frequency depends only on the fraction of water vapor present. For practical purposes this means that attenuation can occur at high altitudes with the same effectiveness as in the lower, denser layers if the humidity mixing ratio is the same.

On the other hand oxygen absorption occurs because of a large number of lines around 60 Gc/s. In the region from 3 to 45 Gc/s the attenuation is proportional to P^2 and $T^{-5/2}$ (Gunn and East, 1954). As the temperature decreases the attenuation increases gradually. At -40°C oxygen attenuation is about 78 per cent higher than at 20°C due to increased density at the low temperature. Table IV shows the pressure and temperature corrections for oxygen attenuation at wavelengths between 0.7 and 10 cm.

Since absorption is so sensitive to the absolute humidity level, it is helpful to have information on the climatic variation of absolute humidity throughout the 1 to 99 per cent probability-of-occurrence range of values normally used in radio engineering problems. As an example estimates of the values of absolute humidity at ground surface expected 50 per cent of the time for the United States for February and August are given in Figs. 3 and 4 respectively (Bean and Cahoon, 1957). It is evident that for either month the coastal regions display greater values of absolute humidity than do the inland regions, and it may be noted that for any location the August values are consistently greater than the February values. Figures 5 through 8 show the values of absolute humidity expected to be exceeded 1 and 99 per cent of the time throughout the United States in both summer and winter.

In addition to oxygen and water vapor, there are a number of other atmospheric gases which have absorption lines in the microwave region from 10 to 50 Gc/s. These gases normally constitute a negligible fraction of the general composition of the atmosphere, but could conceivably contribute to attenuation. Table V shows the resonant frequencies, maximum absorption coefficients at 300°K (attenuation coefficient if the fraction of molecules present were equal to unity), expected concentration in the atmosphere, and expected absorption coefficients due to these trace constituents. The data on molecular absorption coefficients has been taken from Ghosh and Edwards (1956), that on concentrations from the Compendium of Meteorology (1951). It is readily seen that the attenuation due to these sources is negligible compared with the high absorption due to oxygen and water vapor.

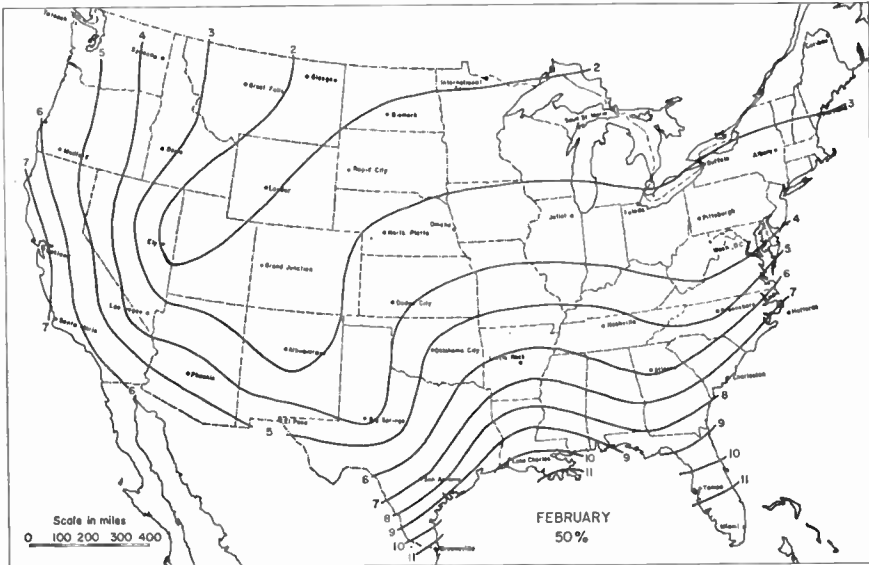


FIG. 3. Estimate of the value of absolute humidity expected 50 per cent of the time for February.

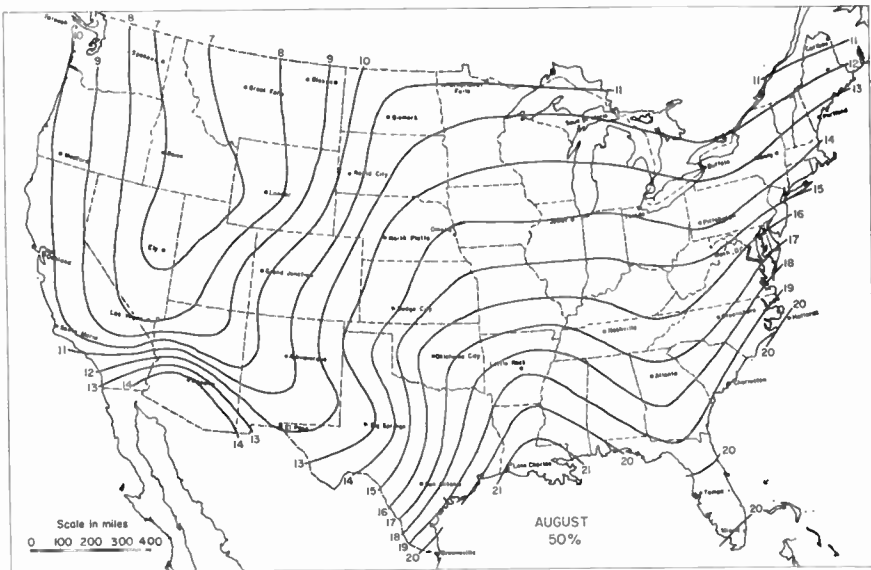


FIG. 4. Estimate of the value of absolute humidity expected 50 per cent of the time for August.

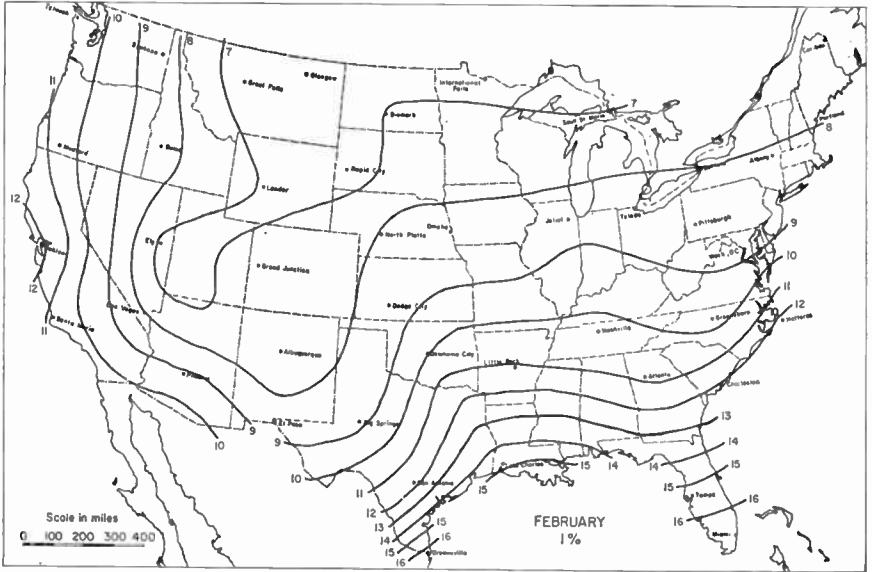


FIG. 5. Values of absolute humidity expected to be exceeded 1 per cent of the time for February.

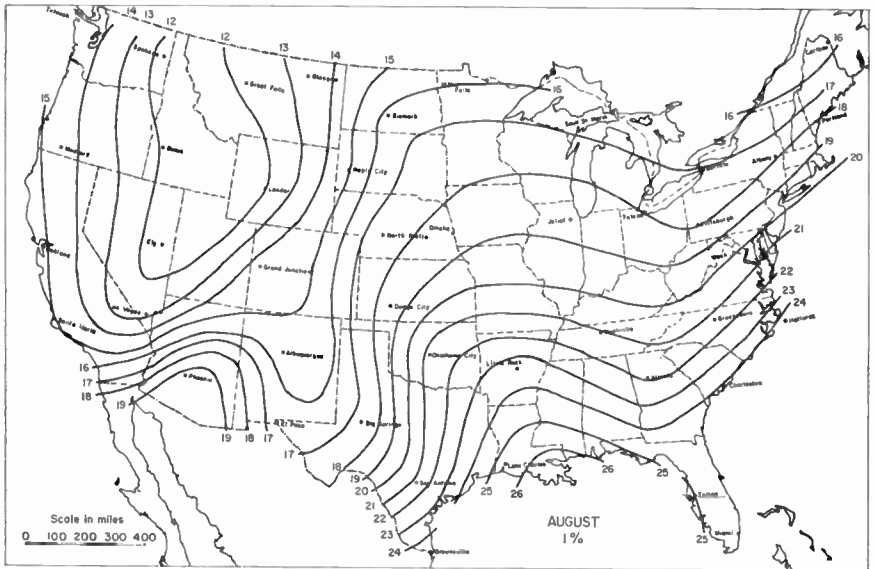


FIG. 6. Values of absolute humidity expected to be exceeded 1 per cent of the time for August.

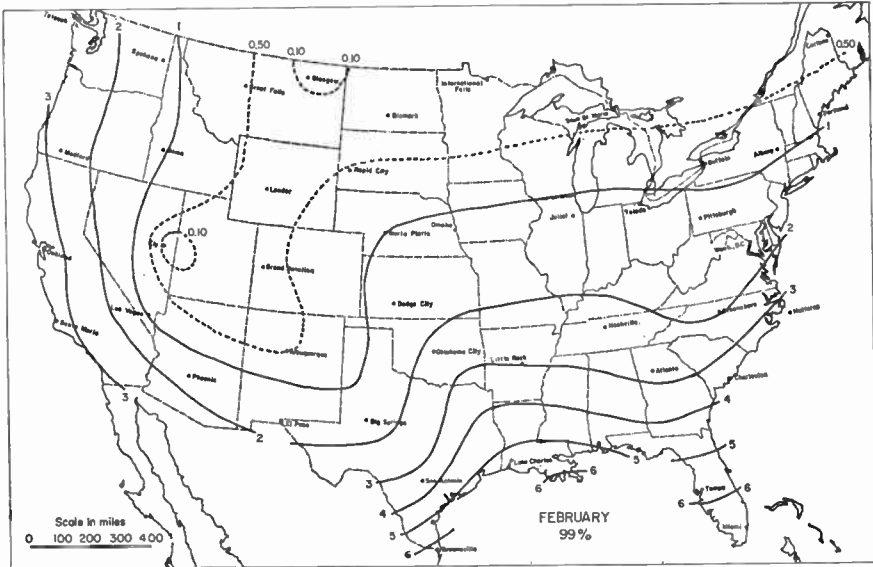


FIG. 7. Values of absolute humidity expected to be exceeded 99 per cent of the time for February.

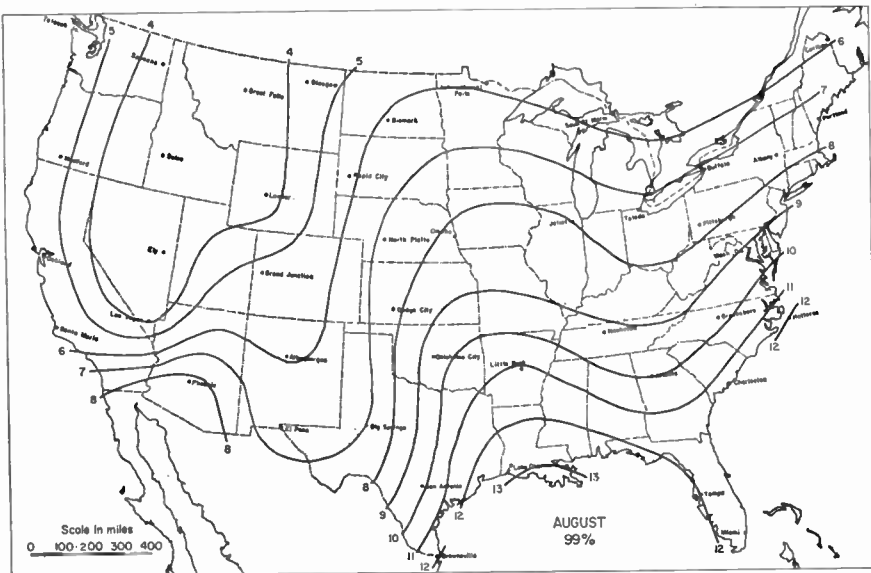


FIG. 8. Values of absolute humidity expected to be exceeded 99 per cent of the time for August.

TABLE V

Gas	ν_0 (Mc/s)	γ_{\max} (db/km)	% by Volume at Ground	γ (db/km) at Ground
SO ₂	12 258·17	1.9×10^{-1}	$(0.1) \times 10^{-6}$	$(0.1.9) \times 10^{-7}$
	12 854·54	8.7×10^{-1}		$(0.8.7) \times 10^{-7}$
	23 433·42	1.2×10^{-1}		$(0.1.2) \times 10^{-7}$
	24 304·96	2.3		$(0.2.3) \times 10^{-6}$
	25 398·22	2.1		$(0.2.1) \times 10^{-6}$
	29 320·36	3.3		$(0.3.3) \times 10^{-6}$
	44 098·62	5.2		$(0.5.2) \times 10^{-6}$
	52 030·60	9.5×10^{-1}		$(0.9.5) \times 10^{-7}$
N ₂ O	24 274·78	2.5	0.5×10^{-6}	1.25×10^{-6}
	22 274·60	2.5		1.25×10^{-6}
	25 121·55	2.5		1.25×10^{-6}
	25 123·25	2.5		1.25×10^{-6}
NO ₂	26 289·6	2.9	$(0.2) \times 10^{-8}$	$(0.5.8) \times 10^{-8}$
	10 247·3	9.5×10^{-2}	Summer $(0.07) \times 10^{-6}$ Winter $(0.02) \times 10^{-6}$	$(0.6.3) \times 10^{-9}$
O ₃	11 075·9	9.1×10^{-2}		$(0.6.3) \times 10^{-9}$
	42 832·7	4.3×10^{-1}		$(0.2.8) \times 10^{-8}$

III. ESTIMATES OF THE RANGE OF TOTAL GASEOUS ABSORPTION

The range in gaseous absorption likely to occur can be seen by considering the data for the months of February and August at Bismarck, North Dakota, and Washington, D.C., two stations with very different climates that represent the range of temperate climate conditions. The values of total gaseous absorption (defined as the sum of γ_1 , γ_2 , and γ_3 , where γ_1 = oxygen absorption in decibels per kilometer, γ_2 = water vapor absorption arising from the 1.35 cm line and γ_3 = additional absorption arising from absorption lines whose frequencies are considerably higher than that corresponding to the 1.35 line) at each station and elevation up to 75 000 ft are shown in Figs. 9 and 10 for each of the four station months for the frequency range of 100 Mc/s to 50 Gc/s. Above 75 000 ft the absorption values for all four station months are identical and are given for each frequency in Fig. 11. The

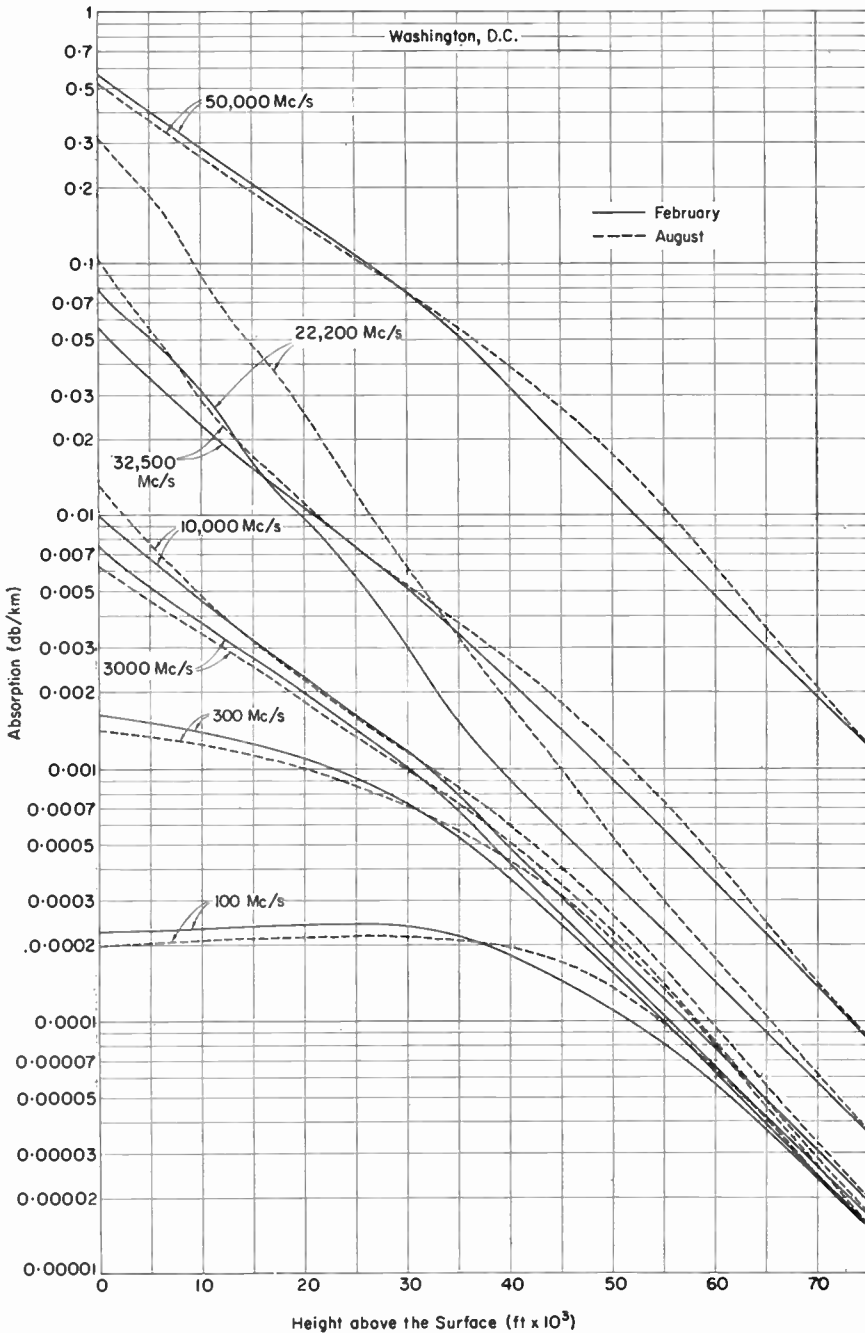


FIG. 9. Total gaseous atmospheric absorption from the surface to 75 000 ft: Washington, D.C.

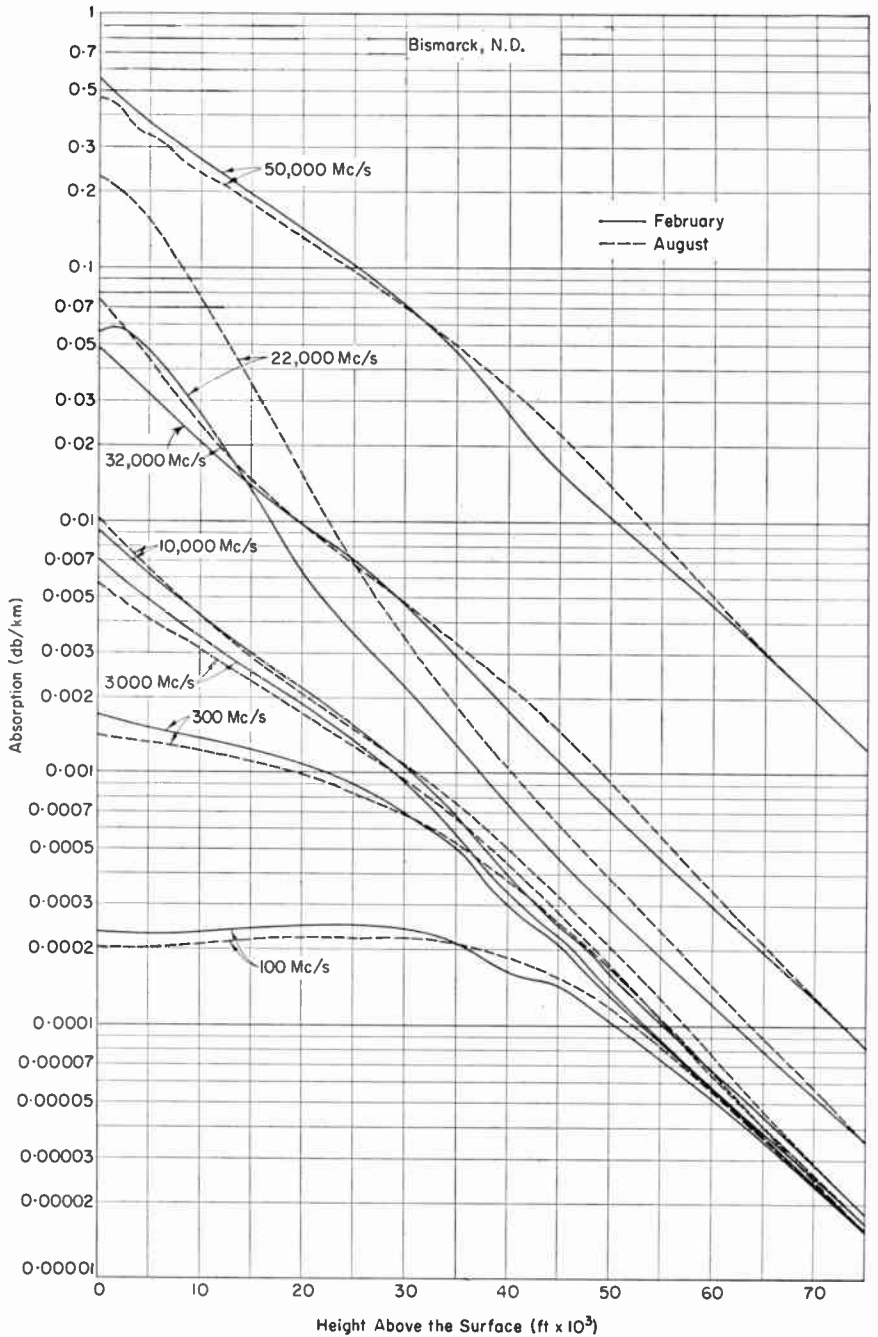


FIG. 10. Total gaseous atmospheric absorption from the surface to 75 000 ft: Bismarck, North Dakota.

absolute humidity was calculated using the upper air monthly average values of temperature, pressure, and humidity as reported by Ratner (1945). Readings for the relative humidity are not generally given in this report for

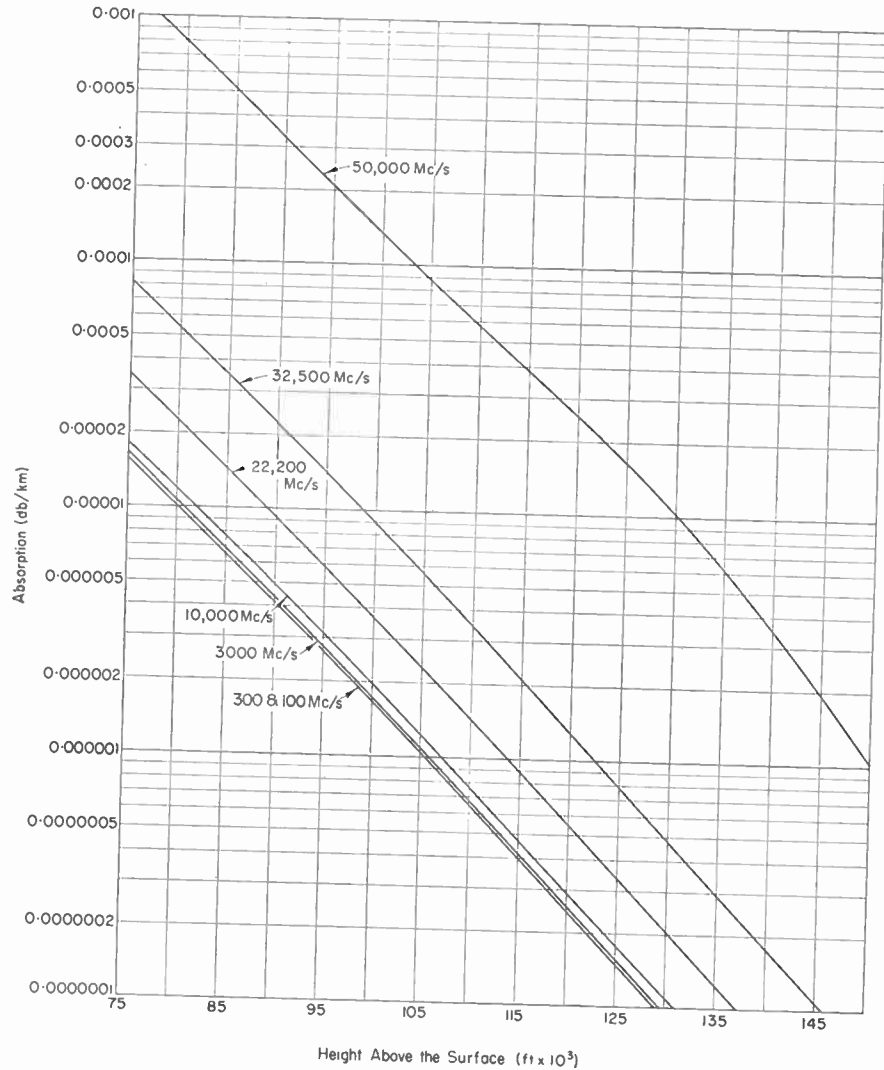


Fig. 11. Common values of total gaseous atmospheric absorption for elevations greater than 75 000 ft.

altitudes greater than about 15 km due to the inability of the radiosonde to measure the small amount of water vapor present at these altitudes. It is believed that the climates represented by these data encompass the range

expected of temperate climates, i.e. excluding arctic, tropic, and desert conditions.

An interesting property of the annual range of absorption as a function of the frequency may be seen in Figs. 9 and 10. For the first 5 000 ft above the surface, it is noted that in the frequency range of 10 to 32.5 Gc/s the summer values are greater than the winter values due to increased humidity of the summer months. Outside of this frequency range, however, the winter values of absorption are greater due to the increased oxygen density.

IV. TOTAL RADIO PATH ABSORPTION

The total path absorption is determined by calculating the various absorption coefficients as functions of the heights along the ray path and then numerically integrating the values along the entire path using standard ray

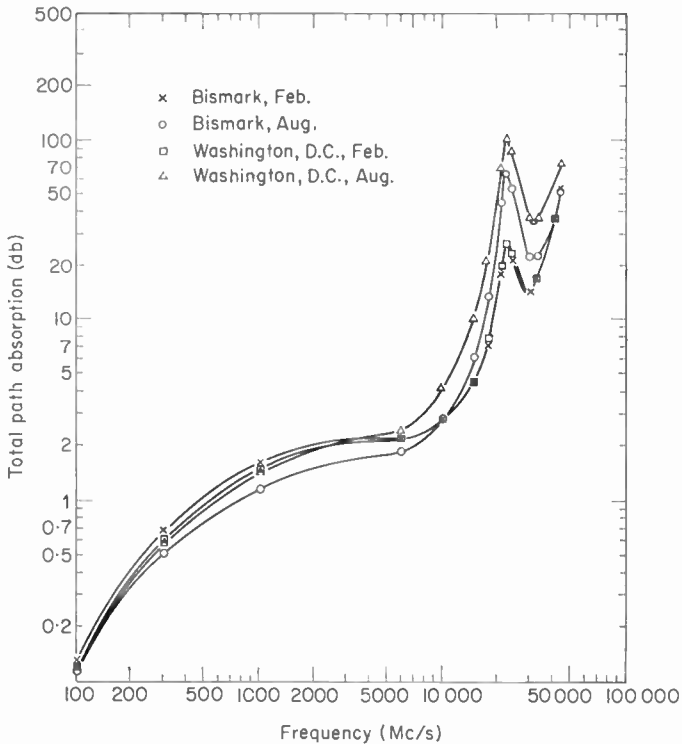


FIG. 12. Total path absorption over a 1 000 km propagation path with the climate of Bismarck, North Dakota, and Washington, D.C.

tracing techniques. The values of total path integrations over a 1 000 km path thus obtained are presented in Fig. 12 for Bismarck, North Dakota, and Washington, D.C. The difference between the two climates is evident principally at the higher frequencies, where the Washington absorptions are

consistently above the Bismarck values. This is apparently due to a combination of generally greater humidities and greater refractive effects. These two effects are related. The increased humidity at Washington enhances the water vapor absorption and increases the refraction causing the radio ray to travel consistently through lower levels of the atmosphere with consequent increase in total path absorption.

V. DERIVATION OF ABSORPTION ESTIMATE FOR OTHER AREAS

The values of total path absorption given above are for two specific locations. For practical use the correlation between total path absorption and the surface value of the absolute humidity, expressed in grams of water vapor per cubic meter may be used to estimate absorption at other times and places. The basis for the correlation between the absolute humidity and the total path absorption is that the absorption at those frequencies for which water vapor absorption is dominant (approximately 10 to 32 Gc/s) varies directly as the absolute humidity, while for those frequencies at which oxygen absorption is dominant, it varies inversely as the absolute humidity due to the inverse relationship of oxygen density and water vapor density. That is, during the warm seasons of the year the total atmospheric pressure tends toward its yearly minimum (as does the oxygen absorption), while the absolute humidity tends toward its yearly maximum (as does the water vapor absorption). Conversely, during the colder seasons of the year the pressure tends toward its maximum value while the absolute humidity tends toward its minimum value (Bean and Abbott, 1957).

As an example of the correlation method, the surface absorption calculated at a water vapor-dominated frequency (22.2 Gc/s) and oxygen-dominated frequency (50 Gc/s) for each month throughout the year, for both Washington and Bismarck, are plotted on Fig. 13. The term surface absorption is used for the values of absorption calculated from standard ground level weather observations. The water-dominated 22.2 Gc/s data fall on a smooth curve despite the pressure and temperature differences of the two stations. The oxygen-dominated 50 Gc/s data, however, display an interesting separation of points for each station, although the distribution of points at the two locations display similar slopes. The 50 Gc/s absorption is more sensitive to the atmospheric density difference between the stations. If the pressure differences were taken into account the Bismarck data would increase about 12 per cent, and the two curves would be distributed along a common line with the same slope as the original two curves. This figure, then, indicates that the absorption is correlated with the absolute humidity. The above illustration is for surface values rather than for integrated propagation path values. Variations in the upper air meteorology that are not reflected in the surface values will tend to diminish the correlation. (For comparison of percentage absorption over a 300-mile path, the first few hundred feet contribute about 5 per cent at 100 Mc/s increasing to 42 per cent at 10 Gc/s and remaining constant to 50 Gc/s.) Keeping these reservations in mind one may utilize the method of least squares to obtain the total path absorption as a linear function of the absolute humidity. The parameters of the statistical

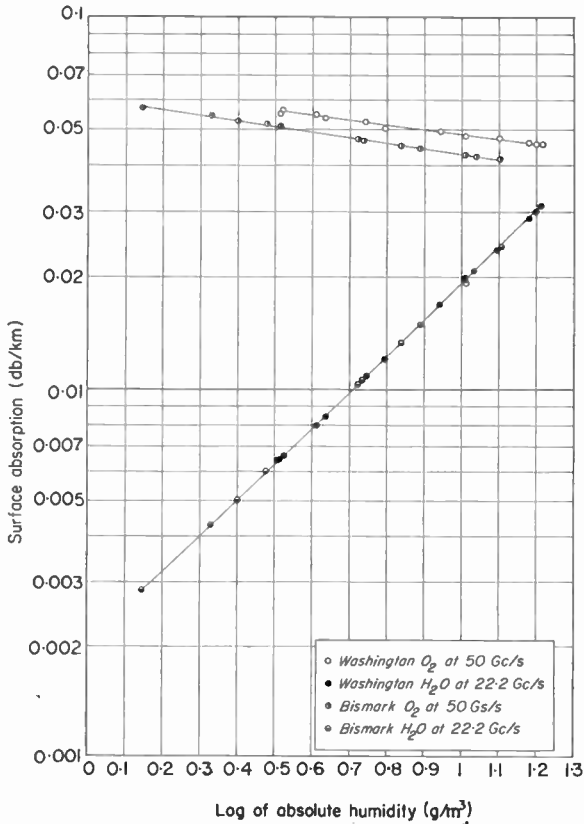


FIG. 13. Surface value of 22.2 and 50 Gc/s absorption versus absolute humidity at Washington, D.C., and Bismarck, North Dakota.

regression line at each frequency for path propagation distances of 100, 300, and 1 000 miles are given in Table VI, and also plotted on Fig. 14, allowing the reader to estimate the regression line as a function of distance and frequency.

Statistics for the variation of absolute humidity have already been given, and contours of the mean values of absolute humidity for the world are given on Figs. 15 and 16 for the months of February and August respectively. More detailed data on water vapor distribution have been given by Tunnell (1958). It is noted that the absolute humidity for either month is greater in the coastal regions than in the continental interiors and that the windward sides of continents have larger values than do the leeward sides. These average values of absolute humidity and the regression parameters of Table VI may be used to estimate the average attenuation at the earth's surface. Similarly, by reference to the statistics of absolute humidity *variation* (Bean and Cahoon, 1957) one may derive estimates of the absorption expected to

TABLE VI. Values of m and b in the regression line $y = mx + b$, where y is the logarithm of the total path attenuation, b is the value of y when the absolute humidity is 1g/m^3 , and x is the logarithm of the absolute humidity.

Distance	100 km		300 km		1 000 km	
Freq. (Mc/s)	m	b	m	b	m	b
100	-0.07263	-3.69822	-0.06324	-2.60042	-0.13298	-1.83711
300	-0.08212	-1.72139	-0.06363	-0.73037	-0.15276	-0.17792
1 000	-0.10203	-0.49427	-0.07078	+0.31846	-0.16932	+0.75687
6 000	+0.06996	-0.24077	+0.06872	+0.54167	-0.04731	+0.96517
10 000	+0.26022	-0.14038	+0.23447	+0.64637	+0.10831	+1.06172
15 000	+0.48097	+0.20891	+0.44214	+0.98393	+0.31506	+1.36994
18 000	+0.62034	+0.65324	+0.58044	+1.42477	+0.46112	+1.77604
21 000	+0.75045	+1.41086	+0.70693	+2.25807	+0.60558	+2.56360
22 406	+0.77630	+1.67001	+0.72874	+2.57270	+0.62885	+2.87766
23 076	+0.77153	+1.69105	+0.72508	+2.57734	+0.62963	+2.87575
24 000	+0.74979	+1.62838	+0.70659	+2.46633	+0.60458	+2.77175
30 000	+0.54155	+1.34408	+0.50126	+2.11161	+0.37634	+2.48455
33 000	+0.46305	+1.51053	+0.42416	+2.28497	+0.29646	+2.67460
42 000	+0.25936	+2.46361	+0.23331	+3.25085	+0.10712	+3.66659
45 000	+0.18460	+2.91681	+0.16668	+3.70472	+0.04360	+4.12531

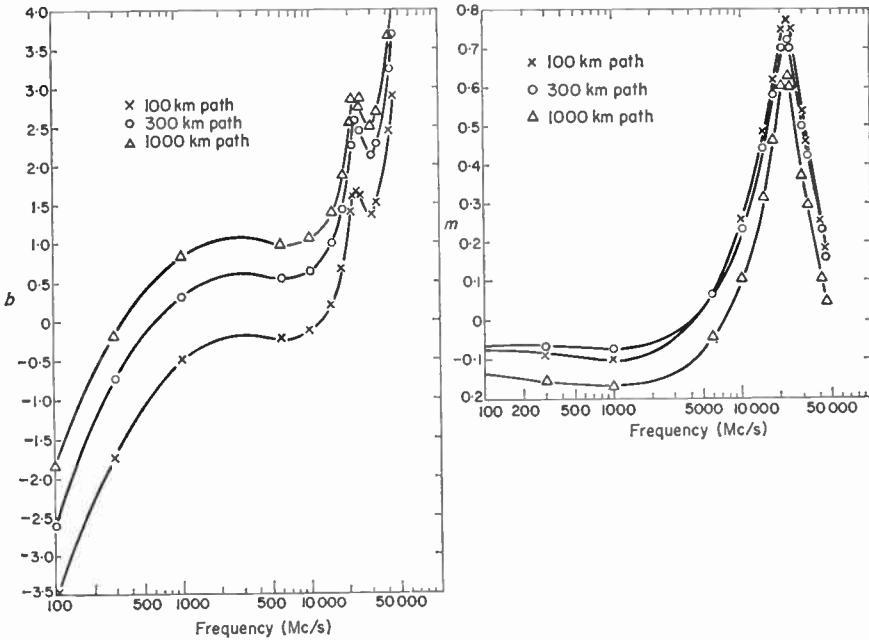


FIG. 14. Values of b and m in the regression line $y = mx + b$, where y is the logarithm of the total path absorption, x is the logarithm of the absolute humidity, b is the value of y when the absolute humidity is 1g/m^3 .

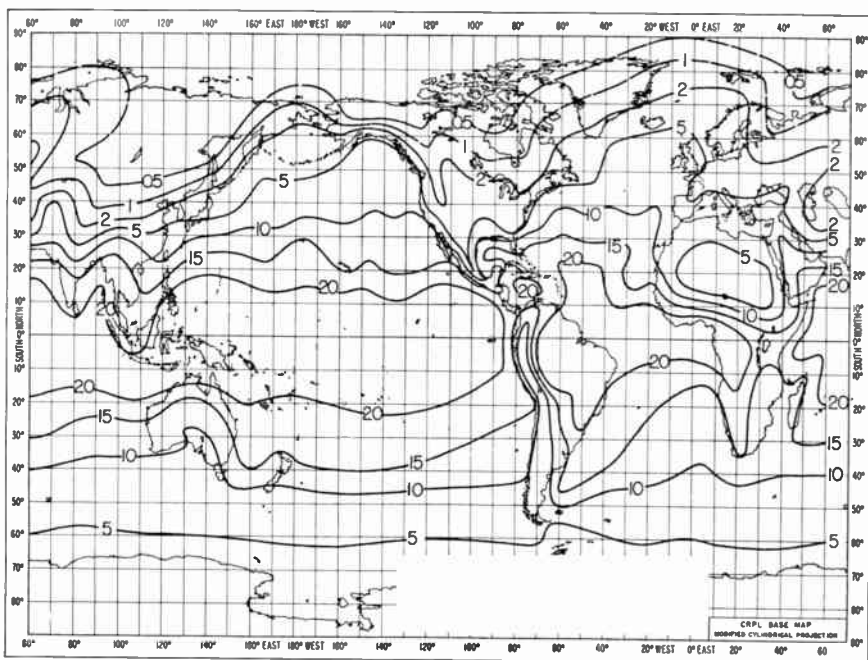


FIG. 15. Average absolute humidity (g/m^3), February.

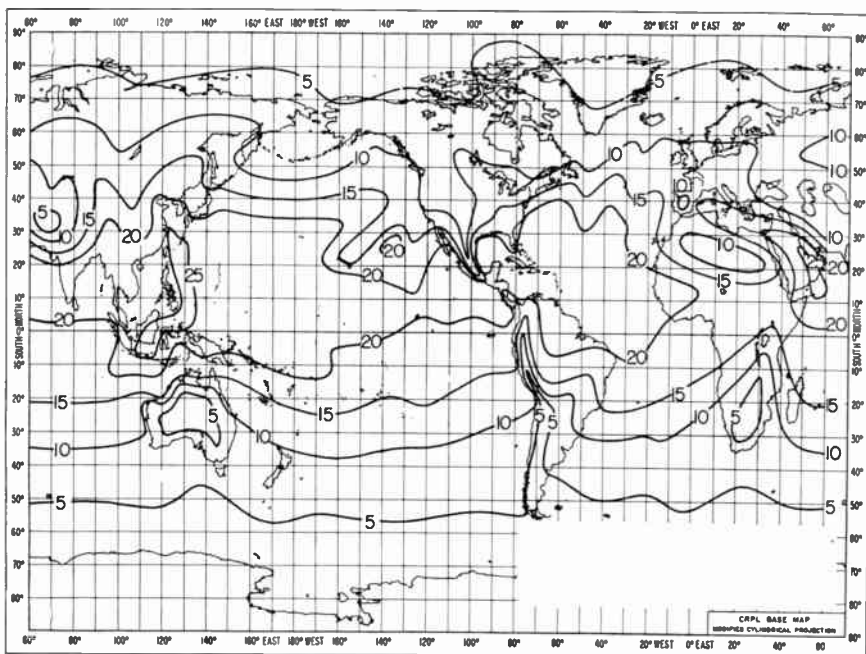


FIG. 16. Average absolute humidity (g/m^3), August.



FIG. 17. August values of 300-mile propagation path absorption loss (in db) to be exceeded 1 per cent of the time for a frequency of 10 Gc/s.

be exceeded for any other percentage of the time. As an example, Fig. 17 gives the values expected to be exceeded 1 per cent of the time over a 300-mile propagation path at 10 Gc/s for the United States during the month of August.

VI. ATTENUATION IN CLOUDS

Cloud droplets are regarded here as those water or ice particles having radii smaller than 0.01 cm. For wavelengths of incident radiation well in excess of 0.5 cm, the attenuation becomes independent of the drop size distribution. The generally accepted equations for attenuation by clouds usually show the moisture component of the equation in the form of the liquid water content (g/m^3). Observations indicate that the liquid water concentration in clouds generally ranges from 1 to 2.5 g/m^3 (Donaldson, 1955), although Weickmann and Kampe (1953) have reported isolated instances of cumulus congestus clouds with a reading of 4.0 g/m^3 in the upper levels. In ice clouds it will rarely exceed 0.5 and is often less than 0.1 g/m^3 . The attenuation due to cloud drops may be written as:

$$K = K_1 M \quad (4)$$

where K = attenuation in db/km
 K_1 = attenuation coefficient in db/km/ g/m^3
 M = liquid-water content in g/m^3 .

Values of K_1 for ice and water clouds are given for various wavelengths and temperatures by Table VII (Gunn and East, 1954).

TABLE VII. *One-Way Attenuation Coefficient, K_1 , in Clouds in db/km/g/m³*

Temperature (°C)	Wave Length (cm)				
	0.9	1.24	1.8	3.2	
Water Cloud	20	0.647	0.311	0.128	0.0483
	10	0.681	0.406	0.179	0.0630
	0	0.99	0.532	0.267	0.0858
	-8	1.25	0.684	0.34 (ex- trapolated)	0.112 (ex- trapolated)
Ice Cloud	0	8.74×10^{-3}	6.35×10^{-3}	4.36×10^{-3}	2.46×10^{-3}
	-10	2.93×10^{-3}	2.11×10^{-3}	1.46×10^{-3}	8.19×10^{-4}
	-20	2.0×10^{-3}	1.45×10^{-3}	1.0×10^{-3}	5.63×10^{-4}

Several important facts are demonstrated by Table VII. The decrease in attenuation with increasing wavelength is clearly shown. The values change by about an order of magnitude for a change of wavelength from 1 to 3 cm. The data presented here also show that attenuation increases with decreasing temperature. Ice clouds give attenuations about two orders of magnitude smaller than water clouds of the same water content, and so can be neglected for all practical purposes (Battan, 1959). The comprehensive papers by Gunn and East (1954) and Battan (1959) on attenuation offer excellent sources of detailed information on this subject.

VII. ATTENUATION BY RAIN

Ryde and Ryde (1945) calculated the effects of rain on microwave propagation and showed that absorption and scattering effects of raindrops become more pronounced at the higher microwave frequencies where the wavelength and the raindrop diameters are more nearly comparable. In the 10 cm band and at smaller wavelengths the effects are appreciable, but at wavelengths in excess of 10 cm the effects are greatly decreased. It is also known that fog and rain have an absorption rate in excess of that of the gaseous constituents. For example, in considering the effect of various attenuations on marine navigational radar, Saxton and Hopkins (1951) conclude that fog would have little effect upon 10 cm radar but that the normal range of 50 km of a 3.2 cm wavelength radar might well be reduced to 30 km in severe arctic fog. A similar reduction in range would not be expected in temperate and tropical-equatorial regions. Attenuation due to rain may, however, be quite serious, especially in heavy tropical cloud-bursts.

In practice it has been convenient to express rain attenuation as a function of the precipitation rate, R , which depends on both the liquid water content

and the fall velocity of the drops, the latter in turn depending on the size of the drops. Ryde studied the attenuation of microwaves by rain and showed that this attenuation in db/km is given approximately by:

$$K_R = K \int_0^r R(r)^\alpha dr \quad (5)$$

where

- K_R = total attenuation in db
- K = constant
- $R(r)$ = rainfall rate
- r = length of propagation path in km
- α = constant.

Laws and Parsons (1943) observed the distribution of drop sizes for various rates of fall on a horizontal surface, and found that the higher the rainfall rate, the larger the drops, and also the greater the range in size of the drops. However, in order to derive the size distributions occurring while the drops are falling freely in the air, each value must be divided by the particular velocity of fall appropriate to the corresponding drop diameter. Figure 18

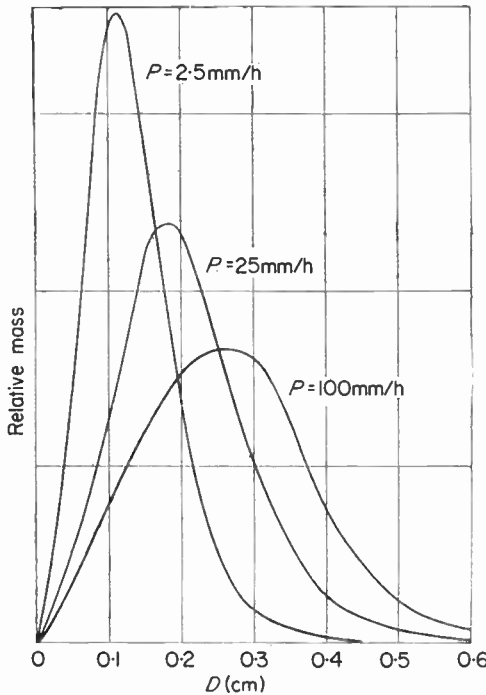


FIG. 18. Relative total mass of liquid water in the air contributed by drops of diameter D for various precipitation rates. (Derived from Laws and Parsons' distributions for a horizontal surface by dividing by the appropriate terminal velocities.)

shows the resulting distribution in air, expressed as the relative mass of drops of given diameter, for three chosen representative values of precipitation rate, p , namely, 2.5 mm/h, 25 mm/h, and 100 mm/h (Ryde, 1946). The excess path loss per mile, according to Ryde, for the three carrier frequency bands of 4, 6, and 11 Gc/s is shown on Fig. 19. Figure 20 (Hathaway and Evans, 1959) is a scatter diagram showing transmission loss versus rainfall rate. For comparison, Ryde's equation is plotted on Fig. 20.

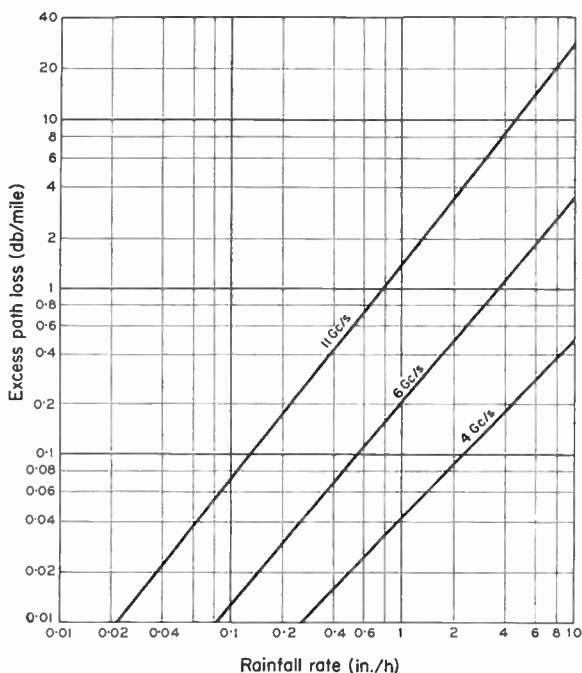


FIG. 19. Rain attenuation versus rainfall rate (Theoretical, after Ryde and Ryde, 1945).

The greatest uncertainty in predictions of attenuation due to rainfall, using theoretical formulae as a basis for calculation, is the extremely limited knowledge of drop size distribution in rains of varying rates of fall observed under differing climatic and current weather conditions. There is little evidence that a rain with a known rate of fall has a unique drop-size distribution, though studies on this problem seem to indicate that a most probable drop size distribution can be attached to a rain of given rate of fall (Laws and Parsons, 1943). Table VIII shows the percentage of total volume of rainfall occupied by raindrops of different diameters (cm) and varying rainfall rates (mm/h). Tables VIII through X enable one to estimate the attenuation of radio waves by raindrops (Burrows and Attwood, 1949). Using Table VIII, the absorption cross-sections of raindrops (Mie, 1908; Burrows and Attwood, 1949) have been computed for use in Table IX. This latter table gives the

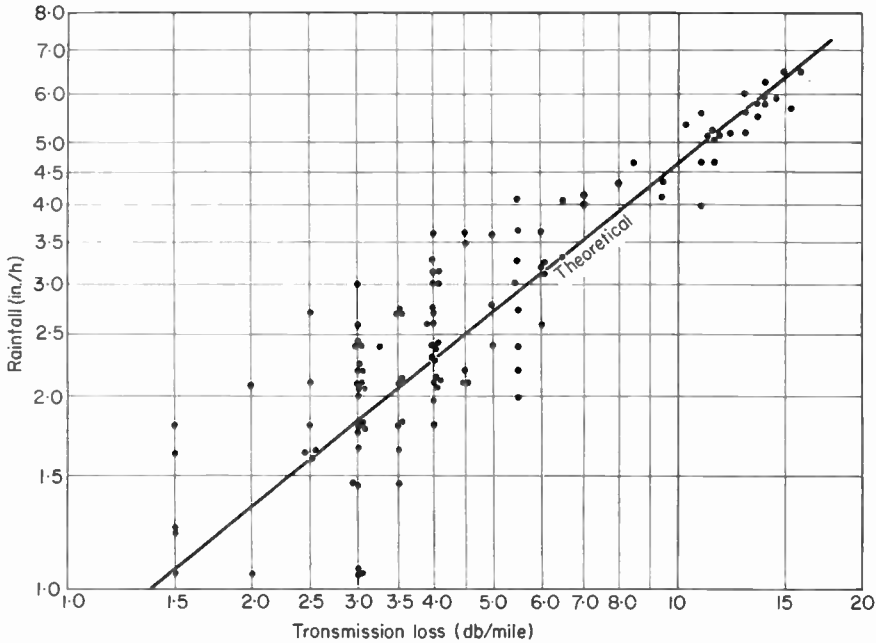


FIG. 20. Transmission loss in decibels per mile versus rainfall in inches per hour. (After Hathaway and Evans, 1959.)

TABLE VIII. Drop Size Distribution (Burrows-Attwood)

Rainfall mm/h	0.25	1.25	2.5	12.5	25	50	100	150
Drop diameter cm	Percentage of total volume							
0.05	28.0	10.9	7.3	2.6	1.7	1.2	1.0	1.0
0.10	50.1	37.1	27.8	11.5	7.6	5.4	4.6	4.1
0.15	18.2	31.3	32.8	24.5	18.4	12.5	8.8	7.6
0.20	3.0	13.5	19.0	25.4	23.9	19.9	13.9	11.7
0.25	0.7	4.9	7.9	17.3	19.9	20.9	17.1	13.9
0.30		1.5	3.3	10.1	12.8	15.6	18.4	17.7
0.35		0.6	1.1	4.3	8.2	10.9	15.0	16.1
0.40		0.2	0.6	2.3	3.5	6.7	9.0	11.9
0.45			0.2	1.2	2.1	3.3	5.8	7.7
0.50				0.6	1.1	1.8	3.0	3.6
0.55				0.2	0.5	1.1	1.7	2.2
0.60					0.2	0.5	1.0	1.2
0.65						0.2	0.7	1.0
0.70								0.3

TABLE IX. Attenuation in db/km for Different Rates of Precipitation of Rain. Temperature 18°C, λ in cm (Burrows-Attwood)

p mm/h	$\lambda=0.3$	$\lambda=0.4$	$\lambda=0.5$	$\lambda=0.6$	$\lambda=1.0$	$\lambda=1.25$	$\lambda=3.0$	$\lambda=3.2$	$\lambda=10$
0.25	0.305	0.230	0.160	0.106	0.037	0.0215	0.00224	0.0019	0.0000997
1.25	1.15	0.929	0.720	0.549	0.228	0.136	0.0161	0.0117	0.000416
2.5	1.98	1.66	1.34	1.08	0.492	0.298	0.0388	0.0317	0.000785
12.5	6.72	6.04	5.36	4.72	2.73	1.77	0.285	0.238	0.00364
25.0	11.3	10.4	9.49	8.59	5.47	3.72	0.656	0.555	0.00728
50	19.2	17.9	16.6	15.3	10.7	7.67	1.46	1.26	0.0149
100	33.3	31.1	29.0	27.0	20.0	15.3	3.24	2.80	0.0311
150	46.0	43.7	40.5	37.9	28.8	22.8	4.97	4.39	0.0481

TABLE X. Attenuation in Rains of Known Drop Size Distribution and Rate of fall (db/km) (Burrows-Attwood)

p mm/h	Wavelength λ in cm					
	1.25	3	5	8	10	15
2.46	$1.93 \cdot 10^{-1}$	$4.92 \cdot 10^{-2}$	$4.24 \cdot 10^{-3}$	$1.23 \cdot 10^{-3}$	$7.34 \cdot 10^{-4}$	$2.80 \cdot 10^{-4}$
4.0	$3.18 \cdot 10^{-1}$	$8.63 \cdot 10^{-2}$	$7.11 \cdot 10^{-3}$	$2.04 \cdot 10^{-3}$	$1.19 \cdot 10^{-3}$	$4.69 \cdot 10^{-4}$
6.0	$6.15 \cdot 10^{-1}$	$1.92 \cdot 10^{-1}$	$1.25 \cdot 10^{-2}$	$3.02 \cdot 10^{-3}$	$1.67 \cdot 10^{-3}$	$5.84 \cdot 10^{-4}$
15.2	2.12	$6.13 \cdot 10^{-1}$	$5.91 \cdot 10^{-2}$	$1.17 \cdot 10^{-2}$	$5.68 \cdot 10^{-3}$	$1.69 \cdot 10^{-3}$
18.7	2.37	$8.01 \cdot 10^{-1}$	$5.13 \cdot 10^{-2}$	$1.10 \cdot 10^{-2}$	$6.46 \cdot 10^{-3}$	$1.85 \cdot 10^{-3}$
22.6	2.40	$7.28 \cdot 10^{-1}$	$5.29 \cdot 10^{-2}$	$1.21 \cdot 10^{-2}$	$6.96 \cdot 10^{-3}$	$2.27 \cdot 10^{-3}$
34.3	4.51	1.28	$1.12 \cdot 10^{-1}$	$2.32 \cdot 10^{-2}$	$1.17 \cdot 10^{-2}$	$3.64 \cdot 10^{-3}$
43.1	6.17	1.64	$1.65 \cdot 10^{-1}$	$3.33 \cdot 10^{-2}$	$1.62 \cdot 10^{-2}$	$4.96 \cdot 10^{-3}$

decibel attenuation per kilometer in rains of different rates of fall and radio wavelengths between 0.3 and 10 cm. In Table X, similar to Table IX, an additional set of results is contained for rains of measured drop-size distribution.

Since the scattering coefficients (Mie, 1908) depend on the temperature (because of its effects on the dielectric properties of water), it is important to evaluate the attenuation of rains whose drops are at different temperatures from those in the preceding tables. Table XI contains the necessary data relative to the change of attenuation with temperature and is to be used with Table IX. For example, in Table IX with a precipitation rate of $p = 0.25$ mm/h, temperature of 18°C, $\lambda = 1.25$ cm, the attenuation is 0.0215 db/km. Using the correction factors obtained from Table XI, for the same general conditions of precipitation and wavelength, for a temperature reading of

TABLE XI. *Temperature Correction for the Data of Table IX (Burrows-Attwood)*

Rate of Rainfall mm/h	λ cm	Correction Factor $\theta(T)$				
		$T = 0^\circ\text{C}$	$T = 10^\circ\text{C}$	$T = 18^\circ\text{C}$	$T = 30^\circ\text{C}$	$T = 40^\circ\text{C}$
0.25	0.5	0.85	0.95	1.0	1.02	0.99
	1.25	0.95	1.00	1.0	0.90	0.81
	3.2	1.21	1.10	1.0	0.79	0.55
2.5	10.0	2.01	1.40	1.0	0.70	0.59
	0.5	0.87	0.95	1.0	1.03	1.01
	1.25	0.85	0.99	1.0	0.92	0.80
12.5	3.2	0.82	1.01	1.0	0.82	0.64
	10.0	2.02	1.40	1.0	0.70	0.59
	0.5	0.90	0.96	1.0	1.02	1.00
50.0	1.25	0.83	0.96	1.0	0.93	0.81
	3.2	0.64	0.88	1.0	0.90	0.70
	10.0	2.03	1.40	1.0	0.70	0.59
150	0.5	0.94	0.98	1.0	1.01	1.00
	1.25	0.84	0.95	1.0	0.95	0.83
	3.2	0.62	0.87	1.0	0.99	0.81
	10.0	2.01	1.40	1.0	0.70	0.58
	0.5	0.96	0.98	1.0	1.01	1.00
	1.25	0.86	0.96	1.0	0.97	0.87
	3.2	0.66	0.88	1.0	1.03	0.89
	10.0	2.00	1.40	1.0	0.70	0.58

0°C the attenuation reads 0.02043 db/km; for a value of 30°C an attenuation of 0.019350 db/km is noted; and for a temperature of 40°C the attenuation is 0.01742 db/km.

VIII. RAIN ATTENUATION EFFECTS ON RADIO SYSTEMS ENGINEERING

Attenuation due to rainfall is obviously a dominating factor in determining the reliability of a communications system, especially at frequencies in excess of 30 Gc/s. Rain varies greatly in frequency of occurrence from one region to another, so it is important to have an effective method of predicting the performance of a radio system in any region in order that the communications engineer will be able to gain the widest possible application and degree of reliability, consistent with cost, in any system of his design

Unfortunately, the present state of meteorological knowledge concerning raindrop size and distribution is such that no conclusions can be drawn on a systematic or climatological basis. However, Bussey (1950) has shown that the absorption due to rainfall exceeds that of gaseous constituents about 5 per cent of the time for frequencies about 6 Gc/s. The 5 per cent figure was obtained by a study of the rainfall rate distribution for various locations in the United States. Figure 21 shows the combined rain and gaseous absorption to be exceeded 1 per cent of the time.

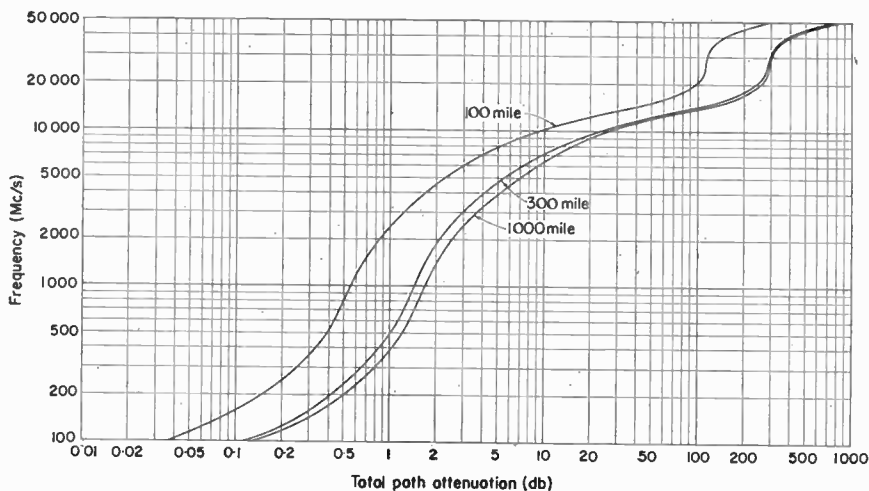


FIG. 21. Combined rain and gaseous absorption to be exceeded 1 per cent of the time.

This section will be concerned, in the main, and by way of illustrative example, with the results of the Bell System's (Hathaway and Evans, 1959) field experiment in the Mobile, Alabama, area, which was designed to establish a relationship between excess path attenuation and instantaneous rate of rainfall and to seek out any relationship between the variation of rate of rainfall along a radio path and rainfall measured at a point. The main problem concerns the ability to predict outage time (time the system noise exceeds the system objective) at 11 Gc/s in all areas of the country that is due to rainfall. This is obviously a difficult problem since, due to reasons of cost, it is not feasible to measure rainfall attenuation in all parts of the country. Therefore it is desirable to be able to use what rainfall data are available and to couple the data, through what are thought to be reasonable assumptions, to the relationships between rainfall and attenuations. In approaching the problem of predicting the outage time due to rainfall, it has been assumed that the annual distribution of 1-h point rainfall rates is indicative of the instantaneous values over 30-mile radio paths (Bussey, 1950) and that the frequency of severe rainfall of the type measured in the Mobile area will be reduced in other parts of the country in proportion to the distribution of annual point rates of one inch or more rainfall per hour.

Figure 22 indicates the expected outage time due to rainfall for various path lengths in different rain areas of the United States. The curves A through H correspond to the areas contoured in Fig. 23, which illustrates contours of constant path length for fixed outage times for different areas of the United States. The longer paths have been somewhat weighted to take into account the less severe rainfall covering larger geographical areas than the intense storms typical of the Gulf region. In a complete point-to-point relay system the rain outages of the individual hops must be added to obtain the performance of the system. It is desirable that the individual hops meet

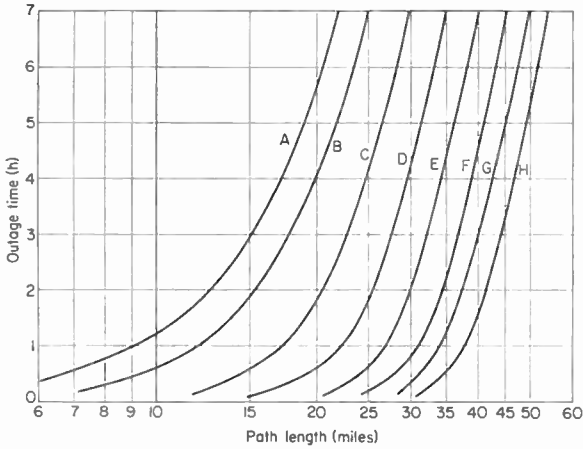


FIG. 22. Expected outage time in hours per year versus path length in miles for various areas of the United States. (After Hathaway and Evans, 1959.)

the same objective, but this is not always possible. Sometimes one or more hops of a system are electrically long; they will have insufficient fading margin (the number of db the receiver input level can be reduced before the noise exceeds the system objective) and hence contribute more than their share of the outage time; and this excess must then be made up by imposing

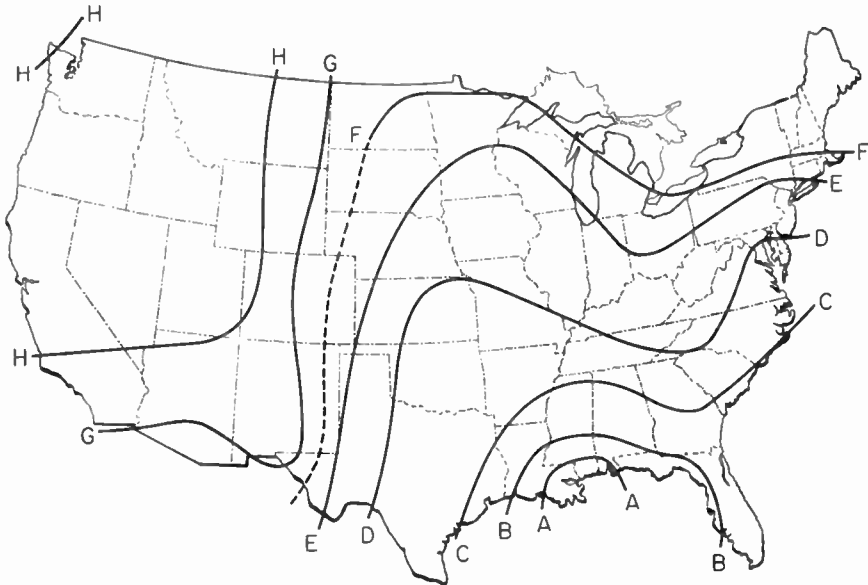


FIG. 23. Contours of constant path length for fixed outage time. (After Hathaway and Evans, 1959.)

tighter requirements on the remaining hops. To meet the over-all objective of a relay system, it is necessary to know the contributions of the long hops—those having a fading margin less than 40 db. Figure 24 shows the excess path loss due to rain versus hours per year for the Mobile area study. The

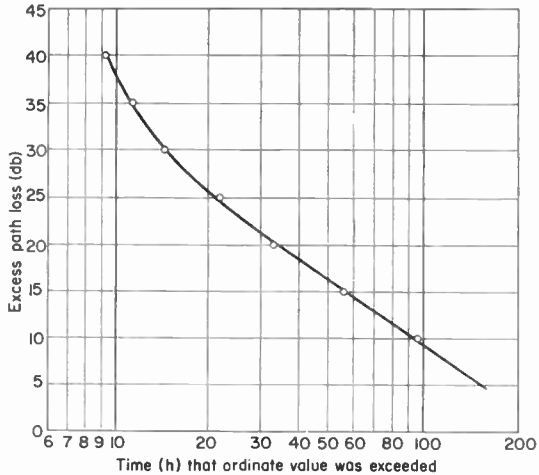


FIG. 24. Excess path loss due to rainfall versus hours per year at Mobile, Alabama. (After Hathaway and Evans, 1959.)

shape of this curve is nearly identical to Bussey's curve of cumulative distribution for point rates in Washington, D.C.; and if it is assumed that this shape is representative of other areas of the country then the additional

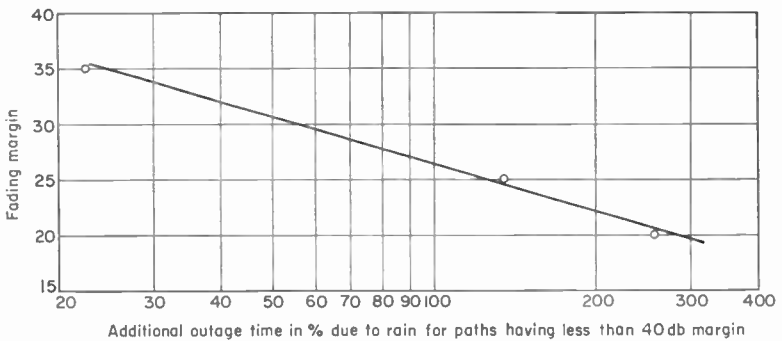


FIG. 25. Additional outage time expected for 11 Gc/s systems having a fading margin less than 40 db.

outage time for path lengths given by Fig. 23 can be estimated for hops having a fading margin less than 40 db. The data shown on Fig. 23 have been rationalized and are shown in Fig. 25 as an estimate of additional outage time. Sometimes it is practical to shorten a proposed path to bring

the fading margin up to 40 db. An approximation of the necessary reduction path length can be made if uniform rainfall rate is assumed over the path. Under this condition the attenuation due to rainfall should be directly proportional to the path length. Thus the path length in Fig. 24 can be shortened to correct for insufficient fading margin.

The experimental results of Hathaway and Evans (1959) indicate that for microwave relay links in the extreme southeastern region of the United States rainfall will limit 11 Gc/s radio systems having a 40 db fading margin to path lengths of approximately 10 to 15 miles, depending on the number of hops, if normal reliability objectives are to be met. Path lengths of 20 to 30 miles should be acceptable in the central area and paths as long as 35 miles should be acceptable in the northwestern part of the country. However, in their existing point-to-point radio relay systems the paths average about 23 miles due to considerations other than those of propagation. An

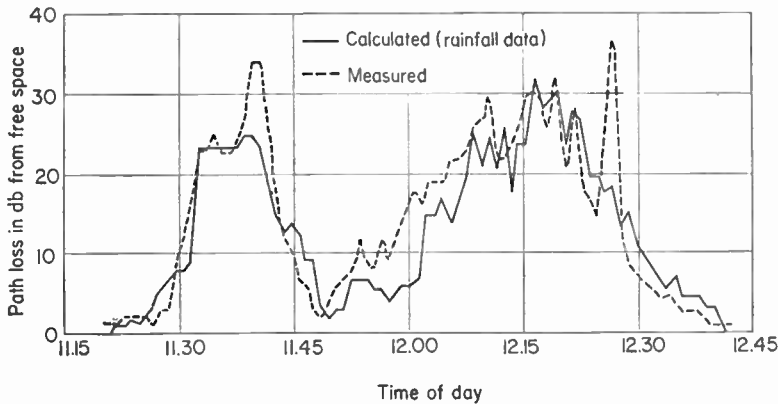


FIG. 26. Correlation between rainfall and path loss, 15 March 1956. (After Hathaway and Evans, 1959.)

illustration of the correlation between the rainfall and path loss on 15 March 1956, of the Mobile study is presented in Fig. 26 in support of the above conclusions.

IX. ATTENUATION BY HAIL

Ryde concluded that the attenuation caused by hail is about one-hundredth of that caused by rain, that ice crystal clouds cause no sensible attenuations, and that snow produces very small attenuation even at the excessive rate of fall of 5 in. an hour. However, the scattering by spheres surrounded by a concentric film of different dielectric constant does not give the same effect that Ryde's results for homogeneously mixed spheres of ice and water would indicate (Hathaway and Evans, 1959; Kerker *et al.*, 1951). For example, when one-tenth of the radius of an ice sphere of radius 0.2 cm melts, the scattering of 10 cm radiation is approximately 90 per cent of the value which would be scattered by an all-water drop.

At wavelengths of 1 and 3 cm with $\gamma = 0.126$ ($\gamma = 2a/\lambda$; a = radius of drop) Kerker *et al.* (1951) found that particles attained total attenuation cross-sections corresponding to all-melted particles when less than 10 per cent of the ice particles were melted. When the melted mass reached about 10–20 per cent, the attenuation was about twice that of a completely melted particle. These calculations show that the attenuation in the melting ice immediately under the 0°C (Best, 1957) isotherm may be substantially larger than in the snow region just above or in the rain below the melting level. Further melting cannot lead to much further enhancement of attenuation, apparently, and may lead to a lessening of the reflectivity of the particle by bringing it to sphericity or by breaking up of the particle. Although the exact process of attenuation by melting particles is not understood, the theoretical results of Kerker *et al.* (1951) appear to give satisfactory agreement with the observed properties of the radar “bright band” found just below the 0°C isotherm of cumulus clouds.

X. ATTENUATION BY FOG

The characteristic feature of fog is the reduction in visibility it causes. Visibility is defined as the greatest distance in a given direction at which it is just possible to see and identify with the unaided eye (a) in the daytime, a prominent dark object against the sky at the horizon, and (b) at night, a known, preferably unfocused moderately intense light source (Glossary of Meteorology, 1957). Although the visibility depends upon both drop size and number of drops and not entirely upon the liquid-water content, yet, in practice, the visibility is indicative of the liquid-water content, and therefore may be used to estimate radio-wave attenuation (Best, 1957). On the basis of Ryde’s work, Saxton and Hopkins (1951) give the figures in Table XII for the attenuation in a fog or clouds at 0°C temperature. The attenuation varies with the temperature because the dielectric constant of water varies with temperature; therefore, at 15°C and 25°C the figures in Table XII should be multiplied by 0.6 and 0.4 respectively.

TABLE XII. *Attenuation Caused by Clouds or Fog (Saxton-Hopkins)*
Temperature = 0°C

Visibility (meters)	Attenuation db/km		
	$\lambda = 1.25$ cm	$\lambda = 3.2$ cm	$\lambda = 10$ cm
30	1.25	0.20	0.02
90	0.25	0.04	0.004
300	0.045	0.007	0.001

It is immediately noted that cloud or fog attenuation is an order of magnitude greater at 3.2 cm than at 10 cm. Nearly another order of magnitude increase occurs between 3.2 cm and 1.25 cm.

XI. THERMAL NOISE EMITTED BY THE ATMOSPHERE

General laws of thermodynamics relate the absorption characteristics of a medium to those of emission. Good absorbers of radiation are also good emitters, and vice versa. Thus, in the microwave region, the atmosphere is also a good emitter, as well as a strong absorber, of radiation. We may therefore describe quantitatively both emission and absorption by the same parameter; namely, the absorption coefficient.

The emission characteristics of any real body at a fixed frequency may be compared to those of a black body at the same temperature. In the microwave region, the noise energy emitted by a black body is given by the Rayleigh-Jeans law:

$$\psi(\nu) = 8\pi k T \left(\frac{\nu}{c}\right)^2 \quad (6)$$

where $\psi(\nu)$ = emitted black body flux density per unit frequency
 ν = frequency
 T = absolute temperature, °K
 c = the velocity of light
 k = Boltzmann's constant (1.38044×10^{16} ergs/K°).

The emission per unit length along an actual ray path may now be expressed as

$$B(\nu) = \gamma(\nu)\psi(\nu) \quad (7)$$

where $\gamma(\nu)$ = absorption per unit length.

Remembering that the fraction of energy absorbed in a path length ds is given by the optical depth $d\tau I = (\gamma(\nu)ds)$, we may obtain the differential equation for transmission of radiation through the atmosphere:

$$\frac{dI(\nu)}{d\tau} = -I(\nu) + \psi(\nu) \quad (8)$$

where $I(\nu)$ is the flux density per unit frequency. The solution to this radiative transfer equation is

$$I_m(\nu) = \sum_m I_m(\nu) \exp\left(-\int_{r_s}^{r_m} d\tau\right) + \int_{r_s}^{\infty} \psi(\nu) \exp\left(-\int_{r_s}^{r_r} d\tau\right) d\tau \quad (9)$$

where the summation extends over all discrete noise sources which may be present, $I_m(\nu)$ is the unattenuated flux density transmitted from the m th discrete source located at position r_m , s is the point of reception of energy, and the other symbols have their previous meaning. It should be recognized that the above integrals extend over a ray path determined by the refractive properties of the medium and cannot be evaluated unless these refractive properties are known.

In the microwave region one may relate the intensity of radiation received

from a particular direction, $I(\nu)$, to an equivalent temperature, $T_n(\nu)$ by the following relation

$$I(\nu) = \frac{8\pi k T_n(\nu)}{\lambda^2} \tag{10}$$

or, from (9):

$$T_n(\nu) = \sum T_{n,m}(\nu) \exp\left(-\int_{\tau_s}^{\tau_{r_n}} d\tau\right) + \int_{\tau_s}^{\tau_{\infty}} T(r) \exp\left(-\int_{\tau_s}^{\tau_r} d\tau\right) d\tau \tag{11}$$

This equivalent temperature is called the thermal noise temperature.

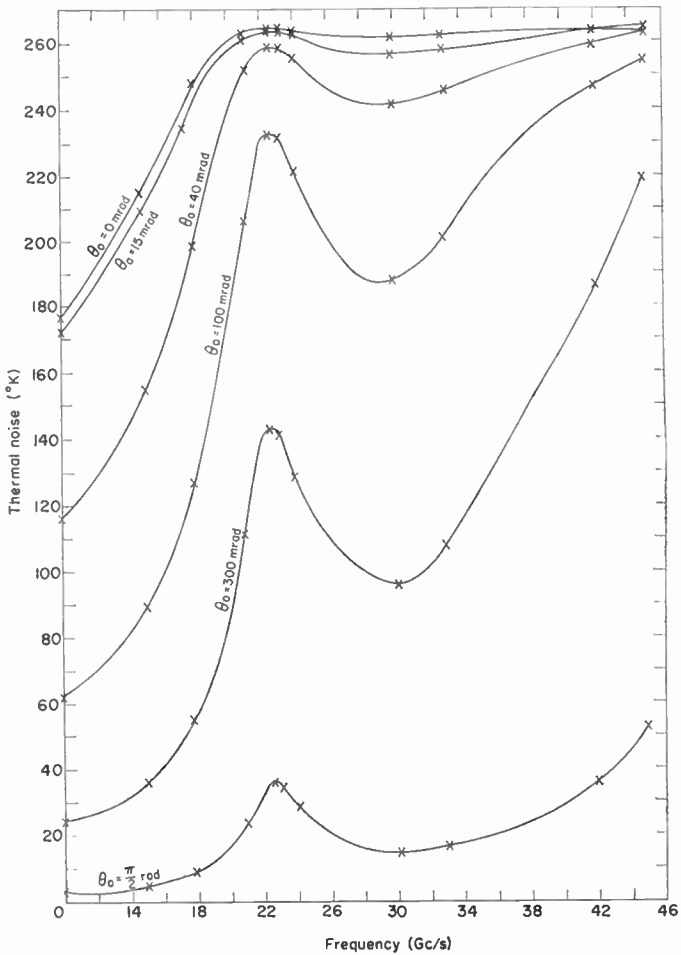


FIG. 27. Thermal noise versus frequency for mean profile conditions, and various antenna elevation angles, θ_0 , at Bismarck, North Dakota.

It is apparent that the thermal noise temperature of the atmosphere, as measured by an antenna, will depend explicitly upon the antenna angle and the frequency, and implicitly upon the atmospheric conditions along the ray path giving rise to absorption and emission of energy. It seems plausible, therefore, that one could exploit this dependence of thermal noise on atmospheric conditions as a probe of atmospheric structure.

Thermal noise is equally important in radio reception since it represents the lowest possible noise level that can be attained by an antenna immersed in the atmosphere. This minimum noise level will, of course, vary, depending on atmospheric conditions, the frequency, and the antenna orientation. For example, in the microwave region, the antenna noise temperature at vertical orientation may be as low as 1°K, and in a horizontal position, where more of the lower layers of the atmosphere are "seen" the noise temperature may be of the same order as the actual temperature of the lower atmosphere; i.e. around 280°K. Figure 27 shows sky temperature as a function of frequency for various antenna elevation angles for mean atmospheric conditions at Bismarck, North Dakota, during February 1940-1943.

REFERENCES

- Artman, J. O. (1953). Absorption of microwaves in the millimeter wavelength region. Columbian Radiation Laboratory Report.
- Artman, J. O., and Gordon, J. P. (1954). *Phys. Rev.* **96**, 1237-1245.
- Battan, L. J. (1959). "Radar Meteorology," p. 43. The University of Chicago Press.
- Bean, B. R. (1953). *Proc. Inst. Radio Engrs, N.Y.* **41**, 549.
- Bean, B. R. (1956). *Trans. Inst. Radio Engrs, N.Y.* **CS-4**, 32-38.
- Bean, B. R., and Abbott, R. L. (1957). *Geofis. pur. appl.* **37**, 127-144.
- Bean, B. R., and Cahoon, B. A. (1957). *Bull. Am. met. Soc.* **38**, 395-398.
- Becker, G. E., and Autler, S. H. (1946). *Phys. Rev.* **70**, 300.
- Beckmann, B. (1957). *NTZ Nachrichtentech. Z.* **10**, 369.
- Best, A. C. (1957). "Physics in Meteorology," Pitman and Sons, London.
- Birnbaum, G., and Maryott, A. A. (1955). *Phys. Rev.* **99**, 1886.
- Burrows, C. R., and Attwood, S. S. (1949). "Radio Wave Propagation," Academic Press, New York.
- Bussey, H. E. (1950). *Proc. Inst. Radio Engrs, N.Y.* **38**, 781.
- "Compendium of Meteorology" (1951). Waverly Press, Baltimore.
- Crawford, A. B., and Hogg, D. C. (1956). *Bell Syst. tech. J.* **35**, 907.
- Davidson, D., and Pote, A. (1955). *Electronics* **35**, 126-131.
- Dinger, H. E. (1953). *Proc. Inst. Radio Engrs, N.Y.* **46**, 1041.
- Donaldson, Ralph J., Jr. (1955). *J. Meteor.* **12**, 238-244.
- Du Castel, F., Misme, P., and Voge, J. (1958). *Ann. Télécomm.* **13**, 209.
- Ghosh, S. N., and Edwards, H. D. (1956). Air Force Surveys in Geophysics, No. 82.
- "Glossary of Meteorology" (1959) **3**, p. 613. American Meteorological Society, Boston.
- Gough, M. W. (1958). *Marconi Rev.* **XXI** 198.
- Gunn, K. L. S., and East, T. W. R. (1954). *Quart. J. Roy. met. Soc.* **30**, 522-545.
- Hathaway, S. D., and Evans, H. W. (1959). *Bell Syst. tech. J.* **38**, No. 1.
- Heer, O. (1955). *NTZ Nachrichtentech. Z.* **8**, 129.
- Hill, R. M., and Gordy, W. (1954). *Phys. Rev.* **93**, 1019.

- Hirao, K. (1956). *J. Radio Res. Labs., Japan* 3, 189.
- Hirao, K., Akita, K., and Shiro, I. (1960). *J. Radio Res. Labs., Japan* 7, 1.
- Hogg, D. C., and Semplak, R. A. (1960). *Proc. Inst. Radio Engrs, N.Y.* 48, 2024–2025.
- Josephson, B., and Blomquist, A. (1958). *Trans. Inst. Radio Engrs, N.Y.* AP-6, 169.
- Kerker, M., Langleben, M. P., and Gunn, K. L. S. (1951). *J. Met.* 8, 424.
- Kieley, D. G. (1956). *Ann. Télécomm.* 11, 233–267.
- Laws, J. O., and Parsons, D. A. (1943). *Trans. Amer. geophys. Un.* 24th Annual Meeting, 452–460.
- Mie, G. (1908). *Ann. Phys.* 25, 377.
- Miller, S. L., and Townes, C. H. (1953). *Phys. Rev.* 90, 537–541.
- Millman, G. H. (1958). *Proc. Inst. Radio Engrs, N.Y.* 46, 1492.
- Onoe, M. (1957). *J. Radio Res. Labs., Japan* 4, 395.
- Planck, Max (1959). “The Theory of Heat Radiation,” Dover Publications, New York.
- Ratner, B. (1945). *Rep. Weather Bur., Wash.* Upper air average values of temperature, pressure, and relative humidity over the United States and Alaska.
- Richtmeyer, F. K., Kennard, E. H., and Lauritsen, T. (1955). “Introduction to Modern Physics,” Ch. 4, McGraw-Hill Book Co., New York.
- Robinson, N. P. (1955). *Proc. Instn. elect. Engrs* 102B, 709.
- Ryde, J. W. (1946). *The Phys. Soc., London*, 169–188.
- Ryde, J. W., and Ryde, D. (1945). See Ryde, J. W. (1946).
- Saxton, J. A., and Hopkins, H. G. (1951). *Proc. Instn. elect. Engrs* 98, Pt. III, 31.
- Straiton, A. W., and Tolbert, C. W. (1960). *Proc. Inst. Radio Engrs, N.Y.* 48, 898–903.
- Tinkham, M., and Strandberg, M. W. P. (1955). *Phys. Rev.* 99, 538.
- Tolbert, C. W. and Straiton, A. W. (1957). *Trans. Inst. Radio Engrs, N.Y.* AP-5, No. 2, 239–241.
- Tunnell, G. A. (1958). *Geophys. Mem., Lond.* No. 100, Her Majesty’s Stationery Office, London.
- Van Vleck, J. H. (1947a). *Phys. Rev.* 71, 413–424.
- Van Vleck, J. H. (1947b). “Propagation of Short Radio Waves,” pp. 646–664, McGraw-Hill Book Co., New York.
- Weber, Eric (1960). *J. Met.* 17, 159.
- Weickmann, H. K., and Kampe, H. J. (1953). *J. Met.* 10, 204–221.

ELECTROMAGNETIC SURFACE WAVES†

JAMES R. WAIT

*Central Radio Propagation Laboratory,
National Bureau of Standards, Boulder, Colorado, U.S.A.*

I.	Introduction	157
II.	Dipole Over an Impedance Plane	159
III.	Related Surface Wave Problems	166
IV.	Axial Waves on Cylindrical Rods	171
V.	Azimuthal Waves on Cylindrical Boundaries	172
VI.	Propagation Over a Homogeneous Spherical Earth	175
VII.	Mixed-Path Propagation	184
	A. Introduction	184
	B. Formulation for a Two-Section Path	184
	C. Reduction to a One-Dimensional Problem	185
	D. Alternative Representations	187
	E. Solution for One Antenna at Great Heights	189
	F. Three-Section Path	190
	G. Numerical Results	193
	H. Some Extensions of the Theory	202
	I. The Integral Equation	203
VIII.	Wave Propagation Over an Inhomogeneous Sphere	204
	References	209
	Acknowledgment	212
	Appendix	212
	References for Appendix	217

I. INTRODUCTION

The basic laws of electricity and magnetism, discovered by Faraday and Ampère, were put in mathematical form by James Clerk Maxwell in 1864—almost a century ago. Maxwell (1873), having formulated the equations which now bear his name, developed the basic properties of electromagnetic waves. Furthermore, he showed that such waves should travel with the velocity of light. However, it was not until sometime later that Hertz (1887, 1888) provided experimental confirmation of Maxwell's deductions. Using a crude form of spark gap generator he actually demonstrated propagation over a distance of some 15 m for a band of wavelengths in the range from about 1 to 10 m. In addition, he showed that a metallic sheet, placed in the vicinity of the receiver, reflected these waves.

Just at the turn of the century, Guglielmo Marconi (1901) made his significant discovery that electromagnetic waves could be transmitted across the Atlantic ocean. His experiments were conducted between Newfoundland and Scotland at a frequency which is believed to have been about 30 kc/s. This astounding discovery led to much speculation about the mechanism of propagation of these waves. At that time, the existence of the ionosphere

† This chapter was written while the author was on a visit to the Radio Research Station, Ditton Park, Slough, England, during the summer of 1962.

had not been established and it was tempting to seek an explanation in terms of waves guided along the earth's surface. Such a motivation led Zenneck (1907) to obtain a solution of Maxwell's equations which was in the form of a wave guided by a plane interface between homogeneous media, one of which is an insulator. This wave which is now known as a Zenneck Surface Wave is polarized such that the magnetic field vector is parallel to the interface. Furthermore, it is bound to the interface since the amplitude of the field decays with distance from the interface. In general, it is a "fast wave" meaning that the phase velocity is greater than that of plane waves in the insulator. Zenneck himself and Hack (1908) in a later paper showed that the electric vector of such a wave traced out a narrow ellipse which was tilted forward slightly in the direction of propagation. They supposed that the characteristics of this Zenneck surface wave were in accord with the behavior of electromagnetic waves on the earth's surface.

In a brilliant memoir Arnold Sommerfeld (1909) obtained a formal solution for a vertical electric dipole in the plane interface between an insulating half-space (i.e. air) and a conducting half-space (i.e. a homogeneous earth). Exact expressions for the field components were obtained in the form of integrals. Sommerfeld evaluated these integrals using an asymptotic method which was valid provided the magnitude of the refractive index of the homogeneous half-space was large compared with unity. In an attempt to explain the physical nature of his solution, he divided the expression for the field into a "space wave" and a "surface wave". Both parts, according to Sommerfeld, are necessary in order to satisfy Maxwell's equations and the appropriate boundary conditions. He found that the "surface wave" part of the solution had almost identical properties to the plane Zenneck surface wave. The field amplitude varied inversely as the square root of the horizontal distance from the source dipole. Furthermore, it was a fast wave and it decayed exponentially with height above the interface.

For some time, it was believed that the Sommerfeld surface wave (or radial form of Zenneck wave) was the predominant component of the field of a vertical antenna over a finitely conducting ground. Sometime later Hermann Weyl (1919) reformulated the problem of a dipole above a conducting half-space. He expressed his solution as an angular spectrum of plane waves which, although in a different form, were equivalent to Sommerfeld's integral formulae. Weyl's results were in a convenient form to obtain asymptotic results for the fields valid at large distances from the source. The radial Zenneck wave did not appear explicitly in his formulae. Some six years later Sommerfeld (1926) published a monumental paper which greatly extended his earlier analysis. He gave exact integral expressions for the fields of vertical and horizontal dipoles for both electric and magnetic types. He redeveloped the asymptotic approximations for the infinite integrals which were valid in the far zone and the resulting field expressions were generalized to permit both source dipole and observer to be at a finite height above the interface. As in the 1909 paper, the asymptotic solution involved an error function whose argument involved the square root of a complex quantity. The prescription for choosing the correct branch of this

square root was changed in the 1926 paper. Unfortunately, however, Sommerfeld did not explain his reasons for making this change of sign which altered the asymptotic behavior of the error function. Consequently, if Sommerfeld had examined the asymptotic expansion of his 1926 formulae he would have found that the radial Zenneck wave fails to emerge as the dominant term.

Using the Weyl formulation as the starting point, van der Pol and Niessen (1930) obtained convenient and slightly more general expressions for the field of the dipole over the homogeneous half-space. Another approach was adopted by Wise (1931) who obtained a rigorous series expansion for the field. The results of these latter investigators can be regarded as modest generalizations of Sommerfeld's basic work.

At this time a set of ground-wave attenuation curves were prepared by Rolf (1930). Unfortunately, he based his calculations on the formulae given by Sommerfeld in his 1909 paper. Consequently, his curves are quite erroneous and, furthermore, computational errors are evident.

It appears that the first explicit statement of the error in Sommerfeld's 1909 paper was published by K. A. Norton (1935) in a letter to *Nature*. It is evident in the exchange of correspondence between Norton and Sommerfeld that the error was never acknowledged. Sommerfeld contended that Rolf and other workers simply misunderstood his attenuation formula and chose the wrong square root of a complex expression. This can hardly be so since Sommerfeld (1910) himself used the incorrect formula and its resulting series expansion. An interesting exposition is found in a paper by Norton (1937a) in which he discusses his concepts of space and surface waves and the implications of the "error in sign" in Sommerfeld's 1909 paper. Burrows (1936, 1937) working apart from Norton, discovered that the results of Weyl, van der Pol, and Niessen differed from those of Sommerfeld. Burrows contended that "the difference between the two results was exactly Sommerfeld's surface wave". Burrows felt the problem could be finally resolved by performing a crucial experiment. Accordingly, he carried out measurements on Seneca Lake in New York state. The experimental data agreed with Weyl's expressions for the field strength as a function of distance.

An independent and thorough discussion of the famous "error" in Sommerfeld's paper was later published by Niessen (1937). As indicated above, it amounts to the incorrect choice of a square root of a complex quantity which appears in the argument of a complex error function.

II. DIPOLE OVER AN IMPEDANCE PLANE

An excellent example of a simple structure which illustrates many of the features of "surface waves" is a flat plane which exhibits the property of boundary impedance (Wait, 1957; Barlow and Fernando, 1956; Furutsu, 1959). To be more explicit, a cylindrical coordinate system (ρ , ϕ , z) is chosen with a vertical electric dipole located at $z = h$, as illustrated in Fig. 1. At the interface, defined by $z = 0$, the boundary conditions are assumed to be

$$E_\rho = -ZH_\phi \quad (1)$$

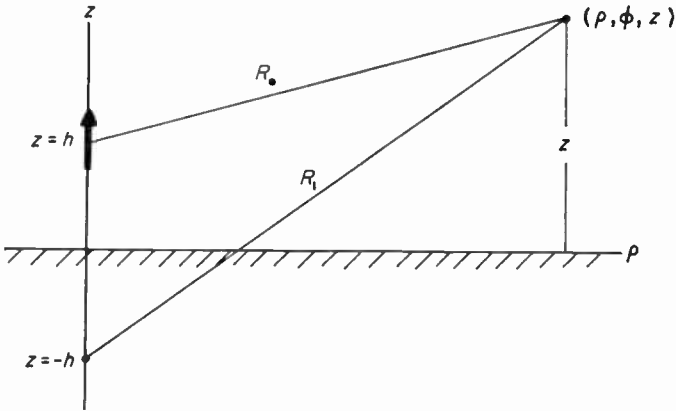


FIG. 1. Cylindrical coordinate system (ρ, ϕ, z) showing location of source dipole with respect to impedance boundary.

where Z is the surface impedance. Such a boundary condition is appropriate when the medium below the interface is, for example, a very good conductor, a dielectric-coated conductor, or a corrugated surface. A short discussion of the scope of the surface impedance is given in the appendix which follows the work of Leontovich (1944), Monteath (1951), and Wait and Surtees (1954). In the present problem, azimuthal symmetry about the source dipole is assumed and, therefore, Z can be regarded as a single complex constant. In view of the restrictions placed on the validity of the surface impedance concept, the generality of the present argument is not further reduced by assuming that

$$|Z| \ll \eta_0$$

where $\eta_0 (\cong 120\pi \Omega)$ is the intrinsic impedance of free space.

For the presently stated problem, the fields may be derived from a Hertz vector which has only a z component, denoted ψ . The form of the solution in the upper half-space (i.e. the free space above the interface) may be written

$$\psi = K \left(\frac{e^{-ikR_0}}{R_0} + \frac{e^{-ikR_1}}{R_1} - 2P \right) \quad (2)$$

where K is a constant and is proportional to the strength of the dipole,

$$R_0 = [\rho^2 + (z-h)^2]^{\frac{1}{2}}, \quad R_1 = [\rho^2 + (z+h)^2]^{\frac{1}{2}}$$

and

$$P = \int_0^{\infty} \frac{(ik\lambda\Delta) e^{-u(h+z)} J_0(\lambda\rho)}{(u+ik\Delta)u} d\lambda, \quad u = (\lambda^2 - k^2)^{\frac{1}{2}} \quad (3)$$

where $\Delta = Z/\eta_0$, $J_0(\lambda\rho)$ is the Bessel function of the first type of order zero. This is the exact formal solution of the problem as may be verified by seeing that $E_\rho = -ZH_\phi$ is satisfied at $z = 0$.

In the (trivial) case when the ground plane is perfectly conducting (i.e. $Z = 0$), the integral P vanishes. The two quantities e^{-ikR_0}/R_0 and e^{-ikR_1}/R_1 can be identified with the primary field and an image field, respectively; the latter field is that due to an image of the source at $z = -h$.

Subject to $|\Delta| \ll 1$, the integral P can be evaluated by the modified saddle point method (Sommerfeld, 1949; Clemmow, 1950). The result, valid in the far field $k\rho \gg 1$, is given by

$$P = \left(\frac{p}{w}\right)^{\frac{1}{2}} [1 - F(w)] \frac{e^{-ikR_1}}{R_1} \quad (4)$$

where

$$F(w) = 1 - i(\pi w)^{\frac{1}{2}} \operatorname{erfc}(iw^{\frac{1}{2}}) e^{-w}$$

$$w = p \left(1 + \frac{z+h}{\Delta R_1}\right)^2$$

$$p = -(ikR_1/2)\Delta^2 = |p| e^{ib}$$

and

$$\operatorname{erfc}(iw^{\frac{1}{2}}) = \frac{2}{\sqrt{\pi}} \int_{iw^{\frac{1}{2}}}^{\infty} e^{-x^2} dx.$$

Allowing both the source dipole and the observer to approach the interface (i.e. $z = h = 0$), the result becomes simply

$$\psi = 2K(e^{-ik\rho/\rho})F(p) \quad (5)$$

The corresponding expression for the vertical electric field is

$$E_z = 2k^2K(e^{-ik\rho/\rho})F(p) \quad (6)$$

The function $F(p)$ can be regarded as the correction to the field of a dipole on the surface of a perfectly conducting plane; for $p \ll 1$, it becomes unity. $F(p)$ has the same functional form as the "attenuation function" introduced originally by Sommerfeld (1909, 1926) in considering the problem of radiation from a vertical electric dipole over a homogeneous conducting half-space. Numerical values of $F(p)$ for this half-space problem have been published by Norton (1936). It is of interest to note at this stage that, if Z is taken to be equal to the ratio of the tangential fields for a plane wave at grazing incidence,

$$\Delta = Z/\eta_0 = (ik/\gamma_1) \left(1 + \frac{k^2}{\gamma_1^2}\right)^{\frac{1}{2}} \quad (7)$$

where γ_1 is the propagation constant of the lower medium. In terms of the conductivity σ_1 and dielectric constant ϵ_1 , $\gamma_1 = (i\sigma_1\mu\omega - \epsilon_1\mu\omega^2)^{\frac{1}{2}}$ where μ is the permeability assumed constant everywhere.

Using the above expression for Δ the "numerical distance" formula becomes

$$p = p_1 = \frac{ik\rho}{2} \left(\frac{k^2}{\gamma_1^2}\right) \left(1 + \frac{k^2}{\gamma_1^2}\right) \quad (8)$$

which is identical to Norton's definition. For a homogeneous half-space the argument of p , denoted b , varies from -90° for a dielectric to 0° for a good conductor. For a stratified conductor, the argument b may be outside this range. For example, in the case of a two layer conducting half-space, the numerical distance may be written (Wait, 1953)

$$p \cong p_1 Q^2 \quad (9)$$

where p_1 is as given above and Q is a correction factor given by

$$Q = |Q| e^{iq} = \frac{(u_2/u_1) + (\gamma_2^2/\gamma_1^2) \tanh u_1 h_1}{(\gamma_2^2/\gamma_1^2) + (u_2/u_1) \tanh u_1 h_1} \quad (10)$$

where $u_1 = (\gamma_1^2 + k^2)^{\frac{1}{2}}$ and $u_2 = (\gamma_2^2 + k^2)^{\frac{1}{2}}$; γ_1 and γ_2 are the propagation constants of the upper and lower layers, respectively, and the thickness h_1 of the upper layer. If displacement currents are very small in the conducting layers, $u_1 \cong \gamma_1 \cong (i\sigma_1\mu\omega)^{\frac{1}{2}}$ and $u_2 \cong \gamma_2 \cong (i\sigma_2\mu\omega)^{\frac{1}{2}}$. It is immediately evident that the argument q may range from $+45^\circ$ to -45° if the upper layer is electrically thin and if the ratio $(\sigma_1/\sigma_2)^{\frac{1}{2}}$ ranges from small to large values. The corresponding range in the argument b is then $+90^\circ$ to -90° . It is to be noted that b now assumes positive values which was not possible in the case of a homogeneous conductor.†

Another limiting case which leads to positive value of b is when the upper medium is a thin dielectric layer and the lower medium is a perfect conductor. Then

$$Z \cong i\mu\omega h_1 \left[1 - \left(\frac{k}{k_1} \right)^2 \right] \quad (11)$$

where $k_1 = (\epsilon_1\mu)^{\frac{1}{2}}\omega$. This "inductive" type surface leads to a b value of $+90^\circ$. A corrugated surface may also exhibit an inductive reactance if the period of the corrugations is sufficiently small compared to the wavelength (Rotman, 1951; Elliott, 1954).

The nature of the attenuation function F depends rather critically on the algebraic sign of b . For example, if $|p| \gg 1$, the error function may be expanded asymptotically and this leads to

$$F(p) \cong -\frac{1}{2p} - \frac{1 \cdot 3}{(2p)^2} - \frac{1 \cdot 3 \cdot 5}{(2p)^3} - \frac{1 \cdot 3 \cdot 5 \cdot 7}{(2p)^4} \dots \quad (12)$$

for $-2\pi < b < 0$, and

$$F(p) \cong -2i(\pi p)^{\frac{1}{2}} e^{-p} - \frac{1}{2p} - \frac{1 \cdot 3}{(2p)^2} - \frac{1 \cdot 3 \cdot 5}{(2p)^3} \dots \quad (13)$$

for $2\pi > b > 0$.

It is immediately seen that when b is negative the vertical electric field E_z varies as $1/\rho^2$ as $\rho \rightarrow \infty$. On the other hand, if b is positive, such as for an inductive surface, E_z varies as $1/\rho^{\frac{1}{2}}$. For the purely inductive boundary,

† Since Norton (1936) uses an $\exp(-i\omega t)$ time factor, his positive values of b correspond to our negative values.

$Z = iX$, $b = 90^\circ$, and the attenuation function may be written

$$F(p) \cong -2 e^{-3\pi/4} e^{-i|p|} + \frac{i}{2|p|} + \frac{3}{4|p|^2} - \frac{15i}{8|p|^3} \dots \quad (14)$$

where
$$|p| = \frac{k\rho X^2}{2\eta_0^2}$$

in terms of the surface reactance X . The leading term in the expansion (for the electric field) varies as

$$\frac{1}{(k\rho)^{\frac{1}{2}}} e^{-ik(1+X^2/2\eta_0^2)\rho}$$

which has the characteristics of a cylindrical wave traveling in the positive ρ direction with a phase velocity

$$c / \left(1 + \frac{X^2}{2\eta_0^2} \right)$$

It is, therefore, a "slow" wave and such a wave is not excited when b is negative. This is really the critical point of the Sommerfeld error since if the sign on b were reversed, the asymptotic expansion of $F(p)$ would yield a Zenneck wave.

When the source dipole and the observer are both raised to heights h and z , respectively, the asymptotic form of the general solution given by equation (4) may be written

$$\psi \cong \psi_a + \psi_b + \varepsilon\psi_s \quad (15)$$

where $\varepsilon = 0$ for $\arg w < 0$ and $\varepsilon = 1$ for $\arg w > 0$ and where

$$\frac{\psi_a}{K} \cong \frac{e^{-ikR_0}}{R_0} + \frac{C - \Delta}{C + \Delta} \frac{e^{-ikR_1}}{R_1} \quad (16)$$

$$\frac{\psi_b}{K} \cong - \left\{ \frac{1}{p(1+C/\Delta)^3} + \frac{1 \cdot 3}{2p^2(1+C/\Delta)^5} + \frac{1 \cdot 3 \cdot 5}{4p^3(1+C/\Delta)^7} + \dots \right\} \frac{e^{-ikR_1}}{R_1} \quad (17)$$

and

$$\frac{\psi_s}{K} \cong - \frac{2\Delta}{\Delta + C} \cdot 2i(\pi w)^{\frac{1}{2}} e^{-w} \frac{e^{-ikR_1}}{R_1} \quad (18)$$

where

$$C = \frac{h+z}{R_1} \quad \text{and} \quad \Delta = \frac{Z}{\eta}$$

The vertical electric field component is obtained simply from

$$E_z = \left(k^2 + \frac{\partial^2}{\partial z^2} \right) \psi \\ \cong k^2(1-C^2)\psi \quad \text{for } k\rho \gg 1 \quad (19)$$

The contribution ψ_a can be described as a "space wave" since it is composed of the primary influence e^{-ikR_0}/R_0 and a specularly reflected component modified by a reflection coefficient $(C-\Delta)/(C+\Delta)$. The term ψ_b when added to ψ_a is the complete description of the field for $b < 0$. This includes the case where the dipole is over a homogeneous conducting half-space. This is the problem which has been discussed in considerable detail by Sommerfeld (1926) and Norton (1936, 1937b). Following the convention adopted by the latter author, it would seem very appropriate to define ψ_b as the *Norton surface wave*. This is a logical step since the "space wave" vanishes as the antenna heights z and h approach zero and, if $b < 0$, ψ_b is then the sole contribution to the field. When $b > 0$ there is no reason to change the suggested nomenclature for ψ_a and ψ_b . In this case, however, the third component ψ_s is present. Because of its properties it is logical to define it as a "trapped surface wave". It is present when the surface has an inductive character; it propagates like a cylindrical wave, decaying exponentially with height above the surface and with relatively small horizontal attenuation. For a highly inductive surface ($b \cong 90^\circ$), this "trapped surface wave" greatly exceeds the "Norton surface wave".

From the asymptotic solution for the total field of a dipole over an impedance plane, it is seen that a logical decomposition of the field may be made into three components (a) Space Wave, (b) Norton Surface Wave, and (c) Trapped Surface Wave. In the asymptotic sense, the latter component, the trapped wave, is excited only if $b > 0$. One may then ask what happens if b is near zero. Surely there cannot be a discontinuity in the field as b passes through zero from positive to negative values? A closer examination reveals that for large numerical distances the damping of the "trapped" surface wave is exceptionally large when b is near zero and thus the magnitude of this component is vanishingly small in this transition zone. For intermediate numerical distances, the behavior is best illustrated by a graphical plot of the function $F(p)$. The amplitude and phase of this quantity is shown in Figs. 2a and 2b for a range of b values. It is seen that when b is zero or negative, $|F|$ is a monotonically decreasing function for all $|p|$. On the other hand, if b is positive corresponding to a partially inductive boundary $|F|$ rises above unity for certain intermediate values of $|p|$. When b is exactly 90° , the propagation factor $|F|$ rises without limit and for large $|p|$ it is proportional to $|p|^{\frac{1}{2}}$. This limiting case corresponds to a purely inductive boundary and the predominant component of the field is an unattenuated "trapped surface wave" whose field components are varying as the square root of the distance.

The plot of the phase of $F(p)$, denoted Φ , is given in Fig. 2b. This quantity is generally positive, corresponding to a phase lag. Thus, for dipole excitation, the total field may always be described as a "slow wave" in contradistinction to the *Zenneck wave* which is a "fast wave".

As can be seen above, it is not always feasible to distinguish between a trapped surface wave and a Norton-type surface wave. It is only in the asymptotic limit that they may be separated. However, for arbitrary values of the numerical distance p it is also possible to split off the space wave ψ_a .

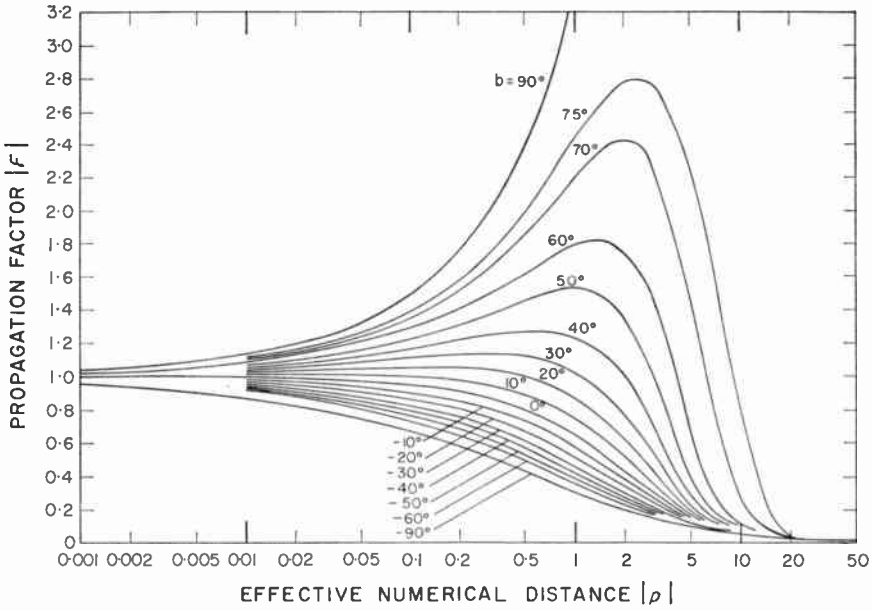


FIG. 2a.

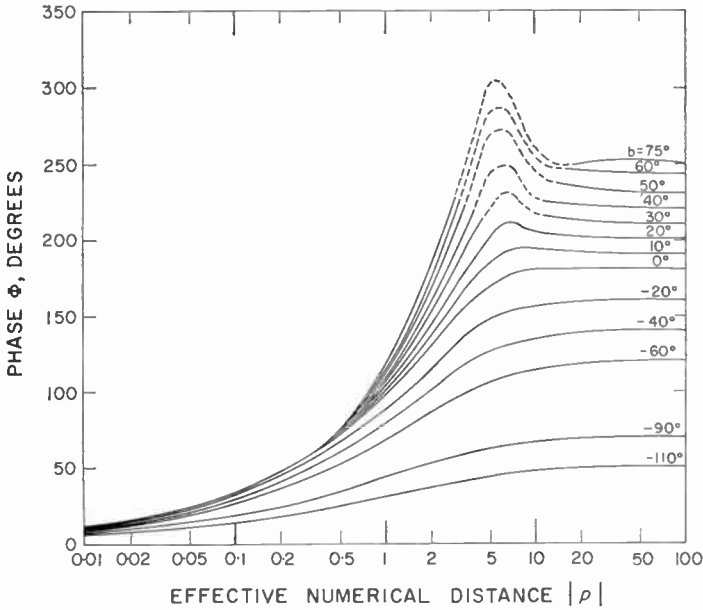


FIG. 2b.

FIGS. 2a, 2b. Propagation factor for an impedance boundary.
 (The precise numerical values for large $|\rho|$ and positive b are somewhat uncertain.)

On using equation (14), the total surface wave may then be written

$$\psi_s = \frac{2K e^{-ikR_1}}{R_1} \left(\frac{\rho}{w}\right)^{\frac{1}{2}} F(w) = \frac{2K e^{-ikR_1}}{R_1(1+C/\Delta)} F(w) \quad (20)$$

When $|\rho| \gg 1$, ψ_s may be written in the form as

$$\psi_s \cong \psi_b + \varepsilon\psi_s \quad (21)$$

where ψ_b and ψ_s are defined above. In the general case, it thus seems appropriate to describe ψ_s as the (total) surface wave.

III. RELATED SURFACE WAVE PROBLEMS

A convenient method to excite surface waves on a reactive boundary is to employ an annular slot which has a constant voltage applied around the circumference (Brown and Sharma, 1959). One such configuration is a circumferential slit around a cylindrical post which projects from the reactive surface as indicated in Fig. 3. This problem can be viewed as an initial value

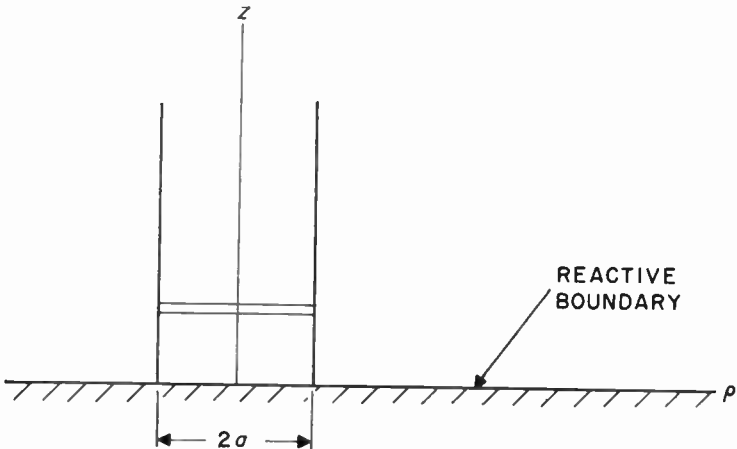


FIG. 3. Excitation of surface waves by a circumferentially slotted cylinder.

problem since the electric field tangential to the cylindrical surface is specified and the resulting fields, external to the cylinder, are to be calculated.

The reactive surface is the plane $z = 0$ with the usual cylindrical coordinates (ρ, ϕ, z) being adopted. The cylindrical surface is defined by $\rho = a$ and $0 \leq z < \infty$. The electric field over the cylinder is specified according to

$$E_z = f(z) \quad \text{for } \rho = a \quad \text{and } 0 \leq z < \infty$$

and approaches zero as $z \rightarrow \infty$. Over the surface $z = 0$ the fields satisfy the condition $E_\rho = -iXH_\phi$ where X is the surface reactance which is assumed constant.

Because of the basic similarity of this problem with the dipole over the impedance plane we expect the fields to be expressible in the form

$$E_z = \int_0^{\infty} [f_1(\lambda) e^{+u z} + f_2(\lambda) e^{-u z}] J_0(\lambda \rho) d\lambda \quad (22)$$

where $u = (\lambda^2 - k^2)^{\frac{1}{2}}$ and $f_1(\lambda)$ and $f_2(\lambda)$ are functions yet to be specified. Writing $u = ip$ and noting that

$$2J_0(\lambda \rho) = H_0^{(1)}(\lambda \rho) + H_0^{(2)}(\lambda \rho) \quad (23)$$

The preceding integral becomes

$$E_z = i \int_{-\infty}^{+\infty} S(p) [e^{+ipz} + R(p) e^{-ipz}] H_0^{(2)}(\sqrt{k^2 - p^2} \rho) \frac{\lambda d\lambda}{\sqrt{\lambda^2 - k^2}} \quad (24)$$

where
$$R(p) = \frac{ip + U}{ip - U} \quad \text{with } U = \varepsilon \omega X \quad (25)$$

The function $S(p)$ is determined from the source distribution; in fact

$$S(p) H_0^{(2)}(\sqrt{k^2 - p^2} a) = \frac{1}{2\pi} \int_0^{\infty} f(z') e^{-ipz'} dz' \quad (26)$$

The integral for E_z can be evaluated by the conventional saddle-point method. The residue at the pole corresponds to the (trapped) surface wave and the dominant contribution at the saddle point is the radiation field or space wave.

It is worthwhile to rewrite the integral for E_z by changing the variable to p and letting p range over real values. This amounts to a change of the path of integration and for a reactive surface in which X is a positive real quantity the pole at $p = -iU$ is crossed. Thus, the residue of the pole must be included in the new representation. Keeping this point in mind, it readily follows that

$$E_z = 4\pi u e^{-U(z+h)} \frac{H_0^{(2)}(\lambda_s \rho)}{H_0^{(2)}(\lambda_s a)} F(iu) + \int_{-\infty}^{+\infty} F(p) [e^{+ipz} + R(p) e^{-ipz}] \frac{H_0^{(2)}(\sqrt{k^2 - p^2} \rho)}{H_0^{(2)}(\sqrt{k^2 - p^2} a)} dp \quad (27)$$

where
$$\lambda_s = i\sqrt{k^2 + U^2} \quad (28)$$

and where
$$F(p) = \frac{1}{2\pi} \int_0^{\infty} f(z') e^{-ipz'} dz' \quad (29)$$

Here it is assumed that $z < z'$ for convenience; a trivial change of signs is

made when $z > z'$. In the case of a thin circumferential slot on the cylinder at $z = h$ excited by a constant voltage V , one may write

$$f(y) = V\delta(z-h)$$

where $\delta(z-h)$ is the (Dirac) unit impulse function at $z = h$. Thus

$$F(p) = \frac{V}{2\pi} e^{-iph}$$

and then

$$E_z = 2uV e^{-u(z+h)} \frac{H_0^{(2)}(\lambda_s \rho)}{H_0^{(2)}(\lambda_s a)} + \frac{V}{2\pi} \int_{-\infty}^{+\infty} \frac{H_0^{(2)}(\sqrt{k^2 - p^2} \rho)}{H_0^{(2)}(\sqrt{k^2 - p^2} a)} [e^{+ip(z-h)} + R(p) e^{-ip(z+h)}] dp \quad (30)$$

which is valid for $z < h$. The only change required for $z > h$ is to replace $\exp[+ip(z-h)]$ by $\exp[-ip(z-h)]$ in the preceding integrand.

The spectral representation given by (24) requires that λ range over all real values. If λ is set equal to $k \sin \theta$ then θ may be regarded as the angle of incidence of plane waves incident onto the reactive boundary. Furthermore, ρ is then equal to $k \cos \theta$. The coefficient $R(p)$ is then equal to

$$\frac{\cos \theta - iX/\eta_0}{\cos \theta + iX/\eta_0} \quad (31)$$

which can be recognized as the appropriate Fresnel reflection coefficient.

The representation given by (24), which requires that $\sin \theta$ takes all real values, contains the surface wave implicitly. On the other hand, the representation given by (30) which includes a spectral representation, involving real values of $\cos \theta$ only, exhibits the surface wave term explicitly. There is no question, however, that the two results are not equivalent. The latter type expansion is often referred to as the angular spectrum of plane waves following the point of view of Booker and Clemmow (1950).

Another closely related approach is to regard the source as composed of a superposition of magnetic current sheets in the horizontal plane. Again, a flat reactive boundary surface is considered with homogeneous free space above. At some height $z = h$ the magnetic current density is taken to be of the form

$$K(\rho) = M_0 J_1(\lambda \rho) \quad (32)$$

Where J_1 is the Bessel function of the first type and M_0 is a constant. The situation is illustrated in Fig. 4.

For the region above, $z > h$ the tangential field components must have the following form

$$E_\rho = A_1 \lambda u e^{-uz} J_1(\lambda \rho) \quad (33)$$

$$H_\phi = A_1 i \omega \epsilon \lambda e^{-uz} J_1(\lambda \rho) \quad (34)$$

remembering that these are to be solutions of Maxwell's equations which are finite at $\rho = 0$.

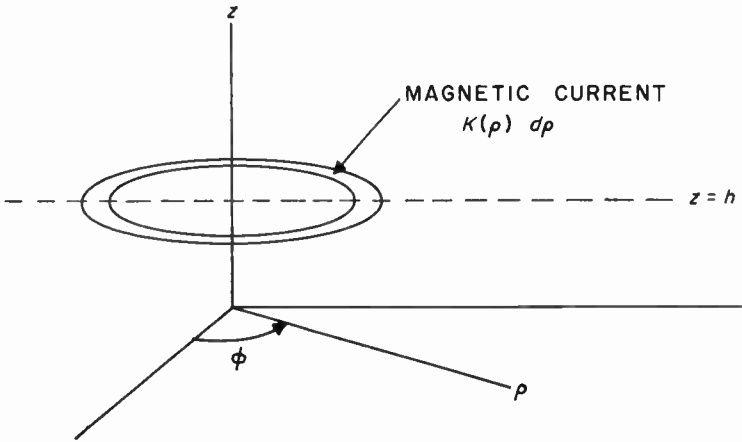


FIG. 4. Excitation of surface waves by a magnetic ring source. The magnetic current $K(\rho)$ flows in the ϕ direction.

For the region below the sheet the appropriate forms are

$$E_\rho = \lambda u [-A_2 e^{uz} + A_3 e^{-uz}] J_1(\lambda \rho) \tag{35}$$

$$H_\phi = i\epsilon\omega\lambda [A_2 e^{uz} + A_3 e^{-uz}] J_1(\lambda \rho) \tag{36}$$

The boundary condition $E_\rho = -iXH_\phi$ at $z = 0$ requires that

$$A_3 = \frac{u+U}{u-U} A_1 \tag{37}$$

The continuity of H_ϕ at $y = h$ leads to

$$A_1 e^{-uh} = A_2 \left[e^{uh} + \frac{u+U}{u-U} e^{-uh} \right] \tag{38}$$

Then, finally, the discontinuity of E_ρ at the sheet $y = h$ is $M_0 J_1(\lambda \rho)$ which gives

$$A_2 = \frac{M_0}{2\lambda U} e^{-uh} \tag{39}$$

Then

$$A_1 = \frac{M_0}{2\lambda U} \left[e^{-uh} + \frac{u+U}{u-U} e^{-uh} \right] \tag{40}$$

The solution for an arbitrary distribution of magnetic current $K(r)$ is obtained by making use of the Fourier-Bessel transforms. Thus

$$K(r) = \int_0^\infty g(\lambda) J_1(\lambda \rho) \lambda d\lambda \tag{41}$$

where

$$g(\lambda) = \int_0^\infty K(\rho) J_1(\lambda \rho) \rho d\rho \tag{42}$$

is an integration over the whole plane. It is assumed, of course, that azimuthal symmetry still prevails.

The solution for the magnetic field then has the following form

$$H_{\phi} = \frac{i\varepsilon\omega}{2} \int_0^{\infty} g(\lambda) \left[e^{\pm u(h-z)} + \frac{u+U}{u-U} e^{-u(h+z)} \right] \lambda J_1(\lambda\rho) d\lambda \quad (43)$$

which is valid for $z \geq h$ if the \pm sign is employed in the exponent. The corresponding solution for a magnetic ring source at $\rho = b$ is obtained by noting that if

$$K(\rho) = A\delta(\rho - b) \quad (44)$$

where A is a constant,

then

$$g(\lambda) = AbJ_1(\lambda b) \quad (45)$$

When b is allowed to shrink to zero the solution has identically the same form as the dipole over the impedance plane discussed in the previous section.

Sharma (1957) has calculated the asymptotic forms of the fields for the case of a ring source of finite radius b . The contribution from the pole leads to the following expression for the surface wave

$$H_{\phi}^s = \pi\varepsilon\omega Ab u J_1(\lambda_s b) e^{-U(h+z)} H_1^{(2)}(\lambda_s \rho) \quad (46)$$

For practical purposes the Hankel function can be replaced by the leading term of its asymptotic expansion which is

$$H_1^{(2)}(\lambda_s \rho) \cong \sqrt{\frac{2i}{\pi\lambda_s \rho}} e^{-i\lambda_s \rho}$$

The contribution from the saddle point gives the radiation field or space wave. Thus

$$H_{\phi}^R \cong \frac{\omega\varepsilon Ab}{2R} J_1(kb \cos \hat{\theta}) F(\hat{\theta}) e^{-ikR} \quad (47)$$

where

$$F(\theta) = e^{ikh \sin \theta} + \frac{ikh \sin \hat{\theta} + U}{ikh \sin \hat{\theta} - U} e^{-ikh \sin \theta} \quad (48)$$

where

$$R = (\rho^2 + z^2)^{\frac{1}{2}} \quad \text{and} \quad \sin \hat{\theta} \cong z/R.$$

This result is valid in the far zone such that terms which vary as $1/R^2$, $1/R^3$, etc., may be neglected. Clearly, these terms must be considered when the surface reactance becomes very small. It is in this situation that the pole and the saddle point are in close proximity. Thus, the condition for the validity of the simple asymptotic result given above is that the "numerical distance" should be very large. Specifically, this requires that

$$k\rho(X/\eta_0)^2 \gg 1$$

This fact is not always appreciated by current workers in the field.

IV. AXIAL WAVES ON CYLINDRICAL RODS

The excitation of surface waves on a cylindrical structure can be treated in much the same fashion. An example to illustrate the approach is a circular rod which has a prescribed surface reactance X at $\rho = a$. The situation is illustrated in Fig. 5. At the plane $z = 0$ the field E_ρ is to be prescribed.

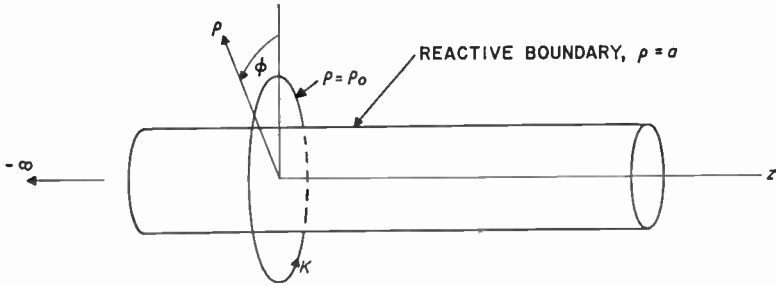


FIG. 5. Excitation of surface waves on a cylindrical rod (of infinite length) by a magnetic ring source.

The source may be regarded as a superposition of magnetic current sheets of the form $K \exp(-i\beta z)$ at $\rho = \rho_0$.

Assuming azimuthal symmetry, the fields for $z > 0$ are taken to have the following form for $\rho > \rho_0$.

$$H_\phi = A_1 \frac{\epsilon\omega}{v} e^{-i\beta z} H_1^{(1)}(iv\rho) \quad (49)$$

$$E_\rho = A_1 \frac{\beta}{v} e^{-i\beta z} H_1^{(1)}(iv\rho) \quad (50)$$

$$E_z = A_1 e^{-i\beta z} H_0^{(1)}(iv\rho) \quad (51)$$

where $v = \sqrt{\beta^2 - k^2}$ and where the Hankel functions are of the first kind. For $\rho < \rho_0$, the expression for the field involves a linear combination of both first and second kinds of Hankel functions. The unknown coefficients are found by imposing the conditions that (a) the H_ϕ field is continuous at $\rho = \rho_0$, (b) the E_z field is discontinuous by an amount $K \exp(-i\beta z)$ at $\rho = \rho_0$, and (c) $E_z = iXH_\phi$ at $\rho = a$. Then, without difficulty, it is found that

$$H_\phi = K \frac{\epsilon\omega\pi\rho_0}{4} [H_1^{(2)}(iv\rho_0) + qH_1^{(1)}(iv\rho_0)] \times H_1^{(2)}(iv\rho) e^{-i\beta z} \quad (52)$$

for $\rho > \rho_0$, where

$$-q = \frac{(i\epsilon\omega X/v)H_1^{(2)}(iva) - H_0^{(2)}(iva)}{(i\epsilon\omega X/v)H_1^{(1)}(iva) - H_0^{(1)}(iva)} \quad (53)$$

When the source is a magnetic current ring at $\rho = \rho_0$ and $z = 0$, one simply

notes that, for $B = \text{constant}$,

$$K(z) = B\delta(z) = \frac{B}{2\pi} \int_{-\infty}^{+\infty} e^{+i\beta z} d\beta \quad (54)$$

therefore, H_ϕ for such a source is

$$H_\phi = \frac{Bk\rho_0}{4} \sqrt{\frac{\epsilon}{\mu}} \int_{-\infty}^{+\infty} H_1^{(1)}(iv\rho) [H_1^{(2)}(iv\rho_0) + qH_1^{(1)}(iv\rho_0)] \times e^{-i\beta z} d\beta \quad (55)$$

To evaluate this field asymptotically Brown and Stachera (1959) use a saddle-point type method. Writing

$$H_\phi = H_\phi^R + H_\phi^S \quad (56)$$

they find that

$$H_\phi^S \cong A \frac{\epsilon\omega}{v_s} e^{-i\beta_s z} H_1^{(1)}(iv_s \rho) \quad (57)$$

where A is a rather complicated coefficient, v_s and β_s are the values of v and β determined at the pole of the integral. The pole is located where

$$(i\epsilon\omega X/v)H_1^{(1)}(iva) = H_0^{(1)}(iva).$$

In most cases the Hankel function which determines the radial decay of the surface wave behaves as a positive exponential. The wave propagates along the wire with attenuation determined only by the imaginary part of β_s . This is proportional to the real part of the surface impedance which can be very small.

The radiation field is found to be of the form

$$H_\phi^R \cong \frac{Bk\rho_0}{4R} \sqrt{\frac{\epsilon_0}{\mu_0}} e^{-ikR} g(k \cos \theta) \quad (58)$$

where

$$g(\beta) = H_1^{(2)}(iv\rho_0) + qH_1^{(1)}(iv\rho_0) \quad (59)$$

Here $R = (\rho^2 + z^2)^{\frac{1}{2}}$ and $\cos \theta = z/R$ so that (R, θ) are spherical coordinates.

It is evident that the radiation field even for a structure of this type is a spherical wave with the typical $\exp(-ikR)/R$ dependence. However, in this case the surface wave does not have an inverse distance dependence and the diminishing of the field is produced only by the ohmic losses in the cylindrical rod.

V. AZIMUTHAL WAVES ON CYLINDRICAL BOUNDARIES

In much of the research and recent applications of surface waves it is possible to regard the guiding reactive boundary as straight in the direction of propagation. Under such a condition the total field can usually be decomposed into a space or radiation wave and a (trapped) surface wave. We will now consider the effect of introducing curvature of the structure in the

direction of propagation. To simplify the discussion a two-dimensional model is adopted.

The source is assumed to be a magnetic line source outside and parallel to a circular cylinder of radius a . Choosing a cylindrical coordinate system (ρ, ϕ, z) the non-zero field components are E_ρ , E_ϕ , and H_z , and the boundary condition is

$$E_\phi = -iXH_z \quad \text{at } \rho = a$$

where X is the surface reactance. Denoting H_z by ψ this can be rewritten

$$\frac{\partial \psi}{\partial \rho} + k \frac{X}{\eta_0} \psi = 0 \quad \text{at } \rho = a \quad (60)$$

The source is located at $\rho = \rho_0$ and $\phi = 0$. The solution for this problem can be written in the form of residues series where each term is regarded as azimuthal-type waves or modes characterized by a factor $\exp(-i\nu\phi)$ where ϕ is the angular distance from the source ($\phi > 0$) and ν is a complex quantity which is determined by the boundary conditions. The radial dependence of the modes is proportional to $H_\nu^{(2)}(k\rho)$, a Hankel function of the second kind, chosen to satisfy the radiation condition at infinity. On physical grounds $Re \nu > 0$ and $Im \nu < 0$. Thus

$$\psi(\phi) = \frac{2i}{ka} \sum_{s=1}^{\infty} \frac{H_{\nu_s}^{(2)}(k\rho) H_{\nu_s}^{(1)}(k\rho_0) e^{-i\nu\phi}}{H_{\nu_s}^{(2)}(ka) \left\{ \frac{\partial}{\partial \nu} \left[H_{\nu_s}^{(2)'}(ka) + \frac{X}{\eta_0} H_{\nu_s}^{(2)}(ka) \right] \right\}_{\nu=\nu_s}} \quad (61)$$

where ν_s is determined from

$$H_{\nu_s}^{(2)'}(ka) + \frac{X}{\eta_0} H_{\nu_s}^{(2)}(ka) = 0 \quad (62)$$

The prime indicates a derivative with respect to the argument.

In writing (61) in this form the cylinder is regarded as an open structure in the sense that ϕ may range from 0 to ∞ . The actual or total field ψ^T for the closed cylinder is, of course, periodic and is obtained from

$$\psi^T(\phi) = \sum_{n=0}^{\infty} \psi(2n\pi + \phi) + \psi(2(n+1)\pi - \phi) \quad (63)$$

Physically these two summations represent waves which have traveled around the cylinder in the clockwise and counterclockwise directions. For present purposes we need discuss only the function $\psi(\phi)$ as it will be dominant for surfaces of large radius of curvature (provided ϕ is not near π).

It is important to see how the residues series representation or sum of modes becomes transformed to the formula for a flat reactive surface when a tends to infinity. To effect this transformation it is necessary to write (62) in the form of a contour integral as follows:

$$\psi(\phi) = -\frac{i}{4} \oint H_v^{(2)}(k\rho_0) \times \left[H_v^{(1)}(k\rho) - \frac{H_v^{(1)'}(ka) + (X/\eta_0)H_v^{(1)}(ka)}{H_v^{(2)'}(ka) + (X/\eta_0)H_v^{(2)}(ka)} H_v^{(2)}(k\rho) \right] e^{-iv\phi} dv \quad (64)$$

where the contour is to enclose the poles (at $v = v_s$) in a clockwise sense. In the above, $\rho < \rho_0$; if $\rho > \rho_0$ one merely interchanges ρ and ρ_0 where they appear in the integrand.

The contour may be replaced by an integration along the real axis from $-\infty$ to $+\infty$ if suitable indentations are made to avoid singularities of the integrand. This step is justified because the contribution from an infinite semi-circle, in the negative half-plane of v , vanishes. Furthermore, in the limiting case of $ka \rightarrow \infty$, the Debye or second-order approximations to the Hankel functions may be used over the principal portions of the contour. For $v < k\rho$, these are

$$H_v^{(1)}(k\rho) \cong (2/\pi)^{\frac{1}{2}} [(k\rho)^2 - v^2]^{-\frac{1}{2}} \exp \left[i \left(\xi - \frac{\pi}{4} \right) \right] \quad (65)$$

and
$$H_v^{(2)}(k\rho) \cong (2/\pi)^{\frac{1}{2}} [(k\rho)^2 - v^2]^{-\frac{1}{2}} \exp \left[-i \left(\xi - \frac{\pi}{4} \right) \right] \quad (66)$$

where
$$\xi = \int_v^{k\rho} [1 - (v/x)^2]^{\frac{1}{2}} dx$$

Then

$$\psi(\phi) \cong -\frac{i}{2\pi} \int_{-\infty}^{+\infty} e^{-iv\phi} \left[e^{-i(\xi_0 - \xi)} + \frac{[1 - (v/ka)^2]^{\frac{1}{2}} - i(X/\eta_0)}{[1 - (v/ka)^2]^{\frac{1}{2}} + i(X/\eta_0)} e^{-i(\xi_0 + \xi - 2\xi_a)} \right] \times \frac{dv}{[(k\rho_0)^2 - v^2]^{\frac{1}{2}} [(k\rho)^2 - v^2]^{\frac{1}{2}}} \quad (67)$$

where
$$\xi_0 = \int_v^{k\rho_0} [1 - (v/x)^2]^{\frac{1}{2}} dx$$

and
$$\xi_a = \int_0^{ka} [1 - (v/x)^2]^{\frac{1}{2}} dx \quad (68)$$

If now ka , $k\rho$, and $k\rho_0$ actually approach infinity in such a way that $\rho - a = h$ and $\rho_0 - a = h_0$ are finite, the integral becomes

$$\psi(\phi) = -\frac{i}{2\pi} \int_{-\infty}^{+\infty} e^{-ikSs} \left[e^{-ikC(h_0 - h)} + \frac{C - i(X/\eta_0)}{C + i(X/\eta_0)} e^{-ikC(h + h_0)} \right] C^{-1} dS \quad (69)$$

where $C = (1 - S^2)^{\frac{1}{2}}$ and $s = a\phi$

It is clear that this result is identical to the integral formula for the field of a magnetic line source over a flat reactive surface (Cullen, 1954). The straightforward application of the saddle-point method leads to the formula for the radiation field and the contribution from the pole of the integrand yields the surface wave.

Actually, the characteristics of azimuthal modes on cylindrical structures are very similar to those for the spherical model. Thus, further discussion of such modes is deferred.

VI. PROPAGATION OVER A HOMOGENEOUS SPHERICAL EARTH

In considering the influence of earth curvature on surface wave propagation it is natural to represent the earth by a sphere with a prescribed surface impedance.

The method of solution is a direct extension of Watson's method (1918, 1919). He treated the (radially oriented) dipole in the presence of a homogeneous sphere. To simplify the analysis, the surface impedance concept is exploited.

The source of the field is considered to be an electric dipole oriented in the radial direction to the spherical earth of radius a . Choosing a spherical coordinate system (r, θ, ϕ) , the surface of the earth is then defined by $r = a$, and the dipole is located at $r = b$ and $\theta = 0$. It is understood that $b > a$. Due to the spherical nature of the problem and because of the azimuthal symmetry, the fields can be derived from a Hertz vector, which has only a radial component rU . Thus, for $r > a$,

$$E_r = \left(k^2 + \frac{\partial^2}{\partial r^2} \right) (rU) \quad (70)$$

$$E_\theta = \frac{1}{r} \frac{\partial^2}{\partial r \partial \theta} (rU) \quad \text{for } r > a \quad (71)$$

$$H_\phi = -i\varepsilon\omega \frac{\partial U}{\partial \theta} \quad (72)$$

and
$$E_\phi = H_r = H_\theta = 0 \quad (73)$$

The function of U satisfies

$$(\nabla^2 + k^2)U = 0 \quad (74)$$

in the exterior region $r > a$ except right at the source dipole. In the immediate vicinity of the source, U must have the following singularity

$$U \rightarrow -\frac{C_0}{bR} e^{-ikR}$$

where $R = (r^2 + b^2 - 2br \cos \theta)^{\frac{1}{2}}$ and $C_0 = -Ids/4\pi i\varepsilon\omega$. This condition is readily verified by noting that the primary fields of the dipole are obtained when the operations are carried out.

The total field U is now written as the sum of two parts, $U_e + U_s$, where U_e has the proper singularity as $R \rightarrow 0$, and U_s remains finite. U_s is now expressed as a superposition of suitable solutions of the homogeneous wave equation. These have the form

$$h_n^{(2)}(kr)P_n(\cos\theta)$$

where $h_n^{(2)}(kr)$ is a spherical Hankel function of the second kind, which assures outgoing waves at infinity, and $P_n(\cos\theta)$ is a Legendre polynomial. The index n takes integral values. Now, making use of the well-known fact that $\exp(-ikR)/R$ can be expressed as an expansion in spherical functions, it readily follows that a suitable expansion for U_e is given by (Wait, 1956a)

$$U_e = \frac{ikC_0}{2} \sum_{n=0}^{\infty} (2n+1)h_n^{(1)}(kr)h_n^{(2)}(kb)P_n(\cos\theta) \quad \text{for } r < b \quad (75)$$

$$\text{and} \quad U_e = \frac{ikC_0}{2} \sum_{n=0}^{\infty} (2n+1)h_n^{(2)}(kr)h_n^{(1)}(kb)P_n(\cos\theta) \quad \text{for } r > b \quad (76)$$

where $h_n^{(1)}(kr)$ is the spherical Hankel function of the first kind.† A corresponding expansion for U_s is

$$U_s = \frac{ikC_0}{2} \sum_{n=0}^{\infty} (2n+1)A_n h_n^{(2)}(kr)P_n(\cos\theta) \quad (77)$$

where A_n is an unknown coefficient. Formally, (75) and (76) which were first used by Bremmer (1949), are divergent expansions. Actually a more rigorous treatment of the problem, avoiding the use of such expansions, is given by Bremmer (1958a) in his *Encyclopedia* article. Apparently, Franz (1962) was not aware of this later work by Bremmer when he criticized the use of these divergent series.

Having U_e and U_s expressed in this form enables the boundary conditions to be applied in a straightforward manner. The important simplification to the solution is that we impose the single boundary condition.

$$E_\theta = -ZH_\phi \quad \text{at } r = a \quad (78)$$

This can be rewritten

$$\frac{1}{r} \frac{\partial}{\partial r} rU = Zi\epsilon\omega U \quad (79)$$

In other words, it is assumed that the influence of the earth can be described adequately by its surface impedance Z . In this problem, Z is taken to be equal to the ratio of the tangential electric and magnetic fields for a vertically polarized plane wave at grazing incidence on a plane stratified earth.

† The spherical Hankel functions are defined as follows:

$$h_n^{(1)}(x) = -i(-1)^n x^n \left(\frac{d}{xdx}\right)^n \left(\frac{e^{ix}}{x}\right) \quad \text{and} \quad h_n^{(2)}(x) = i(-1)^n x^n \left(\frac{d}{xdx}\right)^n \left(\frac{e^{-ix}}{x}\right).$$

By application of (79), it readily follows that

$$A_n = - \frac{h_n^{(1)}(ka)}{h_n^{(2)}(ka)} \left[\frac{\frac{d}{dx} \log x h_n^{(1)}(x) - i\Delta}{\frac{d}{dx} \log x h_n^{(2)}(x) - i\Delta} \right]_{x=ka} h_n^{(2)}(kb) \tag{80}$$

where $\Delta = \epsilon\omega Z/K = Z/\eta_0$, $\eta_0 = 120\pi$

The total field is then of the form

$$U = \sum_{n=0}^{\infty} (2n+1)f(n)P_n(\cos \theta) \tag{81}$$

where $f(n)$ is a known function.

The expansions of the field as developed are not particularly useful in the radio problem since an enormous number of terms would be required in the summations over n .[†] Instead, following the ideas of Watson and others, the summation is transformed into the following contour integral

$$U = i \int_{C_1 + C_2} \frac{n \, dn}{\cos n\pi} f(n - \frac{1}{2}) P_{n-\frac{1}{2}}[\cos(\pi - \theta)] \tag{82}$$

where n is now regarded as a continuous variable. The contour $C_1 + C_2$ encloses the real axis as illustrated in Fig. 6. Noting that the poles of the

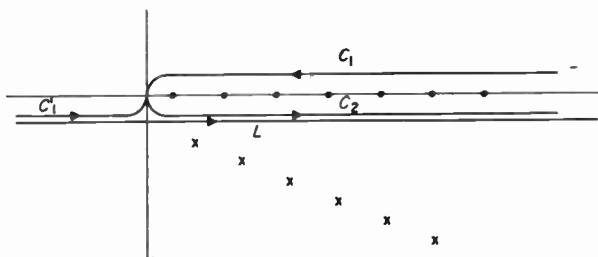


Fig. 6. The contour in the complex n plane showing the location of the real and complex poles.

integrand are located at $n = \frac{1}{2}, \frac{3}{2}, \frac{5}{2}, \dots$ etc., it can be readily verified by the theorem of residues that this integral is equivalent to (81).

Now since $f(n - \frac{1}{2})$ is an even function of n , the part of the contour C_1 above the real axis can be replaced by the contour C_1' which is located just below the negative real axis. The contour $C_1' + C_2$ is now entirely equivalent to L , a straight line running along just below the real axis. Replacing $n - \frac{1}{2}$ by v the contour integral representation for U takes the form

$$U = -i \int_L \frac{(v + \frac{1}{2})}{\sin v\pi} f(v) P_v[\cos(\pi - \theta)] \, dv \tag{83}$$

[†] Recently, however, Johler and Berry (1962) have programmed a series of this kind on a digital computer.

The next step in the analysis is to close L by an infinite semicircle in the negative half-plane. The contribution from this portion of the contour vanishes as the radius of the semicircle approaches infinity. The value of the integral for U along the contour L is now equal to the sum of the residues of the poles of the integrand in the lower half-plane.

The poles are located at the points $\nu = \nu_s$ which are solutions of

$$M(\nu) = 0$$

where
$$M(\nu) = \frac{d}{dx} \log x h_\nu^{(2)}(x) - i\Delta \quad (84)$$

with $x = ka$. It follows then that U is proportional to

$$\sum_s \frac{(v_s + \frac{1}{2}) h_{v_s}^{(2)}(kb) h_{v_s}^{(2)}(kr) P_{v_s}[\cos(\pi - \theta)]}{\sin(\pi v_s) \left[\frac{\partial M(\nu)}{\partial \nu} \right]_{\nu=v_s} [h_{v_s}^{(2)}(ka)]^2} \quad (85)$$

where the summation extends over the complex poles ν_s . The location of these poles in the complex plane is one of the major problems in radio propagation (Logan, 1959). The difficulty stems from the fact that ν_s is of the same order of magnitude as ka . Thus, care must be exercised in approximating the spherical Hankel functions since their order and argument are not appreciably different. Watson (1918, 1919) and Langer (1937) have shown that in this region the spherical Hankel functions may be represented by Hankel functions of order $\frac{1}{3}$. For the present problem this amounts to using the result

$$x h_{\nu - \frac{1}{3}}^{(2)}(x) \cong e^{-i\pi/6} (-2\tau/3)^{\frac{1}{3}} x^{\frac{1}{3}} H_{\frac{1}{3}}^{(2)}[\frac{1}{3}(-2\tau)^{\frac{1}{3}}] \quad (86)$$

where $\nu = x + x^{\frac{1}{3}}\tau$. This relation is often called the Hankel approximation. Apparently it was first used by Lorenz (1890) as pointed out by Logan (1959). The root-determining equation can thus be well approximated by

$$\delta e^{i\pi/3} \frac{H_{\frac{1}{3}}^{(2)}[\frac{1}{3}(-2\tau_s)^{\frac{1}{3}}]}{H_{\frac{1}{3}}^{(2)}[\frac{1}{3}(-2\tau_s)^{\frac{1}{3}}]} = -(-2\tau_s)^{-\frac{1}{3}} \quad (87)$$

where
$$\delta = -i \frac{\eta_0}{(ka)^{\frac{1}{3}} Z} \quad \text{and} \quad \tau_s = \frac{\nu_s - ka + \frac{1}{2}}{(ka)^{\frac{1}{3}}}$$

This equation is valid for $(ka) \gg 1$ and for the important roots (i.e. those leading to small attenuation).

Equation (85) for U can now be considerably simplified; the Legendre function can be replaced by the leading term in its asymptotic expansion and $h_\nu^{(2)}(kb)$ and $h_\nu^{(2)}(kr)$ are replaced by their Hankel approximations. This results in

$$U = 2U_0(2\pi X)^{\frac{1}{3}} e^{-i\pi/4} \sum_s \frac{f_s(h_1) f_s(h_2) e^{-i\tau_s X}}{2\tau_s - 1/\delta^2} \quad (88)$$

where

$$f_s(h_i) = \left[\frac{X_i^2 - 2\tau_s}{-2\tau_s} \right]^{\frac{1}{2}} \frac{H_{\frac{1}{3}}^{(2)} \left[\frac{1}{3} (X_i^2 - 2\tau_s)^{\frac{1}{2}} \right]}{H_{\frac{1}{3}}^{(2)} \left[\frac{1}{3} (-2\tau_s)^{\frac{1}{2}} \right]} \quad (89)$$

$$U_0 = \frac{I ds e^{-ika\theta}}{4\pi i \epsilon \omega a (\theta \sin \theta)^{\frac{1}{2}}} \quad (90)$$

$$h_1 = r - a, \quad h_2 = b - a, \quad X = (ka)^{\frac{1}{2}} \theta$$

and

$$X_i = (ka)^{\frac{1}{2}} (2h_i/a)^{\frac{1}{2}} \quad \text{for } i = 1, 2.$$

The preceding equations are identical in form to those obtained by van der Pol and Bremmer (1937) for the homogeneous earth. Their results are obtained as a special case by letting

$$Z = \eta_0 \Delta \quad (91)$$

with

$$\Delta = \frac{\gamma_0}{\gamma_1} \left(1 - \frac{\gamma_0^2}{\gamma_1^2} \right)^{\frac{1}{2}}$$

where $\gamma_0 = ik$ and where γ_1 is the propagation constant of the homogeneous ground.

The residue series formula given by (88) has also been obtained by Fock (1945). Despite the fact that the notation is very different his final results are very similar. There are a number of reasons why Fock's notation is to be preferred. The main advantage is that it does away with the awkward Hankel functions of order one-third. In their place Airy integrals are used. Now, Fock's solution may be written (for a time dependence $\exp(i\omega t)$) as follows:

$$U = U_0 V(x, y_1, y_2, q) \quad (92)$$

where

$$V = -e^{-i\pi/4} 2(\pi x)^{\frac{1}{2}} \sum_s \frac{e^{-ixt_s}}{1 - t_s/q^2} \frac{w_1(t_s - y_1)}{w_1(t_s)} \frac{w_1(t_s - y_2)}{w_1(t_s)} \quad (93)$$

where

$$y_1 = \left(\frac{2}{ka} \right)^{\frac{1}{2}} kh_1 \quad \text{and} \quad y_2 = \left(\frac{2}{ka} \right)^{\frac{1}{2}} kh_2,$$

$$x = (ka/2)^{\frac{1}{2}} \theta, \quad q = -i(ka/2)^{\frac{1}{2}} \Delta,$$

and $w_1(t)$ is an Airy integral. The roots t_s are solutions of the equation

$$w_1'(t) - qw_1(t) = 0 \quad (94)$$

where the prime indicates a derivative with respect to t . Since

$$w_1(t) = -e^{i\pi/3} (-\pi t/3)^{\frac{1}{2}} H_{\frac{2}{3}}^{(2)} \left[\frac{2}{3} (-t)^{\frac{1}{2}} \right] \quad (95)$$

it is not difficult to see that (93) is *identical* to (88). Furthermore, the root-determining equations (94) and (87) are also equivalent to one another. The Airy integral function $w_1(t)$ is defined by a contour integral as follows:

$$w_1(t) = \frac{1}{\pi^{\frac{1}{2}}} \int_{\Gamma_1} \exp(st - s^3/3) ds \quad (96)$$

where Γ_1 may be taken as a straight line segment from $\infty e^{i\pi/3}$ to the origin and out along the real axis to ∞ . The associated Airy function $w_2(t)$ also occurs frequently and it is defined by

$$w_2(t) = \frac{1}{\pi^{\frac{1}{2}}} \int_{\Gamma_2} \exp(st - s^3/3) ds \quad (97)$$

where Γ_2 is the straight line segment from $\infty e^{-i2\pi/3}$ to the origin and out along the real axis to ∞ .†

For certain applications it is desirable to express V as a contour integral in the complex t plane. This has the form

$$V = e^{in/4} \left(\frac{x}{\pi}\right)^{\frac{1}{2}} \int_{\Gamma_2} e^{-ixt} F(t, y_1, y_2, q) dt \quad (98)$$

where $F = \frac{1}{2}w_1(t - y_2)[w_2(t - y_1) + B(t)w_1(t - y_1)] \quad (99)$

where $B(t) = - \left[\frac{w_2'(t) - qw_2(t)}{w_1'(t) - qw_1(t)} \right] \quad (100)$

When the contour is closed by a circular arc (of infinite radius) in the lower half-plane it is possible to verify that the $-2\pi i$ times the sum of the residues at the poles $t = t_s$ leads back to (93). To demonstrate the equivalence, use is made of the fact that $w_1(t)$ and $w_2(t)$ satisfy the (Airy) differential equation

$$w''(t) - tw(t) = 0 \quad (101)$$

and that $w_1'(t_s) - qw_1(t_s) = 0 \quad (102)$

The form of (98) is particularly suitable for deriving approximate forms which are useful in special cases. This approach has been used extensively by Logan (1959).

The characteristics of the modes propagating around a spherical surface are determined by the solution of (94). The roots t_s of this equation can be conventionally found in series form starting with the solutions for $q = 0$ and $q = \infty$. For example, the solutions of

$$w_1'(t) = 0 \quad (103)$$

are denoted t_s^0 , while the solutions of

$$w_1(t) = 0 \quad (104)$$

are denoted t_s^∞ . The first three sets of roots are given explicitly as follows:

$$\begin{aligned} t_1^0 &= 1.0188 e & t_1^\infty &= 2.3381 e \\ t_2^0 &= 3.2482 e & t_2^\infty &= 4.0879 e \\ t_3^0 &= 4.8201 e & t_3^\infty &= 5.5206 e \end{aligned}$$

† Since Fock employs an $e^{-i\omega t}$ time factor, his definitions of $w_1(t)$ and $w_2(t)$ correspond to our definitions of $w_2(t)$ and $w_1(t)$, respectively.

where $e = \exp(-i\pi/3)$. As indicated by Fock (1945), results to higher accuracy for any order of the root can be obtained from the following relations

$$t_s^0 = (3x_s^0/2)^{\frac{1}{3}}e \quad \text{and} \quad t_s^\infty = (3x_s^\infty/2)^{\frac{1}{3}}e$$

where x_s^0 is a root of

$$J_{-\frac{1}{3}}(x) - J_{\frac{1}{3}}(x) = 0 \quad (105)$$

and x_s^∞ is a root of

$$J_{-\frac{1}{3}}(x) + J_{\frac{1}{3}}(x) = 0 \quad (106)$$

By differentiating (94) with respect to t and making judicious use of (102), it follows that

$$\frac{dt}{dq} = \frac{1}{t - q^2} \quad (107)$$

This equation may be solved with the initial condition $t = t_s^0$ at $q = 0$, to yield

$$t_s(q) = t_s^0 + \frac{1}{t_s^0}q - \frac{1}{2(t_s^0)^3}q^2 + \left[\frac{1}{3(t_s^0)^2} + \frac{1}{2(t_s^0)^5} \right] q^3 - \left(\frac{7}{12(t_s^0)^4} + \frac{5}{8(t_s^0)^7} \right) q^4 + \dots \quad (108)$$

provided $|q/\sqrt{t_s^0}| < 1$. Alternatively, the initial condition may be taken as $t = t_s^\infty$ at $q = \infty$, to give

$$t_s(q) = t_s^\infty + \frac{1}{q} + \frac{t_s^\infty}{3q^3} + \frac{1}{4q^4} + \frac{(t_s^\infty)^2}{5q^5} + \frac{7t_s^\infty}{18q^6} + \left(\frac{(t_s^\infty)^3}{7} + \frac{5}{28} \right) \frac{1}{q^7} + \dots \quad (109)$$

provided $|q/\sqrt{t_s^0}| > 1$. Practically, these expansions can be used everywhere except when $q/\sqrt{t_s^0}$ has a modulus near unity. In this case it is necessary to employ numerical integration of (107).

An interesting situation arises when the phase angle of the surface impedance is in the range $\pi/2 \cong \arg Z > \pi/3$. Then $-\pi/6 < \arg q \leq 0$, and a special root t_0 appears (Wait, 1960). This can be demonstrated as follows:

$$\begin{aligned} \text{If} \quad & |\arg t| < \pi/3 \quad \text{and} \quad |t| \gg 1, \\ & w_1(t) \sim t^{-\frac{1}{3}} \exp \left[\left(\frac{2}{3} \right) t^{\frac{2}{3}} \right], \\ \text{and} \quad & w'_1(t) \sim t^{\frac{1}{3}} \exp \left[\left(\frac{2}{3} \right) t^{\frac{2}{3}} \right]. \end{aligned}$$

Thus, equation (94) has a solution which behaves something like $t \cong q^2$. This can be used as a starting point to obtain a higher approximation. Thus, the second approximation can be written

$$t_0 \cong q^2 - \frac{w'(q^2) - qw(q^2)}{q^2w(q^2) - qw'(q^2)} \quad (110)$$

Higher approximations have been found by successive application of Newton's method to obtain graphical results for the $\text{Im } t_0$ and $\text{Re } t_0$ for real

values of q (Wait, 1960). More recently Logan and Yee (1962) have found asymptotic expansions $t_0(q)$ in the following form

$$\operatorname{Re} t_0(q) \sim q^2 + \frac{1}{2q} + \frac{1}{8q^4} + \frac{5}{32q^7} + \frac{11}{32q^{10}} + \dots \quad (111a)$$

and

$$-\operatorname{Im} t_0(q) \sim 2q^2 \exp \left[-\frac{4}{3}q^3 - 1 - \frac{7}{12q^3} - \frac{31}{48q^6} - \frac{829}{576q^9} + \dots \right] \quad (111b)$$

These are usable when $|q| > 3$. In the limiting case of zero curvature (i.e. $ka \rightarrow \infty$) this root can be identified with the trapped surface wave on a flat inductive surface. The present development shows that the influence of curvature on this mode of propagation is indeed small.

When q is not large the value of t_0 must be found from a numerical integration of the differential equation

$$\frac{dt}{dq} = \frac{1}{t - q^2} \quad (112)$$

In the case of real q the following values were found by N. A. Logan (private communication).

q	$\operatorname{Re} t_0(q)$	$-\operatorname{Im} t_0(q)$
0.00	0.5094	0.8823
0.10	0.5633	0.7974
0.20	0.6270	0.7132
0.30	0.7010	0.6305
0.40	0.7857	0.5499
0.50	0.8815	0.4722
1.00	1.5487	0.1551
1.50	2.6229	0.0141
2.00	4.2597	0.0063×10^{-2}
2.50	6.4535	0.0040×10^{-6}

The residue series formula given by (88) enables field strength calculations to be carried out. In fact, there are many curves available in the literature (Burrows and Gray, 1941; Norton, 1941) for terrestrial ground wave propagation which are based on this van der Pol-Bremmer theory. However, at short distances and in some cases at low frequencies, the residue series formula becomes quite poorly convergent. A new type of expansion has recently been developed in which the first term corresponds to the radiation of a dipole over a flat surface or a plane (stratified) earth (Bremmer, 1958b; Wait, 1956a). Succeeding terms are then proportional to inverse powers of ka .

The first step is to re-express U in the form of a contour integral or inverse Laplace transform as follows:

$$\frac{iU(g)}{2g^{\frac{1}{2}}U_0} = \frac{1}{2\pi i} \int_{c-i\infty}^{c+i\infty} \frac{\pi^{\frac{1}{2}} f(P, h_1) f(P, h_2) e^{Pg}}{1 + e^{i\pi/3} P^{\frac{1}{2}} A(P)} dP \tag{113}$$

where c is some small positive constant

$$g = iX/(2\delta^2) \tag{114}$$

$$A(P) = \frac{H_{\frac{2}{3}}^{(2)}\left(\frac{P^{\frac{2}{3}}}{3\delta^3}\right)}{H_{\frac{1}{3}}^{(2)}\left(\frac{P^{\frac{1}{3}}}{3\delta^3}\right)} \tag{115}$$

and
$$f(P, h_i) = \left[\frac{X_i^2 + (P/\delta^2)}{(P/\delta^2)} \right]^{\frac{1}{2}} \frac{H_{\frac{2}{3}}^{(2)}\left[\frac{1}{3}(X_i^2 + (P/\delta^2)^{\frac{2}{3}})\right]}{H_{\frac{1}{3}}^{(2)}\left[\frac{1}{3}(P/\delta^2)^{\frac{1}{3}}\right]} \tag{116}$$

It can be noted that the poles p_s of the integrand are determined by the solution of

$$H_{\frac{2}{3}}^{(2)}\left(\frac{P_s^{\frac{2}{3}}}{3\delta^3}\right) + e^{i\pi/3} P_s^{\frac{1}{2}} H_{\frac{1}{3}}^{(2)}\left(\frac{P_s^{\frac{1}{3}}}{3\delta^3}\right) = 0 \tag{117}$$

If P_s is replaced by $2\delta^2 \tau_s e^{i\pi}$, this equation is identical to equation (87). It can be verified that the sum of the residues evaluated at the poles P_s leads back to equation (88).

The procedure is now to expand the integrand in powers of $1/P$. Each term is then a fairly simple inverse Laplace transform. Inverting each of these can be carried out if certain results from the operational calculus are employed. The details of this rather tedious process are given elsewhere (Wait, 1956a). The final formula is given as follows:

$$\begin{aligned} \frac{U}{2U_0} = W \cong G \left\{ F(p) - \frac{\delta^3}{2} [1 - i(\pi p)^{\frac{1}{2}} - (1 + 2p)F(p) \right. \\ \left. + \delta^6 \left[1 - i(\pi p)^{\frac{1}{2}}(1 - p) - 2p + \frac{5}{6}p^2 + \left(\frac{p^2}{2} - 1\right)F(p) \right] \right. \\ \left. + \text{terms in } \delta^9, \delta^{13}, \text{ etc.} \right\} \tag{118} \end{aligned}$$

where

$$F(p) = 1 - i(\pi p)^{\frac{1}{2}} \operatorname{erfc}(ip^{\frac{1}{2}}) e^{-p}, \quad \delta^3 = \frac{i}{ka\Delta^3} \tag{119}$$

$$p = -ika\theta\Delta^2/2 \quad \text{and, finally,}$$

$$G \cong (1 + ikh_1\Delta)(1 + ikh_2\Delta) \tag{120}$$

This series formula is valid for relatively small heights such that kh_1^2 and

$kh_2^2 \ll 2a\theta$. A more general version of equation (118) for greater heights is available (Wait, 1956).

VII. MIXED-PATH PROPAGATION

A. INTRODUCTION

In many problems dealing with the propagation of surface waves the properties of the bounding surface are inhomogeneous. A striking example occurs when radio waves pass from land to sea. In such a case it is important to be able to predict the characteristics of the wave for various conditions. In radio engineering this has been called the mixed-path problem and a great deal of attention has been given to this topic.

An excellent semiempirical approach to the problem of calculating fields over an inhomogeneous earth has been given by Millington (1949). Sometime earlier Feinberg (1946) had formulated a general method for treating mixed paths over a flat earth. Similar results were obtained independently by Clemmow (1953) and Bremmer (1954). The author (Wait, 1956b) showed that the integral formula for a two-section path could be easily derived by an application of the compensation theorem (Monteath, 1951). It was also indicated in this paper (Wait, 1956b) that the results could be readily generalized to a spherical earth. In a further paper (Wait and Householder, 1957) extensive numerical results were given for propagation over a two-section path on a spherical earth. Furutsu (1956) has also considered propagation over a spherical earth under mixed-path conditions. His general method is based on solving the dual integral equations for the problem by an iterative procedure. The mixed-path problem has also been discussed by Godzinski (1958).

The theory for mixed-path propagation over both two- and three-section paths on a smooth spherical earth is given here in condensed form and some attention is given to the various representations which may be used in practical field computations. The situation when one terminal is at great height is also considered in some detail since this solution describes the radiation pattern of an antenna when the ground plane is inhomogeneous. Where possible, a physical interpretation of the results is given. Finally, some numerical results are given in convenient graphical form.

B. FORMULATION FOR A TWO-SECTION PATH

The mutual impedance Z_{ab} between two vertical antennas located at A and B over a spherical earth of radius a is considered. The situation is illustrated in Fig. 7 where a vertical cross-section of the earth is shown. The great circle distance A and B (measured along the surface of the earth) is d . The earth medium to the left of the boundary line has a conductivity σ and dielectric constant ϵ . The corresponding constants for the medium to the right of the boundary are σ_1 and ϵ_1 . A variable P on the great circle path is a distance α from B . Then, for $\alpha > d_1$, the surface impedance is

$$Z \cong [i\mu_0\omega/(\sigma + i\epsilon\omega)]^{\frac{1}{2}} \left[1 - \frac{i\epsilon_0\omega}{\sigma + i\epsilon\omega} \right]^{\frac{1}{2}} \quad (121)$$

while for $\alpha < d_1$

$$Z_1 \cong [i\mu_0\omega/(\sigma_1 + i\varepsilon_1\omega)]^{\frac{1}{2}} \left[1 - \frac{i\varepsilon_0\omega}{\sigma_1 + i\varepsilon_1\omega} \right]^{\frac{1}{2}} \quad (122)$$

where μ_0 is the permeability of the whole space which is assumed to be constant.

The mutual impedance between the dipoles A and B for the two-section

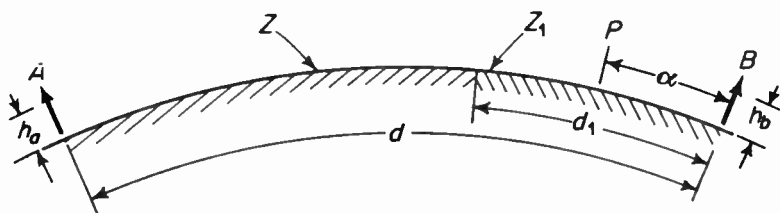


FIG. 7. Two-section path on a spherical earth.

mixed path illustrated in Fig. 7 is denoted Z'_{ab} . It was shown previously (Wait, 1956b) that it could be expressed in the form

$$I^2(Z'_{ab} - Z_{ab}) \cong (Z_1 - Z) \int_S (\vec{H}_{at} \cdot \vec{H}'_{bt}) dS \quad (123)$$

where Z_{ab} is the mutual impedance if the surface of the earth were homogeneous with surface impedance Z everywhere. \vec{H}_{at} is the tangential magnetic field of dipole A over the homogeneous earth while \vec{H}'_{bt} is the tangential magnetic field of dipole B over the inhomogeneous earth. The currents in the dipoles are both taken equal to I for convenience. The surface of integration S extends over the region of the earth which is characterized by a surface impedance Z_1 . Equation (123) also follows directly from the work of Montearth (1951).

C. REDUCTION TO A ONE-DIMENSIONAL PROBLEM

Equation (123) is essentially a two-dimensional integral equation for the fields. On a straightforward application of the principle of stationary phase, the surface integral can be reduced to a line integral from $\alpha = 0$ to d_1 along the great circle path. Before stating this result it is convenient to introduce certain attenuation functions, W and W_1 , as follows:

$$Z_{ab} = \frac{l_a l_b i\mu_0\omega}{2\pi d} e^{-ikd} W(d, Z) \quad (124)$$

and

$$Z'_{ab} = \frac{l_a l_b i\mu_0\omega}{2\pi d} e^{-ikd} W'(d, Z, Z_1) \quad (125)$$

where l_a and l_b are the effective lengths of the dipoles A and B . It is to be understood that W and W' are also functions of h_a and h_b , the height of dipole A and B above the ground. The functions W and W' are normalized

such that they would approach 1 if the earth were flat and perfectly conducting—and provided $h_a = h_b = 0$. Consistently in what follows it is assumed that h_a and $h_b \ll d \ll a$.

The resulting one-dimensional integral equation is given by

$$\begin{aligned}
 W'(d, Z, Z_1) &\cong W(d, Z) \quad \text{for } d_1 < 0 \\
 W'(d, Z, Z_1) &\cong W(d, Z) - \left(\frac{ikd}{2\pi}\right)^{\frac{1}{2}} \left(\frac{Z_1 - Z}{\eta_0}\right) \\
 &\quad \times \int_0^{d_1} \frac{W(d - \alpha, Z)W'(\alpha, Z_1, Z)}{[\alpha(d - \alpha)]^{\frac{1}{2}}} d\alpha \quad \text{for } d_1 > 0 \quad (126)
 \end{aligned}$$

where

$$\eta_0 = (\mu_0/\epsilon_0)^{\frac{1}{2}} \cong 120\pi$$

This result was obtained in an earlier paper (Wait and Householder, 1957) where certain numerical results were given for a two-section path in the frequency range 20 to 200 kc/s. In the present work, it is desirable to introduce certain dimensionless parameters. These are defined by

$$\begin{aligned}
 iq &= (ka/2)^{\frac{1}{2}}(Z/\eta_0) \\
 iq_1 &= (ka/2)^{\frac{1}{2}}(Z_1/\eta_0) \\
 x &= (ka/2)^{\frac{1}{2}}(d/a) \\
 \hat{x} &= (ka/2)^{\frac{1}{2}}(\alpha/a) \\
 x_1 &= (ka/2)^{\frac{1}{2}}(d_1/a)
 \end{aligned}$$

Thus

$$W'(x, q, q_1) \cong W(x, q) \quad \text{for } x_1 < 0$$

and

$$W'(x, q, q_1) \cong W(x, q) + \left(\frac{x}{\pi i}\right)^{\frac{1}{2}} (q_1 - q) \int_0^{x_1} \frac{W(x - \hat{x}, q)W'(\hat{x}, q_1, q)}{[\hat{x}(x - \hat{x})]^{\frac{1}{2}}} d\hat{x} \quad (127)$$

for $x_1 > 0$. It is immediately observed that $W'(\hat{x}, q_1, q)$ in the integrand may be replaced by $W(\hat{x}, q_1)$ since $\hat{x} < x_1$ over the range of integration. Therefore

$$W'(x, q, q_1) \cong W(x, q) + \left(\frac{x}{\pi i}\right)^{\frac{1}{2}} (q_1 - q) \int_0^{x_1} \frac{W(x - \hat{x}, q)W(\hat{x}, q_1)}{[\hat{x}(x - \hat{x})]^{\frac{1}{2}}} d\hat{x} \quad (128)$$

An alternative form of this equation is easily obtained by regarding the left-hand portion of the path as a modification to the homogeneous earth of surface impedance Z_1 . Thus

$$W'(x, q_1, q) \cong W(x, q_1) + \left(\frac{x}{\pi i}\right)^{\frac{1}{2}} (q - q_1) \int_0^{x-x_1} \frac{W(x - \hat{x}, q_1)W(\hat{x}, q)}{[\hat{x}(x - \hat{x})]^{\frac{1}{2}}} d\hat{x} \quad (129)$$

D. ALTERNATIVE REPRESENTATIONS

Equations (128) and (129) are explicit integral formulas to permit the computation of the attenuation function W' in terms of the attenuation functions W appropriate for a homogeneous earth. From equation (93) it follows that

$$W(x, q) = \left(\frac{\pi x}{i}\right)^{\frac{1}{2}} \sum_{s=1, 2, 3, \dots}^{\infty} \frac{e^{-ixt_s}}{t_s - q^2} \frac{w_1(t_s - y_a)}{w_1(t_s)} \frac{w_1(t_s - y_b)}{w_1(t_s)} \quad (130)$$

where

$$x = (ka/2)^{\frac{1}{2}}(d/a), \quad y_a = (2/ka)^{\frac{1}{2}}kh_a, \quad y_b = (2/ka)^{\frac{1}{2}}kh_b.$$

The coefficients t_s are solutions of the equation (94).

In a similar fashion,

$$W(x, q_1) = \left(\frac{\pi x}{i}\right)^{\frac{1}{2}} \sum_{r=1}^{\infty} \frac{e^{-ixt_r^{(1)}}}{t_r^{(1)} - q_1^2} \frac{w_1(t_r^{(1)} - y_a)}{w_1(t_r^{(1)})} \frac{w_1(t_r^{(1)} - y_b)}{w_1(t_r^{(1)})} \quad (131)$$

where $t_r^{(1)}$ are solutions of

$$w_1'(t) - q_1 w_1(t) = 0. \quad (132)$$

Using (130) and (131), the integration in (128) may be readily carried out to yield

$$W'(x, q, q_1) - W(x, q) = \left(\frac{\pi x}{i}\right)^{\frac{1}{2}} (q_1 - q) \sum_s \sum_r \frac{e^{-ixt_s} [e^{-ix(t_r^{(1)} - t_s)} - 1]}{(t_r^{(1)} - t_s)(t_s - q^2)(t_r^{(1)} - q_1^2)} \frac{w_1(t_s - y_a)}{w_1(t_s)} \frac{w_1(t_r^{(1)} - y_b)}{w_1(t_r^{(1)})} \quad (133)$$

The double summation converges quite rapidly if x_1 is of the order of unity or greater and provided that either y_a and y_b are not large compared with unity.

When x_1 is small, the double series expansion given in (133) becomes very poorly convergent. An alternative expansion for the case $h_b = 0$ is obtained by using the following representation

$$W(\hat{x}, q_1) = \sum_{m=0, 1, 2, \dots} A_m e^{im\pi/4} q_1^m (\hat{x})^{m/2} \quad (134)$$

where

$$\begin{aligned} A_0 &= 1, & A_1 &= -i\sqrt{\pi}, & A_2 &= -2, \\ A_3 &= i\sqrt{\pi} \left(1 + \frac{1}{4q_1^3}\right), & A_4 &= \frac{4}{3} \left(1 + \frac{1}{2q_1^3}\right), \\ A_5 &= -\frac{i\sqrt{\pi}}{2} \left(1 + \frac{3}{4q_1^3}\right), & A_6 &= -\frac{8}{15} \left(1 + \frac{1}{q_1^3} + \frac{7}{32q_1^6}\right), \text{ etc.} \end{aligned}$$

This is a variation of (118) quoted above. Using this result along with the residue series representation for $W(x - \hat{x}, q)$ enables (128) to be expressed in

the form

$$W'(x, q, q_1) = W(x, q) - ix^{\frac{1}{2}}(q_1 - q) \sum_{s=1}^{\infty} \sum_{m=0}^{\infty} A_m e^{im\pi/4} q_1^m I_{\frac{m-1}{2}} \frac{w_1(t_s - y_a)}{w_1(t_s)} \tag{135}$$

where

$$I_{\frac{m-1}{2}} = \int_0^{x_1} e^{-i(x-\hat{x})t_s} (\hat{x})^{\frac{m-1}{2}} d\hat{x}. \tag{136}$$

The integral $I_{\frac{m-1}{2}}$ may be reduced by the following recurrence relation

$$I_{\frac{m}{2}} = \frac{1}{it_s} \left[e^{-i(x-\hat{x})t_s} (\hat{x})^{m/2} - \left(\frac{m}{2}\right) I_{\frac{m-1}{2}} \right] \tag{137}$$

Successive application of this equation enables $I_{\frac{m-1}{2}}$ to be expressed in terms of I_0 and $I_{-\frac{1}{2}}$. These are given by

$$I_0 = e^{-ixt_s} \int_0^{x_1} e^{i\hat{x}t_s} d\hat{x} = \frac{e^{-ixt_s}}{it_s} (e^{ix_1t_s} - 1) \tag{138}$$

and

$$I_{-\frac{1}{2}} = e^{-ixt_s} \int_0^{x_1} \frac{e^{i\hat{x}t_s}}{(\hat{x})^{\frac{1}{2}}} d\hat{x} = \left(\frac{i\pi}{t_s}\right)^{\frac{1}{2}} e^{-ixt_s} \text{erf}(\sqrt{-it_s x_1}) \tag{139}$$

where erf (Z) is the error integral of argument Z .

The double series expansion given by (135) is highly convergent if x is somewhat greater than 1 and x_1 is somewhat less than unity. In fact, if $|q_1^2 x_1| \ll 1$, only the $m = 0$ terms need be retained. Furthermore, if in addition $x_1 \ll 1$,

$$I_{-\frac{1}{2}} \cong 2 e^{-ixt_s} (x_1)^{\frac{1}{2}}$$

And thus,

$$W'(x, q, q_1) \cong W(x, q) \left[1 + \frac{q_1 - q}{(\pi i)^{\frac{1}{2}}} 2x_1^{\frac{1}{2}} \right] \tag{140}$$

The term in square brackets can be regarded as the correction to the attenuation function as a result of the portion of the path from $\hat{x} = 0$ to x_1 . In terms of the original parameters of the problem, the square bracket term becomes

$$\left[1 - \left(\frac{i}{\pi}\right)^{\frac{1}{2}} \frac{Z_1 - Z}{\eta_0} (2k d_1)^{\frac{1}{2}} \right] \tag{141}$$

This same correction emerged from the corresponding theory for the flat-earth case (Wait, 1956a).

E. SOLUTION FOR ONE ANTENNA AT GREAT HEIGHTS

When one terminal becomes elevated to a large height such that y_a or $y_b \gg 1$, it is desirable (following Fock, 1945) to replace the attenuation function W by an auxiliary function V . This function V actually characterizes the far zone radiation pattern of a vertical antenna on the curved surface (Wait and Conda, 1958). First it is noted that if $|y-t| \gg 1$

$$w_1(t-y) \cong e^{-i\pi/4} (y-t)^{-\frac{1}{2}} \exp[-i\frac{2}{3}(y-t)^{\frac{3}{2}}] \quad (142)$$

Furthermore, if also $y \gg t$,

$$w_1(t-y) \cong e^{-i\pi/4} y^{-\frac{1}{2}} e^{-i\frac{2}{3}y^{3/2}} e^{iy\frac{1}{2}t} \quad (143)$$

This latter asymptotic relation enables $W(x, q)$ to be written in the form

$$W(x, q) \cong e^{-i\frac{2}{3}y_a^{3/2}} V(x-\sqrt{y_a}, q) \frac{x^{\frac{1}{2}}}{y_a^{\frac{1}{2}}} \quad (144)$$

where

$$V(X, q) = -i\pi^{\frac{1}{2}} \sum_s \frac{e^{-iXt_s}}{(t_s-q^2)w_1(t_s)} \frac{w_1(t_s-y_b)}{w_1(t_s)} \quad (145)$$

This suggests that the radiation pattern function $V'(X, q, q_1)$ for the mixed path be defined by the relation

$$W'(x, q, q_1) = e^{-i\frac{2}{3}y_a^{3/2}} V'(x-\sqrt{y_a}, q, q_1) \frac{x^{\frac{1}{2}}}{y_a^{\frac{1}{2}}} \quad (146)$$

The integral formula for V' may then be obtained directly from (128), thus

$$V'(X, q, q_1) = V(X, q) + \frac{(q_1-q)}{(\pi i)^{\frac{1}{2}}} \int_0^{x_1} \frac{V(X-\hat{X}, q)W(\hat{X}, q_1)}{(\hat{X})^{\frac{1}{2}}} d\hat{X} \quad (147)$$

where

$$X = x - \sqrt{y_a} \cong \left(\frac{ka}{2}\right)^{\frac{1}{2}} \frac{d - \sqrt{2ah_a}}{a}$$

It should be noted that X can be positive or negative, depending on whether d is greater or less than $(2ah_a)^{\frac{1}{2}}$.

An alternate form for V' is obtained from (129), thus

$$V'(X, q, q_1) = V(X, q_1) + \frac{(q-q_1)}{(\pi i)^{\frac{1}{2}}} \int_{-\sqrt{y_a}}^{x_1} \frac{W(X-\hat{X}, q_1)V(\hat{X}, q)}{(X-\hat{X})^{\frac{1}{2}}} d\hat{X} \quad (148)$$

where

$$X_1 = x_1 - \sqrt{y_a}$$

Since $y_a \gg 1$, the lower limit of this integral is effectively $-\infty$.

Series formulas for $V'(X, q, q_1)$ can be readily obtained in the manner discussed above for $W'(x, q, q_1)$. However, these are applicable only in the present situation if $X > 0$, since the series given in (145) is divergent for

$X < 0$. A more suitable approach is to use the contour integral representation for $V(X, q)$. This is given by

$$V(X, q) = \frac{1}{2\pi^{\frac{1}{2}}} \oint \frac{e^{-iXt}}{w_1'(t) - qw_1(t)} \frac{w_1(t - y_b)}{w_1(t)} dt \tag{149}$$

The contour is chosen so that it encloses (in a clockwise sense) the poles of the integrand at $t = t_s$. It is readily verified that $-2\pi i$ times the sum of the residues leads back to (145). It is now convenient to write

$$V(X, q) = \sum_{n=0}^{\infty} a_n(q) X^n \tag{150}$$

where
$$a_n(q) = \frac{e^{-in\pi/2}}{2\pi^{\frac{1}{2}} n!} \oint \frac{t^n}{[w_1'(t) - qw_1(t)]} \frac{w_1(t - y_b)}{w_1(t)} dt \tag{151}$$

Methods for evaluating the coefficients $a_n(q)$ have been discussed by Logan (1959).

The above representation for V and the series form for the W given by (134) enable the integration in (147) for V' to be readily carried out. The result is

$$V'(X, q, q_1) - V(X, q) = \frac{q_1 - q}{\pi i} \sum_{n=0}^{\infty} \sum_{m=0}^{\infty} a_n(q) A_m(q_1) e^{im\pi/4} q_1^m P_{n, \frac{m-1}{2}} \tag{152}$$

where
$$P_{n, \frac{m-1}{2}} = \int_0^{d_1} (X - \hat{x})^n (\hat{x})^{\frac{m-1}{2}} d\hat{x} \tag{153}$$

The integral $P_{n, \frac{m-1}{2}}$ can be reduced by using the following formula

$$P_{n, \frac{m}{2}} = \frac{(X - x_1)^n (x_1)^{\frac{m}{2} + 1}}{\frac{m}{2} + 1} + \frac{n}{\frac{m}{2} + 1} P_{n-1, \frac{m}{2} + 1} \tag{154}$$

Successive applications enable $P_{n, \frac{m-1}{2}}$ to be expressed in terms of $P_{0, \frac{m}{2}}$ where

$$P_{0, \frac{m}{2}} = \int_0^{x_1} (\hat{x})^{\frac{m}{2}} d\hat{x} = \frac{(x_1)^{\frac{m}{2} + 1}}{\frac{m}{2} + 1} \tag{155}$$

The above double-series representation for V' converges very rapidly when both $|X|$ and x_1 are reasonably small compared to 1.

F. THREE-SECTION PATH

The next most obvious extension is to a three-part medium. The situation is illustrated in Fig. 8. The approach used amounts to a successive application

of the theory for the two-part medium. The path, between *A* and *B*, consists of three segments whose surface impedances are *Z*, *Z*₂ and *Z*₁. The length of the latter two segments are *d*₂ and *d*₁. Using the above-mentioned method,

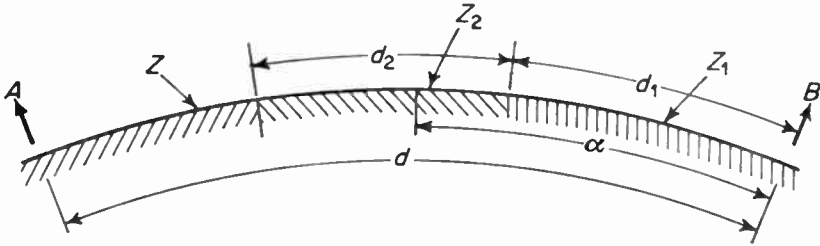


FIG. 8. Three-section path on a spherical earth.

it readily follows that the expression for the resultant attenuation function may be written

$$\begin{aligned}
 W'(d, Z, Z_2, Z_1) = & W(d, Z) - \left(\frac{ikd}{2\pi}\right)^{\frac{1}{2}} \frac{Z_1 - Z}{\eta_0} \int_0^{d_1} \frac{W(d-\alpha, Z)W(\alpha, Z_1)}{[\alpha(d-\alpha)]^{\frac{1}{2}}} d\alpha \\
 & - \left(\frac{ikd}{2\pi}\right)^{\frac{1}{2}} \frac{Z_2 - Z}{\eta_0} \int_{d_1}^{d_1+d_2} \frac{W(d-\alpha, Z)W'(d, Z_1, Z_2)}{[\alpha(d-\alpha)]^{\frac{1}{2}}} d\alpha \quad (156)
 \end{aligned}$$

where *W*(*d*, *Z*) is the attenuation function characteristic of propagation from *A* to *B* over a homogeneous earth of surface impedance *Z*. *W*(*d*−*α*, *Z*) and *W*(*α*, *Z*₁) are attenuation functions for propagation over homogeneous surfaces of surface impedances *Z* and *Z*₁, respectively. The integration variable *α* can be regarded as a great circle distance measured from *B*. The *W'*(*α*, *Z*₁, *Z*₂) occurring in the second integral is the appropriate attenuation function for propagation over the two-part medium from *B* to a point *α* on the middle segment.

For numerical work it is again convenient to introduce the dimensionless parameters used for the two-section theory. Thus

$$\begin{aligned}
 W'(x, q, q_2, q_1) = & W(x, q) + \left(\frac{x}{\pi i}\right)^{\frac{1}{2}} (q_1 - q) \int_0^{x_1} \frac{W(x-\hat{x}, q)W(\hat{x}, q_1)}{[\hat{x}(x-\hat{x})]^{\frac{1}{2}}} d\hat{x} \\
 & + \left(\frac{x}{\pi i}\right)^{\frac{1}{2}} (q_2 - q) \int_{x_1}^{x_1+x_2} \frac{W(x-\hat{x}, q)W'(\hat{x}, q_1, q_2)}{[\hat{x}(x-\hat{x})]^{\frac{1}{2}}} d\hat{x} \quad (157)
 \end{aligned}$$

where $iq_2 = (ka/2)^{\frac{1}{2}}(Z_2/\eta_0)$ $x_2 = (ka/2)^{\frac{1}{2}}(d_2/a)$

and the other quantities have their usual meaning. From (128) and (129)

we may deduce that

$$W'(\hat{x}, q_1, q_2) = W(\hat{x}, q_1) + \left(\frac{x}{\pi i}\right)^{\frac{1}{2}} (q_2 - q_1) \int_0^{\hat{x} - x_1} \frac{W(\hat{x} - x', Z_1)W(x', Z_2)}{[(\hat{x} - x')x']^{\frac{1}{2}}} dx' \quad (158)$$

$$= W(\hat{x}, q_2) + \left(\frac{x}{\pi i}\right)^{\frac{1}{2}} (q_1 - q_2) \int_0^{x_1} \frac{W(\hat{x} - x', Z_2)W(x', Z_1)}{[(\hat{x} - x')x']^{\frac{1}{2}}} dx' \quad (159)$$

Of course, it would be possible to obtain various series formulas for W' for a three-section path, but in general these would be cumbersome. It is considered to be preferable to work directly with (157) and carry out the integration numerically, since presumably $W'(x, q_1, q_2)$ would be known from the two-section theory.

There is a simple limiting case of (157) which is particularly interesting. We take $q = q_1$ and $x_2 \ll x$ and x_1 . To this approximation, the first integral on the right-hand side of (157) vanishes and the integrand in the second integral is essentially a constant over the range x_1 to $x_1 + x_2$. Thus

$$W'(x, q, q_2, q_1) \cong W(x, q) + \left(\frac{x}{\pi i}\right)^{\frac{1}{2}} (q_2 - q) \frac{x_2}{[x_1(x - x_1)]^{\frac{1}{2}}} W(x - x_1, q)W(x_1, q) \quad (160)$$

This simple formula has a clear physical interpretation. The second term on the right-hand side can be regarded as the field scattered by the strip of width x_2 . It is proportional to $q_2 - q$ (or $Z_2 - Z$), which is the surface impedance contrast and it also is proportional to the attenuation functions $W(x - x_1, q)$ and $W(x_1, q)$ which respectively account for the attenuation from A to the strip, and from the strip to B . Such an equation is analogous to the first Born approximation in scattering theory.

In the foregoing discussion of the three-section theory the antenna heights h_a and h_b , of A and B respectively, may be arbitrary (provided that h_a and $h_b \ll a$). When the height of one terminal is large, such that $y_a \gg 1$, for example, it is again convenient to define a radiation pattern function V' . In this case,

$$W'(x, q, q_2, q_1) = e^{-i\frac{1}{2}y_a^{3/2}} V'(X, q, q_2, q_1) \frac{x^{\frac{1}{2}}}{y_a^{\frac{1}{2}}} \quad (161)$$

where

$$V'(X, q, q_2, q_1) = V(X, q) + \frac{(q_1 - q)}{(\pi i)^{\frac{1}{2}}} \int_0^{x_1} \frac{V(X - \hat{x}, q)W(\hat{x}, q_1)}{(\hat{x})^{\frac{1}{2}}} d\hat{x} \\ + \frac{(q_2 - q)}{(\pi i)^{\frac{1}{2}}} \int_{x_1}^{x_1 + x_2} \frac{V(X - \hat{x}, q)W'(\hat{x}, q_1, q_2)}{(\hat{x})^{\frac{1}{2}}} d\hat{x} \quad (162)$$

where all quantities on the right-hand side have their usual meaning.

G. NUMERICAL RESULTS

It is obvious that any attempt to present curves and tables which completely cover all cases of practical interest is futile. The large number of parameters involved quickly lead us to an enormous number of curves. However, with some care it is possible to limit these to several hundred curves if the user is asked to interpolate to some extent. It is hoped to publish such an atlas of curves in the future. In the meantime, it is considered worthwhile to present a sampling of those results in graphical form (Wait and Walters, 1963).

For the most part, the cases shown in the following figures are for propagation over a two-part path consisting of homogeneous sea and land portions, (Figs. 9 through 14). One example of a three-part path is also shown (Fig. 15). The electrical constants for the land were taken as $\sigma = 10^{-2}$ mhos/m and $\epsilon/\epsilon_0 = 15$ corresponding to well conducting land, and $\sigma = 10^{-3}$ mhos/m and $\epsilon/\epsilon_0 = 15$ corresponding to poorly conducting land. For sea water, $\sigma = 4$ mhos/m and $\epsilon/\epsilon_0 = 80$. To allow for standard atmospheric refraction the effective radius concept was utilized (Norton, 1941). For the results shown here, a was set equal to four-thirds times the actual radius.

In each case the amplitude of $W(d, Z, Z_1)$ and the phase lag (i.e. $-\arg W$) are plotted as a function of distance d in kilometers. For these calculations, the heights of the antennas above ground are assumed to be zero. The frequencies chosen are 1 000, 100 and 20 Kc/s. The length of the second section d_2 is indicated on each curve.

The preceding formulation was in terms of mutual impedance between vertical dipoles A and B . For further discussion it is probably better to express the results in terms of the vertical electric field at B for a standard source at A . For example,

$$E = E_0 W = E_0 |W| e^{-i\Phi} \quad (163)$$

where $|W|$ is the amplitude of the relative field, Φ is the phase lag, and $E_0 = \frac{100}{d} \left[1 - \frac{1}{(kd)^2} - \frac{i}{kd} \right] e^{-ikd}$ V/m. For a flat perfectly conducting plane E would be equal to the field E_0 . The strength of the source is thus chosen so that the radiation field is 0.1 V/m at $d = 1$ km. In most cases of practical interest, $kd \gg 1$ and

$$E_0 \cong (100/d) e^{-ikd} \quad (164)$$

Thus, in the far field, W is proportional to the actual field times distance. Speaking loosely, W can be described as the actual field divided by the "inverse-distance" field.

It should be kept in mind that at short distances, where d is comparable with or less than a wavelength, the terms corresponding to $1/(ikd)$ and $1/(ikd)^2$ in equation (163) should be retained. These correspond to what are often called the induction and static fields, respectively. It is also worth mentioning that if the receiving antenna (at B) were a vertical loop, the horizontal magnetic field component H would be measured. Thus

$$H = H_0 W \quad (165)$$

where

$$\eta_0 H_0 = \frac{100}{d} \left[1 - \frac{i}{kd} \right] e^{-ikd} \tag{166}$$

is also expressed in V/m if $\eta_0 = 120\pi \Omega$. Again, on a flat perfectly conducting earth $\eta_0 H_0 = 0.1$ V/m at $d = 1$ km, provided $kd \gg 1$. In this case there is no static field component.

There are many other situations in which the W functions enter into the field formulas. In general, they characterize the vertical polarized component of any physical source placed on or near the earth's surface. Furthermore, the source or receiver may be buried in the ground or submerged in the sea.

Some specific features of the curves are now worth discussing. In this portion, the W functions will be referred to as the "relative field".

In Fig. 9a, for 1 000 kc/s, the path of propagation is from land to sea. It is apparent that the relative field increases beyond the coast line in each

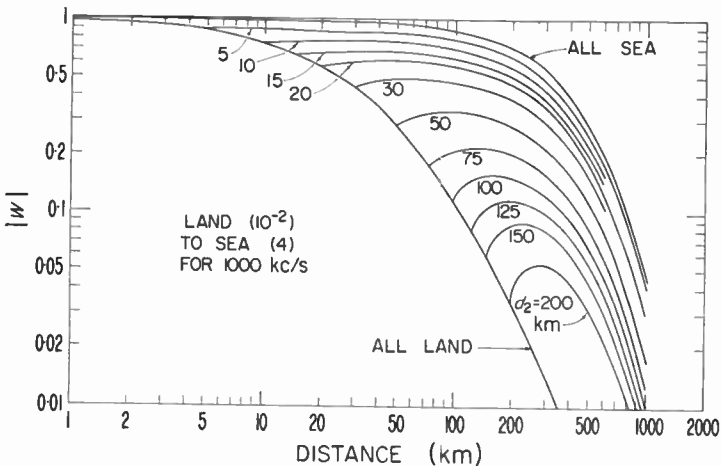


FIG. 9a. Amplitude of the relative field of the ground wave as a function of distance for propagation from land towards the sea. The coast line is a distance d_2 from the transmitter (which is on the land).

case. For the greater distances the effect is very marked. Such a phenomenon has been observed experimentally by Millington (1949) and has been called the recovery effect. The corresponding phase curves are shown in Fig 9b. The rather abrupt drop in the phase just beyond the coast line could be called a phase recovery. Such an effect has been confirmed experimentally by Pressey *et al.* (1956).

An additional set of land-to-sea curves for 1 000 kc/s is given in Figs. 10a and 10b. Here, the relatively poor conductivity of the land (i.e. 10^{-3}) leads to very marked recovery effects beyond the coast line. The right-hand portion of the amplitude curves in Fig. 10a is shown dashed to emphasize that under these conditions the ionospheric reflected waves may overwhelm the ground wave. However, in certain pulsed-type transmissions such as

used in Loran, the ground wave may be observed separately from the sky waves even at very great ranges. Nevertheless, it is well to keep in mind that ionospheric influences are not considered in these curves.

Ground wave propagation at 1000 kc/s from sea to land is illustrated in Fig. 11, where the amplitude of the relative field is plotted as a function of distance. In this case, the transmitter is located over the sea. Here, as expected, the field drops abruptly as the coast line is crossed. Actually, there is no new information in Fig. 11 that was not in Fig. 9a since, by

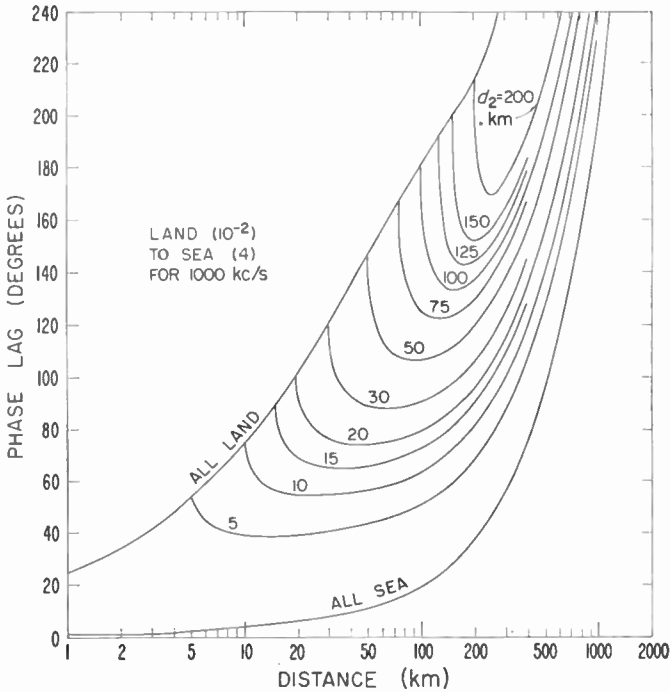


FIG. 9b. Phase of the relative field corresponding to conditions of Fig. 9a.

reciprocity, the transmitter and receiver locations can always be exchanged. Consequently, it would be somewhat redundant to show the phase curves.

At lower frequencies the phenomena described above also occur. However, as indicated in Fig. 12 for 100 kc/s and a land conductivity of 10^{-2} , the recovery phenomenon is not so marked. In fact, for the amplitude of the field there is hardly any difference between an all-land path and an all-sea path. This is consistent with the well-known fact that the characteristics of ground wave propagation at low frequencies are determined mainly by the curvature of the earth rather than its electrical properties. However, for poorer ground conductivity, the recovery effects, even at 100 kc/s, are significant. Examples of these are shown in Figs. 13a and 13b for a land conductivity of 10^{-3} .

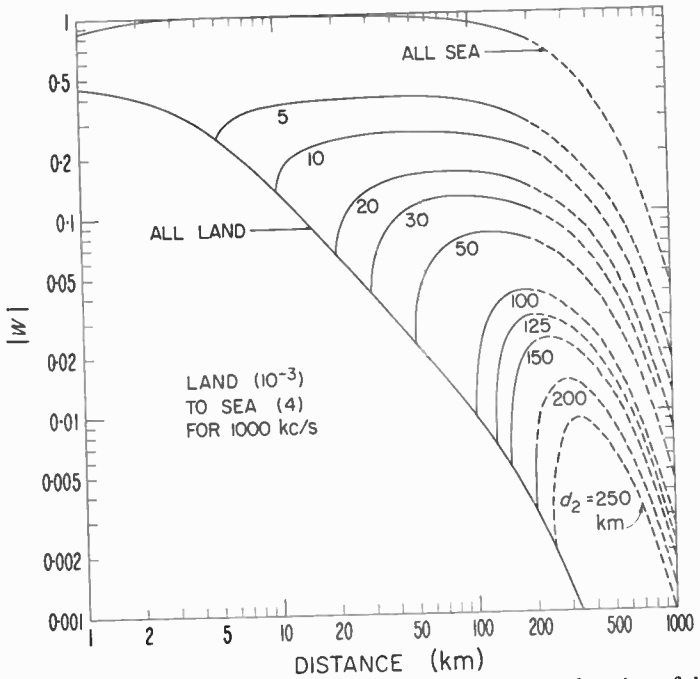


FIG. 10a. Amplitude of the relative field of the ground wave as a function of distance for propagation from land towards the sea. The coast line is a distance d_2 from the transmitter (which is on the land).

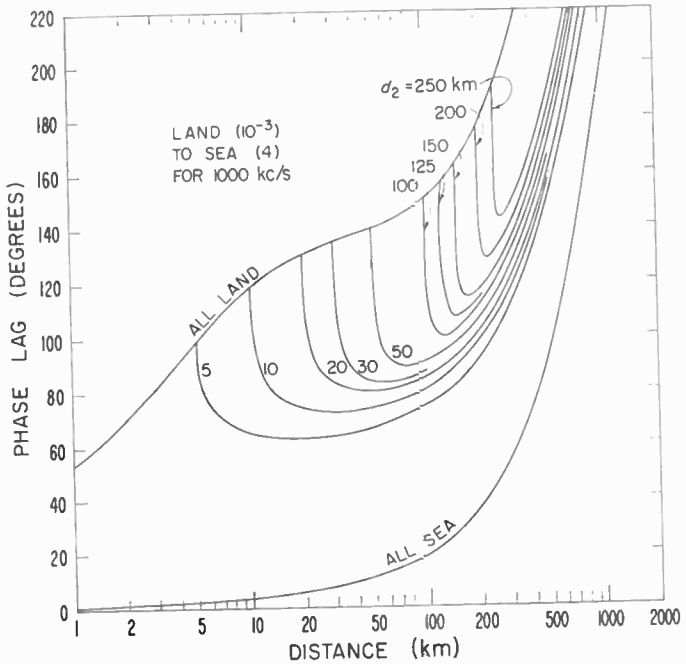


FIG. 10b. Phase of the relative field corresponding to conditions in Fig. 10a.

Ground wave propagation from land to sea at very low frequencies is illustrated in Fig. 14 for a land conductivity of 10^{-3} . Here, even though a poor land conductivity has been chosen, the recovery effects are not marked.

Finally, in Fig. 15 an example of a three-part path is shown. The propagation, for 1000 kc/s, is from land to sea to land. In each case it is noted that a recovery effect takes place as the first coast line is crossed. Then, at the second coast line the field drops abruptly. In each of the three cases shown the amplitude curves, asymptotically, at large distances, approach the curve for an all-land path. However, in each case there is residual vertical displacement which is approximately proportional to the length of the intermediate sea-portion of the path. This phenomenon was discussed previously (Wait, 1961).

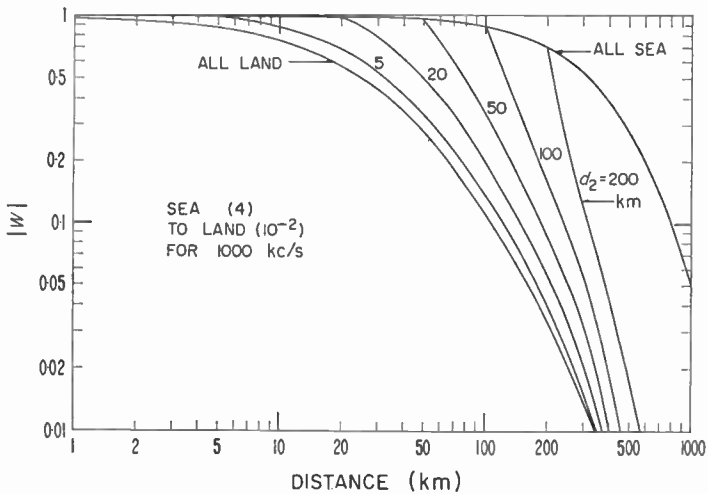


FIG. 11. Amplitude of the relative field of the ground wave as a function of distance for propagation from sea towards the land. The coast line is a distance d_2 from the transmitter.

The curves presented here are all based on the assumption that the heights of the transmitting and receiving antennas are effectively zero. Without additional computation it is not possible to say much about the height variation of the fields over mixed paths. However, it is to be expected that the recovery effects are less marked as the receiving antenna is raised. In fact, this is necessary from a physical basis since energy must be supplied from greater heights if the field is to actually increase with distance on the earth's surface. This is confirmed by an examination of the structure of the general formula for arbitrary heights (Wait, 1961). Such a mechanism was also suggested by Millington (1949).

Most of the complications in the height-gain function would occur at or just near the coast lines. Somewhat beyond the coast line the situation

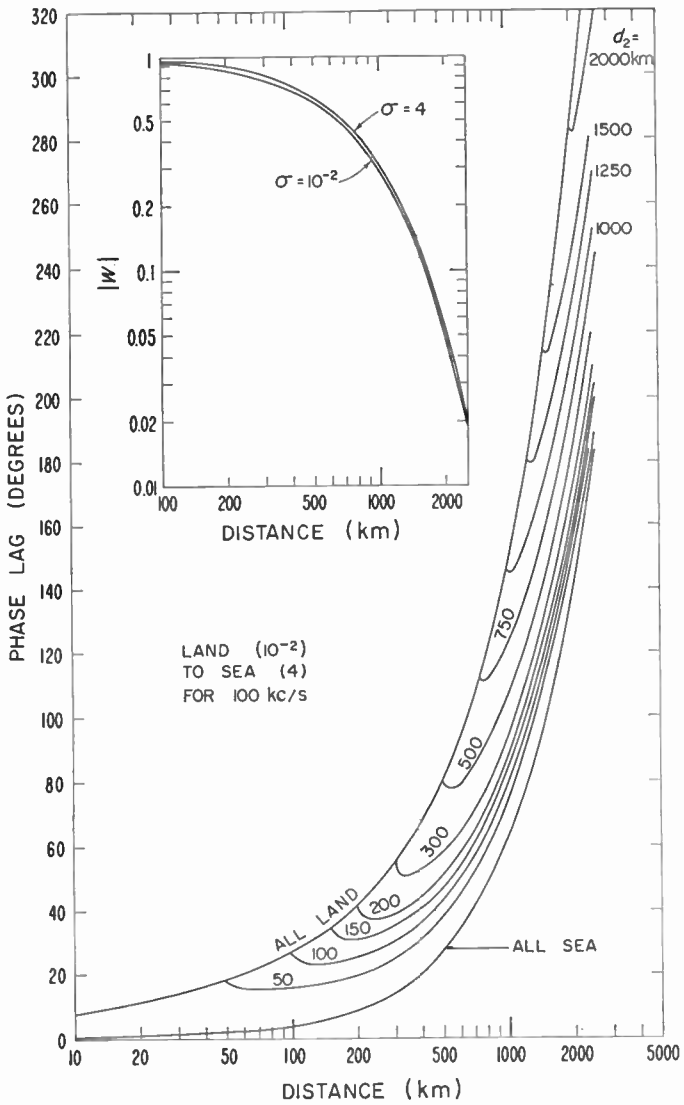


FIG. 12. Amplitude and phase of the relative field as a function of distance for propagation from land to sea.

becomes much simpler. For example, on examining any of the curves in Figs. 9a to 14, it is noted that the field variations with distance always approach that expected for a homogeneous medium. This is also observed in the structure of the theoretical forms (Wait, 1961). Consequently, in these limiting cases, it may be asserted that the height-gain functions are characteristic only of the underlying medium. In fact, for low heights

$$\frac{E \text{ (at height } z\text{)}}{E \text{ (at height } 0\text{)}} \cong 1 + ikz(Z/\eta_0) \quad (167)$$

where Z is the surface impedance of the underlying earth's surface, $\eta_0 = 120\pi$, and $k = 2\pi/\text{wavelength}$. This simple formula is valid provided $(ka)^{-2/3}(kz)^2 \ll 1$ (Wait, 1956a) and also, as mentioned, it must only be used sufficiently far from the coast line.

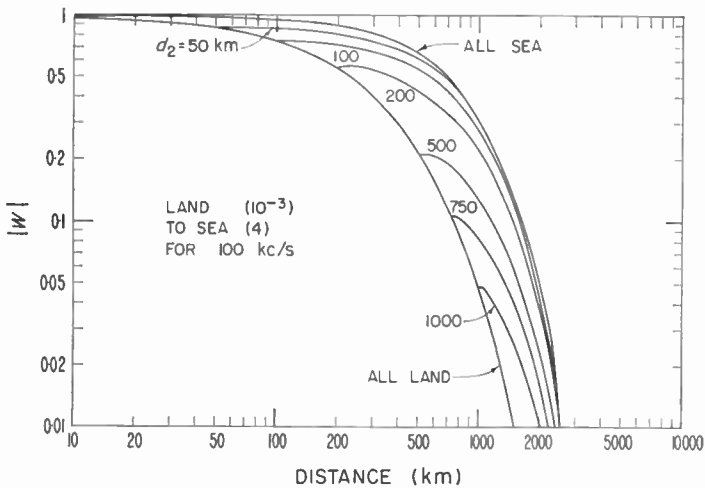


FIG. 13a. Amplitude of the relative field of the ground wave as a function of distance for propagation from land towards the sea. The coast line is a distance d_2 from the transmitter (which is on the land).

Some of the important features of the characteristics of mixed-path propagation have been observed experimentally as mentioned above. While the observed effects are consistent with theory, it is difficult to find conditions which are suitably idealized. For example, the land portions of the path are usually inhomogeneous and not sufficiently smooth. A much better way to experimentally confirm theory is to set up a model experiment. With this motivation an extensive laboratory investigation of mixed-path propagation has been initiated. Some of the first results (Maley, 1962) obtained in this study indicate very satisfactory agreement with theory.

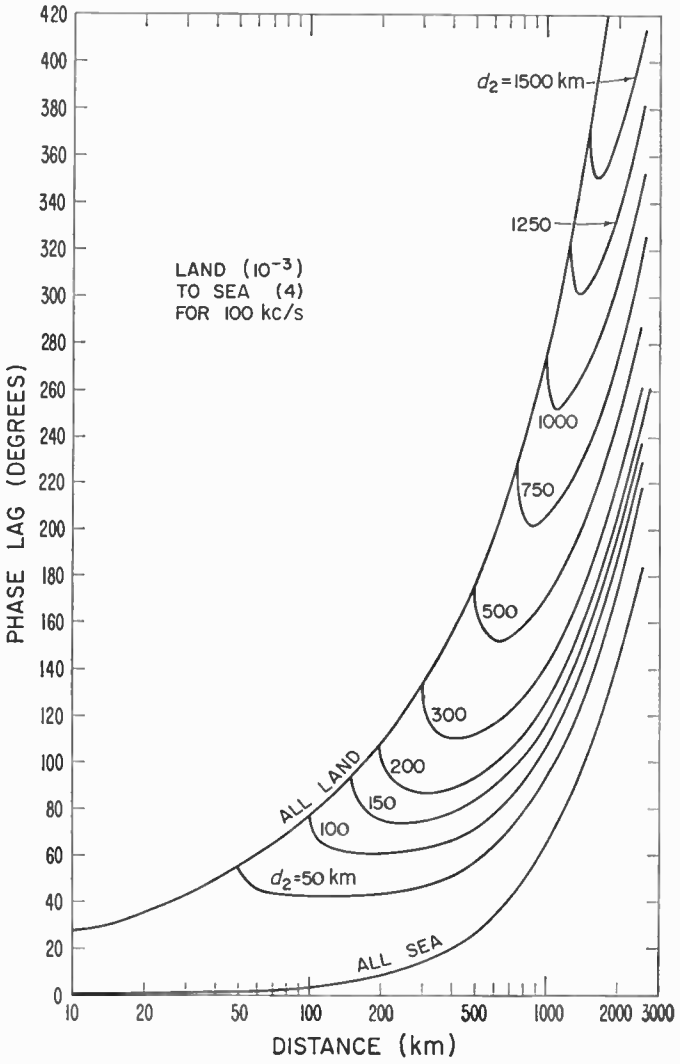


FIG. 13b. Phase of the relative field corresponding to conditions of Fig. 13a.

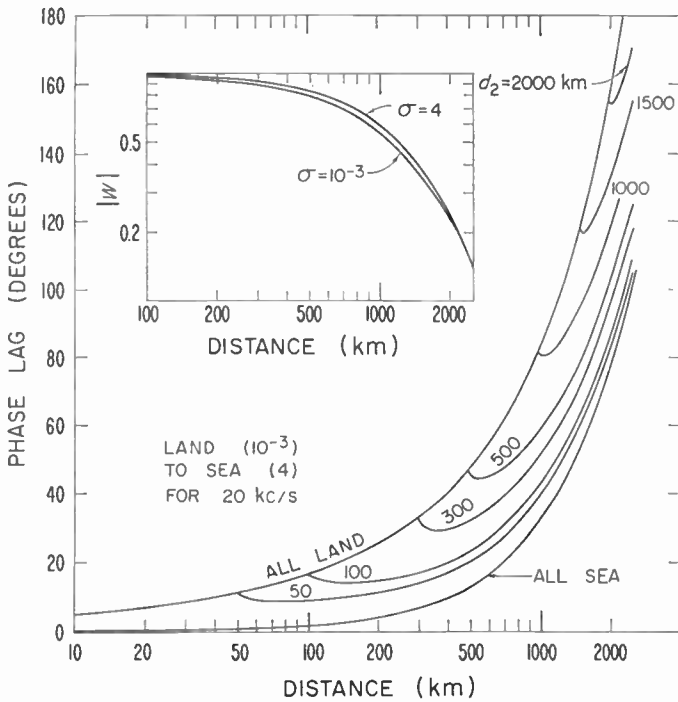


FIG. 14. Amplitude and phase of the relative field as a function of distance for propagation from land to sea.

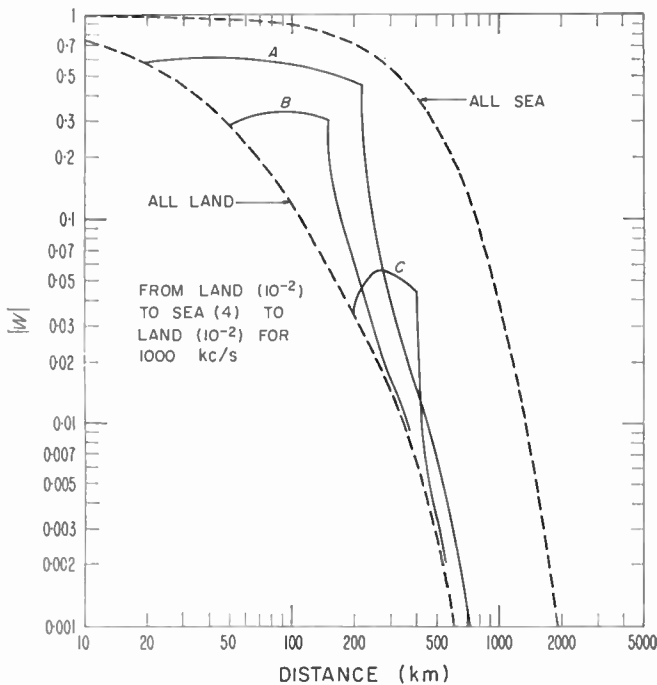


FIG. 15. Amplitude of the relative field for propagation over a three-section path consisting of two land portions separated by a sea portion.

H. SOME EXTENSIONS OF THE THEORY

It is of interest to apply the compensation theorem as expressed by (123) to a spherical earth in the case when the surface impedances are a function of distance along the great circle distance d between A and B . The one-dimensional form of (123) may be written in terms of the attenuation functions as follows:

$$W'(q, q_1, x) = W(q, x) + \left(\frac{x}{\pi i}\right)^{\frac{1}{2}} \int_0^{x_1} [q_1(\hat{x}) - q(\hat{x})] \frac{W(x - \hat{x}, q) W'(\hat{x}, q_1, q)}{[\hat{x}(x - \hat{x})]^{\frac{1}{2}}} d\hat{x} \quad (168)$$

where q_1 and q are now functions of \hat{x} (or α) the great circle distance from B . Of course, if q_1 and q are constant, (168) is identical to (127).

It is believed that (168) could be solved directly by numerical means if q is taken as a constant corresponding to the unmodified homogeneous earth and $q_1(\hat{x})$ is some specified function of \hat{x} over the range from 0 to x_1 . Equation (168) also permits an approximate treatment of transition regions. To illustrate this latter point we consider a three-section path as shown in Fig. 8. Now, however, the middle section is considered to have a surface impedance which is a function of α . Thus, q_2 is a function of \hat{x} over the region from x_1 to $x_1 + x_2$. The attenuation function for this particular path may be expressed by

$$W'(x, q, q_2(x), q_1) = W'(x, q, q_1) + \left(\frac{x}{\pi i}\right)^{\frac{1}{2}} \times \int_{x_1}^{x_1 + x_2} [q_2(\hat{x}) - q] \frac{W(x - \hat{x}, q) W'(\hat{x}, q_1, q_2(x), q)}{[\hat{x}(x - \hat{x})]^{\frac{1}{2}}} d\hat{x} \quad (169)$$

where $W'(x, q, q_1)$ is the appropriate two-section attenuation function and is given explicitly by (128). Now on the assumption that x_2 is small compared with both x_1 and x it is permissible to replace W' in the integral in (169) by $W(x_1, q_1)$. Admittedly, this is a first-order approximation, but it should be adequate since the relative contribution of the integral is expected to be small in any case. To the same approximation $W(x - \hat{x}, q)$ in the integrand can be replaced by $W(x - x_1, q)$. Thus

$$W'(x_1, q, q_2(x), q_1) \cong W'(x, q, q_1) + \left(\frac{x}{\pi i}\right)^{\frac{1}{2}} \times (\bar{q}_2 - q) \frac{x_2}{[x_1(x - x_1)]^{\frac{1}{2}}} W(x - x_1, q) W(x_1, q_1) \quad (170)$$

where $\bar{q}_2 = \frac{1}{x_2} \int_{x_1}^{x_1 + x_2} q_2(\hat{x}) d\hat{x}$ is the average value of $q_2(\hat{x})$

THE INTEGRAL EQUATION

In the foregoing discussion the attenuation function W for a homogeneous earth consistently appears. It is of interest to see that an integral equation for W in the case $h_a = h_b = 0$ emerges directly from (168). To show this we allow x_1 to approach zero in (168) and then we imagine the unmodified surface to be a flat, perfectly conducting plane between A and B . Thus, the appropriate value $W(x, q)$ is simply $\exp(ix^3/12)$. (The quantity $x^3/12$ is the difference between the arc and the chord between A and B .) Furthermore, the appropriate value of the surface impedance along the arc AB over a conducting plane is easily found to be given by

$$Z \cong -\eta_0 \frac{d-\alpha}{2a}$$

or
Thus

$$q(\hat{x}) \cong i(x-\hat{x})/2$$

$$W'(x, q_1(x)) = e^{ix^3/12} + \left(\frac{x}{\pi i}\right)^{\frac{1}{2}} \int_0^x \left[q_1(x) - i \frac{(x-\hat{x})}{2} \right] e^{i(x-\hat{x})^3/12} W'(\hat{x}, q_1(\hat{x})) d\hat{x} \quad (171)$$

Now if q_1 is a constant throughout the length of the path, W' in the above equation becomes by definition the attenuation function for a homogeneous path. Thus

$$W(x, q_1) = e^{ix^3/12} + \left(\frac{x}{\pi i}\right)^{\frac{1}{2}} \int_0^x \left[q_1 - i \frac{(x-\hat{x})}{2} \right] \times [\hat{x}(x-\hat{x})]^{-\frac{1}{2}} e^{i(x-\hat{x})^3/12} W(\hat{x}, q_1) d\hat{x} \quad (172)$$

This integral equation has been derived by Hufford (1952), who also shows that its solution is the residue series

$$W(x, q_1) = \left(\frac{\pi x}{i}\right)^{\frac{1}{2}} \sum_{r=1,2,3,\dots} \frac{e^{-ixt_r}}{t_r - q_1^2} \quad (173)$$

where t_r are roots of

$$w_1'(t) - q_1 w_1(t) = 0$$

In a similar manner it may be shown that

$$V(X, q_1) = e^{iX^3/12} + \left(\frac{i}{\pi i}\right)^{\frac{1}{2}} \int_{-\infty}^X \left[q_1 - i \frac{(X-\hat{X})}{2} \right] \times [X-\hat{X}]^{-\frac{1}{2}} e^{i(X-\hat{X})^3/12} V(\hat{X}, q_1) d\hat{X} \quad (174)$$

$$\text{where} \quad V(X, q_1) = -i\pi^{\frac{1}{2}} \sum_{r=1,2,3,\dots} \frac{e^{-ixt_r}}{(t_r - q_1^2)w_1(t_r)} \quad (175)$$

These particular integral equations have also been discussed by Logan (1959).

VIII. WAVE PROPAGATION OVER AN INHOMOGENEOUS SPHERE

In Section VII the mutual impedance between two dipoles on a sectionally homogeneous earth was considered. To obtain convenient formulas for computation, the integral representations were reduced to a single integration along a great circle connecting the two dipoles. The derivation of the relevant formulas, given here, illustrate some important principles in wave propagation on an inhomogeneous spherical surface. Furthermore, certain assumptions, which are inherent in the previous results, are clarified when the three-dimensional nature of the problem is preserved.

The vertical electric dipole (of lengths l_a and l_b) at A and B which are both taken to be on the surface of a smooth spherical earth of radius a . As before, the great circle distance between A and B is denoted by d . The situation, in perspective, is shown in Fig. 16, where the center of the earth is denoted by

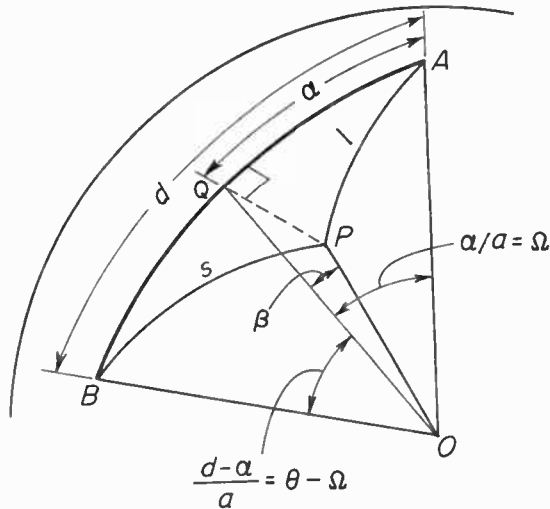


FIG. 16. Coordinates for describing wave propagation on a spherical surface.

O . As in Section VII, the mutual impedance is denoted Z_{ab} between A and B when the earth is homogeneous with surface impedance Z everywhere. From the results of Section VI, it is known that

$$Z_{ab} = \frac{l_a l_b i \mu_0 \omega}{2\pi d} e^{-ikd} \left[1 + \frac{1}{ikd} - \frac{1}{k^2 d^2} \right] W(d, Z) \tag{176}$$

where $W(d, Z)$ is the attenuation function given by equation (130). In the present case the attenuation function is given by

$$W(d, Z) \cong \left(\frac{\pi x}{i} \right)^{\frac{1}{2}} \left[\sum_{s=1,2,3} \frac{e^{-ixt_s}}{t_s - q^2} \right] \left[\frac{(d/a)}{\sin(d/a)} \right]^{\frac{1}{2}} \tag{177}$$

where
and

$$x = (ka/2)^{\frac{1}{2}}(d/a)$$

$$q = -i(ka/2)^{\frac{1}{2}}(Z/\eta_0)$$

The complex factors t_s are found from the roots of

$$w'_1(t) - qw_1(t) = 0$$

The representation of the attenuation function given above is a slightly extended version of equation (131). It is valid everywhere on the globe except near the antipode. When $d/a \ll 1$, equation (176) reduces to unity when $kd \gg 1$ and then this equation becomes identical to (124).

In the same manner as in Section VII, the mutual impedance for the sphere is denoted by Z'_{ab} when the surface impedance is changed from Z to Z' . Then the attenuation function $W'(d, Z, Z')$ is defined by

$$Z'_{ab} = \frac{I_a I_b i \mu_0 \omega}{2\pi d} e^{-ikd} \left[1 + \frac{1}{ikd} - \frac{1}{k^2 d^2} \right] W'(d, Z, Z') \quad (178)$$

It is assumed that a current I_b applied at the terminals of dipole B would produce electric and magnetic fields \vec{E}_b and \vec{H}_b when the surface impedance of the earth is Z everywhere. On the other hand, a current I_a applied at the terminals of dipole A would produce electric and magnetic fields \vec{E}'_a and \vec{H}'_a when the surface impedance of the earth is Z' .

It now follows from an application of the Lorentz reciprocity theorem, or directly from the work of Monteath (1951), that

$$Z'_{ab} - Z_{ab} = \frac{1}{I_a I_b} \iint_S [\vec{E}_b \times \vec{H}'_a - \vec{E}'_a \times \vec{H}_b] \cdot \vec{i}_r dS \quad (179)$$

where S is the surface of the sphere, dS is an element of area and \vec{i}_r is the unit vector normal to the sphere. Over the surface of the sphere the tangential field vectors satisfy the approximate boundary conditions specified by

$$\vec{i}_r \times \vec{H}_{bt} = Z \vec{E}_{bt} \quad (180a)$$

and
$$\vec{i}_r \times \vec{H}'_{at} = Z' \vec{E}'_{at} \quad (180b)$$

On making use of equations (179), (180a), and (180b), it now follows that

$$I_a I_b (Z'_{ab} - Z_{ab}) = \iint_S (\vec{H}'_{at} \cdot \vec{H}_{bt}) (Z' - Z) dS \quad (181)$$

which reduces to equation (123) for a sectionally homogeneous surface.

The next step is to express the tangential magnetic field vectors, at the point P in Fig. 16, in terms of the attenuation functions. Thus

$$\vec{H}_{bt} = \frac{ik I_b h_b}{2\pi s} e^{-iks} \left(1 + \frac{1}{iks} \right) W(s, Z) (\vec{i}_r \times \vec{i}_s) \quad (182)$$

and
$$\vec{H}'_{at} = \frac{ik I_a h_a}{2\pi l} e^{-ikl} \left(1 + \frac{1}{ikl} \right) W(l, Z, Z') (\vec{i}_r \times \vec{i}_l) \quad (183)$$

where \vec{i}_s and \vec{i}_l are unit vectors in the directions of increasing s and l , respectively.

Equation (181), when combined with (178), (182), and (183), is now reduced to

$$W'(d, Z, Z') = W(d, Z) + \frac{ikd}{2\pi} \int_s \int \frac{e^{-ik(s+l-d)}}{sl} (Z' - Z) \left(1 + \frac{1}{iks}\right) \times \left(1 + \frac{1}{ikl}\right) W(s, Z) W'(l, Z, Z') (\cos \delta) dS \quad (184)$$

where δ is the angle subtended by \vec{i}_s and \vec{i}_l .

This is an integral equation for the unknown attenuation function $W'(l, Z, Z')$. To solve such an equation directly appears to be out of the question. Therefore, some simplifications are made at this stage in order to achieve tractability.

The function $\exp[-ik(s+l-d)]$ is rapidly varying compared with other factors in the integrand. Therefore, one may expect that the principal contribution to the integrand will occur when $(s+l) \cong d$, provided that the surface impedance contrast $(Z' - Z)$ does not change rapidly in a direction transverse to the path. Therefore, in the other factors in the integrand l may be replaced by α and s by $d - \alpha$, where α is the great circle distance from A to the point Q on the great circle between A and B . (The arc QP is perpendicular to AB .) Furthermore, over most of the region of integration, $(1/ks)$ and $(1/kl)$ can be neglected compared with unity and, finally, $\cos \delta$ is replaced by -1 .

The reduced form of integral equation is

$$W'(d, Z, Z') = W(d, Z) - \frac{ikd}{2\pi\eta_0} \int_s \int \frac{e^{-ik(s+l-d)}}{\alpha(d-\alpha)} [Z'(\alpha) - Z] \times W(d-\alpha, Z) W'(\alpha, Z, Z') dS \quad (185)$$

where all quantities, except the exponential factor, vary with α only. To effect a further reduction of the integral, a suggestion by Z. Godzinski (personal communication) is adopted. The idea is to express the exponent $s+l-d$ in terms of the angle coordinates Ω and β shown in Fig. 1. These angles are defined by $\Omega = \alpha/a = QA/a$ and $\beta = QP/a$.

From spherical trigonometry

$$\cos(AOP) = \cos \Omega \cdot \cos \beta$$

and $\cos(BOP) = \cos(\theta - \Omega) \cdot \cos \beta$

Thus

$$(AOP) = \frac{l}{a} = \Omega + \left[\frac{\cot \Omega}{2}\right] \beta^2 + \text{terms in } \beta^4, \beta^6, \dots \quad (186)$$

and $(BOP) = \frac{s}{a} = \theta - \Omega + \left[\frac{\cot(\theta - \Omega)}{2}\right] \beta^2 + \text{terms in } \beta^4, \beta^6, \dots \quad (187)$

and therefore to a first order in β^2 ,

$$s + l - d \cong \frac{a}{2} [\cot \Omega + \cot(\theta - \Omega)] \beta^2 \tag{188}$$

Within the region of validity of the present approximations, the element of area dS may be approximated by $a^2 d\Omega d\beta$. The integral now has the form

$$W'(d, Z, Z') = W(d, Z) - \frac{ikda}{2\pi\eta_0} \int_{\alpha_1}^{\alpha_2} \frac{Z'(\alpha) - Z}{\alpha(d - \alpha)} W(d - \alpha, Z) W'(\alpha, Z, Z') \\ \times \left[\int_{\beta_1(\alpha)}^{\beta_2(\alpha)} \exp \left[-i \frac{ka}{2} [\cot \Omega + \cot(\theta - \Omega)] \beta^2 \right] d\beta \right] d\alpha \tag{189}$$

where the limits of the surface S are $y_1(\alpha) \leq y \leq y_2(\alpha)$ and $\alpha_1 \leq \alpha \leq \alpha_2$.†

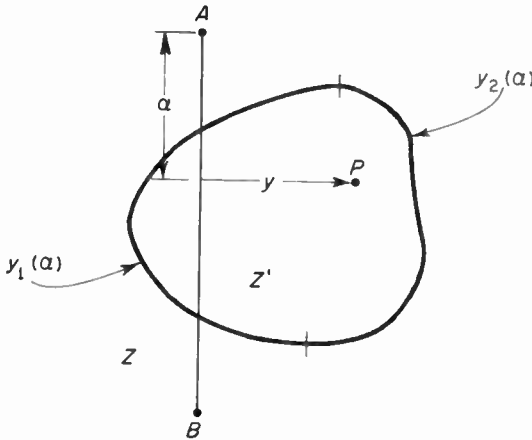


FIG. 17. Plane view of inhomogeneous surface showing coordinates (α, y) and the boundary curves $y_1(\alpha)$ and $y_2(\alpha)$. The horizontal scale is exaggerated somewhat.

The integral involving β is of a Fresnel type and, therefore,

$$\int_{\beta_1}^{\beta_2} \exp[\dots] d\beta = \left(\frac{\pi}{ka} \right)^{\frac{1}{2}} [\cot \Omega + \cot(\theta - \Omega)]^{-\frac{1}{2}} \int_{u_1}^{u_2} \exp \left(-i \frac{\pi}{2} u^2 \right) du \tag{190}$$

where $u_1 = \left(\frac{ka}{\pi} \right)^{\frac{1}{2}} [\cot \Omega + \cot(\theta - \Omega)]^{\frac{1}{2}} \beta_1$

and $u_2 = \left(\frac{ka}{\pi} \right)^{\frac{1}{2}} [\cot \Omega + \cot(\theta - \Omega)]^{\frac{1}{2}} \beta_2$

† As indicated in Fig. 17.

Equation (189) may now be written

$$W'(d, Z, Z') = W(d, Z) - \left(\frac{ika}{2\pi}\right)^{\frac{1}{2}} d \int_{\alpha_1}^{\alpha_2} \frac{Z'(\alpha) - Z}{\eta_0} \left[\cot\left(\frac{\alpha}{a}\right) + \cot\left(\frac{d-\alpha}{a}\right) \right]^{-\frac{1}{2}} \times \frac{W(d-\alpha, Z)W'(\alpha, Z, Z')}{(d-\alpha)\alpha} F(u_1, u_2) d\alpha \quad (191)$$

where
$$F(u_1, u_2) = (i/2)^{\frac{1}{2}} \int_{u_1}^{u_2} \exp\left(-i\frac{\pi}{2}u^2\right) du \quad (192)$$

It may be observed that when $(-u_1)$ and u_2 are somewhat greater than $+1$, the Fresnel integral function $F(u_1, u_2)$ can be replaced by unity. Also, if the angular distance d/a is much less than 1 the cotangents can be replaced by the reciprocal of their arguments. With these approximations the integral equation reduces to the form

$$W'(d, Z, Z') = W(d, Z) - \left(\frac{ikd}{2\pi}\right)^{\frac{1}{2}} \int_{\alpha_1}^{\alpha_2} \left[\frac{Z'(\alpha) - Z}{\eta_0} \right] \frac{W(d-\alpha, Z)W'(\alpha, Z, Z')}{[\alpha(d-\alpha)]^{\frac{1}{2}}} d\alpha \quad (193)$$

When considering propagation over a two-part path this equation would reduce to the integral formula given by (126).

The rapidly varying function $\exp[-ik(s+l-d)]$ in the integrand of (184) determines the portions of the earth's surface between A and B which are significant. The phenomena may be described in terms of Fresnel zones.† These are determined by the locus of the points where

$$k(s+l-d) = m\pi/2 \quad (\text{for } m = 1, 2, 3, \dots)$$

or within a good approximation

$$\frac{ka}{2} \left[\cot\left(\frac{\alpha}{a}\right) + \cot\left(\frac{d-\alpha}{a}\right) \right] \beta^2 = m\pi/2 \quad (194)$$

The width, f_m , of the Fresnel zone at any point α is then obtained from

$$f_m = 2\beta a = (2ma\lambda)^{\frac{1}{2}} \left[\cot\left(\frac{\alpha}{a}\right) + \cot\left(\frac{d-\alpha}{a}\right) \right]^{-\frac{1}{2}} \quad (195)$$

The maximum width, denoted f_m , occurs where $\alpha = d/2$. Explicitly,

$$f_m = (m\lambda d/2)^{\frac{1}{2}} X \quad (196)$$

where
$$X = \frac{\tan [d/(2a)]}{d/(2a)} = 1 + \frac{[d/(2a)]^2}{6} + \dots$$

Under most conditions C can be replaced by unity even when d is comparable with the earth's radius a . Within this approximation the Fresnel

† In the classical sense, the first Fresnel zone corresponds to $m = z$.

zones are ellipses and the minor axes are $\hat{f}_m/2$. The requirement that the function $F(u_1, u_2)$ may be replaced by unity in equation (191) is really equivalent to saying that the width of the surface S is greater than several Fresnel zones.

REFERENCES

- Barlow, H. E. M., and Fernando, W. M. G. (1956). An investigation of the properties of radial surface waves launched over flat reactive surfaces. *Proc. Instn elect. Engrs* **103**, 307–318.
- Booker, H. G., and Clemmow, P. C. (1950). The concept of an angular spectrum of plane waves and its relations to that of a polar diagram and aperture distribution. *Proc. Instn elect. Engrs* **97**, Pt. III, 11.
- Bremmer, H. (1949). "Terrestrial Radio Waves," Elsevier Publ. Co., New York and Amsterdam.
- Bremmer, H. (1954). The extension of Sommerfeld's formula for the propagation of radio waves over a flat earth to different conductivities of the soil. *Physica's Grav.* **20**, 441.
- Bremmer, H. (1958a). Propagation of electromagnetic waves. *Handb. der Phys.* **16**, 423–639.
- Bremmer, H. (1958b). Applications of operational calculus to ground wave propagation, particularly for long waves. *Trans. Inst. Radio Engrs, N. Y.* **AP-6**, 267–272.
- Brown, J., and Sharma, K. P. (1959). The launching of radial cylindrical surface waves by a circumferential slot. *Proc. Instn elect. Engrs* **106**, Pt. B, 123.
- Brown, J., and Stachera, H. S. (1959). Annular slot launchers for single conductor transmission lines. *Proc. Instn elect. Engrs* **106**, Pt. B, *Suppl.* no. 13, 143.
- Burrows, C. R. (1936). Existence of a surface wave in radio propagation, *Nature, Lond.* **138**, p. 284. (See also Burrows, C. R. (1937), *Proc. Inst. Radio Engrs, N. Y.* **25**, 219.)
- Burrows, C. R. (1937). Radio propagation over plane earth-field strength curves. *Bell Syst. tech. J.* **16**, 45–77 and 1203–1236.
- Burrows, C. R., and Gray, M. C. (1941). The effect of the earth's curvature on ground wave propagation. *Proc. Inst. Radio Engrs* **29**, 16–24.
- Clemmow, P. C. (1950). Some extensions to the method of integration by steepest descents. *Quart. J. Mech.* **3**, 241–256.
- Clemmow, P. C. (1953). Radio propagation over a flat earth across a boundary separating two different media. *Trans. roy. Soc. (London)* **246**, 1.
- Cullen, A. L. (1954). The excitation of plane surface waves. *Proc. Instn elect. Engrs* **101**, Pt. IV, 225–234.
- Editorial Comment (1901). Marconi signals across the Atlantic. *Elect. World, N. Y.* **38**, 1023.
- Elliott, R. S. (1954). On the theory of corrugated plane surfaces. *Trans. Inst. Radio Engrs, N. Y.* **AP-2**, 71–81.
- Feinberg, E. (1946). On the propagation of radio waves along an imperfect surface. *J. Phys., Moscow* **10**, 410–440.
- Fock, V. A. (1945). Diffraction of radio waves around the earth's surface. *J. Phys., Moscow* **9**, 256–266 and *J. theor. exp. Phys.* **15**, 480–490.
- Franz, K. (1962). The Watson transformation in diffraction theory (preprint volume of the "Symposium on Electromagnetic Theory and Antennas, Copenhagen").

- Furutsu, K. (1956). The calculation of field strength over mixed paths on a spherical earth. *J. Radio Res. Labs. (Japan)* 3, 391–407.
- Furutsu, K. (1959). On the electromagnetic radiation from a vertical dipole over a surface of arbitrary surface impedance. *J. Radio Res. Labs. (Japan)* 6, 269–292. (This paper was also presented at the URSI Symposium on Electromagnetic Theory, Toronto, June 1959).
- Godzinski, Z. (1958). The theory of ground wave propagation over an inhomogeneous earth. *Proc. Instn elect. Engrs* 105, Pt. C, 448.
- Hack, F. (1908). The propagation of electromagnetic waves over a plane conductor. *Ann. Phys., Ppz.* 27, 43.
- Hertz, H. (1887). Ueber sehr schnelle elektrische Schwingungen. *Wiedemanns Ann.* 31, 421.
- Hertz, H. (1888). Ueber elektrodynamische Wellen im Luftraume und deren Reflexion. *Wiedemanns Ann.* 34, 609.
- Hufford, G. A. (1952). An integral equation approach to the problem of wave propagation over an irregular surface. *Quart. appl. Math.* 9, 391.
- Johler, J. R., and Berry, L. A. (1962). Propagation of terrestrial radio waves of long wavelength—theory of zonal harmonics with improved summation techniques. *J. Res. nat. Bur. Stand.* 66D (Radio Prop.), no. 6, 737–774.
- Langer, R. E. (1937). On the connection formulas and the solutions of the wave equation. *Phys. Rev.* 51, 669.
- Leontovich, M. A. (1944). Approximate boundary conditions for the electromagnetic field on the surface of a good conductor. *Bull. Acad. Sci. U.R.S.S., Ser. Phys.* 9, 16.
- Logan, N. A. (1959). “General Research in Diffraction Theory,” I-II, Lockheed Missiles and Space Co., Sunnyvale, Calif.
- Logan, N. A., and Yee, K. S. (1962). A simple expression for propagation constants associated with a reactive convex surface. *Trans. Inst. Radio Engrs, N.Y.* AP-10, 103.
- Lorenz, L. V. (1890). Lysbevoegelsen i og uden for en plane Lysbølger belyst Kugle. *Vid. Selsk. Skr. (6)* 6, 403.
- Maley, S. W. (1962). Private communication.
- Marconi, G. (1901). (See Editorial Comment). *Elect. World, N.Y.* 38, 1023.
- Maxwell, J. C. (1873). “A Treatise on Electricity and Magnetism.” Clarendon Press, Oxford.
- Millington, G. (1949). Ground wave propagation over an inhomogeneous smooth earth, Pt. I. *Proc. Instn elect. Engrs* 96, 53. See also *Nature, Lond.* 163, 128 and 164, 114.
- Monteath, G. D. (1951). Application of the compensation theorem to certain radiation and propagation problems. *Proc. Instn elect. Engrs* 98, Pt. 4, 23–30.
- Niessen, K. F. (1937). Zue Entscheidung den zwischen den beiden Sommerfeldschen Formeln für Fortpflanzung von drahtlosen Wellen. *Ann. Phys. Lpz.* 29, 585.
- Norton, K. A. (1935). Propagation of radio waves over a plane earth. *Nature, Lond.* 135, 954.
- Norton, K. A. (1936). The propagation of radio waves over the surface of the earth and in the upper atmosphere, I. *Proc. Inst. Radio Engrs, N.Y.* 24, 1367–1387.
- Norton, K. A. (1937a). Physical reality of space and surface waves in the radiation field of radio antennas. *Proc. Inst. Radio Engrs, N.Y.* 25, 1192–1202.
- Norton, K. A. (1937b). The propagation of radio waves over the surface of the earth and in the upper atmosphere, II. *Proc. Inst. Radio Engrs, N.Y.* 25, 1203–1236.
- Norton, K. A. (1941). The calculation of the ground wave field intensity over a finitely conducting spherical earth. *Proc. Inst. Radio Engrs, N.Y.* 29, 623–639.

- Pressey, B. G., Ashwell, G. E., and Fowler, C. S. (1956). Change of phase of a low-frequency ground wave propagated across a coast line. *Proc. Instn elect. Engrs* 103B, 527.
- Rolf, B. (1930). Graphs to Prof. Sommerfeld's attenuation formula for radio waves. *Proc. Inst. Radio Engrs, N.Y.* 18, 391.
- Rotman, W. (1951). A study of single surface corrugated guides. *Proc. Inst. Radio Engrs, N.Y.* 39, 952-959.
- Sharma, K. P. (1957). An investigation of the excitation of radiation from surface waves. Ph.D. Thesis, University of London.
- Sommerfeld, A. (1909). Ueber die Ausbreitung der Wellen in der Drahtlosen Telegraphie. *Ann. Phys. Lpz.* (4) 28, 665.
- Sommerfeld, A. (1910). The propagation in wireless telegraphy. *Jahrb. d Drahtl. Tel.* 4, 157.
- Sommerfeld, A. (1926). Ueber die Ausbreitung der Wellen in der Drahtlosen Telegraphie. *Ann. Phys. Lpz.* 81, 1135.
- Sommerfeld, A. (1949). "Partial Differential Equations," Academic Press, New York.
- van der Pol, B., and Bremmer, H. (1937, 1938, 1939). The diffraction of electromagnetic waves from an electrical point source round a finitely conducting sphere. *Phil. Mag. Ser. 7* 24, 141-176; 24, 825-864; 25, 817-834; and 26, 261-275.
- van der Pol, B., and Niessen, K. F. (1930). Ueber die Ausbreitung elektromagnetischer Wellen ueber eine eben Erde. *Ann. Phys. Lpz.* (5) 6, 273. [See also B. van der Pol and K. F. Niessen (1931). *Ann. Phys. Lpz.* (5) 10, 485-510; B. van der Pol (1931). *Z. fur Hochfreq. Tech.* 37, 152; B. van der Pol (1931). *Physics* 2, 843; K. F. Niessen (1933a). *Ann. Phys. Lpz.* (5) 16, 810; K. F. Niessen (1933b). *Ann. Phys. Lpz.* (5) 18, 893.]
- Wait, J. R. (1953, 1954). Radiation from a vertical dipole over a stratified ground, I. *Trans. Inst. Radio Engrs, N.Y.* AP-1, 9-12 (1953); II. AP-3, 144-146 (1954).
- Wait, J. R. (1956a). Radiation from a vertical antenna over a curved stratified ground. *J. Res. nat. Bur. Stand.* 56, No. 4, 237-244.
- Wait, J. R. (1956b). Mixed path ground wave propagation, 1. Short distances. *J. Res. nat. Bur. Stand.* 57, 1-15.
- Wait, J. R. (1957). Excitation of surface waves on conducting, stratified, dielectric-clad, and corrugated surfaces. *J. Res. nat. Bur. Stand.* 59, 376-377.
- Wait, J. R. (1960). On the excitation of electromagnetic surface waves on a curved surface. *Trans. Inst. Radio Engrs, N.Y.* AP-8, 445-448.
- Wait, J. R. (1961). On the theory of mixed-path ground propagation on a spherical earth. *J. Res. nat. Bur. Stand.* 65D, 401-410.
- Wait, J. R., and Conda, A. M. (1958). Pattern of an antenna on a curved lossy surface. *Trans. Inst. Radio Engrs, N.Y.* AP-6, 348-359.
- Wait, J. R., and Householder, J. (1957). Mixed path ground wave propagation, 2. Larger distances. *J. Res. nat. Bur. Stand.* 59, 19-26.
- Wait, J. R., and Surtees, W. J. (1954). Impedance of a top-loaded antenna of arbitrary length over a circular grounded screen. *J. appl. Phys.* 25, 553-555.
- Wait, J. R., and Walters, L. C. (1963). Curves for ground wave propagation over mixed land and sea paths. *Trans. Inst. elect. Engrs* AP-11, 38-45.
- Watson, G. N. (1918). The diffraction of radio waves by the earth. *Proc. roy. Soc.* A95, 83-99.
- Watson, G. N. (1919). The transmission of electric waves around the earth. *Proc. roy. Soc.* A95, 546-563.
- Weyl, H. (1919). Ausbreitung elektromagnetischer Wellen ueber einem ebenen Leiter. *Ann. Phys. Lpz.* (4) 60, 481.

- Wise, W. H. (1931). The grounded condenser antenna radiation formula. *Proc. Inst. Radio Engrs, N.Y.* **19**, 1684.
- Zenneck, J. (1907). Über die Fortpflanzung ebener electromagnetischer Wellen einer ebenen Leiterfläche und ihre beziehung zur Drahtlosen Telegraphie. *Ann. Phys. Lpz.* (4) **23**, 846.

ADDITIONAL REFERENCES

- Belkina, M. G. (1949). "Tables to Calculate the Electromagnetic Field in the Shadow Region for Various Soils." Soviet Radio Press, Moscow.
- Davis, P., and Rabinowitz, P. (1956). Abscissas and weights for Gaussian quadratures of high order. *J. Res. nat. Bur. Stand.* **56**, 35-37.
- Feinberg, E. L. (1959). Propagation of radio waves along an inhomogeneous surface. *Nuovo Cim., Ser. X* **11** (Suppl.), 60-91. (This paper contains an extensive bibliography of Russian papers on the subject.)
- Furutsu, K. (1955). Propagation of electromagnetic waves over a flat earth across two boundaries separating three different media. *J. Radio Res. Labs. (Tokyo)* **2**, 239-279; and Propagation of electromagnetic waves over the spherical earth across boundaries separating different earth media. *Ibid.* **2**, 345-398.
- Gerks, I. H. (1962). Use of a high-speed computer for ground wave calculations. *Trans. Inst. Radio Engrs, N.Y.* *AP-10*, 292-299.
- Johler, J. R., and Lilley, C. M. (1961). Evaluation of convolution integrals occurring in the theory of mixed path propagation. *Tech. Notes nat. Bur. Stand.* no. 132 (PB 161633).
- Johler, J. R., Walters, L. C., and Lilley, C. M. (1960). Amplitude and phase of the low and very-low radio frequency ground wave. *Tech. Notes nat. Bur. Stand.* no. 60 (PB 161561).
- Wait, J. R. (1958). On the theory of propagation of electromagnetic waves along a curved surface. *Canad. J. Phys.* **36**, 9-17.
- Wait, J. R., and Howe, H. H. (1956). Amplitude and phase curves for ground wave propagation in the band 200 c/s to 500 kc/s. *Circ. nat. Bur. Stand.* no. 574.

ACKNOWLEDGMENT

The author thanks Mrs. L. C. Walters for extensive assistance in the numerical calculations and Mrs. Eileen Brackett for preparing the manuscript and helping to arrange the bibliography. Permission to reproduce illustrations from the paper (Wait and Walters, 1963) has been kindly granted by the Institute of Electrical and Electronics Engineers.

APPENDIX

A NOTE ON PROPAGATION ALONG NON-PLANAR AND INHOMOGENEOUS SURFACES

In studying the propagation of radio waves along the surface of the earth it is really necessary to consider the roughness. Also, in many artificial structures which are employed to guide surface waves, the imperfections of the surface may play a significant role. A rigorous theory of propagation on a rough surface appears to be out of the question. Furthermore, even if such a theory were available, the actual conditions of the problems are not usually known precisely. For example, the inhomogeneities of the earth's surface are specified only in general terms.

In this note an approximate boundary condition for a non-planar surface is developed. At the same time the inhomogeneous conductivity structure of the earth is included in the analysis. The development follows the work of Feinberg (1944-46, 1944) rather closely, although a number of simplifications are made without losing any generality.

The local surface impedance of the earth is denoted by the function $\eta(x, y)$ which depends only upon the horizontal coordinates x and y . The surface shape is represented by the function $\zeta(x, y)$ which is the height above some reference plane $z = 0$. It is convenient to introduce a dimensionless shape parameter S by writing

$$\zeta(x, y) = \zeta_0 S(x/l, y/l) \quad (1)$$

where l characterizes the length at which ζ undergoes a change in order of magnitude of average value ζ_0 .

It is fundamental to the present derivation that the character of the field at the $z = \zeta(x, y)$ surface differs only slightly from the field at the reference surface $z = 0$. It is apparent that the degree of variation caused by the inhomogeneity is determined by two independent geometrical factors: surface slope and distance. For example, on a smooth section of an ideally conducting ground, an inclination of the surface to any desired height will not disrupt the normal lines of force. On the other hand, any abrupt surface discontinuity, such as a small sudden change of height, will cause the field close to the discontinuity to be changed significantly from the unperturbed condition.

The nature of the geometric perturbation is determined usually by two small parameters. However, when the assumed mutual independence of the slopes in the two mutually perpendicular directions is taken into consideration, three parameters must be considered. These are: (1) distance $\zeta(x, y)$, and its average value ζ_0 , from the reference plane $z = 0$,

$$(2) \text{ slope parameter } \gamma_x = \frac{\partial}{\partial x} (\zeta_0 S)$$

$$(3) \text{ slope parameter } \gamma_y = \frac{\partial}{\partial y} (\zeta_0 S)$$

The respective mean slopes are designated γ_x^0 and γ_y^0 , while for an "isotropic" surface $\gamma_x^0 = \gamma_y^0 = \gamma^0$. In accordance with the basic assumptions stated above,

$$|\gamma_x^0| \ll 1 \quad \text{and} \quad |\gamma_y^0| \ll 1$$

The applicability of the surface impedance to a local region of the surface requires that the depth of penetration into the medium is small compared with the local radius of curvature R . This restriction can be stated in the form

$$k^2 R l \gg |\eta/\eta_0|$$

where $\eta_0 \cong 120\pi$ is the characteristic impedance of free space.

A further restriction, which must be stipulated, is that electric properties of the ground should vary slowly in a distance equal to the "skin depth" in the ground. For example, if b denotes a distance over which η changes appreciably, then

$$kb \gg |\eta/\eta_0|$$

With these requirements, the boundary conditions for the surface $z = \zeta(x, y)$ are now formulated. Initially, the earth is assumed to be plane. Also, for simplicity, the atmosphere is taken to be homogeneous with dielectric constant ϵ_0 . The fields \vec{E}, \vec{H} in the atmosphere then satisfy

$$\text{curl } \vec{H} = i\epsilon_0\omega\vec{E} \quad \text{and} \quad \text{div } \vec{E} = 0$$

for a time factor $\exp(i\omega t)$.

Letting the earth's surface be the (x, y) plane with the z axis directed towards the atmosphere (i.e. upwards) and introducing the surface impedance

$$E_x/H_y = -\eta \quad \text{and} \quad E_y/H_x = +\eta$$

it follows from the divergence equation that

$$\left\{ \frac{\partial E_z}{\partial z} = \eta \left(\frac{\partial H_y}{\partial x} - \frac{\partial H_x}{\partial y} \right) + \frac{\partial \eta}{\partial x} H_y - \frac{\partial \eta}{\partial y} H_x \right\}_{z=0} \quad (2)$$

On making use of the curl equation, this can be rewritten

$$\left\{ \frac{\partial E_z}{\partial z} = i\epsilon_0\omega\eta E_z - \frac{1}{\eta} (\vec{E}_t \cdot \text{grad } \eta) \right\}_{z=0} \quad (3)$$

under the assumptions that the changes in the horizontal direction are very gradual. For the special case when the electric properties of the earth are constant in a vertical direction, the equation (3) reduces to

$$\left\{ \frac{\partial E_z}{\partial z} = \frac{ik}{(\epsilon_g - i\sigma_g/\omega)} E_z + \frac{1}{2(\epsilon_g - i\sigma_g/\omega)} [\vec{E}_t \cdot \text{grad}(\epsilon_g - i\sigma_g/\omega)] \right\}_{z=0} \quad (4)$$

where σ_g and ϵ_g are the conductivity and dielectric constant of the ground which, in this case, are regarded as functions of x and y only.

Equation (3), which is the approximate boundary condition for E_z , can be simplified if η changes sufficiently slowly that

$$\left| \frac{1}{\eta^2} (\vec{k} \cdot \text{grad } \eta) \right| \ll k$$

where \vec{k} is a vector in the direction of propagation of magnitude equal to k . Then

$$\left\{ \frac{\partial E_z}{\partial z} = i\epsilon_0\omega\eta E_z \right\}_{z=0} \quad (5)$$

The generalization to a planar and inhomogeneous surface is now considered for a given point on the surface $z = \zeta(x, y)$. An orthogonal system of curvilinear coordinates (u_1, u_2, u_3) is introduced at which it is assumed that u_1 runs along the normal to the surface at the point in question. The other two coordinates then define the tangent plane. Identifying u_1 with the normal n while u_1 and u_2 are proportional to the polar angles, θ_1 and θ_2 , in the corresponding principal planes, an element of length can be expressed by

$$ds^2 = dn^2 + R_1^2 d\theta_1^2 + R_2^2 d\theta_2^2 \quad (6)$$

where R_1 and R_2 are the main curvature radii.

It is convenient to observe that

$$\frac{\partial R_1}{\partial n} = \frac{\partial R_2}{\partial n} = 1 \quad (7)$$

and

$$\frac{1}{R_1} + \frac{1}{R_2} = -\frac{\partial \gamma_x}{\partial x} - \frac{\partial \gamma_y}{\partial y} \quad (8)$$

Then, on expressing $\text{div} \vec{E}$ and $\text{div} \vec{E}_g$ in curvilinear coordinators and making use of the continuity of the tangential components of \vec{E} and \vec{E}_g , it readily follows that

$$\frac{\partial E_n}{\partial n} = \frac{\partial E_{gn}}{\partial n} + (E_{gn} - E_n) \left(\frac{1}{R_1} + \frac{1}{R_2} \right) + \frac{1}{\hat{e}_g} (\vec{E}_g \cdot \text{grad} \hat{e}_g) \quad (9)$$

at $z = \zeta$

In this equation E_n is the normal component of the electric field in the air, E_{gn} is the normal component of the electric field in the ground, and $\hat{e}_g = \epsilon_g - i\sigma_g/\omega$ is the complex dielectric constant in the ground.

Because $|\hat{e}_g/\epsilon_0| \gg 1$ and, in view of the identity, $\hat{e}_g E_{gn} = \epsilon_0 E_n$ at $z = 0$, it appears that E_{gn} can be neglected compared with E_n . Furthermore, since R_1 and R_2 are large compared with a wavelength in the ground, E_{gn} is propagating as a plane wave just below the interface. Thus

$$\frac{\partial E_{gn}}{\partial n} \cong ik\sqrt{\epsilon_g/\epsilon_0} E_{gn} = i\epsilon_0 \omega \eta E_{gn} \quad (10)$$

at $z = \zeta$. Then

$$\frac{\partial E_n}{\partial n} = \left[i\epsilon_0 \omega \eta - \left(\frac{1}{R_1} + \frac{1}{R_2} \right) \right] E_n + \frac{1}{\hat{e}_g} (\vec{E}_t \cdot \text{grad} \hat{e}_g) \quad (11)$$

where \vec{E}_t is the electric field vector tangential to the surface. In the case of a flat surface this equation reduces to (3).

The derived boundary condition for E_n is now transferred to the reference plane $z = 0$ by making use of the following relations

$$(1) \quad E_n \cong E_z \sim \exp[-i(k_x x + k_y y)] \quad (12)$$

where k_x and k_y are the x and y components of the horizontal wave number.

$$(2) \quad E_x \cong \left(-\gamma_x + \frac{k_x \eta}{k \eta_0} \right) E_z, \quad z = \zeta \quad (13)$$

and

$$E_y \cong \left(-\gamma_y + \frac{k_y \eta}{k \eta_0} \right) E_z, \quad z = \zeta \quad (14)$$

$$(3) \quad E_n = -\gamma_x E_x - \gamma_y E_y + \gamma_z E_z \quad (15)$$

$$\frac{\partial}{\partial n} = -\gamma_x \frac{\partial}{\partial x} - \gamma_y \frac{\partial}{\partial y} + \gamma_z \frac{\partial}{\partial z} \quad (16)$$

where

$$\gamma_z = (1 - \gamma_x^2 - \gamma_y^2)^{\frac{1}{2}} \quad (17)$$

Terms in the second order in γ and ζ are retained while neglecting terms involving $(\eta/\eta_0)\gamma$ and $(\eta/\eta_0)\zeta$. Then, the boundary condition on the plane $z = 0$, becomes

$$\begin{aligned} \frac{\partial E_z}{\partial z} = i\epsilon_0 \omega \eta \left[1 + \frac{i}{k^2} \left(k_x \frac{\partial}{\partial x} + k_y \frac{\partial}{\partial y} \right) \log_e \left(\frac{\eta}{\eta_0} \right) \right] E_z \\ + \frac{\partial}{\partial x} \left(\gamma_x E_z + \zeta \frac{\partial E_x}{\partial z} \right) + \frac{\partial}{\partial y} \left(\gamma_y E_z + \zeta \frac{\partial E_y}{\partial z} \right) \end{aligned} \quad (18)$$

To within a first order in γ and ζ , the terms involving the derivative of E_x and E_y may be neglected.

To obtain an integral equation for \vec{E} , the field in the air, Feinberg (1944) makes use of Green's theorem. Thus

$$\vec{E} = \frac{\vec{E}_a}{2} - \frac{1}{4\pi} \iint \left(\frac{\partial \vec{E}}{\partial z'} v - \frac{\partial v}{\partial z'} \vec{E} \right) dx' dy' \quad (19)$$

where the integration extends over the whole plane and \vec{E}_a corresponds to a volume integral over the source. The auxiliary function v may be chosen arbitrarily. However, for convenience, it is desirable to regard v as the field of a dipole located on the surface of an auxiliary or reference flat earth of constant surface impedance η_c at $z = 0$. Thus

$$v = \frac{e^{-ikr}}{r} W \quad (20)$$

where $r = [(x-x')^2 + (y-y')^2 + z^2]^{\frac{1}{2}}$, and W is the Sommerfeld attenuation function (Sommerfeld, 1949) for a homogeneous flat earth. The latter is given by

$$W \cong 1 - i(\pi p)^{\frac{1}{2}} e^{-w} \operatorname{erfc}(iw^{\frac{1}{2}}) \quad (21)$$

where $w = p \left(1 + \frac{\eta_0 z}{\eta_c r} \right)^2$, $p = -(ikr/2) (\eta_c/\eta_0)^2$, and erfc is the complement

of the error function. At the surface $z = 0$ it may be verified that

$$\frac{\partial W}{\partial z} = i\epsilon_0 \omega \eta_c W \quad (22)$$

The integral equation E_z , in the limit $z \rightarrow 0$, now becomes

$$E_z = E_{az} - \frac{1}{2\pi} \iint_{z'=0} \left[\frac{\partial E_z}{\partial z'} - i\epsilon_0 \omega \eta_c E_z' \right] \frac{e^{-ikr}}{r} W dx' dy' \quad (23)$$

where the specific form of $(\partial E_z / \partial z')$ is obtained from (18). E_{az} can now be regarded as the z component of the field when the surface is plane with surface impedance η_c . To within the first order of smallness of γ and ζ , the explicit form of the integral equation becomes

$$\begin{aligned} E_z = E_{az} - \frac{i\epsilon_0 \omega}{2\pi} \iint \left\{ \eta \left[1 + \frac{i}{k^2 \eta} \left(k_{x'} \frac{\partial \eta}{\partial x'} + k_{y'} \frac{\partial \eta}{\partial y'} \right) \right] - \eta_c \right\} E_z' \\ \times \frac{e^{-ikr}}{r} W dx' dy' - \frac{1}{2\pi} \iint \left[\frac{\partial}{\partial x'} (\gamma_{x'} E_z') \right] \frac{e^{-ikr}}{r} W dx' dy' \\ - \frac{1}{2\pi} \iint \left[\left(\frac{\partial}{\partial y'} \right) (\gamma_{y'} E_z') \right] \frac{e^{-ikr}}{r} W dx' dy' \quad (24) \end{aligned}$$

where

$$r = [(x-x')^2 + (y-y')^2]^{\frac{1}{2}}$$

$$\gamma_{x'} = \frac{\partial \zeta}{\partial x'} \quad \gamma_{y'} = \frac{\partial \zeta}{\partial y'}$$

$$W \cong 1 - i(\pi p)^{\frac{1}{2}} e^{-p} \operatorname{erfc}(ip^{\frac{1}{2}})$$

and

$$p = -(ikr/2)(\eta_c/\eta_0)^2 \quad (25)$$

This integral equation may be used as the starting point for various theoretical investigations of mixed-path propagation of radio waves. In some senses the results turn out to be equivalent to more recent approaches (e.g. Wait, 1962) which utilize the compensation theorem. The choice between these methods is really a matter of convenience.

REFERENCES FOR APPENDIX

- Feinberg, E. L. (1944-1946). On the propagation of radio waves along an imperfect surface. *J. Phys. (U.S.S.R.)* **8**, No. 6, 317-330 (1944); **9**, No. 1, 1-6, (1945); and **10**, No. 5, 410-418 (1946).
- Feinberg, E. L. (1944). Propagation of radio waves along an actual surface. *Bull. Acad. Sci. (U.R.S.S.) Phys. Series* **8**, 109-131 (in Russian).
- Sommerfeld, A. N. (1949). "Partial Differential Equations", Academic Press, New York.
- Wait, J. R. (1962). The propagation of electromagnetic waves along the earth's surface. In "Electromagnetic Waves" (R. E. Langer, ed.) University of Wisconsin Press.

AUTHOR INDEX

*Numbers in italics refer to the pages on which references are listed
at the end of each article*

A

Abbott, R. L., 121, 137, *155*
 Adey, A. W., 24, *50*
 Akita, K. T., 36, *51*, *155*
 Ament, W. S., 38, 40, 46, *50*
 Anderson, L. J., 90, *119*, *120*
 Anderson, W. L., 112, *119*
 Anway, A. C., 109, 111, *119*
 Artman, J. O., 124, 126, *155*
 Ashwell, G. E., 194, *211*
 Attwood, S. S., 144, *155*
 Autler, S. H., 124, *155*

B

Barghausen, A. F., 113, *120*
 Barlow, H. E. M., 159, *209*
 Barrell, H., 5, *50*
 Battan, L. J., 142, *155*
 Bean, B. R., 4, 35, 36, *50*, 56, 57, 58,
 65, 77, 78, 81, 87, 89, 94, 96, 97, 103,
 105, 106, *119*, 121, 128, 137, 138, *155*
 Becker, G. E., 124, *155*
 Beckmann, B., *155*
 Belkina, M. G., *212*
 Bennett, C. A., 116, *119*
 Berry, L. A., 117, *210*
 Berry, R. L., 34, *50*
 Best, A. C., 152, *155*
 Beyers, N. J., 112, *119*
 Birnbaum, G., 5, 7, 14, 23, 37, 41, 49,
 50, 124, *155*
 Blomquist, A., *156*
 Boggs, J. E., 14, 16, 49, *50*, *51*, *52*
 Booker, H. G., 56, *119*, *168*, *209*
 Bremmer, H., 176, 179, 182, 184, *209*,
 211
 Brooks, C. E. P., 117, *119*
 Brown, J., 166, 172, *209*
 Burgoyne, R. H., 35, *50*
 Burrows, C. R., 59, *120*, 144, *155*, 159,
 182, *209*
 Bussey, H. E., 14, 23, 37, 41, *50*, 121,
 147, 148, *155*

C

Cahoon, B. A., 57, 58, 105, *119*, 128,
 138, *155*
 Campen, C. M., 46, *51*
 Carruthers, N., 117, *119*
 Catterjee, S. K., 5, *50*
 Chapman, C. M., 46, *51*
 Clapp, J. K., 33, *50*
 Clemmow, P. C., 161, 168, 184, *209*
 Clinger, A. H., 36, *50*
 Cogdell, J. R., 30, *50*
 Conda, A. M., 189, *211*
 Condron, T. P., 79, *119*
 Crain, C. M., 5, 7, 9, 20, 23, 34, 36, 38,
 41, 46, 49, 50, *50*, *51*, *52*
 Crawford, A. B., *155*
 Cullen, A. L., 175, *209*
 Cunningham, R. M., 49, *51*
 Cunningham, R. W., 38, 46, *52*

D

Dakin, T. W., 14, 16, *52*
 Davidson, D., 121, *155*
 Davis, P., *212*
 Deakins, G. E., 50, *51*
 Deam, A. P., 7, 26, 30, 37, 41, 49, *50*,
 51, *52*
 Debye, P., 3, *51*
 Dinger, H. E., *155*
 Donaldson, Ralph J., Jr., 141, *155*
 Du Castel, F., *155*
 Dubin, M., 66, *119*
 Dutton, E. J., 87, *119*

E

East, T. W. R., 128, 141, 142, *155*
 Edmonds, F. N., 41, *51*
 Edwards, H. D., 128, *155*
 Elliott, R. S., 162, *209*
 Essen, L., 5, *51*
 Evans, H. W., 144, 145, 148, 149, 150,
 151, *155*

F

- Fehlhaber, L., 65, 119
 Feinberg, E. L., 184, 209, 212, 213, 216, 217
 Fernando, W. M. G., 159, 209
 Ferrell, E. B., 59, 120
 Fock, V. A., 179, 181, 189, 209
 Fowler, C. S., 194, 211
 Franeau, J., 14, 50
 Franklin, N. L., 116, 119
 Franz, K., 176, 209
 Freethey, F. E., 20, 24, 52
 Froome, D. S., 14, 24, 51
 Froome, K. D., 5, 51
 Furutsu, K., 159, 184, 210, 212

G

- Galloway, W. C., 12, 52
 Gerhardt, J. R., 7, 36, 38, 41, 46, 51
 Gerks, I. H., 212
 Ghosh, S. N., 128, 155
 Godzinski, Z., 184, 210
 Gordon, J. P., 124, 126, 155
 Goroy, W., 124, 155
 Gough, M. W., 155
 Gray, M. C., 182, 209
 Grosskopf, J., 65, 119
 Gunn, K. L. S., 128, 141, 142, 151, 152, 155, 156

H

- Hack, F., 158, 210
 Hathaway, S. D., 144, 145, 148, 149, 150, 151, 155
 Hay, D. R., 33, 51
 Hector, L. G., 5, 51
 Heer, O., 155
 Herbstreit, J. W., 113, 120
 Hertz, H., 157, 210
 Hill, R. M., 124, 155
 Hinze, J. O., 37, 51
 Hirao, Kunio, 36, 51, 78, 120, 155
 Hogg, D. C., 155, 156
 Hopkins, H. G., 142, 152, 156
 Horn, J. D., 36, 50, 81, 87, 119
 Hornberg, K. O., 113, 120
 Householder, J., 184, 186, 211
 Howe, H. H., 212

- Hufford, G. A., 203, 210
 Humphreys, W. J., 64, 119

J

- Janes, H. B., 113, 120
 Jehn, K. H., 36, 51
 Jöhler, J. R., 177, 210, 212
 Johnson, W. E., 113, 120
 Jona, M. J., 4, 5, 32, 51
 Josephson, B., 156

K

- Kampe, H. J., 141, 156
 Katz, I., 78, 119
 Kennard, E. H., 156
 Kerker, M., 151, 152, 156
 Kerr, D. E., 56, 94, 119
 Kerr, F. J., 6, 51
 Kieley, D. G., 156
 Kirkpatrick, A. W., 113, 120
 Kolmogoroff, A. N., 37, 51
 Kryden, S. J., 5, 50

L

- Lane, J. A., 14, 24, 51
 Langer, R. E., 178, 210
 Langleben, M. P., 151, 152, 156
 Lauritsen, T., 156
 Laws, J. O., 143, 144, 156
 Leontovich, M. A., 160, 210
 Lilley, C. M., 212
 Logan, N. A., 178, 180, 182, 192, 203, 210
 Lorenz, L. V., 178, 210
 Lyons, H., 5, 50

M

- McConnell, G. J., 14, 24, 51
 MacDonald, F. C., 40, 52
 McGavin, R. E., 2, 51
 Magee, J. B., 49, 51
 Martin, H. C., 33, 51
 Maley, S. W., 199, 210
 Marconi, G., 157, 210
 Maryott, A. A., 124, 126, 155
 Maxwell, J. C., 157, 210
 Meaney, F. M., 35, 50

- Mie, G., 144, 146, 156
 Miller, S. L., 156
 Millington, G., 184, 194, 197, 210
 Millman, G. H., 156
 Minzner, R. A., 79, 119
 Misme, P., 78, 105, 119, 155
 Mohan, T. J., 34, 50
 Monteath, G. D., 160, 184, 185, 205, 210
 Montgomery, C. G., 14, 51
- N
- Niessen, K. F., 159, 210, 211
 Norton, K. A., 65, 113, 119, 159, 161, 162, 164, 182, 193, 210
- O
- Onoe, M., 156
 Ozanich, A. M., Jr., 87, 119
- P
- Parsons, D. A., 143, 144, 156
 Peterson, C. F., 113, 120
 Phillips, W. E., 5, 51
 Planck, Max, 156
 Plank, V. G., 46, 51
 Pote, A., 121, 155
 Pound, R. V., 9, 12, 52
 Pressey, B. G., 194, 211
- R
- Rabinowitz, P., 212
 Rainey, R. J., 112, 119
 Ramaswamy, K. L., 5, 52
 Rao, G. O., 5, 52
 Ratner, B., 81, 120, 135, 156
 Rice, P. L., 65, 120
 Richtmeyer, F. K., 156
 Riggs, L. P., 36, 50
 Ringwalt, D. L., 40, 52
 Ripley, W. S., 79, 119
 Robinson, N. P., 156
 Rolf, B., 159, 211
- Rotman, W., 162, 211
 Ryde, D., 142, 144, 156
 Ryde, J. W., 142, 144, 156
- S
- Sanger, R., 5, 6, 52
 Sargent, J. A., 49, 52
 Saxton, J. A., 6, 46, 52, 142, 152, 156
 Schelling, J. C., 59, 120
 Schulkin, M., 58, 120
 Schunemann, R., 16, 52
 Sears, J. E., 5, 50
 Semplak, R. A., 156
 Severin, J. A., 34, 52
 Sharma, K. P., 166, 170, 209, 211
 Shaw, R. H., 38, 46, 52
 Sherr, P. E., 26, 41, 52
 Shiro, I., 155
 Smart, W. M., 120
 Smith, E. K., 4, 6, 52
 Sommerfeld, A. N., 158, 159, 161, 164, 211, 216, 217
 Stachera, H. S., 172, 209
 Steffan, W., 16, 52
 Stickland, A. C., 63, 120
 Stout, C. D., 34, 50
 Straiton, A. W., 24, 30, 31, 36, 37, 38, 41, 50, 51, 52, 126, 156
 Stranathan, J. D., 5, 6, 34, 52
 Strandberg, M. W. P., 124, 156
 Surtees, W. J., 160, 211
- T
- Tao, Kazohiko, 78, 120
 Thayer, G. D., 56, 58, 77, 78, 89, 97, 103, 105, 106, 119
 Thompson, C. M., 49, 50
 Thompson, M. C., Jr., 14, 20, 24, 52, 113, 114, 120
 Thorn, D. C., 24, 49, 51, 52
 Tinkham, M., 124, 156
 Tolbert, C. W., 31, 52, 126, 156
 Townes, C. H., 156
 Tregidga, A. C., 6, 52
 Troitskii, V. S., 78, 87, 120
 Tuller, W. G., 12, 52
 Tunnell, G. A., 138, 156
 Turner, H. E., 33, 51

V

Van Der Pol, B., 159, 179, 211
 Van Vleck, J. H., 122, 123, 156
 Vetter, M. J., 14, 16, 52, 113, 120
 Voge, J., 155
 Vogler, L. E., 65, 120
 Von Rosenberg, C. E., 38, 41, 51

W

Wagner, N. K., 44, 52
 Wait, J. R., 159, 160, 176, 181, 182, 183,
 184, 185, 186, 188, 189, 193, 197, 199,
 211, 212, 217, 217
 Walker, G. B., 37, 41, 52
 Walkinshaw, W., 56, 119
 Walters, L. C., 193, 211, 212
 Waters, D. M., 20, 24, 52
 Watson, G. N., 175, 178, 211
 Watson, H. E., 5, 52
 Weber, Eric, 156
 Weickmann, H. K., 141, 156

Weintraub, S., 4, 6, 52
 Weisbrod, S., 90, 120
 Wells, P. I., 113, 120
 Weyl, H., 158, 211
 Wilkerson, R. E., 113, 120
 Williams, C. E., 20, 23, 38, 51
 Wise, W. H., 159, 212
 Woernly, D. L., 5, 51
 Wong, Ming S., 38, 52, 91, 120
 Works, C. N., 14, 16, 52

Y

Yee, K. S., 182, 210

Z

Zaffarano, F. P., 12, 52
 Zahn, C. T., 6, 52
 Zenneck, J., 158, 212
 Zhevankin, S. A., 78, 87, 120

SUBJECT INDEX

A

- A-unit, 87–89
- Absolute humidity, 123, 128–131, 137 foll.
 - contours, 129–131, 140
- Absorption of radio waves, atmospheric,
 - correlation with absolute humidity, 137–141
 - by gases, 122–141, 147 foll.
 - line width factors, 124–126
 - total path, 136–141
 - by trace constituents, 128, 132
- Aerial noise temperature, 155
- Aerosols, effect on refractivity, 49
- Angular spectrum of plane waves, 168
- Antenna, *see* Aerial
- Arctic climate, refraction for, 106–108
- ARDC (Air Research and Development Command) Model Atmosphere, 66, 68
- Atmosphere,
 - attenuation of radio waves in, 121–156
 - effect of horizontal inhomogeneities on ray tracing, 91–100, 119
 - radio refractive index measurements, 1–52
 - refractivity structure models, 59–89
 - thermal noise emission, 153–155
- Atmospheric gases,
 - radio wave absorption by, 122–141, 147 foll.
 - total absorption range, 132–136
- Attenuation of radio waves
 - by atmospheric gases, 122–141
 - in clouds, 141–142, 152
 - by fog, 152
 - by hail, 151–152
 - by rain, 142–151
 - in troposphere, 121–156
- Axial waves on cylindrical rods, 171–172
- Azimuthal waves on cylindrical boundaries, 172–175

B

- Bending of radio ray, 53 foll., 72–78, 94–101
 - comparisons for model atmospheres, 71–76
 - graphical computation method, 90–91
 - high-angle, 57–58
 - initial gradient correction, 77–78
 - methods of calculation, 57–59, 77–78, 87–89
 - prediction errors, 77, 85–86
- Birnbaum refractometer, 7, 14–17, 24–26

C

- Calibration of aircraft refractometers, 22
- Canterbury Project, 91 foll.
- Capacitor-type refractometers, 9, 32–34
- Cape Canaveral–Nassau path, meteorological profile for, 94–100
- Clapp oscillator, 33
- Clouds,
 - radio wave attenuation in, 141–142, 152
 - refractive index changes in, 46–49
- Condensation effects in refractometers, 23–24, 30, 34
- Crain refractometer, 7–14, 21 foll., 38–42
- CRPL (Central Radio Propagation Laboratory)
 - Corrected Exponential Reference Atmosphere, 97–98
 - Exponential Reference Atmosphere, 67–78, 85 foll.
 - Reference Refractivity Atmosphere, 66–77
 - Standard *N*-profile Sample, 100–119

D

- Deam refractometer, 9, 26–30, 39 foll.
- Dipole
 - above conducting half-space, 158–166

Dipole

- above homogeneous spherical earth, 175-184
- above impedance plane, 159-166, 170
- above plane stratified earth, 182

Dropsonde, 34

Ducting, 56, 92, 94, 99

Dust effect on refractivity, 49

E

Earth,

- plane stratified, 182
- spherical
 - homogeneous, propagation over, 175-184
 - inhomogeneous, propagation over, 204-209

Effective earth's radius (4/3 earth) model, 59-62, 193

modification of, 62-67

Elevation angle error, 55, 100 foll., 117

fluctuations, 110-112

Excess path loss due to rainfall, 148 foll.

F

Fog attenuation of radio waves, 152

Frequency dependence of refractivity, 4-5

G

Ground waves, *see* Propagation

H

Hail attenuation of radio waves, 151-152

Hay refractometer, 9, 32-34

Height-gain function for ground wave propagation, 197, 199

Hygrometers based on refractometer, 49

I

ICAO (International Civil Aviation Organization) standard atmosphere, 79-80

Ice clouds, 141-142, 151

Impedance plane, 159-166, 170

Ionization measurement by refractometer, 49-50

M

Microwave attenuation

- by atmospheric gases, 122-141
- in clouds, 141-142, 152
- by fog, 152
- by hail, 151-152
- by rain, 142-151

Microwave relay links, path loss and rainfall, 151

Microwaves,

- atmospheric absorption of, 121-156
- scattering in atmosphere, 121-122
- scattering by hail, 151-152
- scattering by raindrops, 142-147

N

N-units, *see* Refractivity

Noise

- of refractometer system, 17
- thermal, emitted by atmosphere, 153-155

Norton surface wave, 164

O

Oxygen, absorption by, 122 foll., 128, 137

microwave attenuation, 126-128

P

Polarizability, 3

Pound stabilized oscillators, 9-12, 26, 50

Pressure effects on refractometer cavities, 22-23

Propagation, ground-wave,

- land-to-sea, 193 foll.
- over land-sea-land path, 197, 201
- sea-to-land, 195, 197

Propagation, surface-wave,

- along non-planar and inhomogeneous surfaces, 212-217
- over homogeneous spherical earth, 175-184
- over inhomogeneous spherical earth, 204-209
- over mixed path on spherical earth, 184-203
- laboratory investigation of, 199
- three-section path, 190-192
- two-section path, 184-190

Propagation factor
for impedance boundary, 164–165

R

Radar,

effect of fog and rain on, 142
tropospheric echoes, 45–46

Radiation pattern, far-zone, for aerial
on curved surface, 189

Radio hole, 38

Radio range error, 56, 100 foll., 117
fluctuations, 113–115

Radio sextant, 109–110

Radio systems,

outage time predictions, 148–151
rain attenuation effects on, 147–151

Radio waves, *see under* Absorption;
Attenuation; Microwaves; Refraction

Radiosonde,

data for refractivity profiles, 35–36,
58–59, 62–64, 81, 92 foll.

with direct refractive index output, 36

Rain attenuation of microwaves,

effects on radio systems, 147–151
as function of rainfall rate, 142–147
for known drop size distribution,
146

Rainfall rate, drop size distribution for,
143–146

Ray tracing, 53–56

effect of atmospheric horizontal
inhomogeneity on, 91–100
limitations of, 56–57

Recovery effect, 194 foll.

Refraction of radio waves, tropo-
spheric, 53–120

predicted from surface weather ob-
servations, 100–119

of 1.85-cm λ solar radiation, 109, 111
Refractive index of atmosphere, 2–5, 53
calculated from meteorological data,
35–36

in clouds, 46–49

fluctuations, 41–46

horizontal inhomogeneities, 91–100,
119

isopleths, 92 foll.

measurements, 1–52

by airborne refractometer, 38–49,
94 foll.

ground based, 36–38

Refractive index of atmosphere,
measurements,
in laboratory, 5–6
on tower, 37, 43–44
nomograms, 35

Refractive index of water vapour,
frequency dependence of, 4–5
microwave measurement, 6

Refractivity of atmosphere, 4
bi-exponential model, 78–87

definition of N , 3–4, 56

distribution

above 20 000 ft, 66

for ICAO standard atmosphere,
79–80

dry- and wet-term scale heights, 78,
81–85, 87

exponential model, 67–77, 85 foll.

frequency dependence, 4–5

as function of altitude above sea level,
63–64

models of, 59–89

profiles,

comparison with reference atmo-
spheres, 67–77

CRPL Standard Sample, 100–119

departure from normal, 87–89

typical, 62–63

surface value, for predicting refrac-
tion, 100–119

Refractometer capacitors, 32–34

Refractometer cavities,

coaxial-type, 26–31

condensation in, 30

refractive index variations along,
30–31

temperature compensation, 30

microwave-type, 17–26

ceramic, 20

frequency variations in, 19–20

interference with airflow, 24–26

invar, 20

pressure effects on, 22–23

reduction of thermal effects, 20–22

resonant frequency of, 19

ventilation of, 24–26

wall condensation in, 23–24

Refractometer techniques,

applications of, 49–50

Refractometers (atmospheric)

airborne measurements, 38–49, 94 foll.

- Refractometers (atmospheric)
 balloon-borne, 9, 29, 33
 Birnbaum-type, 7, 14-17, 24-26
 Crain-type, 7-14, 21 foll., 38-42
 Deam-type, 9, 26-30, 39 foll.
 free-falling, 39-40
 ground-based measurements by, 36-38
 Hay-type, 9, 32-34
 history of, 6-9
 Tolbert phase-shift type, 31-32
 tower-mounted, 37
- S
- Scattering of microwaves,
 in atmosphere, 121-122
 by hail, 151-152
 by raindrops, 142-147
 Schulkin's method of calculating ray
 bending, 58-59
 Servomechanism for refractometer
 tuning, 14, 17
 Sky temperature, 154-155
 Smoke, effect on refractivity, 49
 Snell's law, 53
 graphic representation, 90
 Sommerfeld surface wave, 158-159
 Space wave, 164, 170, 172
 Subrefraction, 94, 97 foll.
 Superrefraction, 94, 100
 Surface ducts, 92, 94, 99
 Surface waves (electromagnetic), 157-
 217
 axial, on cylindrical rod, 171-172
 azimuthal, on cylindrical boundaries,
 172-175
 excitation by circumferentially slotted
 cylinder, 166-168
 excitation by magnetic ring source,
 168-170
 of Norton, 164
 propagation, *see* Propagation, sur-
 face-wave
 of Sommerfeld, 158-159
 trapped, 164, 172
 of Zenneck, 158-159, 163
 Synoptic radio meteorology, 36
- T
- Temperate climate, refraction for, 106-
 108
 Temperature measurement of refracto-
 meter cavities, 22
 Thermal effects on refractometer
 cavities, 20-22, 30
 Thermal noise temperature, 154-155
 Tolbert phase-shift refractometer, 31-32
 Total path absorption, correlation with
 absolute humidity, 137-141
 Transmission loss versus rainfall rate,
 144-145
 Trapping of radio ray, 56
 Tropical climate, refraction for, 106-108
 Tropopause, *N* value at, 79-80, 86
 Troposphere,
 attenuation of radio waves in, 121-156
 radar echo and refractive index data,
 45-46
 refraction of radio waves in, 53-120
 subrefractive layers in, 99-100
- V
- Van der Pol-Bremmer theory for pro-
 pagation over homogeneous earth,
 179, 182
 Ventilation of refractometer cavities,
 24-26
- W
- Water vapour, absorption by, 122 foll.,
 137
 microwave attenuation, 126-128
 Wave propagation, *see* Propagation
 Waveguide mode of propagation, 56
 Waves, electromagnetic, *see* Propaga-
 tion; Surface waves
 Weather observations, refraction pre-
 dicted from, 100-119
 Wiresonde, 92
- Z
- Zenneck surface wave, 158-159, 163



